2019

EXPLORING THE SENSITIVITY OF MANTLE CELL LYMPHOMA TO INHIBITORS OF BRUTON'S TYROSINE KINASE

Hannah Patricia Thompson

PHD

EXPLORING THE SENSITIVITY OF MANTLE CELL LYMPHOMA TO INHIBITORS OF BRUTON'S TYROSINE KINASE

Thompson, Hannah Patricia

Award date:
2019

Awarding institution:
University of Plymouth

UNIVERSITY OF
PLYMOUTH

EXPLORING THE SENSITIVITY OF MANTLE CELL LYMPHOMA TO INHIBITORS OF BRUTON'S TYROSINE KINASE

by

HANNAH PATRICIA THOMPSON

A thesis submitted to the University of Plymouth
in partial fulfilment for the degree of

DOCTOR OF PHILOSOPHY

Peninsula Medical School

July 2019

ACKNOWLEDGEMENTS

I would like to express my sincere gratitude to my director of studies Dr Claire Hutchinson, for her continued support and guidance throughout the duration of my PhD studies, for teaching me the essential techniques required for this research, and for her motivation and encouragement which has developed my skills and passion for research in the haematology field.

I am grateful to Professor Simon Rule for his additional supervision of this project, for offering his expert knowledge on the clinical features of Mantle cell lymphoma patients treated with BTK inhibitor therapy, and for his enthusiasm and interest in my scientific findings.

I am extremely grateful to Dr Dave Tucker for his invaluable support and friendship during my PhD, and would also like to thank Frances Frend and Elliot Thomas for all their help in the lab during my final year.

I am extremely thankful to all the MCL patients who consented to participate in this study, and to the clinical staff at Derriford hospital in Plymouth for collecting and supplying the blood samples.

I would like to thank Dr Martin Dyer for supplying the REC-1 cells (an important cell line in this study), and the CD40L-expressing and non-expressing fibroblast cell lines used in co-culture experiments with primary lymphocytes. I am also grateful to the clinical scientists at Derriford hospital radiotherapy department for staying after hours to irradiate the fibroblast monolayers.

I would also like to thank Dr Karen Rees Unwin and Dr John Burthem for carrying out the mass spectrometry analysis on the IRF4 protein precipitations, and Dr Michele Kiernan for sequencing the chromatin precipitations prepared in this study.

I am extremely grateful to University Hospitals Plymouth NHS trust for funding this research project, and would also like to thank Plymouth and District Leukaemia fund (PDLF) for their generous contribution towards laboratory equipment.

Finally, I would like to acknowledge my family for all their help and support during my PhD, especially Rick and Harry for their patience and understanding.

AUTHOR'S DECLARATION

At no time during the registration for the degree of Doctor of Philosophy has the author been registered for any other University award without prior agreement of the Doctoral College Quality Sub-Committee.

Work submitted for this research degree at the University of Plymouth has not formed part of any other degree either at the University of Plymouth or at another establishment.

This study was financed with the aid of a studentship from University Hospitals Plymouth NHS Trust.

Word count of main body of thesis: 56,834

Signed……..

Date……

ABSTRACT

Hannah Patricia Thompson

EXPLORING THE SENSITIVITY OF MANTLE CELL LYMPHOMA TO INHIBITORS OF BRUTON'S TYROSINE KINASE

Mantle cell lymphoma (MCL) is an incurable B-cell lymphoma which responds poorly to conventional chemotherapy. Inhibitors of Bruton's tyrosine kinase (BTKi) have shown a significant clinical effect; despite this success however, approximately one third of MCL patients have primary resistance to the drug, and patients who initially respond to treatment frequently acquire secondary resistance with aggressive relapse of the disease. The purpose of this study was to understand how BTKi-resistance or sensitivity is mediated, aiming to identify new targets for therapy or predictive biomarkers of response.

Combining a range of cell culture, biochemical and molecular techniques, the work presented describes the development of *in vitro* models of MCL with different sensitivity or resistance to BTKi. These models identify distinct functional and signalling responses of sensitive or resistant cell lines during BTKi treatment in the presence or absence of stromal cell support. The REC-1 cell line demonstrated reduced survival, proliferation, inhibition of BTK and ERK signalling, and downregulation of IRF4 expression in response to BTK inhibition. In contrast, resistant cell lines (G519, JEKO-1 and JVM2) or REC-1 cells with acquired resistance to BTKi did not downregulate IRF4. The stromal microenvironment also supported BTKi resistance and opposed IRF4 downregulation. These findings were reproduced using *ex vivo* primary MCL cells taken before and during clinical BTKi therapy, identifying IRF4 as a potential mediator and biomarker of BTKi treatment sensitivity or resistance in a clinical setting.

Further detailed assessment of IRF4 protein interactions using molecular and proteomic approaches in BTKi sensitive cells identified a novel potential association with proteins involved in mitochondrial function that may be involved in resistance to treatment with BTKi. Further investigation of these interactions may indicate novel targets for the design of therapeutic combinations which can overcome BTKi resistance in MCL.

TABLE OF CONTENTS

LIST OF TABLES

LIST OF FIGURES

LIST OF ABBREVIATIONS

Ab	Antibody
Ag	Antigen
ABC DLBCL	Activated B cell diffuse large B cell lymphoma
ABT-199	Venetoclax
Acal	Acalabrutinib
AKT	Protein kinase B
AP-1	Activator protein 1
APC	Allophycocyanin
APS	Ammonium persulphate
ATF2	Activating transcription factor 2
ATP	Adenosine triphosphate
BAD	BCL2-associated agonist of cell death
BAFF	B cell activating factor F
BAK	BCL2 antagonist/killer 1
BALL	B cell acute lymphoblastic leukaemia
BATF	Basic leucine zipper transcription factor, ATF-like
BAX	BCL2-associated X protein
BCA	Bicinchoninic acid assay
BCL2	B cell lymphoma 2
BCL-W	BCL2-like 2
BCL-XL	B-cell lymphoma-extra large
BCR	B-cell receptor
BD	Becton Dickinson
BGB-3111	Zanubrutinib
BH	TEC homology
BIM	BCL2-like 11
BIRC3	Baculoviral IAP Repeat Containing 3
BLF-1	BCL2-related protein A1
BLIMP-1	B lymphocyte-induced maturation protein-1
BLNK	B cell linker
BSA	Bovine serum albumin
BTK	Bruton's tyrosine kinase
BTKi	Bruton's tyrosine kinase inhibitor’s

bp	Base pair
BZM	Bortezomib
CAM-DR	Cell adhesion mediated drug resistance
CARD11	Caspase Recruitment Domain 11
CBM	CARD11-BCL10-MALT1 complex
CC-292	Spebrutinib
CD (5, 19, 20, 10, 23, 40)	Cluster of differentiation proteins
CD40-L	CD40-ligand
CD40L-NT	CD40-ligand-non-transfected (murine stroma)
CD40L-T	CD40-ligand-transfected (murine stroma)
cDNA	Complementary DNA
CFLAR	CASP8 and FADD-like apoptosis regulator
ChIP	Chromatin immunoprecipitation
CHOP	Cyclophosphamide, doxorubicin, vincristine, and prednisone
cIAP	Cellular inhibitor of apoptosis
CLL	Chronic lymphocytic leukaemia
CR	Complete response
CSR	Class switch recombination
Cys (481)	Cysteine 481
DAPI	4’,6-diamidino-2-phenylindole
DECP	Diethyl pyrocarbonate
DLBCL	Diffuse large B-cell lymphoma
DMSO	Dimethyl-sulfoxide
DNA	Deoxyribonucleic acid
DSMZ	Deutsche Sammlung von Mikroorganismen & Zellkulturen GmbH
EBV	Epstein Barr virus
ECL	Enhanced chemiluminescence
EDTA	Ethylenediaminetetraacetic acid
EDTA 4Na	EDTA tetrasodium salt, tetrahydrate
EGFR	Epidermal growth factor receptor
EICE	ETS/Interferon consensus element
ELK1	ETS Like-1 protein
ERK1/2	Extracellular Signal-Regulated Kinases 1 and 2
ETOH	Ethanol
ETS	E-twenty-six

FACS	Fluorescence-activated cell sorting
FBS	Fetal bovine serum
FDA	US Federal Drug Administration
FDC	Follicular dendritic cell
FITC	Fluorescein isothiocyanate
FN	Fibronectin
FSC	Forward scatter
FTH	Follicular T helper cell
G519	Granta-519
GC	Germinal centre
GCB DLBCL	Germinal centre B cell diffuse large B cell lymphoma
GDP	Gaunosine diphosphate
GEF	Gaunine exchange factor
GS/ONO-4059	Tirabrutinib
GTP	Gaunosine triphosphate
Gy	Gray
HCL	Hydrochloric acid
HL	Hodgkin lymphoma
HRP	Horseradish peroxidase
Ibr	Ibrutinib
IC50	Half maximal inhibitory concentration
Ig	Immunoglobulin
IGH	Immunoglobulin gene heavy-chain
IGHV	Immunoglobulin gene heavy-chain variable gene
IκB	Inhibitory kappa B
IKK	Inhibitory kappa B kinase
IL1	Interleukin-1
Ion PGM	Ion personal genome machine
IP	Immunoprecipitation
IRF	Interferon regulatory factor
IRF4	Interferon regulatory factor 4
JAK3	Janus kinase 3
JNK	c-jun NH2-terminal kinase
LB	Laemmli buffer
LIMD1	LIM domain-containing protein 1

LINAC	Linear accelerator
LPD	Lymphoproliferative disorder
LS buffer	Low stringency lysis buffer
LYN	Lck/Yes novel tyrosine kinase
ISRE	Interferon stimulated response element
MAPK	Mitogen-activated protein kinases
MAX	MYC associated factor X
MCL	Mantle cell lymphoma
MCL-1	Myeloid cell leukemia sequence 1
MFI	Median fluorescence intensity
MFIR	Median fluorescence intensity ratio
mg	Milligrams
β-ME	β-mercaptoethanol
mRNA	Messenger RNA
MSC	Mesenchymal stromal cells
mTOR	Mammalian target of rapamycin
MV	Megavolts
MZL	Marginal zone lymphoma
Na deoxycholate	Sodium deoxycholate
NCBI	National centre for biotechnology information
NEMO	NF-κB essential modulator
NF-kB	Nuclear factor kappa B
NFAT	Nuclear factor of activated T cells
NGS	Next generation sequencing
NHL	Non-Hodgkin lymphoma
NIK	NFκB inducing kinase
nM	Nanomolar
NTC	Non template control
NT-CD40L	Murine fibroblast cell line not transfected with CD40L
ORR	Overall response rate
PAX5	Paired box -5
PBMC	Peripheral blood mononuclear cell
PBS	Phosphate buffered saline
pBTK	Phosphorylated BTK
PCR	Polymerase chain reaction

PE	Phycoerythrin
pERK	Phosphorylated ERK1/2
PEST	Proline, glutamic acid, serine, and threonine
PFA	Paraformaldehyde
PFS	Progression free survival
PH	Pleckstrin homology
PI	Propidium iodide
PI3K	Phosphoinositide 3-kinase
PLCy2	Phospholipase C gamma (y) 2
pM	Picomolar
PS	Phosphatidylserine
PR	Partial response
PU.1	ETS-domain transcription factor
PUMA	BCL2 binding component 3
PVDF	Polyvinylidene fluoride
qPCR	Real-time quantitative PCR
RAS	Rapidly accelerated fibrosarcoma
RB	Retinoblastoma
rcf	Relative centrifugal force
RIPA buffer	Radio immunoprecipitation assay buffer
RNA	Ribonucleic acid
RPM	Revolutions per minute
RPMI	Roswell Park Memorial Institute
R/R	Relapsed/Refractory
R-CHOP	CHOP chemotherapy + Rituximab
SDS	Sodium dodecyl sulfate
SDS-PAGE	Sodium dodecyl sulphate polyacrylamide gel electrophoresis
SEM	Standard Error of the Mean
SH (2,3)	Src homology 2 and 3
SHM	Somatic hypermutation
SNP	Single nucleotide polymorphism
SOS	Son of sevenless
SRC	Non receptor tyrosine kinases
SSC	Side-scatter
STAT3	Signal transducer and activator of transcription 3

SYK	Spleen tyrosine kinase
TEC	Tyrosine protein kinase
TEMED	N,N,N',N'-tetramethylethylenediamine
Tyr (Y)	Tyrosine
TK	Tyrosine kinase
TBE	Tris-borate-EDTA
TBS	Tris buffered saline
TBST	Tris buffered saline with 0.1 % TWEEN 20
TLR	Toll like receptor
TNF	Tumour necrosis factor
TRAF	TNF receptor-associated factor
Tris	Tris(hydroxymethyl)aminomethane
V	Volts
VCAM-1	Vascular cell adhesion protein 1
V(D)J	Variable diversity joining region
VH CDR3	Stereotyped heavy complementarity-determining region 3
VLA4	Very late antigen -4
WM	Waldenstrom's Macroglobulinaemia
XLA	X-linked agammaglobulinaemia
Y223	(pBTK) tyrosine 223
µg	Micrograms
µl	Microlitres
µM	Micromolar
~	Approximately

DEDICATION

In memory of my grandfather,

TREVOR WILLIAM THOMPSON

Chapter 1- Introduction

1.1 Mantle cell lymphoma

Mantle cell lymphoma (MCL) is currently classified by the World Health Organisation (WHO) as a mature B-cell neoplasm which represents up to 10% of all cases of Non-Hodgkin's Lymphoma (NHL).[1,2] The incidence of MCL is approximately 1 in 100,000 in Europe and the USA[3] and is marginally higher among Caucasians (~0.6 in 100,000) than among black and Asian populations (~0.3 in 100,000).[4] MCL can develop at a young age, but diagnosis of the disease is more common in elderly individuals with a median age of 65 years,[5] and the frequency of males diagnosed is greater than that of females (3:1 ratio, respectively).[2,6]

The majority of MCL patients (75%) are diagnosed at a late clinical stage (stage III-IV) with an aggressive form of MCL, characterised by progressive nodal disease indicated by widespread dissemination of MCL cells to the lymph nodes (>90%), bone-marrow (70-80%), spleen (60%), liver (30%), peripheral blood (30%) and gastrointestinal tract (lymphomatous polyposis) (20-30%).[1,7,8] Patients with aggressive MCL have the worst long term survival of all NHL subtypes with a median overall survival of 3-5 years and require immediate treatment.[8-10]

However, a minority of MCL patients display a more indolent form of the disease, characterised by a non-nodal leukaemic presentation with only bone marrow involvement and an enlarged spleen.[11,12] These indolent cases are less common but have a progression free survival ranging from 7 to 10 years in the absence of treatment.[8,13,14]

1.1.1 The biological characteristics of mantle cell lymphoma

MCL is a heterogeneous disease and has several different phenotypes. However, the characteristic hallmark of MCL and the primary oncogenic mechanism in the development of MCL, is the t(11; 14) (q13; q32) translocation which occurs at the pre-B stage of differentiation, during recombination of the V(D)J genes of the immunoglobulin heavy chain variable region (IGHV) in the bone marrow.[15,16] This translocation event joins the IGHV enhancer-promotor on chromosome 14 (14q32), to the transcription unit of the proto-oncogene *CCND1* on chromosome 11 (11q13) which encodes the protein cyclin D1.

Cyclin D1 is a key regulator of the G1/S transition of the cell cycle.[17,18] In normal B-cells, cyclin D1 is transiently expressed and binds to cyclin dependant kinase (CDK)4 and CDK6 to form a CDK/cyclin complex which phosphorylates the tumour suppressor retinoblastoma (*RB1*) gene. This leads to activation of E2F transcription factors which promote cyclin E/CDK2 activation to trigger entry into the S phase of the cell cycle.[1,17] In MCL, cyclin D1 is overexpressed which enables cells to bypass these cell cycle control mechanisms and leads to uncontrolled cell proliferation.[19]

Although the t(11; 14) (q13; q32) translocation is found in the majority of MCL cases, a small number of cases lack cyclin D1 overexpression and instead overexpress cyclin D2 or D3.[20,21] In addition, the translocation exists in blood cells in approximately 2% of healthy individuals.[1,22] This suggests that deregulation via *CCND1* and cyclin D1 overexpression is not the only cause for MCL development.

MCL has a high degree of genomic instability. Several genomic aberrations are frequently observed in MCL which can increase cyclin D1 expression and are thought

to contribute to disease progression. Some of these include mutations in *ATM* and *TP53* genes [23] causing alterations in DNA damage response, mutations in epigenetic modifiers including MLL2, MLL3 and SMARCA4,[24] mutations in *NOTCH1/2* [25] causing deregulated Notch signalling, and mutations in TNF receptor-associated factor 2 (*TRAF2)* and Baculoviral IAP Repeat Containing 3 *(BIRC3)* which affect the NFκB signalling pathway.[26,27]

1.1.2 Cell of origin of mantle cell lymphoma

MCL cells proliferate in the mantle zone, surrounding germinal centres (GC) within lymphoid follicles.[28,29] However, the cell of origin of MCL remains a topic of debate. In most cases, the MCL cells express an un-mutated (germ line configuration) *IGHV* gene indicating a pre B-cell (antigen-naïve) origin. However *IGHV* somatic hyper-mutations have been reported in 15 - 40% of MCL cases [30-32] which indicate a GC B-cell (antigen-exposed) origin. In around 10% of these cases, stereotyped heavy complementarity-determining region 3 (VH CDR3) sequences have been detected which has indicated that the development of MCL cells can be driven by antigen selection.[16,30]

1.1.3 Immunophenotype of mantle cell lymphoma cells

MCL cells have a unique immunophenotype which can be determined by the cluster of differentiation (CD) proteins they express on their surface. These markers assist in identifying their stage in B cell development, and can be useful for differentiating MCL from other cell types and from other lymphomas with similar cell morphology. MCL cells reflect the phenotype of a mature B-cell with a moderate to strong expression of surface immunoglobulins IgM and IgD (mainly lambda).[8,33] MCL cells also express the pan B-cell antigens including CD19, CD20 and CD22 and the T-cell and chronic lymphocytic leukaemia (CLL)-associated antigen CD5.[34] However MCL cells do not

normally express CD10 (a GC associated antigen), or CD23 (a cell surface molecule for B-cell activation and growth).[8] The absence of CD23 is particularly useful for identifying chronic lymphocytic leukaemia (CLL) cells which strongly express CD23.[35,36] Occasionally, some MCL cells have expression of CD10 and CD23 [37] which pinpoints a later stage in B-cell development and therefore suggests a different subtype of NHL however the cells still display features that are characteristic of MCL.

1.1.4 Histological subtypes of mantle cell lymphoma

There are three different histologic patterns of MCL including mantle zone, nodular, and diffuse which correspond to different stages in the progression of the disease.[38] The majority of aggressive MCL cases show a diffuse pattern, while indolent MCL cases show a growth pattern restricted to the mantle zone, thus it is thought that the behavior of indolent cells may correspond to early stages in the development of aggressive MCL.[16]

Four cytological variants have also been described including classical small-cell, blastoid, pleomorphic and marginal zone-like.[1,39-41] The classical small-cell variant is the most common but the blastoid and pleomorphic variants have a higher Ki67 proliferation index and are generally more aggressive.[8]

1.1.5 Treatment of mantle cell lymphoma

Conventional treatment for newly diagnosed patients is a combination chemotherapy regime which is tailed to the age and co-morbidities of the patient. For those patients not suitable for autologous stem cell transplant then an anthracycline-based chemotherapy regime incorporating rituximab, a chimeric monoclonal antibody (mAb) which specifically targets the CD20 protein expressed on B-cells (R-CHOP;

cyclophosphamide, doxorubicin, vincristine and prednisone) can achieve remissions in 60-90% of patients.[42] However, for most of these patients the remission period is only temporary and is followed by relapse (return of disease and symptoms), while other patients may be refractory (not responding) to treatment. The median overall survival after relapse is between 1 and 2 years.[43] More intensive cytarabine based regimes followed by an autologous transplant in complete remission offers better long term outcomes but is usually only an option for younger MCL patients without comorbidity who can tolerate the toxicities associated with these intense chemotherapy regimens.[44]

Other agents which have been explored in the treatment of patients with MCL include bortezomib, lenalidomide and temsirolimus. Bortezomib is a reversible proteasome inhibitor which induces cell cycle arrest and apoptosis in MCL cells.[45] In initial clinical trials, bortezamib demonstrated overall response rates (ORR) of 32% as a single agent in relapsed and refractory MCL, increasing to 71% when given in combination with chemotherapy.[46] Lenalidomide and temsirolimus, have shown only moderate activity as single agents in relapsed and refractory MCL (ORR 35% and 22%, respectively).[47,48]

Within the last decade, there has been a fundamental change in the management of patients with MCL with the development of Bruton's tyrosine kinase (BTK) inhibitors (BTKi). This will be discussed in more detail in later sections and although these agents have improved treatment outcomes in MCL, they are not effective in all patients, and those who do respond eventually develop acquired resistance and suffer relapse of the disease. Therefore there is a continued need for drug development for patients with MCL.

1.2 Mantle cell lymphoma and the tissue microenvironment

The tissue microenvironment is an important component in the development of many forms of cancer[49-51] and has been implicated in the pathogenesis and drug resistance of several haematological malignancies, including MCL.[52-54]

In addition to the intrinsic pathways that lead to the development and progression of MCL, there is growing evidence to suggest that interactions between MCL cells and accessory cells in the tissue microenvironment lead to disease progression.[55,56] While the majority of MCL cells can be eliminated by conventional treatments, a minority of lymphoma cells reside in protective tissue niches (residual disease), where they receive signals from accessory cells that promote lymphoma cell survival, growth and drug-resistance which lead to relapses.[57]

1.2.1 Cellular interactions in the tissues; the role of CD40L

The cellular components which make up the MCL microenvironment are found within the primary lymphoid organs (bone-marrow) and secondary lymphoid tissue (lymph nodes, spleen and mucosa-associated lymphoid tissues). Collectively, these include T cells, macrophages, follicular dendritic cells (FDCs) and mesenchymal stromal cells (MSCs).[55]

An important interaction within the MCL microenvironment involves Follicular T helper cells (FTH). In normal B-cell maturation, FTH cells are required along with B-cells to produce a series of signals in order for the adaptive immune system to elicit a response to antigen.

The first of these signals involves engagement of the FTH cell receptor with various antigens. These can either be peptides that are presented on the surface of antigen

presenting cells (APCs) in the context of the major histocompatibility complex II (MHC II), or unprocessed innate antigens binding to a cognate B-cell receptor (BCR).[58]

The second step involves co-stimulatory signals between activated FTH cells and either APCs or B cells. One essential signal is produced by the CD40 Ligand (CD40L) (also known as CD154) expressed on activated FTH cells when it engages with the CD40 receptor expressed on B-cells and APCs.[59]

The CD40L is a type II transmembrane protein of the tumour necrosis factor (TNF) superfamily. Although primarily expressed by activated T-cells and B-cells, CD40L can also be expressed on dendritic cells, granulocytes, macrophages and platelets.[60-62] CD40L may be cleaved into a soluble form (sCD40L) that has a cytokine-like activity. Both forms bind to several receptors, including CD40.[60]

Engagement of CD40L to CD40 stimulates the formation of germinal centres (GC) and is critical for B cell proliferation, differentiation, antibody class switch recombination and affinity maturation. These processes are essential for the generation of memory B cells and long-lived plasma cells**.**

During B cell differentiation within the GC (Figure 1.1), somatic hyper-mutation takes place to allow maturing B-cells to diversify the variable region of their surface immunoglobulin; through the addition of mutations in the V(D)J regions of both the heavy and light chains. This produces antibodies with high antigen affinity BCRs.[63]

GC B-cells expressing BCRs with high affinities for antigen are selectively engaged by FTH cells and receive CD40 survival signals through their BCR, whereas GC B-cells expressing BCRs with weak affinities for antigen do not receive sufficient CD40 survival signals and are deleted via the extrinsic Fas-dependent apoptosis pathway.[59]

The CD40 signal is transduced through the ligand-dependent recruitment of adaptor proteins of the TNF receptor-associated factor (TRAF) family. This leads to activation of proximal protein kinases and subsequent activation of survival pathways (described in section 1.2.3) including the mitogen activated protein kinase (MAPK) pathway, the phosphatidylinositol 3-kinase (PI3K) cascade and the nuclear factor kappa-light-chain enhancer of activated B cells (NF-κB) pathways. Stimulation of these pathways leads to transcription of pro-survival proteins including the B-cell lymphoma-2 (BCL2) proteins (described in section 1.2.3) which protects the cell from apoptosis.[59,64,65]

The observation from our group and others[53,63-67] that *ex vivo* primary MCL cells undergo spontaneous apoptosis *in vitro* suggests that they depend on these signals within the *in vivo* environment for their survival.

Established *In vitro* models have been described in the literature [53,64-67] which exploit various interactions within the tissue microenvironment and can be used to facilitate survival of primary cells in culture and to explore drug resistance pathways in MCL.

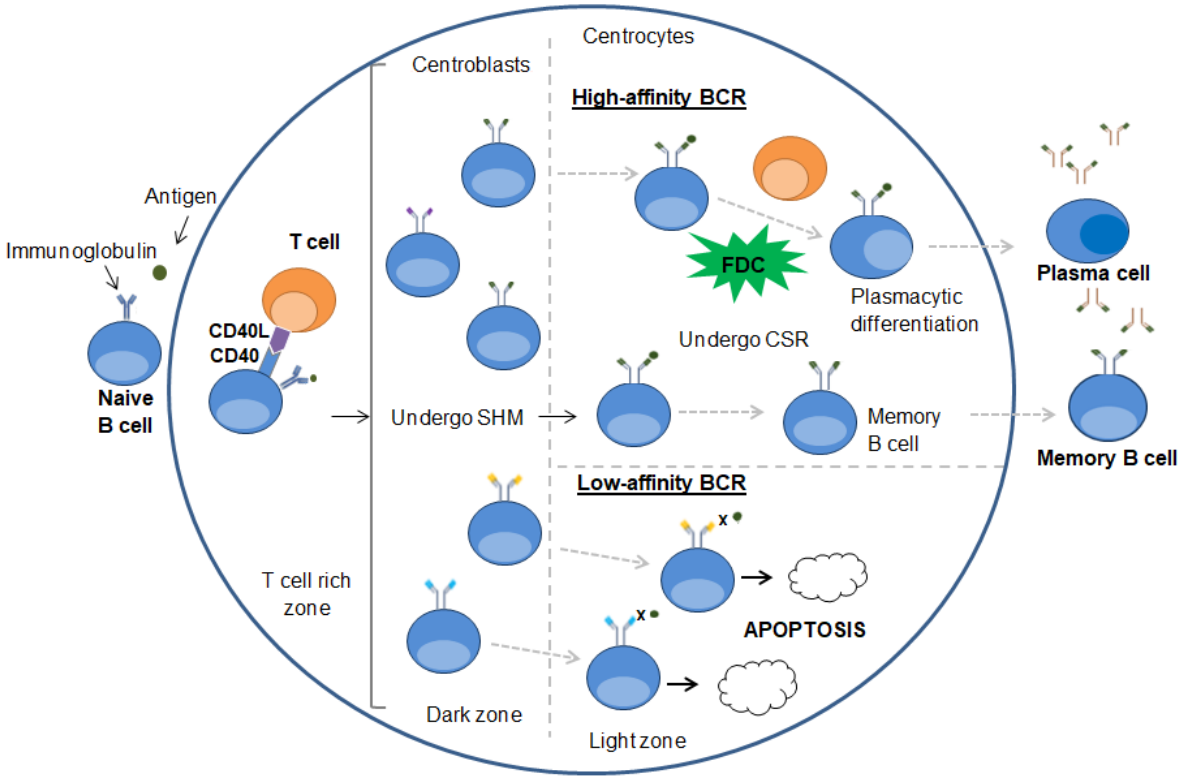

Figure 1.1: B cell differentiation and survival through the germinal centre. After encountering an antigen, naïve B cells are activated by their CD40L/CD40 interactions in the T cell rich zone of the lymph node, and the germinal centre reaction is initiated. B cells proliferate rapidly as centroblasts in the dark zone of the lymph node. These cells undergo somatic hypermutation (SHM) to diversify the heavy and light chain regions of their surface immunoglobulins. In the light zone, proliferation is reduced and some of these centrocytes undergo class switch recombination (CSR) of their immunoglobulin isotype. Interactions with follicular dendritic cells and T cells select the cells with highest antigen affinity. These cells then differentiate into plasma cells or memory B cells. B-cells with a low-affinity BCR undergo apoptosis. (Figure adapted from Marr 2016 [68]).

1.2.2 Chemokines, adhesion and migration

MCL cells have a high propensity for dissemination and homing to different tissue compartments. The movement and homing of B lymphocytes is a regulated process during which the cells are attracted and retained in the tissues in response to chemokine gradients produced by mesenchymal stromal cells (MSCs) such as fibroblasts and associated macrophages. This is dependent on the responsiveness of chemokine receptors and the expression of various adhesion molecules on the MCL cell.[52]

MCL cells express high levels of surface adhesion markers, such as the C-X-C motif chemokines CXCR4 and CXCR5, and the very late antigen 4 (VLA-4/CD49d), which are thought to be important for retaining the cells in their tissue microenvironment, and also integrin β1-containing receptors (α4β1 and α5β1) which are major mediators of cell adhesion to stroma.[65] It is thought that the high expression of these receptors facilitates cell adhesion mediated drug resistance (CAM-DR) in MCL which may be responsible for characteristic relapses observed in MCL and the reason for the incurability of patients following chemotherapy.[52,65]

Several studies are focusing on disrupting these homing and adhesion interactions by blocking external micro environmental signals.[69,70] One study has demonstrated that inhibition of VLA-4 and CXCR4 adhesion increases sensitivity to chemotherapy in MCL cell lines.[70]

1.2.3 BCR signalling and downstream survival pathways

The major signalling pathway in B-cell activity is the BCR pathway (Figure 1.2). The BCR is linked to downstream pathways which regulate the growth, differentiation and survival of normal B cells. BCR signalling pathways are critically involved in the progression of mantle cell lymphoma and thus components of the BCR signalling pathway are molecular targets for therapeutic approaches.[73]

Important proteins required for B-cell signalling and activation are non-receptor tyrosine kinases. The BCR is composed of a membrane immunoglobulin (in most cases this is IgM) non-covalently bonded to a heterodimer composed of CD79a and CD79b. These molecules have cytoplasmic domains that contain Immunoreceptor Tyrosine-based Activation Motifs (ITAMs) Igα and Igβ.[71] When a specific antigen binds to a BCR, the tyrosine residues of the ITAMs are phosphorylated by SRC family kinases including LCK/YES novel tyrosine kinase (LYN), and spleen tyrosine kinase (SYK).[72,73] The phosphorylation results in recruitment of many kinases and adaptor proteins, including LYN, SYK, PI3K, BTK, the guanine exchange factor VAV proteins, the growth factor receptor-bound protein 2 (GRB2) and the B-cell linker (BLNK).[74]

Following recruitment of LYN and SYK to the phosphorylated ITAM of the BCR, BLNK is recruited to the non-ITAM portion of CD79a and is rapidly phosphorylated by SYK. Activated BLNK then recruits BTK for phosphorylation by SYK.[75] This enables BTK to phosphorylate its direct substrate phospholipase C gamma (γ) 2 (PLCγ2), which hydrolyses phosphatidylinositol 4,5-bisphosphate (PIP2) into inositol 1,4,5-trisphosphate (IP_3) and diacylglycerol (DAG).[76] This event leads to calcium (Ca+2) mobilisation by IP_3, and activation of protein kinase C (PKC) by DAG[77,78]. The influx of calcium directly activates a number of transcription factors, including NF-κB, and

activator protein 1 (AP-1) which regulate important genes required for cell proliferation and survival, and nuclear factor of activated T cells (NFAT) which regulates cytokine production and other effectors of the immune response[74].

In addition to calcium influx, the β isoform of PKC (PKCβ) can lead to activation of NF-κB by phosphorylating the caspase recruitment domain-containing protein (CARMA1) which activates the CARD11-BCL10-MALT1 (CBM) complex. The CBM activates NFκB which translocates to the nucleus to regulate transcription of NFAT and the myelocytomatosis viral oncogene homolog (c-MYC).[83,84] In normal B cells, MYC activates transcriptional programs that favour cell growth and proliferation, and suppresses programs that cause cell growth arrest.[79]

Activation of PKCβ also leads to activation of the MAPK pathway. The MAPK pathway includes the extracellular signal-regulated kinase 1/2 (ERK1/2) which is constitutively active in MCL [88,89] and therefore represents an additional target for investigation in this thesis.

The MAPK pathway can also be activated via the PLC-γ2 signal which is transduced to the rapidly accelerated fibrosarcoma (RAS) protein through VAV and GRB2, which complexes with the son of sevenless (SOS) protein.[80] These proteins which are recruited by BLNK after BCR ligation activate RAS in the form of RAS-gaunosine triphosphate (GTP). RAS-GTP then binds to the serine/threonine kinases B-RAF and C-RAF. Stimulated RAF kinases phosphorylate and activate mitogen-activated protein kinase kinase (MEK1/2), which results in the phosphorylation of ERK1/2. Phosphorylated ERK1/2 kinases form dimers, which can then be translocated into the nucleus to regulate genes such as c-MYC and the transcriptional activator ETS Like-1 protein (ELK1).[81] The MAPK pathway regulates several other transcription factors

including AP-1 and the activating transcription factor 2 (ATF2) through c-Jun N-terminal kinase (JNK), and the MYC associated factor X (MAX) through p38 MAPK, leading to proliferation and survival or apoptosis [74,82].

There is an increasing body of evidence implicating deregulated BCR signalling in the pathogenesis and progression of several lymphomas, including MCL.[81] In a phospho-proteomic analysis of MCL cell lines, the most abundant phosphorylated peptides identified were those generated following BCR activation, including SYK, LYN, BTK, and PKC. Inhibition of key molecules of these pathways caused apoptosis in MCL cells *in vitro* [81]. As mentioned, BTK is an essential protein linked to important BCR survival pathways in MCL and has a critical role in the amplification of the BCR signal. Inhibition of BTK has produced profound effects in the treatment of MCL patients (discussed in detail in section 1.3).

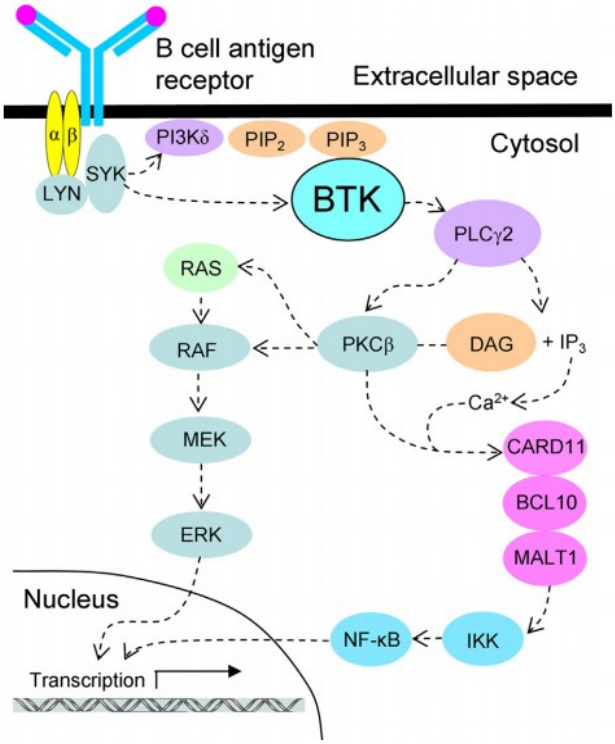

B-cell activation/ proliferation/differentiation /survival

Figure 1.2: The key BCR signalling pathways involved in the progression of mantle cell lymphoma. BTK is an essential protein linked to important BCR survival pathways in MCL. The dashed arrows indicate that several steps may be involved in the activation of each component shown (Figure adapted from Roskoski 2016.[81] Permission to reproduce this figure was granted by Elsevier).

As mentioned above, NFkB transcription factors can be activated by several BCR signalling components to regulate the growth and survival of B-cells. The NF-κB family has five monomers: RelA (p65), RelB, c-Rel, p50/p105 (NF-kB1) and p52/p100 (NF-kB2), which homo or hetero dimerise to form up to 15 different NF-κB complexes to regulate expression of growth factors, cytokines, chemokines, adhesion molecules, and apoptosis inhibitors.

The two primary pathways for NF-κB activation are the canonical and non-canonical pathways (Figure 1.3) and these pathways are frequently deregulated in MCL [83].

The canonical pathway is triggered by toll-like receptors (TLRs) and pro-inflammatory cytokines such as tumour necrosis factor alpha (TNFα) and interleukin-1 (IL-1), which initiate inflammatory responses, immune regulation, and cell proliferation.

The non-canonical pathway is activated by TNF family cytokines, including lymphotoxin β (TNFSF3), CD40L and B cell-activating factor (BAFF), which promotes B cell maturation and lymphoid organogenesis.

The common regulatory step in both of these cascades is activation of an inhibitory kappa B (IκB) kinase (IKK) complex consisting of catalytic kinase subunits (IKKα and/or IKKβ) and the regulatory non-enzymatic scaffold protein NEMO (NF-κB essential modulator also known as IKKγ).

The NF-κB dimers are activated by IKK-mediated phosphorylation of IκB, which triggers proteasomal IκB degradation. This enables the active NF-κB transcription factor subunits to translocate to the nucleus and induce target gene expression.

Stimulation of the canonical pathway by TLR leads to the recruitment of adaptors (such as TRAF) to the cytoplasmic domain of the receptor. These adaptors in turn recruit the

IKK complex, which leads to phosphorylation and degradation of the IκB inhibitor resulting in nuclear translocation of NF-κB dimers, predominantly the NF-κB heterodimer RelA/p50.

Activation of canonical NFkB signalling by BCR also leads to nuclear translocation of RelA/p50 but occurs via an alternative pathway, involving activation of BTK, PKC and the CBM complex which leads to the activation of the IKK complex.

The non-canonical pathway involves an IKK complex that contains two IKKα subunits, but not NEMO. Under non-stimulation, TNF associated factor proteins (TRAF) 2 and TRAF3 form a complex with cellular inhibitor of apoptosis 1 and 2 (cIAP 1 and cIAP 2) and the NFκB inducing kinase (NIK). Stimulation by TNF family cytokines such as CD40L destabilises the complex and releases NIK which phosphorylates and activates the IKKα complex leading to phosphorylation of the p52 precursor p100, and the persistent activation of the RelB/p52 heterodimer.

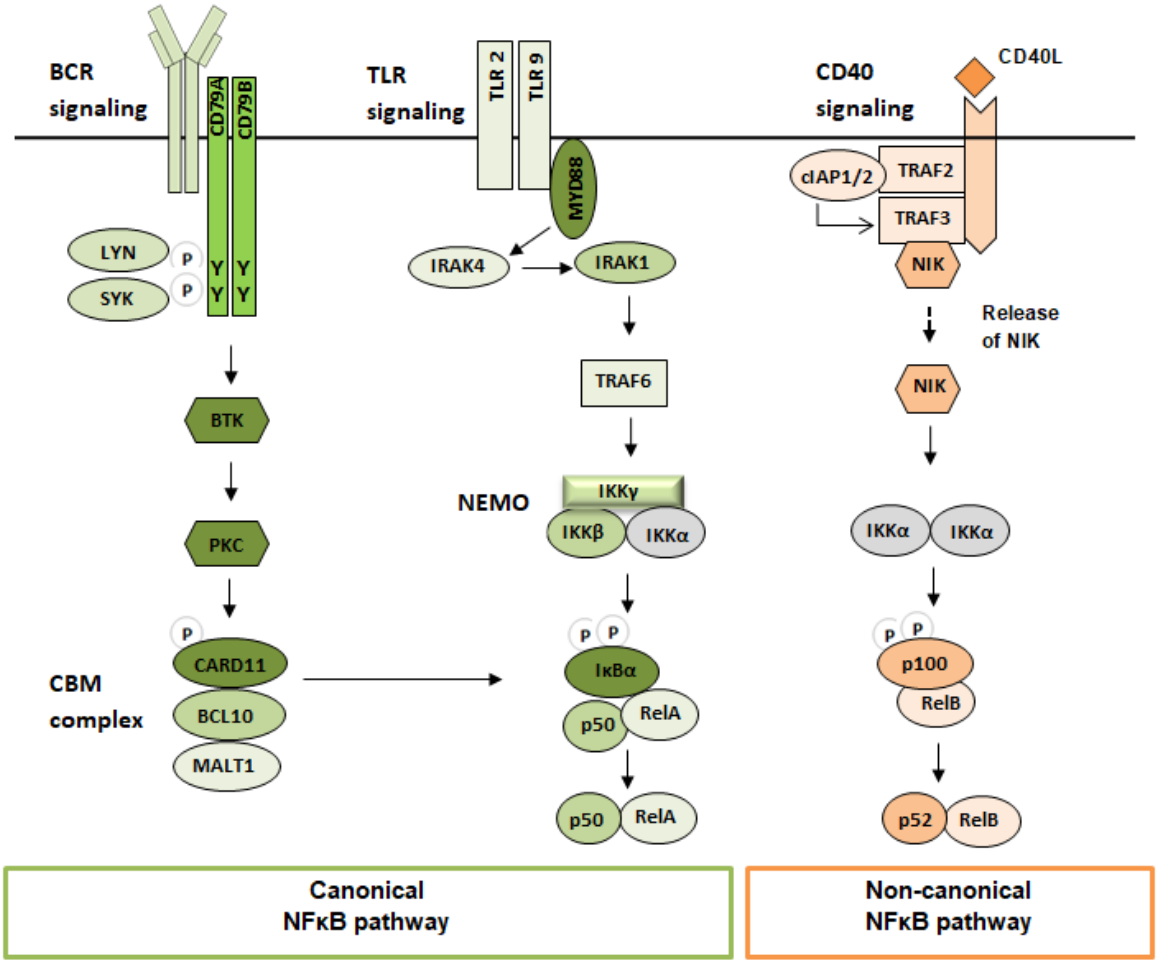

Figure 1.3: The canonical and non-canonical NF-kB signalling pathways. In the canonical pathway, ligand binding to a receptor leads to the recruitment and activation of an IKK complex comprising IKK alpha and/or IKK beta catalytic subunits and two molecules of NEMO. The IKK complex then phosphorylates IκB leading to proteasomal degradation. NF-κB then translocates to the nucleus to activate target genes. Non-canonical NF-kB activation involves phosphorylation and processing of the p52 precursor p100 into the mature protein and subsequent nuclear translocation of the RelB/p52 heterodimer to the nucleus to activate target genes. Chronic active BCR (A) or Toll-like receptor (TLR) (B) signalling activate the canonical NF-kB pathway. CD40 signalling (C) activates the non-canonical NF-kB pathway (Figure adapted from Colomer & Campo 2014.[83] Permission to reproduce this figure was granted by Elsevier).

Important targets of NF-κB signalling include the BCL2 protein family which are the key regulatory proteins governing the intrinsic pathway of mitochondrial apoptosis[84].

The group of pro-apoptotic proteins includes BCL2-associated X protein (BAX), BCL2 antagonist/killer 1 (BAK), BCL2-associated agonist of cell death (BAD), BCL2-like 11 (BIM), BCL2 binding component 3 (PUMA) and NOXA which all promote cell death.

The group of anti-apoptotic proteins to which BCL2 belongs also includes B-cell lymphoma-extra large (BCL-XL), the myeloid cell leukemia sequence 1 (MCL-1), BCL2-like 2 (BCL-W) and the BCL2-related protein A1 (BFL-1), which all promote cell survival.

As mentioned in section 1.2.1, levels of the BCL2 proteins increase in response to CD40 stimulation which is important for the survival of mature B cells. CD40 signalling stimulates the non-canonical NFκB pathway leading to activation of RelB/p52 which induces expression of BCL2, BCL-XL and MCL-1 (Figure 1.4). In the absence of CD40 stimulation, the cIAP1/2 complex degrades NIK which inhibits further signalling through the non-canonical NFkb pathway and promotes B cell apoptosis.

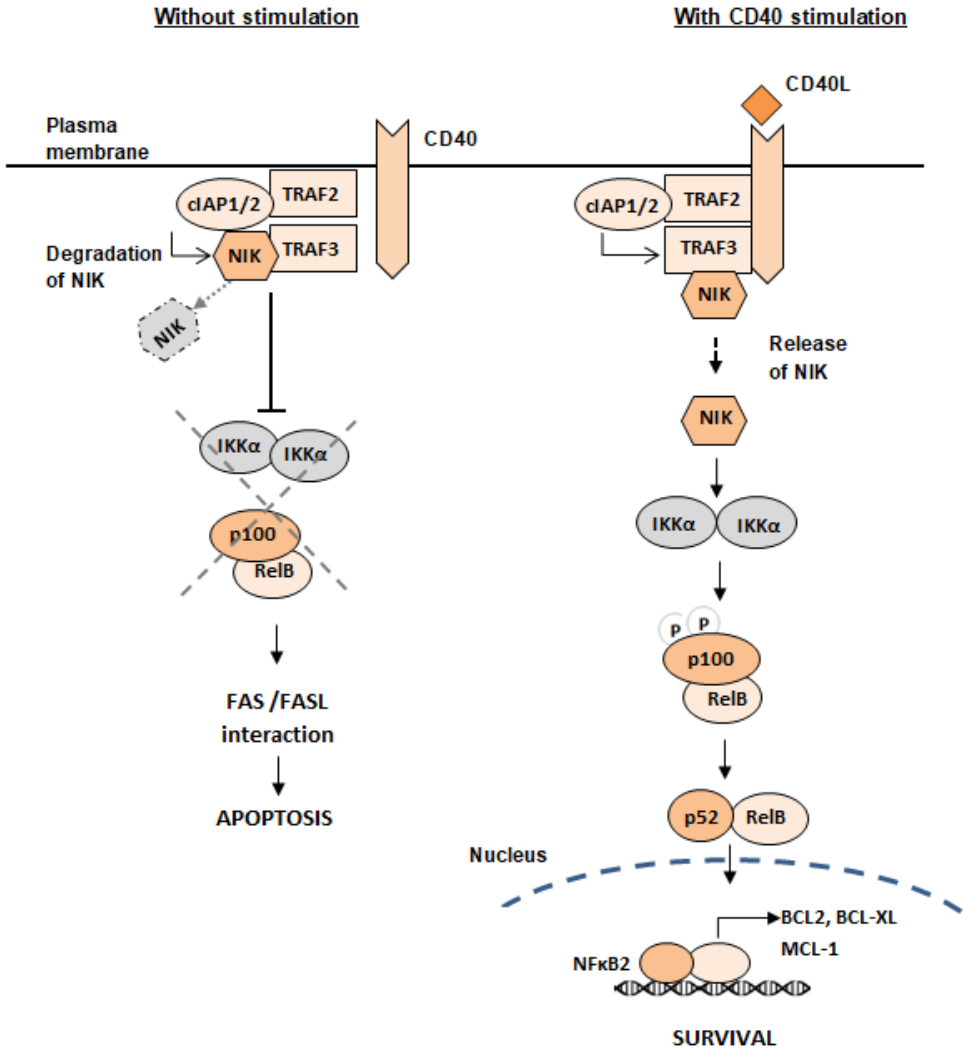

Figure 1.4: Survival of B cells in the presence and absence of CD40 signalling through the non canonical NFkB pathway. Under non-stimulation, TRAF 2 and TRAF3 form a complex with cIAP 1 and cIAP 2 and NIK. In the absence of CD40 stimulation, the cIAP1/2 complex degrades NIK which inhibits further signalling through the non-canonical NFkb pathway and promotes B cell apoptosis. In the presence of CD40 stimulation, the complex is destabilised, permitting the release of NIK from the complex and continued signalling through the non-canonical NFκB pathway. The non-canonical NF-κB pathway targets activation of the p52/RelB NF-κB complex via processing of p100. Nuclear translocation of the p52/RelB dimer activates transcription of anti-apoptotic BCL2 family proteins thereby promoting survival (Figure adapted from Elgueta *et al* 2009 [59] and Braun *et al* 2006 [85]).

In normal B cells, the balance of anti- and pro-apoptotic BCL2 proteins protects cells in response to cellular stress, but also induces death in damaged cells. Cancer cells can manipulate this system by skewing the balance toward anti-apoptotic proteins, thereby facilitating prolonged tumour-cell survival.[86]

BCL2 proteins are overexpressed in several B cell malignancies including MCL.[86-88] In a tissue microarray of 62 MCL samples,[89] BCL2 expression positively correlated with expression of BTK, which as mentioned, is an essential component of the BCR signalling complex. BTK (discussed in detail in section 1.3) upregulated BCL2 transcription through the canonical NF-κB pathway. In addition, the high BCL2 levels were thought to result from a defect in protein degradation due to a deficiency of FBXO10 (the E3 ubiquitin ligase which targets BCL2 for proteasomal degradation).[90]

It has also been indicated that the high BCL2 levels in MCL may be due to mutations in the tumour suppressor protein TP53 which lies directly upstream from BCL2 and causes resistance to chemotherapy.[86]

Several agents which specifically target BCL2 have been explored in B cell malignancies, including ABT-199 (Venetoclax). However, resistance to BCL2 inhibitors has been observed in CLL and MCL patients, and in CLL has been linked to modulation of BCL2 proteins by the tumour microenvironment, particularly in response to CD40 signalling.[88,91,92] Venetoclax is currently being evaluated in combination with BTK inhibitors for the treatment of CLL and MCL.[93,94]

1.3 BTK and BTK inhibitors

1.3.1 BTK

BTK (MW: 76 KDa) belongs to the TEC family of non-receptor tyrosine kinases and is expressed in most haematopoietic cells of both lymphoid and myeloid lineages, with the exception of T-cells and plasma cells.[95] BTK is constitutively expressed from the early stages of B-cell maturation until the stage prior to terminally differentiated plasma cells.[96]

The *BTK* gene is situated on the long (q) arm of the X chromosome at the g21.1-22 locus and encodes a 659 amino acid protein.[97] The structure of BTK is characterised by five domains, similar to that of other TEC family members (ITK, BMX, TXK and TEC). Starting at the N-terminus, these include PH (pleckstrin homology) and BH (TEC homology) domains, followed by SH3 (Src homology 3) and SH2 (Src homology 2) domains, and end with a tyrosine kinase (TK) domain at the C-terminus [98,99] (Figure 1.5). Amino acid 481 in the adenosine triphosphate (ATP) binding cleft of the kinase domain is a cysteine residue (Cys481) and is crucial for the activity of BTK inhibitors [81] (described later).

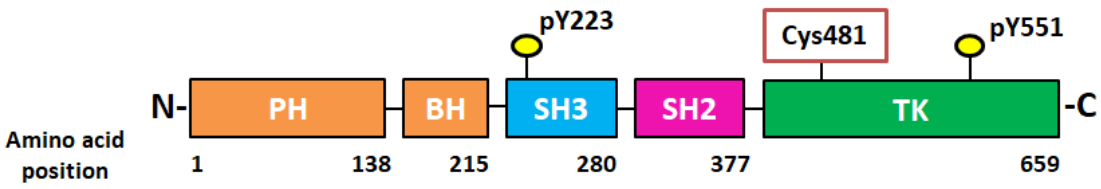

Figure 1.5: BTK protein structure. BTK is a 659 amino acid protein which has five structural domains. From the N-terminus: PH (pleckstrin homology), BH (TEC homology), SH3 (Src homology 3), SH2 (Src homology 2), TK (tyrosine kinase). The BTK phosphorylation site pY223 is located in the SH3 domain and the pY551 site in the TK domain. A crucial cysteine residue (Cys481) is located in the TK domain (Figure adapted from Hutchinson and Dyer 2014 [98]).

The *BTK* gene was identified in 1993, during which time a loss of function mutation was discovered and found to be responsible for the production of the defective protein which leads to human X-linked agammaglobulinemia (XLA).[100,101] This immunodeficiency syndrome was originally identified in 1952 by an American Navy paediatrician, Colonel Ogden Carr Bruton, who observed a condition in a group of young boys characterised by recurrent bacterial infections and caused by an absence of mature B lymphocytes and failure of immunoglobulin production.[102] Consequently, the gene was named after Dr Bruton, in recognition of his initial work. These studies demonstrated that BTK was an essential protein tyrosine kinase required for B-cell maturation and thus a key protein in BCR signalling events.

BTK is located downstream of the BCR, predominantly in the cytoplasm (but also in the nucleus), and translocates to the plasma membrane via the PH domain for phosphorylation and activation. There are two main tyrosine phosphorylation sites within BTK. Phosphorylation of tyrosine (Y) 551 within the kinase domain regulates the transition between active and inactive states and occurs on localisation to the membrane by LYN and SYK kinase.[103] A conformational change in the protein then enables auto-phosphorylation at Y223 in the SH3 domain[98] and subsequent activation of PLCy2 which as mentioned, activates pathways for survival, proliferation and migration. In addition, BTK stimulates actin polymerization at the cell cortex, leading to a reconfiguration of the actin cytoskeleton required for BCR aggregation.[80,104]

In addition to its involvement in BCR signalling pathways, BTK is also involved in co-stimulatory pathways involving chemokine receptor binding and TLR signalling. BTK is activated by chemokine binding to CXCR4 and CXCR5 via interactions with G-protein sub-units of the chemokine receptors.[98,105] The ligands for these receptors are tissue

homing chemokines CXCL12 and CXCL13 (respectively) thus it is believed that BTK has a role in B-cell migration and homing. In addition, BTK regulates integrin-mediated interaction of tumour cells with the microenvironment and has a role in the secretion of chemokine ligands (CCL) CCL3 and CCL4 by MCL cells.[106]

1.3.2 First in class BTK inhibitor - Ibrutinib

Ibrutinib (previously known as PCI-32765) was among a panel of small molecule BTKi initially synthesised by Celera Genomics to study BTK function, and was later developed by Pharmacyclics.[107] The ibrutinib compound demonstrated the most favourable activity in animal models of autoimmune disease and arthritis and was therefore selected over the alternative compounds for use in further pre-clinical studies and subsequent clinical trials.[108]

Ibrutinib (trade name: Imbruvica), is an irreversible, small molecule inhibitor of BTK with a half maximal inhibitory concentration (IC50) of 0.5nM. The drug is an oral tablet administered once daily at an optimal dose of 560 mg in MCL. The irreversibility of the drug is attributed to an electrophilic group, which binds covalently to the cystine (Cys) 481 region within the catalytic ATP binding site of the BTK kinase domain[107] which prevents its auto-phosphorylation at Y223 and downstream cascade of signals.[109] The existence of a cysteine residue in the catalytic site is uncommon and therefore enhances specificity of ibrutinib to BTK and other TEC kinases.[97] Several other BTKi have been developed which bind to BTK at the same cysteine residue but with even more selectively, one of these is acalabrutinib (discussed later). Figure 1.6 shows the binding of acalabrutinib to the ATP binding pocket of BTK.[110]

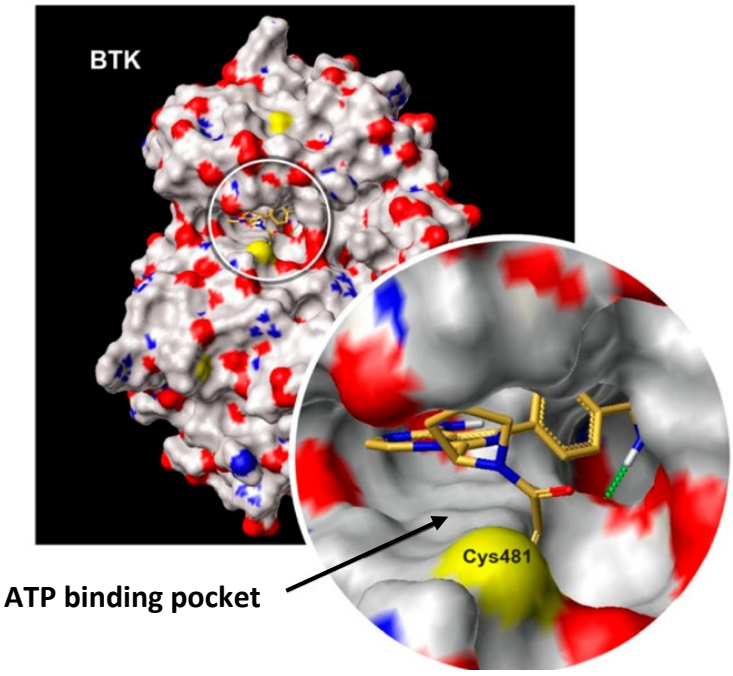

Figure 1.6: Binding model of acalabrutinib (gold) in the ATP binding pocket of BTK. Figure adapted from Barf *et al* 2017.[110]

1.3.3 Pre-clinical studies with ibrutinib

The therapeutic potential of BTK inhibition for treating lymphoma was first demonstrated by its effects on malignant cell lines and primary cells *in vitro.*

In CLL cell lines, ibrutinib inhibited BCR signalling proteins ERK, PI3K and NF-κB which reduced the survival of CLL cells and inhibited CD40, BAFF, TLR and cytokine signalling.[111] Ibrutinib was also found to inhibit DNA replication, and block pro-survival pathways in CLL cells by downregulating CCL3 and CCL4 expression.[112] Furthermore, ibrutinib disrupted integrin α4β1-mediated adhesion of CLL cells to stromal elements such as fibronectin and Vascular cell adhesion protein 1 (VCAM1) and reduced migration of primary cells to tissue homing chemokines CXCL12, CXCL13 and CCL19.[113]

In MCL cell lines, ibrutinib increased apoptosis and reduced levels of anti-apoptotic proteins BCL-2, BCL-XL, and MCL-1.[114] In addition, knockdown of BTK in MCL cells using siRNA (short interfering RNA) was shown to reduce phosphorylated levels of the signal transducer and activator of transcription 3 (STAT3) and inhibit the NF-κB pathway, which is required for MCL growth and migration.[115]

In a study by Honigberg *et al*,[109] ibrutinib selectively blocked BCR signalling and induced an objective clinical response of 38% in Canines with naturally occurring B-cell NHL. Shortly after this study, ibrutinib entered clinical trials.

1.3.4 Clinical studies with ibrutinib

The clinical efficacy of ibrutinib as a single agent was first reported in patients with various relapsed and refractory (R/R) B-cell malignancies. Despite the irreversibility of the drug, it did not cause any major side effects and demonstrated durable objective responses, particularly in CLL and MCL.[116] In a subsequent phase Ib/II trial, an overall response rate of approximately 71% was achieved in R/R CLL patients on continuous treatment with ibrutinib.

A phase II trial was then initiated in MCL (PCYC-1104), which enrolled 111 patients with R/R MCL who had received at least one prior therapy.[117] A total of 68% of MCL patients had a response to ibrutinib, of which 21% had a complete response (CR) and 47% a partial response (PR). Ibrutinib was also found to be highly active in previously treated patients with Waldenström's macroglobulinemia (WM).[118]

Due to its significant clinical activity and safety in these B-cell malignancies, ibrutinib received a breakthrough designation and accelerated approval by the US Food and Drug Administration (FDA) for the treatment of R/R MCL in November 2013, for CLL in

July 2014 and for WM in January 2015. Ibrutinib has since been approved in Europe for R/R MCL and CLL and for other indications including previously untreated CLL with the del(17p13.1) karyotype, and for patients with untreated WM.

However not all lymphoma subtypes have achieved high response rates following ibrutunib treatment. For example, in R/R Follicular lymphoma (FL), 37.5% of patients responded to ibrutinib and 12.5% had a complete response.[116] In R/R Marginal zone lymphoma (MZL), approximately 50% of patients have responded to ibrutinib.[119] In R/R Diffuse large B-cell lymphoma (DLBCL), complete or partial responses of 37% have been achieved in patients with the activated B-cell (ABC) subtype of DLBCL but responses of only 5% have been achieved in patients with the germinal centre B-cell (GCB) subtype.[120]

1.3.5 Therapeutic mode of action of ibrutinib

Despite the clinical success of ibrutinib, its mechanisms of action are still not entirely understood. It is currently unknown why this class of drug has such a profound effect in certain B cell lymphoproliferative disorders, particularly in MCL where there is dependence on cyclin D1. However, a particular feature of ibrutinib treatment is that a peripheral lymphocytosis is observed which is accompanied by a rapid reduction in lymph node size and represents the migration of neoplastic cells from tissues to blood.[117]

A peripheral lymphocytosis is observed in most MCL patients responding to ibrutinib, and increases by more than 50% from baseline in 34% of cases. The lymphocytosis peaks at a median of 4 weeks and falls to near baseline level after approximately 3 months.[117] This effect is also seen in CLL patients treated with ibrutinib where a lymphocytosis is seen in approximately 80% of cases and takes longer to resolve.[121]

These observations have suggested that there is a similar mechanism of action of BTKi on adhesion and migration of the neoplastic lymphocytes in patients with CLL and MCL.

Another feature of ibrutinib therapy is the absence of tumour lysis. Tumour lysis syndrome is commonly observed following conventional treatment when large numbers of tumour cells die rapidly causing metabolic disturbances.[122] The absence of tumour lysis suggests that apoptosis or inhibition of survival is not a primary mechanism of ibrutinib action.

The findings from pre-clinical studies (section 1.3.3) suggest that ibrutinib may have more than one mechanism of action, whereby it acts to inhibit intrinsic B-cell signalling pathways resulting in reduced proliferation and survival, and also disrupts the extrinsic interactions necessary for homing and retention of malignant cells to the tissues.

It has also been suggested that the outcome of ibrutinib treatment may result from the combined inhibition of BTK and other kinases, acting in synergy. Ibrutinib has a broad kinome which includes irreversible inhibition of several other kinases with a corresponding cysteine residue in the ATP binding site.[123] Analysis of 491 kinase sequences revealed 9 additional kinases with a cysteine at position 481. These include four other TEC-family kinases (ITK, BMX, TEC, TXK), three epidermal growth factor receptor (EGFR) family kinases (EGFR, ErbB2/HER2 and ErbB4/HER4), and two other kinases (B lymphoid tyrosine kinase (BLK) and Janus Kinase 3 (JAK3)). In addition, ibrutinib binds strongly to SRC family kinases.[109,110,121]

It is thought that this broad specificity could be the cause of off-target side effects observed in MCL such as bleeding, arthralgia, atrial fibrillation and diarrhoea.[124] For

example, diarrhoea is also seen in patients treated with EGFR inhibitors [125] and therefore might be caused by off target inhibition of EGFR by ibrutinib.

1.3.6 Second generation BTK inhibitors

Due to the broad specificity of ibrutinib for BTK and its multiple modes of action, several second generation BTKi have been developed which have enhanced selectivity for BTK. These include acalabrutinib (ACP-196), tirabrutinib (GS/ONO-4059) and zanubrutinib (BGB-3111) which are currently being evaluated for the treatment of several B-cell malignancies. Table 1.1 summarises the data of completed trials in MCL, showing the response rates achieved in MCL patients following single agent treatment with several second generation BTKi compared with response rates achieved by ibrutinib as a single agent and in combination with rituximab.

The furthest second generation BTKi in development is acalabrutinib (trade name CALQUENCE®) (formally known as ACP-196). Acalabrutinib is an irreversible BTKi which like ibrutinib, forms a covalent bond with cysteine 481 in the BTK kinase domain. In comparison to ibrutinib, it has higher selectivity for BTK as determined in a competition binding assay on a panel of 456 human kinases.[110] The improved selectivity is thought to be due to the reduced intrinsic reactivity of acalabrutinib's propiolamide electrophile compared to ibrutinib's acrylamide electrophile which causes fewer off-target interactions with other kinases such as ITK, EGFR, ERBB2/4, JAK3, LYN, and SRC.[110,126]

In the competition binding assay, acalabrutinib inhibited BTK at a higher concentration than ibrutinib (IC50 of 5.1 and 1.5nmol/L, respectively), however the IC50 against other kinases was much greater.[110] The figure below (Figure 1.7) shows the chemical

structures and kinome scan images for acalabrutinib and ibrutinib and compares their binding affinities to all kinases which contain a cysteine residue at position 481 in BTK.

The first pre-clinical study of acalabrutinib in canine models of NHL demonstrated enhanced *in vivo* potency compared to ibrutinib.[127]

In a phase II study (ACE-LY-004), acalabrutinib was given to 124 patients with R/R MCL who had received 1 to 5 prior lines of therapy. The drug achieved an ORR of 82% and CR of 40%. At a median follow-up of 12 months, 72% of patients remained in response.[128] As a result of this trial, acalabrutinib was granted accelerated approval by the FDA in October 2017 for the treatment of MCL patients whose disease has progressed after receiving at least one prior therapy.

Since acalabrutinib has a shorter half-life, it is taken twice a day at a dosage of 100 mg in MCL. It is believed that this dosing improves BTK inactivation since BTK synthesis in malignant lymphocytes may be faster than the 24 hour dosing interval of ibrutinib [128]

Therapeutic regimen	Patient population	Phase	Efficacy	Reference
Ibrutinib (PCI-32765)	R/R MCL	Phase II	ORR (68%), CR (21%)	Wang *et al* [117]
Ibrutinib (PCI-32765)	R/R MCL	Phase III	ORR (72%), CR (19%)	Dreyling *et al* [129]
Ibrutinib (PCI-32765) + Rituximab	R/R MCL	Phase II	ORR (88%), CR (44%), PR (44%)	Wang *et al* [130]
Acalabrutinib (ACP-196)	R/R MCL	Phase II	ORR (81%), CR (40%), PR (41%)	Wang *et al* [128]
Tirabrutinib (GS/ONO-4059)	R/R MCL	Phase I	ORR (92%)	Walter *et al* [124]
Zanubrutinib (BGB-3111)	R/R MCL	Phase Ib	ORR (88%)	Tam *et al* [131]

Table 1.1: Results of completed clinical trials evaluating the efficacy of several BTK inhibitors as single agents in MCL. *R/R* Relapsed or refractory, *MCL* Mantle cell lymphoma, *ORR* overall response rate, *CR* complete response, *PR* partial response.[132]

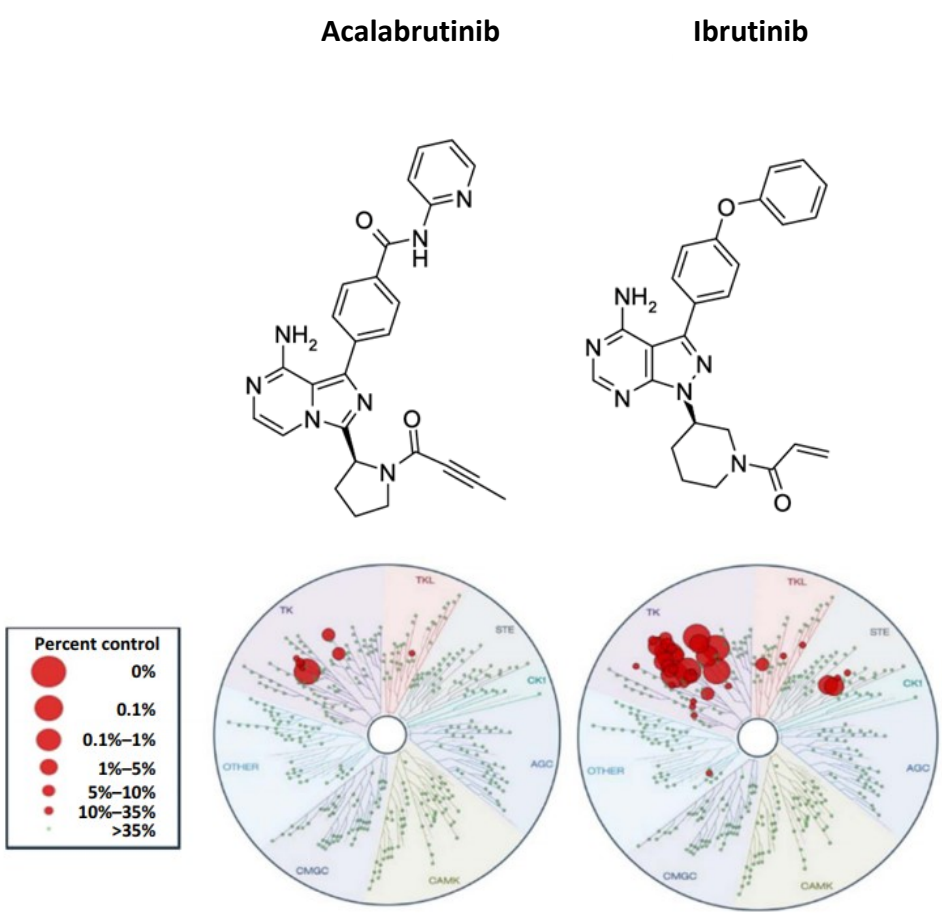

	IC50 (nM)	
Kinase	**Acalabrutinib**	**Ibrutinib**
BTK	5.1	1.5
BMX	46	0.8
ITK	>1000	4.9
TEC	93	7.0
TXK	368	2.0
EGFR	>1000	5.3
ERBB2	~1000	6.4
ERBB4	16	3.4
JAK3	>1000	32
BLK	>1000	0.1

Figure 1.7: Chemical structures and kinase inhibition of acalabrutinib and ibrutinib. Recombinant enzymes were used to profile the *in vitro* activity of acalabrutinib compared with ibrutinib. Each BTK inhibitor was profiled at 1mM in a competition binding assay on a panel of 456 human kinases (using KINOMEscan at DiscoverX, Fremont, CA). The size of the circles represents intervals of the percentage of remaining activity versus the untreated control. The table shows the IC50s for the kinases that contain a cysteine residue aligning with cysteine 481 in BTK. IC50 denotes half-maximal inhibitory concentration (Figure adapted from Barf *et al* 2017[110] and Herman *et al* 2017[133]).

In addition to using BTKi as single agents for treating MCL, various combinations are also being explored incorporating BTKi and other targeted therapies into standard chemo immunotherapy regimens.

Currently, there are 20 ongoing clinical trials evaluating the efficacy of BTKi in MCL (Table 1.2). These include either single agent BTKi, or BTKi in combination with other agents (including monoclonal antibodies and/or chemotherapy) in previously treated as well as untreated MCL.

Some combinations have already been shown to be beneficial for improving treatment outcomes. For example, the response rate of ibrutinib as a single agent in the phase II trial was 68%, however in combination with rituximab, the ORR increased to 88%. When both agents were combined with bendamustine the ORR in 12 MCL patients was 94% and 76% had a complete remission. However results from these trials are on-going and will help to determine optimal treatment combinations for patients with MCL.

	Therapeutic regimen	Patient population	Phase	Identifier
1	Novel BTK inhibitor (BGB-3111)	R/R MCL	Phase II	NCT03206970
2	Novel BTK inhibitor (M7583)	R/R MCL	Phase II	NCT02825836
3	Novel BTK inhibitor (CT-1530)	R/R NHL (including MCL)	Phase II	NCT02981745
4	Novel BTK inhibitor (AC0010)	R/R NHL (including MCL)	Phase I	NCT03060850
5	Novel BTK inhibitor (CC-292) + Lenolidamide	R/R NHL (mixed cohort)	Phase Ib	NCT01766583
6	Acalabrutinib/ Bendamustine/ Rituximab	Previously untreated MCL	Phase III	NCT02972840
7	Ibrutinib (long-term)	B cell lymphoma (including MCL)	Phase II	NCT01109069
8	Ibrutinib after induction therapy	Previously untreated MCL	Phase II	NCT02242097
9	Ibrutinib and Obinutuzumab	R/R MCL	Phase II	NCT02736617
10	Ibrutinib and Carfilzomib	R/R MCL	Phase I/II	NCT02269085
11	Ibrutinib and Palbociclib	R/R MCL	Phase I	NCT02159755
12	Ibrutinib and Lenolidamide	R/R NHL (including MCL)	Phase I	NCT01955499
13	Ibrutinib and Pembrolizumab	R/R NHL (including MCL)	Phase I	NCT02950220
14	Ibrutinib and Selinexor	Aggressive NHL (including MCL)	Phase I	NCT02303392
15	Ibrutinib and Pevonedistat	R/R NHL (including MCL)	Phase I	NCT03479268
16	Ibrutinib and Cirmtuzumab	Cirmtuzumab treated MCL	Phase II	NCT03088878
17	Ibrutinib/ Bendamustine/ Rituximab	Relapsed MCL or Indolent NHL	Phase I	NCT01479842
18	Ibrutinib/ Bendamustine/ Rituximab	Newly diagnosed MCL	Phase III	NCT01776840
19	Ibrutinib and Lenalidomide / Rituximab	R/R MCL	Phase I	NCT02446236
20	Ibrutinib, Avelumab, Utomilumab, Rituximab and Combination Chemotherapy	R/R MCL	Phase I	NCT03440567

Table 1.2: On-going clinical trials evaluating BTK inhibitors (as single agents and in combination therapy) in MCL. *BTK* Bruton's tyrosine kinase, *R/R* Relapsed or refractory, *MCL* Mantle cell lymphoma, *NHL* Non-Hodgkins Lymphoma.[134]

1.3.7 Primary and acquired resistance to BTK inhibitors

Despite the success of BTKi, approximately 30% of MCL patients display primary resistance to these agents and patients who initially respond eventually develop acquired BTKi resistance and aggressive relapse of the disease. About 25% of patients discontinue ibrutinib therapy after 20 months due to progression.[135] The 1 year survival rate for those who experience disease progression after ibrutinib treatment is only 22%.[103] Current available therapies for patients who have relapsed on BTKi treatment are often not effective which therefore indicates the need to discover biomarkers of BTKi resistance so that agents which target specific resistance mechanisms can be developed to overcome them.

Nearly 700 unique mutations have been detected in the *BTK* gene which cause XLA[136] although none of these leads to its constitutive activity in MCL. However, several mutations have been identified in patients who have relapsed following BTKi therapy. These mutations can either affect BTK directly, or it's downstream signalling components including PLCγ2. The first mutation identified was a point mutation causing a protein substitution (cysteine to serine) at the ibrutinib binding site (C481S) resulting in ineffective BTK inhibition due to loss of covalent binding.[137] The C481S mutation has been observed following BTKi therapy with both ibrutinib and acalabrutinib,[121,137-141] and results in chronic activation of downstream BTK and mammalian target of rapamycin (mTOR) / Protein kinase B (AKT) pathways.

In R/R CLL patients with this mutation, the activity of BTK was restored even in the presence of ibrutinib, demonstrating reactivation of BCR signalling which enabled proliferation to proceed.[137]

The BTK C481S mutation has been characterised by many studies as the most common mechanism of ibrutinib resistance. In a study by Sharma *et al* [135] the C481S mutation showed 25-fold less sensitivity to ibrutinib than the wild type.

In another study, Chiron *et al* [138] identified C481S in 2 out 5 MCL patients who initially responded to ibrutinib but then progressed. The C481S mutation resulted in increased BTK and AKT activation which was driven by the cell cycle regulator CDK4. The mutation was only present in patients who had prolonged exposure to ibrutinib, and was not present in 6/6 patients with primary resistance, nor in patients who only partially responded to ibrutinib.

Other BTK mutations have been found in ibrutinib refractory cases of CLL including C481F/Y/R, T474I/S, and L528W.[135] These mutations all occur in the kinase domain of BTK and either directly attenuate (T474I/S) or hinder (L528W) ibrutinib binding.

There has also been one report of a mutation T316A located in the SH2 domain in a R/R CLL patient.[135] This mutation did not directly interfere with ibrutinib binding but prevented inhibition of CLL proliferation compared to the wild type cells.

Mutations in molecules other than BTK have been identified. A gain-of-function substitution (R665W) has been reported in PLCγ2 which produces a constitutively active enzyme, which no longer needs to be phosphorylated by BTK.[137] This mutation is thought to involve PI3K-AKT activation which overrides the inhibitory mechanism of BTK.

Thus far, *BTK* mutations have only been detected in patients exposed to ibrutinib. However it has been suggested that the mutations may be present in tiny clones prior

to therapy which undergo subsequent clonal selection and expansion with continued use of ibrutinib.[142,143]

Whole exome/transcriptome profiling of serial biopsies from the start of ibrutinib treatment until drug resistance in a patient with MCL, showed the evolution of the BTK C481S mutation.[138]

Chronic exposure to ibrutinib has been shown to result in kinome reprogramming and activation of the PI3K-AKT-mTOR pathway in MCL cells, causing acquired ibrutinib resistance.[144] However, some ibrutinib relapsed MCL and CLL patients do not have mutations in BTK or PLCy2 [135,138] which suggests that other mechanisms for ibrutinib resistance exist.

Primary resistance to ibrutinib in MCL is thought to involve PI3K-AKT activation since inhibition of ERK1/2 and AKT correlates with cellular response to BTK inhibition *in vitro.*[145]

In other *in vitro* experiments, proliferation of ibrutinib resistant MCL cell lines was found to be mediated through the alternative NF-κB pathway, via *TRAF2*, *TRAF3* and *BIRC3* mutations.[26,27]

In addition, as with conventional treatment, it is thought that interactions between MCL cells and accessory cells in the MCL microenvironment may be involved in resistance to BTKi. Amplified activation of the CXCR4-CXCL12 pathways have been detected in an MCL patient with ibrutinib resistance.[26]

These studies demonstrate the need to identify biomarkers which can predict response to treatment so that patients with primary BTKi resistance do not receive unnecessary exposure to a drug which has no effect, and so that patients who do

respond to BTKi can be offered alternative therapies before these BTK mutations fully evolve and result in relapse.

This thesis will particularly focus on the transcription factor Interferon Regulatory Factor 4 (IRF4) to determine whether this could represent a biomarker of BTK sensitivity or resistance in MCL.

1.4 Interferon regulatory factor 4 (IRF4)

IRF4 is implicated in the pathogenesis of several B-cell malignancies. Overexpression of IRF4 is seen in cases of ABC DLBCL and multiple myeloma (MM), both of which respond well to treatment which suppresses levels of IRF4. The role of IRF4 in the pathogenesis of MCL or in response to treatment (particularly with BTKi) is currently unknown and therefore represents an important area of investigation.

IRF4 (MW: 50 KDa) (also known as MUM1, LSIRF, Pip, NFEM5 and ICSAT) is one of nine members (in humans and mice) of the interferon regulatory factor (IRF) family of transcription factors and has critical functions in various cell types of the immune system including B cells, macrophages and DCs.[146]

Most IRF members are induced by type I and II interferons and cytokines in response to viral infections, however IRF4 is unique in that its expression is regulated by pathways of lymphocyte activation including BCR, LPS and CD40 signalling in response to various stimuli.[147] These stimuli all activate the Rel/NF-kB pathway, which leads to activation of the IRF4 promoter.[148,149]

1.4.1 Structure and function of IRF4 in normal B cells

IRF4 is a 450 amino acid protein which has an N-terminal DNA binding domain (DBD) and a C-terminal interferon activation domain (IAD) (separated by a flexible linker)

(Figure 1.8) through which it can form homo or hetero-dimers with other members of the IRF family and with other proteins to activate transcription of its target genes.[150] At the C terminal, there is an auto regulatory (AR) domain comprising an auto inhibitory region which interacts with the DBD to maintain the protein in an inactive state.[151] The DBD is highly homologous to other IRF members due to the presence of five tryptophan sequences repeated at 10-18 amino acid intervals.[150] Here, homo-or hetero-dimers formed between IRF4 and other IRF family members (predominantly IRF8) bind DNA with low affinity at Interferon-Stimulated Response Elements (ISREs 5'-GAAANNGAAA-3').[150,152]

In addition to its interaction with other IRFs, IRF4 can also form heterodimers with members of the E-twenty-six (ETS) family, or the activator protein-1 (AP-1) family of transcription factors.[153-156]

In B-cells, the principal co-binding partners for IRF4 are the ETS family members PU.1 and SPI-B, which are critical for B-cell development and maturation. Hetero-dimers formed between IRF4 and PU.1 bind at ETS Interferon Composite Elements (EICEs: 5'-GGAANNGAAA-3')[157] in the IAD. ETS proteins contain a sequence rich in proline, glutamic acid, serine, and threonine (PEST). Interaction of the IAD with the PEST region of an ETS protein relieves the auto-inhibitory effect and allows IRF4 to bind its target sequence with much greater affinity.

Heterodimers formed by IRF4 and AP-1 family members such as the Basic leucine zipper transcription factor, ATF-like (BATF), regulate genes containing AP-1-IRF Composite Elements (AICEs: 5'-GAAATGAGTCA-3' or 5'-GAAANNNNTGAGTCA-3') [154-156] which are important for regulating cellular functions in DCs and T-cells particularly in response to CD40 signalling.

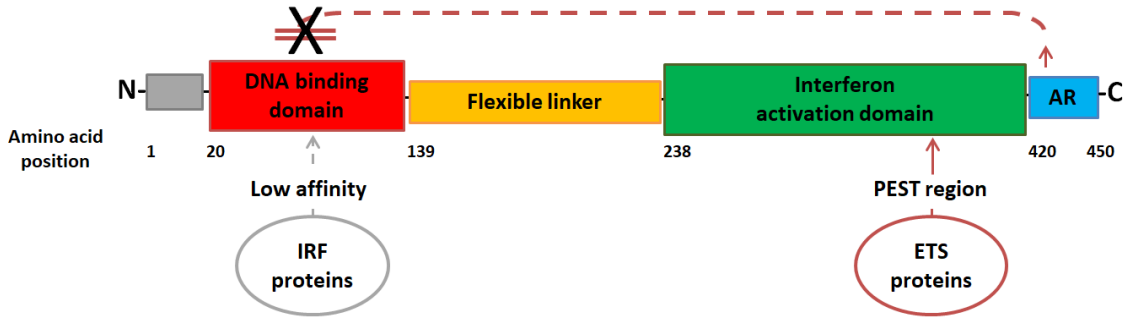

Figure 1.8: IRF4 protein structure. IRF4 is a 450 amino acid protein which has an N-terminal DNA binding domain (DBD) and a C-terminal interferon activation domain (IAD), separated by a flexible linker. An auto regulatory (AR) domain comprising an auto inhibitory region is located at the C terminal and maintains the protein in an inactive state. The DBD of IRF4 binds to other IRFs with low affinity. Interaction of the IAD with an ETS protein through its PEST domain, triggers the DBD to relieve the autoinhibition, allowing IRF4 to bind to its target with high affinity (Figure adapted from Marr 2016 [68]).

IRF4 controls important events during B-cell development and maturation by transducing signals from various receptors to either activate or repress gene expression.

During the early stages of B-cell development in the bone marrow, IRF4 interacts with its close family member IRF8 to coordinate the transition from the large pre B-cell to small pre B-cells.[150] These events are mediated by several transcription factors including the paired box 5 (PAX5), a B-cell lineage specific activator.[158] IRF4 and IRF8 are direct targets of PAX5 and function with PU.1 to regulate PAX5 expression by binding to an enhancer region in the PAX5 locus.[150]

At the pre-B cell stage, IRF4/8 and PU.1 regulate the rearrangement and expression of the immunoglobulin light chain by binding to the 3' κ enhancer and λ enhancer regions, where EICE motifs were first identified.[151,159,160]

Downstream to pre-B cell receptor signalling, IRF4 and IRF8 induce the expression of the transcription factors ikaros and aiolos which function as negative regulators of BCR signalling and cell cycle progression.[150] Ikaros and aiolos repress the expression of the surrogate light chain (SLC), an essential component of the pre-B cell receptor complex,[161] and also inhibit large pre-B cell expansion by directly binding and repressing MYC.[162]

IRF4 has been shown to regulate the expression of CXCR4 in pre-B cells by shifting pre-B cells towards CXCL12 expressing stromal cells and away from IL-7 secreting stromal cells.[163,164] IL-7 signalling inhibits pre-B cell differentiation by directly repressing light chain rearrangements.

In mature B-cells, IRF4 is involved in the initiation and termination of the GC reaction, and cooperates with IFR8 to control plasma cell differentiation and class-switch recombination (CSR).[165-168] At low levels, IRF4 binds cooperatively with ETS and AP-1 family members at EICE/AICE motifs and induces expression of BCL6, OCT-Binding Factor 1 (OBF1) and Activation-induced cytidine deaminase (AID) which are required in order to initiate the GC reaction. BCL6 is a master regulator for GC reaction, while AID is critical for somatic hyper-mutation to generate high avidity BCRs, and CSR. Mice lacking IRF4 specifically in B-cells failed to form GCs due to insufficient induction of BCL6, OBF1 and AID.[166]

Within the centrocytes of GCs, high levels of IRF4 are induced by antigen binding to high avidity BCRs. This causes a shift in the binding of IRF4 from EICE/AICE motifs, to binding low affinity ISRE motifs. IRF4 binding to ISRE induces the B lymphocyte-induced maturation protein-1 (BLIMP-1) and represses BCL6 which is required to end the GC reaction and to initiate plasma cell differentiation.[166]

IRF4 also has a role in the positioning of mature B lymphocytes within lymphoid microenvironments by its regulation of NOTCH2.[169]

1.4.2 IRF4 in B cell malignancies

Deregulation of the processes controlled by IRF4 has been linked to the pathogenesis of several types of B cell malignancies which correspond to specific developmental stages.[146,147,170,171] This has highlighted that IRF4 can function both as an oncogene as well as a tumour-suppressor in different lymphoma subtypes (Figure 1.9).

IRF4 has oncogenic roles in several GC and post-GC lymphomas, including Hodgkin lymphoma (thought to be derived from GC cells), the ABC subtype of DLBCL (thought to be derived from post GC cells), and multiple myeloma (MM) (a malignancy derived from plasma cells). On the other hand, IRF4 acts as a tumour suppressor in B cell acute lymphoblastic leukaemia (B-ALL) (derived from immature B cells) and in CLL (derived from quiescent mature B cells).[150]

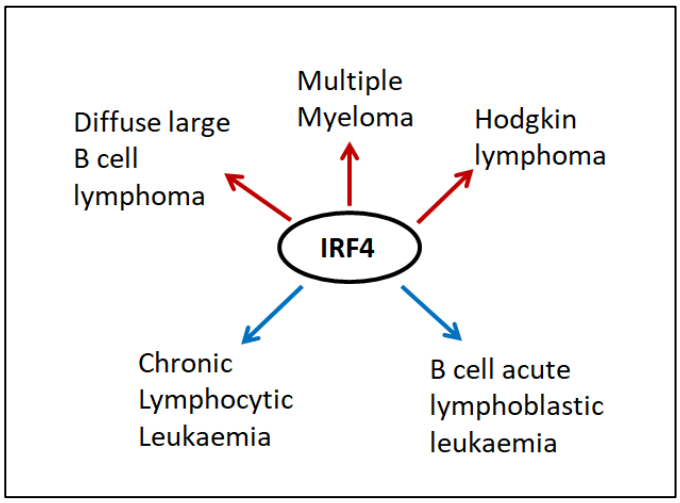

Figure 1.9: IRF4 in B cell malignancies. Red arrows point towards malignancies where IRF4 functions as an oncogene, blue arrows point towards malignancies where IRF4 functions as a tumour suppressor.

IRF4 overexpression is seen in cases of ABC DLBCL.[172] In DLBCL cell lines, IRF4 functions with ETS family member SPI-B to repress type I interferon responses.[173] Specifically, IRF4 and SPI-B co-bind to EICE motifs to suppress IRF7 causing subsequent inhibition of interferon β production and interferon response mediated cell death.[150,173]

The role of IRF4 in MM is unusual in that it directs plasma cell differentiation while it also functions as a survival factor for MM cells, a concept described as non-oncogene addiction.[147,171] Studies have identified *MYC* as a direct target of IRF4 in MM. Upregulation of IRF4 and *MYC* contributes to cell proliferation and aggressiveness but it is thought that *MYC* deregulation is the critical factor in the pathogenesis of MM, and IRF4 functions in part as a survival factor by directly regulating *MYC* expression.[171]

In CLL, higher IRF4 expression has been associated with better prognosis.[170] Single nucleotide polymorphisms (SNPs) have been identified in the 3' untranslated region (UTR) of the IRF4 locus[174] and are associated with increased susceptibility for developing CLL. The risk alleles harbouring the SNPs are linked to downregulation of IRF4 and are associated with poor prognosis.[174-176]

In NHL as a whole, IRF4 is associated with several genes including *BATF,* LIM domain-containing protein 1 (*LIMD1*)*,* CASP8 and FADD-like apoptosis regulator (*CFLAR*)*,* serine/threonine-protein kinase pim-2 (*PIM2*)*, and CCND2* which are involved in B-cell development, oncogenesis, cell cycle regulation, and cell death[157] However the molecular targets regulated by IRF4 specifically in MCL and in response to BTKi are unknown and require investigation.

1.4.3 Expression of IRF4 in mantle cell lymphoma

Little is known about the involvement of IRF4 in MCL. In a gene expression profiling study, *IRF4* was shown to be over expressed in MCL along with several other lymphoma subtypes[157] although this was only representative of 8 MCL cases.

The majority of MCL tumour biopsies are usually negative for IRF4 expression, however IRF4 was expressed in 35% of MCL tumour biopsies (45/ 127 cases) with a characteristic GC or post-GC phenotype.[149] As mentioned in section 1.1.2, MCL cells are derived mainly from antigen naïve pre GC B-cells, however up to 40% of MCL cases carry somatic mutations of the IGVH genes, indicative of a GC or post GC phenotype therefore IRF4 expression is likely to vary depending on the phenotypic subtype.

In a small number of cases, it has been demonstrated that MCL cell clones can undergo plasma cell differentiation.[177,178] A partial plasmacytic phenotype has been identified displaying stronger CD38 and IRF4 expression, identifying a biologically distinct subset of MCL.[179]

IRF4 is expressed to varying degrees in several MCL cell lines including REC-1, HBL2, JEKO-1 and MINO[179] and it has been demonstrated that REC-1 cells depend on IRF4 expression for survival.[179] IRF4 is also expressed in G519 and JVM2 cells[180] however it should be noted that these cell lines have been transformed into lymphoblastoid cell lines by Epstein Barr Virus (EBV). IRF4 expression can be regulated through modulation of NF-κB signalling by viral proteins such as EBV.[181]

1.4.4 IRF4 in response to treatment

The immunomodulatory agent lenolidamide has demonstrated clinical responses in lymphomas which are characterised by IRF4 overexpression, including MM and DLBCL.

In the ABC subtype of DLBCL, IRF4 and SPI-B transcription factors prevent interferon beta (IFNβ) production by repressing *IRF7* and amplify pro-survival NF-κB signalling by transactivating *CARD11*.[173] Lenalidomide kills ABC DLBCL cells by downregulating IRF4 and SPI-B, thereby increasing production of IFNβ and reducing the pro-survival effects of NF-κB signalling. Lenalidomide has also demonstrated clinical activity in R/R MCL as a single agent[117,182] which suggests involvement of IRF4 in aggressive relapse of MCL.

IRF4 has been proposed as a potential marker of bortezomib (BZM) resistance in MCL.[179] MCL cells from patients with poorer clinical responses to BZM showed high expression of IRF4 and *MYC*. Gene knockdown of *IRF4* repressed expression of *MYC in vivo*, and was toxic for the subset of MCL cells with plasmacytic differentiation.[180]

1.4.5 IRF4 in response to BTK inhibitors

A small number of studies have demonstrated downregulation of IRF4 in response to ibrutinib *in vitro*. Ibrutinib induced downregulation of IRF4 has been demonstrated in DLBCL and MCL *in vitro* [106,173,183] and has also been shown previously by our group in *ex vivo* primary CLL cells (unpublished data).

In MCL, Sun *et al* [183] showed that IRF4 was downregulated by ibrutinib in sensitive MCL cell lines and was rescued by a PKC agonist through reactivation of the NFkB pathway.

IRF4 has also been shown to be downregulated in MCL cell lines in response to a combination of the BTKi spebrutinib (CC-292) and lenolidamide.[106] In this study, the REC-1 cell line demonstrated enhanced sensitivity to both ibrutinib and CC-292 by inducing apoptosis, although only marginal apoptosis was induced by CC-292 (10-15%) after 72 hours treatment. Phosphorylated BTK Y223 was reduced in all cell lines (REC-1, MINO, UPN-1, MAVER-1 and Z138) regardless of their sensitivity to ibrutinib. However,

CC-292 downregulated the expression of the surrogate marker for NF-κB activation pIkB, only in MCL cell lines sensitive to CC-292. It has been described previously that lenolidamide (which directly targets NF-kB) downregulates IRF4 in sensitive cell lines [180] and this study demonstrated that co-treatment with CC-292 significantly enhanced this effect in REC-1 cells. These results are of particular note given the results we will describe in this thesis.

1.5 Summary of introduction and aims of thesis

General Background to approach

MCL is often an aggressive lymphoma that has very poor outcome for patients. BTK inhibitors have shown a significant clinical activity in patients with particular subtypes of NHL; importantly this includes patients with MCL. Research has shown that modifying the intracellular-signalling downstream of the BCR through inhibition of BTK alters the interaction between the neoplastic cells and their environment, with that there is an associated controlled regression of the MCL.[117] This allows patients with MCL to achieve a clinical remission. However, despite the promise of these agents in this difficult-to-treat disease, one third of MCL patients have primary resistance to BTKi, and most patients who initially respond eventually acquire secondary resistance with aggressive relapse of the disease.

Hypothesis

This clinical promise offered by BTKi provides an impetus for this project, it was hypothesised that study of relevant protein expression could identify processes that underlie sensitivity or resistance to BTKi in MCL, and that findings could be exploited to suggest new avenues for therapy as well as highlighting predictive biomarkers for treatment response that could be used to rationally direct therapy.

Selection of IRF4 as a candidate molecule and Aims of thesis

At the start of this PhD little was known about the mechanism(s) of action of BTK inhibitors in MCL, and importantly the mechanisms of BTKi resistance were unclear. However, preliminary work within this research group had suggested a protective role for the cellular microenvironment, and a potential role for IRF4 in mediating protection from the effects of BTKi. This provided the basis for the approach.

The Aims were:

1. To identify, characterise and develop cell line models of MCL that reproduced the relevant features of disease behaviour including responsiveness or resistance to two BTKi drugs used clinically to treat MCL.
2. To use these models to explore key elements of the biological response of MCL cells to BTKi with particular emphasis on the chemo-protective effects of the cellular microenvironment and on the potential role of IRF4.
3. To expand on these findings to look at possible mechanisms of those chemo-protective changes that were identified.
4. To confirm findings using primary MCL cells.

Chapter 2- Materials and Methods

2.1 Reagents and buffers

2.1.1 Buffers for cell culture

Culture media

RPMI 1640 growth media with GlutaMAX^{TM}, supplemented with 10% Fetal Bovine Serum (FBS) and 1% penicillin/ streptomycin (Gibco, Fisher Scientific).

Freezing media

90% FBS containing 10% dimethylsulphoxide (DMSO).

General wash buffer

1X phosphate buffered saline (PBS) (Fisher Scientific).

1 X Trypsin-EDTA

1X Trypsin- EDTA, diluted in 1X PBS from 10X liquid (0.5% Trypsin, 5.3mM EDTA 4Na) (Gibco, Fisher Scientific #10779413).

RIPA lysis buffer

20mM Tris, 150mM NaCl, 1mM EDTA, 1% Triton-X-100, with protease and phosphatase inhibitors (10µl/mL) (Sigma Aldrich #P8340/#P5726).

Low stringency lysis buffer:

1M Tris base pH8 (0.2mL), 3M NaCl, 10% Triton-X-100, MilliQ H_2O. Protease inhibitor (Sigma Aldrich #P8340) was added before use.

2.1.2 Buffers for flow cytometry

1X Annexin-V binding buffer

Diluted from 10X Annexin-V binding buffer (BD Biosciences).

Fixation buffer

Paraformaldehyde (PFA) diluted to 4% in 1X PBS

Permeablisation buffer

Triton X- 100 detergent diluted to 0.1% or 0.2% in 1X PBS

Staining buffer

0.5% Bovine serum albumin (BSA) diluted in 1X PBS containing 0.1% Triton-X-100.

2.1.3 Buffers for 1D SDS-PAGE, western blotting and immunohybridisation

10% (w/v) SDS

For 100mL: 10g SDS dissolved in 90mL deionised water (dH_2O).

10% (w/v) Ammonium pursulphate (APS)

For 1mL: 100mg APS dissolved in 900µl dH_2O. For 10mL: 1g APS dissolved in 9mL dH_2O.

1.5 M Tris-HCl, pH 8.8 (MW 121.14)

18.17g Tris base dissolved in 70mL dH_2O, and brought up to 100mL with dH_2O.

0.5 M Tris-HCl, pH 6.8 (MW 121.14)

6g Tris base dissolved in 60mL dH_2O, and brought up to 100mL with dH_2O.

10X Tris buffer

30.2g of 24mM Tris-HCL, 144g of 191mM Glycine, dissolved and brought up to 1000mL with dH_2O.

10X Tris buffered saline (TBS)

24.2g of Trizma base, 80.06g of Sodium chloride (NaCl) dissolved in 800mL of dH_2O.

Resolving gel (10% acrylamide)

1.5M Tris (pH 8.8), 10% (w/v) SDS, 10% APS, dH_2O, 30% acrylamide (National diagnostics ProtoGel EC-890, Fisher Scientific # 12381469), 10µl N,N,N',N'-tetramethylethylenediamine (TEMED) (Sigma Aldrich).

Stacking gel (4% acrylamide)

0.5M Tris (pH 6.8), 10% (w/v) SDS, 10% APS, dH_2O, 30% acrylamide, 6.7µl TEMED.

2X Laemmli sample buffer (SDS reducing)

0.5M Tris-HCL (pH 6.8), Glycerol, 10% (w/v) SDS, 0.5% (w/v) Bromophenol blue, dH_2O + β-mercaptoethanol (BME) at 5% of the sample volume added just before use.

1X Running buffer

24mM Tris, 191mM Glycine, 10% SDS.

1X Transfer buffer

24mM Tris, 191mM Glycine, 20% MeOH

Wash buffers

1 X TBS diluted from 10X TBS
1X TBST: 1 X TBS with 0.1% Tween-20.

Blocking buffer and antibody dilution buffer

5% BSA diluted in 1X TBST.

Immunoprecipitation (IP) buffer

1X PBST (1X PBS with 0.1% Tween-20)

2.1.4 Buffers for agarose gel electrophoresis

1X Tris Borate EDTA (TBE)

Diluted from 10X TBE (89mM Tris, 89mM boric acid, 2mM EDTA) (Thermo Fisher Scientific #B52).

DNA loading dye buffer

6X DNA loading dye buffer (10mM Tris-HCL (pH 7.6), 0.03% bromophenol blue, 0.03% xylene, 60% glycerol 60mM EDTA, (Thermo Fisher Scientific #R0611).

2.1.5 Buffers/reagents for chromatin immunoprecipitation

1X enzymatic lysis buffer A

(50µl of 4X Buffer A (CST #7006) + 750ul dH_2O)) + 0.5µl 1M Dithiothreitol (DTT) and 5µl of 200X protease inhibitor cocktail (PIC), per IP preparation.

1X enzymatic lysis buffer B

(275µl of 4X Buffer B (CST #7007) + 825ul dH_2O)) + 0.55µl 1M DTT, per IP preparation.

1X ChIP buffer

(10µl of 10X ChIP Buffer (CST #7008) + 90µl dH_2O)) + 0.5µl 200X PIC, per IP preparation.

Low salt wash

(300µl of 10X ChIP Buffer + 2.7mL dH_2O)

High salt wash

(100µl of 10X ChIP Buffer + 900µl dH_2O) + 70µl 5M NaCl (CST #7010)

1X ChIP elution buffer

(75µl 2X ChIP Elution Buffer (CST #7009) + 75µl dH_2O, per IP preparation.

Other reagents for ChIP

- 37% Formaldehyde (Fisher Scientific)
- 10X Glycine solution (CST #7005)
- Micrococcal nuclease (CST #10011)
- 0.5M EDTA (CST #7011)
- 5M NaCl (CST #7010
- RNAse A (10 mg/mL) (CST #7013)
- Proteinase K (20mg/mL) (CST #10012)
- ChIP-Grade Protein G magnetic beads (CST #9006)
- Human RPL30 Exon 3 Primers 1 (CST #7014)
- 1M DTT (192.8mg DTT (CST #7016) + 1.12mL dH_2O)

(All provided in the SimpleChIP® enzymatic chromatin IP kit, CST #9003) except for formaldehyde.

2.1.6 Buffers for DNA purification

DNA binding buffer

Containing chaotropic salts: guanadinium hydrochloride (Gu-HCl)/ sodium iodide (NaI).

DNA wash buffer

10mM Tris-HCl pH 7.5, 80% Ethanol (EtOH)

DNA elution buffer

10mM Tris pH 8-9

(All provided in the SimpleChIP® DNA Purification kit (CST #14209).

2.1.7 Buffers for RNA extraction

Buffer RLT

Denaturing buffer containing guanidine-thiocyanate. 10µl of β-ME was added per 1mL of buffer RLT.

Buffer RW1

Stringent wash buffer containing guanidine salt and EtOH.

Buffer RPE

Mild wash buffer supplied as concentrate and diluted in 4 volumes of EtOH (96–100%).

(All provided in the RNeasy Mini kit (Qiagen # 74104).

2.2 Cells and general culture

2.2.1 Cells and characterisation

Blood samples from MCL patients were obtained by the clinical research team at Derriford hospital (University Hospitals Plymouth NHS trust, UK). MCL cases were confirmed by the presence of the t(11; 14) translocation by fluorescence *in situ* hybridisation and /or detection of cyclin D1 expression (by molecular , immunohistochemistry) and for the characteristic immunophenotypic cell surface expression by flow cytometry.

All blood samples were obtained following informed consent (Integrated Research Application System project ID number: 145245), and under existing regulatory approval granted by the NHS Health Research Authority National Research Ethics Service Committee East of England – Cambridge East.

Human MCL cell lines Granta 519 (G519), JEKO-1 and JVM2 were purchased from Deutsche Sammlung von Mikroorganismen and Zellkulturen (DSMZ, Braunschweig,

Germany). The REC-1 cell line was a kind gift from Professor Martin Dyer (University of Leicester, UK). The authenticity of the selected MCL cell lines is summarised in Table 2.1.[184,185]

The NIH3T3 murine bone marrow fibroblast cell lines, one transfected with CD40-Ligand (T-CD40L), and the other, non-transfected (NT-CD40L) were also provided by Professor Martin Dyer.

Cell line	Source	Diagnosis	t(11;14)	CCND1/ cyclin D1	EBV transformed
REC-1	Peripheral blood/lymph node	B-NHL, diffuse large cell progressing to transformed mantle cell, blastoid variant	✓	✓	
G519	Peripheral blood	B-NHL (leukemic transformation of mantle cell lymphoma, stage IV)	✓	✓	✓
JEKO-1	Peripheral blood	Mantle cell lymphoma	✓	✓	
JVM2	Peripheral blood	B-prolymphocytic leukaemia (B-PLL)	✓	✓	✓

Table 2.1: Authentication summary of MCL cell lines used in this study.[184,185]

2.2.2 Peripheral blood mononuclear cell preparation

Whole blood samples were processed in a sterile laminar flow hood within 16 hours from the time of collection. Peripheral blood mononuclear cells (PBMCs) were separated by density-gradient centrifugation using Lymphoprep™ (AXIS SHIELD #1114545) or Ficoll-Paque PLUS (Fisher Scientific #11768538) following manufacturer's instructions. Four to five 5mL EDTA tubes of whole blood was collected from each patient and was very slowly added on top of an equal volume of lymphoprep/Ficoll in a 50mL falcon tube held at a 45 degree angle. In order to isolate the PBMCs, the tube containing the blood and lymphoprep/Ficoll was centrifuged at 2000rcf for 30 minutes

at room temperature, with zero brake speed. The PBMCs were extracted from the interface between lymphoprep/Ficoll and plasma using a pasteur pipette and added to a fresh 50mL falcon tube. The cells were washed with 1X PBS and the supernatant was discarded. The pellet of cells was re-suspended in 10mL of culture media and a cell count was performed (section 2.2.7).

2.2.3 Cellular cryopreservation

Cell lines and primary lymphocytes were re-suspended in 1mL freezing media (section 1.1). Cell lines were divided into aliquots containing 5 X 10^6 cells, and the primary lymphocytes were divided into aliquots containing 2 x 10^7 cells (low lymphocyte count) or 1 x 10^8 cells (high lymphocyte count) and added to 2mL cryopure tubes (Sarstedt). Cells were frozen gradually (1 degree per minute) to -80°C in a cryopreservation container filled with isopropyl alcohol (C3H8O). Cells were stored in liquid nitrogen (-180°C) for future use. Cell pellets were prepared at 5 x 10^7 for protein assays and were frozen dry at -80°C.

Cryopreserved PBMCs were thawed from liquid nitrogen in a water bath set to 37°C, and transferred to a 50mL falcon tube (Sarstedt). To remove the 10% DMSO, a volume of 9mL of warmed culture media was slowly added to the 1mL of cells to avoid temperature shock. The cells were centrifuged at 1500rcf for 5 minutes at room temperature and the supernatant containing DMSO was discarded. The cell pellet was re-suspended in 1mL of fresh culture media and topped up to the required volume.

2.2.4 Culture of suspension cell lines

Suspension cell lines were grown in culture media in $25cm^2$ or $75cm^2$ vented flat-bottom culture flasks (Sarstedt) and maintained in a humidified incubator at 37°C with 5% CO_2. All cell lines were passaged two to three times per week depending on their doubling time, to maintain optimal cell density. After every 28 culture passages, the cells were discarded and fresh aliquots of cells were obtained from liquid nitrogen.

Suspension cell lines were tested for mycoplasma contamination by indirect staining with the fluorescent dye; 4',6-diamidino-2-phenylindole (DAPI) which binds to DNA[186] and can be visualised by fluorescence microscopy. The figure below (Figure 2.1) shows DAPI fluorescence from the nuclei of two MCL cell lines, REC-1 (at passage 25) and G519 (at passage 28) with the detailed method described in the figure legend. Mycoplasma DNA (visualised as small white dots or flecks of fluorescence) was not detected within the cells or in the surrounding medium of either cell line.

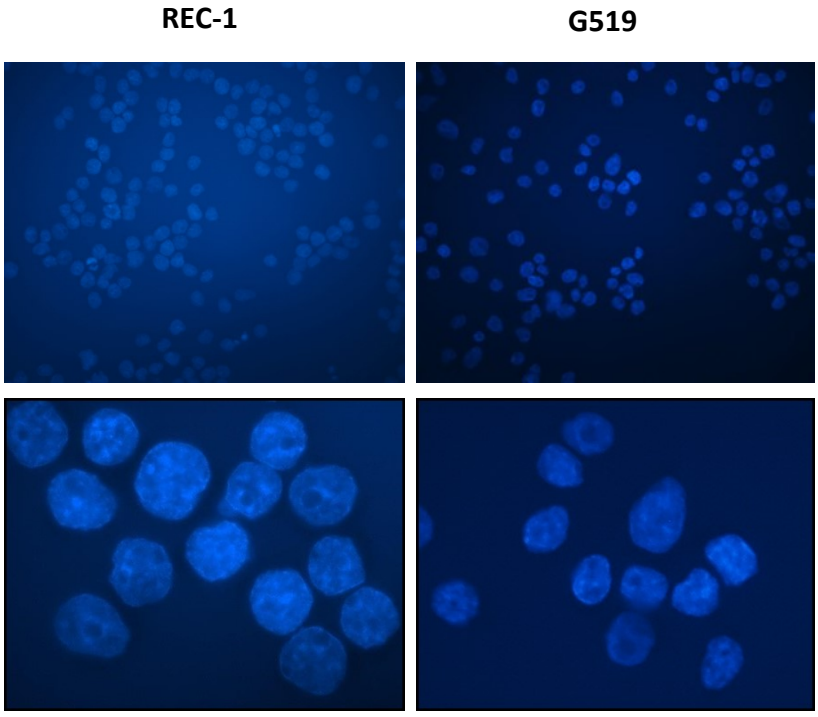

Figure 2.1: Immunofluorescent analysis of REC-1 and G519 cell nuclei by DAPI staining. REC-1 and G519 cells were seeded onto 5mm coverslips within a standard 24 well plate (Sarstedt) in culture media and left to settle overnight at 37°C. The media was carefully removed leaving the remaining cells attached to the coverslip surface. Cells were fixed in 200µl of 4% paraformaldehyde for 10 minutes, washed twice in 200µl of 1X PBS for 5 minutes and permeablised using 200µl of 0.1% Triton X-100 for 5 minutes. Cells were washed twice in 1X PBS for 5 minutes and blocked in 200µl of 1% BSA blocking buffer for 30 minutes at room temperature. The coverslips were removed from the 24 well plate and left to air dry overnight at room temperature. Cells were stained with 20µl of VectorSheild Hard Set Antifade Mounting Medium (containing DAPI) (Vector laboratories #H-1500), and mounted on to standard glass slides and left to cure for 4 hours. A NIKON fluorescent microscope with NIS-Elements imaging software was used to visualise DAPI fluorescence. Left-REC-1 cell nuclei, right-G519 cell nuclei. Top-20X magnification, bottom- 100X magnification.

2.2.5 Culture of T-CD40L and NT-CD40L murine bone marrow fibroblasts

The murine bone marrow fibroblasts were previously transfected with a human CD40L sequence and were supplied to our group along with the non-transfected control fibroblasts by Professor Martin Dyer (University of Leicester, UK). The CD40L transfected cells (T-CD40L) and the non-transfected cells (NT-CD40L) were grown in culture media in sterile 75cm^2 vented flat-bottom flasks with a special coating to support cell surface adhesion (Sarstedt). Once 70-80% confluent, the cells were washed in 1 X PBS and detached from surface of the culture flask using 1 x Trypsin-EDTA (section 1.1), then passaged 1 in 5 into fresh culture medium for ongoing culture.

Surface expression of CD40L was determined by detection of a phycoerythrin (PE) dye, conjugated to a mouse-anti-human CD40-ligand monoclonal antibody (BD #555700) and assessed using both fluorescence microscopy (Figure 2.2) and flow cytometry (Figure 2.3).

For assessment of CD40L by fluorescent microscopy, the T-CD40L and NT-CD40L fibroblasts were cultured on 5mm coverslips within standard 24 well plates in culture media for 48 hours until 70% confluent. The media was discarded leaving the remaining cells attached to the coverslip surface. Each coverslip was stained with 50µL of anti-human CD40L-PE and incubated in the dark for 20 minutes. The coverslips were washed with 1X PBS and the cells were fixed with 200µL of 4% PFA for 10 minutes. The coverslips were washed with 1X PBS for 5 minutes, then removed from the 24 well plate and left to air dry overnight in the dark at room temperature. Cells on each coverslip were stained with 20µL of VectorSheild Hard Set Antifade Mounting Medium (containing DAPI), then mounted on to standard glass slides and left to cure for 4 hours.

The slides were then visualised using a NIKON fluorescent microscope with NIS-Elements imaging software. The figure below (Figure 2.2) shows the images obtained following fluorescence microscopy indicating the presence of CD40L on the surface of the T-CD40L fibroblasts but not on the surface of the NT-CD40L fibroblasts.

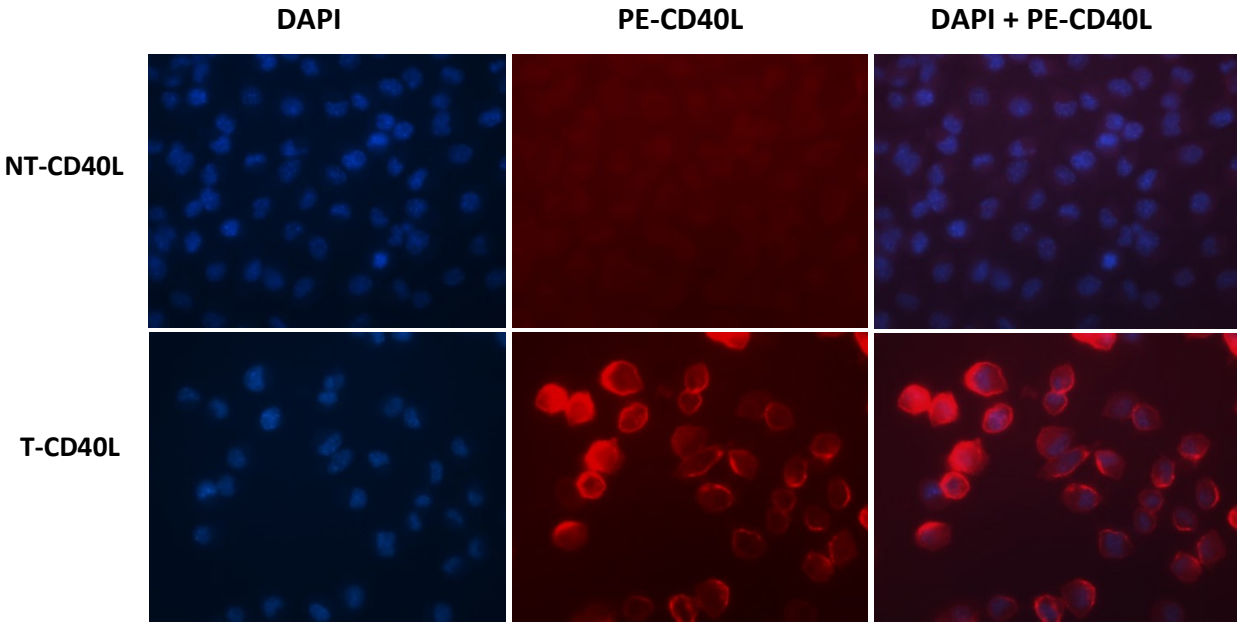

Figure 2.2: Characterisation of CD40L expression by fluorescence microscopy. Top images – NT-CD40L fibroblasts; bottom images – T-CD40L fibroblasts. Left images - cells stained with DAPI alone (blue); middle images - cells stained with PE-anti-CD40-ligand mAb alone (red); right images – merged images of cells stained with DAPI (blue) and PE-anti-CD40-ligand mAb (red), 60X magnification.

For assessment of CD40L by flow cytometry, the detached T-CD40L and NT-CD40L fibroblasts were added to individual FACS tubes and stained with 20µl of anti-human CD40L- PE along with a corresponding IgG-PE isotype control and incubated in the dark for 20 minutes (extracellular antibody conjugation method, section 2.3.1).

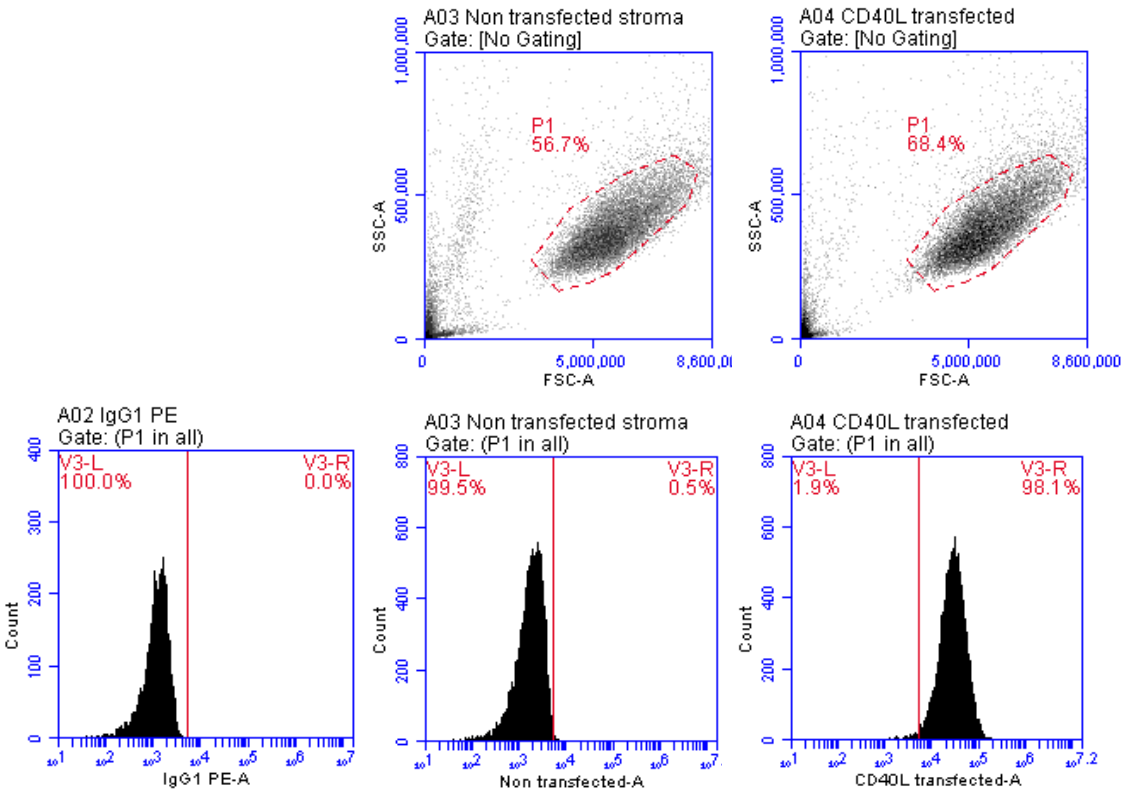

Figure 2.3: Characterisation of CD40L expression by flow cytometry. A gate was placed around the fibroblast population (P1) of the T-CD40L cells and the NT-CD40L cells. Expression of CD40L-PE was constricted to P1. Top row: forward and side scatter plots of fibroblast cells gated on P1. bottom row: peak plots showing the percentage of CD40L expression. Left: the PE isotype control (IgG1-PE), middle: the non-transfected fibroblasts and right: the CD40L transfected fibroblasts.

2.2.6 Culture of primary MCL cells

The murine fibroblasts (T-CD40L and NT-CD40L) were seeded into standard flat-bottomed 6 well plates (for protein assays) or 12 or 24 well plates (Sarstedt) (for functional assays) at a concentration of 5 x 10^5/mL, and returned to the incubator until 70% confluent.

To slow the proliferation rate of the fibroblasts, the well plates were irradiated through external beam radiation delivered through a linear accelerator (LINAC) by clinical physicists at Derriford Hospital Radiotherapy Department (University Hospitals Plymouth NHS Trust, UK). In brief, the cells were irradiated in the well plate using a 6MV photon beam at the machine isocentre. The sample was at a depth of 5cm in a solid water phantom and the field size used was 20cm^2. The dose of radiation delivered to the cells was 15Gy (Gray) in a single fraction.

Once the irradiated fibroblasts had settled and adhered to the surface of the wells, the media was removed and the two monolayers of fibroblasts were washed in 1X PBS. Primary MCL cells were seeded at 4 x 10^6/mL (REC-1 cells at 5 x 10^5/mL) on to each fibroblast monolayer and returned to the incubator. The figure below (Figure 2.4) shows phase-contrast images of the murine fibroblast monolayers and the primary MCL cells after 48 hours in co-culture.

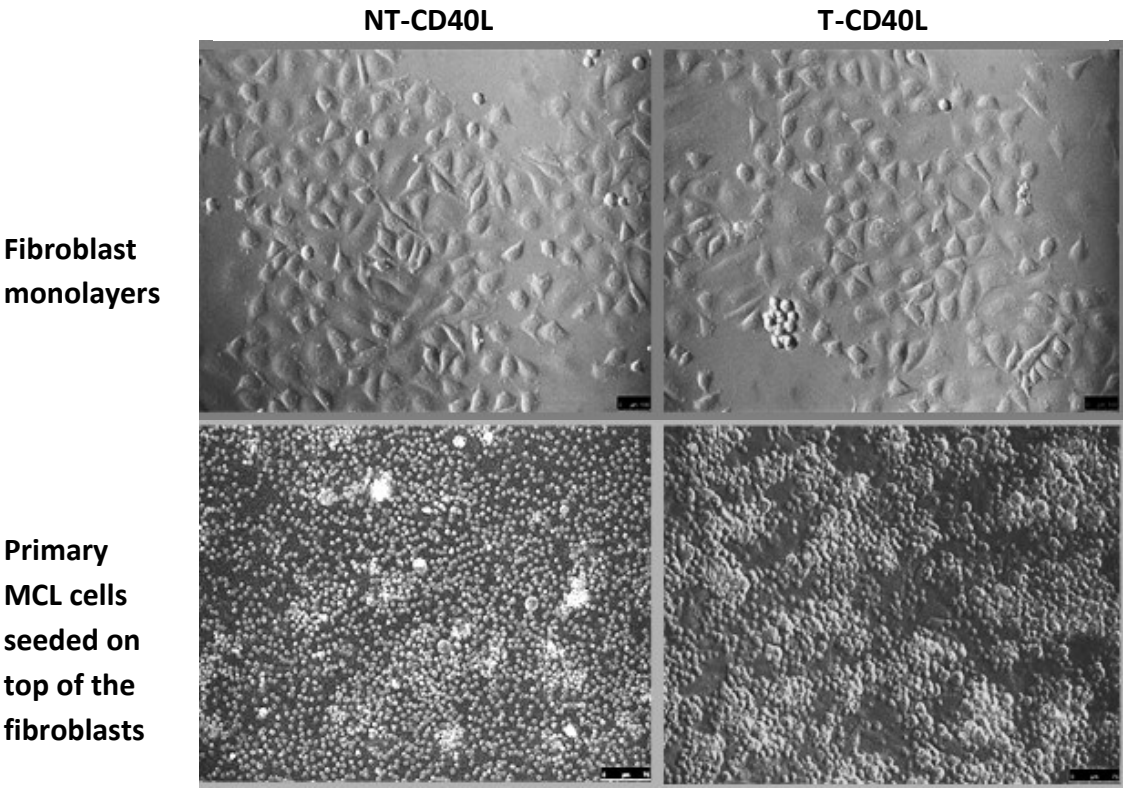

Figure 2.4: Phase-contrast images of murine fibroblast monolayers and co-culture with primary MCL cells. Top: fibroblast monolayers, Left: NT-CD40L, and Right: T-CD40L. Bottom: Primary MCL cells (seeded at 4 X 10^6/mL) on top of the fibroblast layers after 48h in co-culture.

2.2.7 Assessment of cell number

A cell count was performed by counting the number of viable cells on a neuabauer haemocytometer using a trypan blue assay. On occasions, the trypan blue stained cells were counted with a TC20^{TM} automated cell counter (Bio-rad).

2.2.8 B-cell receptor activation

The B-cell receptor (BCR) was stimulated by crosslinking IgM. Activating the BCR by stimulating IgM rather than IgG was preferred since most mature B-cell malignancies derived from antigen dependant BCR signalling express a functional IgM type BCR which promotes NFkB activation and cell proliferation.[187,188] Cells were stimulated with

Goat Fab' 2 anti-human IgM antibody (0.5mg/mL) (Bio-Rad AbD Serotec, STAR146), diluted to 3µg/mL and signalling responses assessed after a time-dependent period as described in the results chapters.

2.2.9 In vitro drug treatments

The two BTK inhibitors used in this study were ibrutinib (Ibr) and acalabrutinib (Acal). Ibr was purchased from Selleckchem (Houston, Texas, USA), and Acal was supplied as a gift by Acerta Pharma (San Francisco, USA) prior to FDA approval. A ten millimolar stock solution of each drug was prepared in DMSO and stored at -20°C or -80°C for short and long term use (respectively). Ten millimolar stocks were diluted in DMSO to various working concentrations within the range of 10mM-1nM. Drugs were added to cell cultures using a 1 in 1000 dilution.

2.2.10 Acquired BTK inhibitor resistant cell lines

Cells from a cell line demonstrating sensitivity to BTKi (REC-1) were cultured at a density of 2 x 10^5 in 12mL of culture media (+10% FBS) in 25cm^2 flasks. The cells were treated with increasing concentrations of Ibr at the following doses: 1nM, 3nM, 10nM, 30nM, 100nM, 300nM, 1µM, 3µM.

At the lower doses (<100nM), cells were passaged every 2-3 days and 3 times at each dose. At higher doses (>100nM), the density of REC-1 cells was increased to 5 x 10^5 in 12mL and cells were passaged every 3-4 days, and 6 times at each dose, until the cells were proliferating at the same rate as untreated parent REC-1 cells cultured under the same conditions. The sensitised cells were then treated continuously for 8 weeks at 1µM and 3µM, above the *in vivo* dose for Ibr (400nM),[116,145] and grown for use in subsequent experiments.

Before each passage, the cells were centrifuged at 1500rcf and the supernatant was discarded. To wash the cells and remove the drug from the previous culture, the pellet was re-suspended in 10mL of serum free media, re-centrifuged at 1500rcf and the supernatant was discarded. The washed pellet of cells was then re-suspended in 12mL fresh culture media (+10% FBS) and split 1 in 2 into two fresh culture flasks. The cells were then treated directly with a 1 in 1000 dilution of Ibr and incubated at 37°C with 5% CO^2 until the next passage.

At a later stage in the study, REC-1 cells were also sensitised to Acal in the same way to generate a cell line model of acquired Acal resistance. The continuous dosage did not exceed 1µM for Acal and therefore cells were sensitised to just below the *in vivo* dose for Acal which is 2µM (personal communication from Acerta Pharma).

2.3 Flow cytometric assays

Each antibody was conjugated to a specific fluorochrome which emits different wavelengths of fluorescence when activated and can be quantified by flow cytometry.

2.3.1 Extra cellular antibody conjugation method

This method was required for the detection of cellular antigens on the surface of cells. The below method was required for the detection of CD40L expression and for defining the primary MCL cell population.

Fluorochrome-conjugated antibody (recommended amount per test described in relevant results chapters) was added to a volume of 100-200µl of cell suspension media. Tubes were incubated in the dark for 20 minutes at room temperature unless indicated otherwise. Cells were diluted in 300µl of staining buffer, and analysed by

flow cytometry. Fluorescence was measured against an isotype control of the same IgG subclass and fluorochrome.

2.3.2 Intracellular antibody conjugation method

An intracellular antibody conjugation method was required for the detection of the nuclear antigen Ki67 (for assessment of proliferation) and for the detection of intracellular BTK (for assessment of BTK activity).

Each assay had different culture requirements before fixation and are therefore described separately.

For the proliferation assay, cells were cultured in 12 or 24 well plates in cell culture media at a concentration of 5 x 10^6/mL. A volume of 200µl was removed, pelleted by centrifugation at 13000rpm for 5 minutes, and then fixed in 200µl of 4% PFA for 10 minutes at room temperature.

For the BTK assay, cells were cultured in 1.5mL Eppendorf tubes and fixed in suspension. Cell lines were cultured at 1 x 10^6/mL in 1mL of serum free culture media and fixed with 200µl of PFA to a final concentration of 4% for 10 minutes at room temperature.

For primary MCL cells, 200µl of cells (at 5 x 10^6/mL) in culture media (+ 10% FBS) were pre-labelled with anti-CD5 and anti-CD19 on ice for 20 minutes prior to fixation (as described above).

Following fixation, cells were washed in 1 x PBS and permeablised with 0.2% Triton X-100 on ice for 10 minutes. Cells were re-suspended in 100µl of staining buffer and stained with fluorescein conjugated monoclonal antibodies directed against Ki67 or BTK (and an IgG isotype control) and incubated in the dark for 20-25 minutes. Cells

were diluted in 300µl of staining buffer, transferred to a FACS tube and analysed by flow cytometry.

2.3.3 Apoptosis staining method

For the apoptosis assay, cell lines were cultured at 1 x 10^6/mL in standard 12 well or 24 well plates. A volume of 100µl of cell suspension was collected into FACS tubes and stained with 5µl annexin V-FITC (BD #556419), gently vortexed and incubated in the dark for 20 minutes. Cells were analysed in 400µl of 1X annexin-V binding buffer (section 2.1).

Primary MCL cells were cultured at 4 x 10^6/ml and 200µl of cells were pre-labelled with MCL surface markers on ice for 20 minutes before the addition of annexin-V- FITC.

2.3.4 Analysis of flow cytometry data

Samples were analysed on a BD AccuriTM C6 flow cytometer (BD Biosciences). Data were collected and plotted onto a 2D forward and side scatter plot. Analysis was performed on a minimum of 20,000 events per experimental condition using BD AccuriTM CFlow Plus software (BD Biosciences). Cells were vortexed immediately prior to analysis to promote a single cell population.

Gating was used to isolate the lymphocyte population based on forward and side scatter which allowed for exclusion of debris and cell clumps. In addition, assessment of the pulse area (FSC-A) vs the pulse height (FSC-H) was used to exclude doublets.

The appropriate gating was then applied to a histogram which was used to determine the proportion of activated fluorescence of the specified cell population against an unstained or isotype control. The analysis applied to define the MCL population and to determine apoptosis, proliferation and phosphorylation of BTK in cell lines and primary

MCL cells is described in detail in the Appendix. In brief, apoptosis was determined by analysing the percentage of annexin V-FITC positive cells against viable cells. Cell proliferation was determined by analysing the percentage of KI67-FITC positive cells against an isotype control of the same IgG subclass. BTK phosphorylation was assessed by obtaining the median fluorescence intensity values of the BTK positive cells.

The percentages and the median fluorescence intensity values were exported to Microsoft Excel™ and GraphPad Prism™ (version 5) for statistical analysis. The proportion of cells expressing pBTK-Y223 was determined by calculation of the median fluorescence intensity ratio (MFIR) = median fluorescence intensity of pBTK-Y223 antibody divided by median fluorescence intensity of isotype control.

2.4 Biochemical assays

2.4.1 Cell lysis

Whole cell protein extracts were prepared by lysing ~1 x 10^7 cells in 100µl of RIPA buffer (section 2.1). The cells were incubated on ice for 30 minutes and vortexed every 10 minutes. The lysed cells were pelleted by centrifugation at 13500rpm and the supernatant containing the protein was transferred to a fresh tube. The extracted protein was then quantified and stored at -20°C.

2.4.2 Protein quantification

Protein concentrations were estimated using the BCA (Bicinchoninic acid) Protein Assay Reagent kit (Thermo Fisher UK) according to the manufacturer's instructions. One Bovine Albumin Standard Ampule (Thermo Scientific Pierce #11811345), was diluted into 9 different dilutions in 1X PBS to make a set of protein standards. Ten

microliters of each BSA standard was added in triplicate to a 96 well plate (Fisher Scientific) to construct a standard calibration curve.

Protein lysates were diluted 1 in 5 in 1 X PBS, to bring them to within the detection range of the kit (0.2-2mg/mL). Ten microliters of each diluted sample was added in duplicate to the 96 well plate. An adequate volume of working reagent (BCA reagent A and BCA reagent B, mixed at a ratio of 50:1) was prepared and 190µl was added to each sample including the BSA standards. The plate was then incubated at 37°C for 30 minutes. The mean absorbance values of the samples were measured at 562nm using a microplate reader and protein concentrations were corrected against the standard curve. A multiplication factor of 5 was applied to the resulting sample values to account for the 1 in 5 sample dilutions.

2.4.3 Gel preparation, sample loading and 1D electrophoretic separation

A fresh 10% resolving gel mixture was prepared (section 2.1) and poured into a 1.5mm chamber between two glass plates up to three quarters of the length of the inner plate and left to polymerise for 45 minutes. A fresh 4% stacking gel mixture was prepared and was added on top of the resolving gel to the top of the inner glass plate. A 10 or 15 well comb was added and the gel was left to polymerise for 45 minutes.

The glass plates containing the gels were placed in a Mini – PROTEAN Tetra cell system (Biorad; 165-8004) filled with 1X running buffer (section 2.1) and placed inside a gel tank.

Protein was added to 1.5mL Eppendorf tubes and diluted in dH_2O to achieve equal protein concentrations between all samples. Protein was denatured by adding an

equal volume of 2 X Laemmli sample buffer containing 5% β-mercaptoethanol to the protein, and heating the samples at 95°C on a heat block for 5 minutes.

Samples were loaded into individual wells of the stacking gel along with 5µl of protein standard (Biorad) used as a marker to identify proteins based on their molecular weight. Samples were electrophoresed at 70 volts (V) using a Bio-Rad power pack, for 35 minutes or until protein had lined up at the bottom of the stacking gel. The voltage was then increased to 140V and proteins were separated based on mass through the resolving gel for 1 hour.

2.4.4 Co-immunoprecipitation (Co-IP)

REC-1 cells were seeded at 10 x 10^7/mL and lysed in 1mL of low stringency lysis buffer (100µl lysis buffer/ 1 x 10^7 cells) (section 2.1).

The cells were sheared using a needle and syringe to gently break the nuclear membrane. The protein concentration was estimated using the BCA assay (section 2.4.2). For each immunoprecipitation, 600µg of protein was diluted in 200µl of 1X PBST.

Prior to immunoprecipitation, a pre clearing step was performed to eliminate any non-specific binding to the beads. The diluted protein lysate was incubated with 50µl of protein G magnetic dynabeads (Novex) in a 1.5mL Eppendorf tube and agitated on a daisy wheel for 30 minutes at 4°C. The magnetic beads were pulled out of solution using a magnetic separator (Cell signalling technology #7017) and the pre-cleared lysate was transferred to a fresh 1.5mL Eppendorf tube.

Immunoprecipitations (IP) were performed indirectly by adding antibodies specific to the protein(s) of interest to the diluted REC-1 protein lysate at concentrations

indicated on the data sheet, and incubating with agitation over night at 4°C. A volume of 50µl of the protein G beads was added to each IP sample and incubated with agitation for 2 hours at 4°C.

The samples were placed on a magnetic separator and the magnetic beads bound to the protein of interest were attracted to the side of the tube. The post IP fraction (remaining solution) was removed and saved for SDS-PAGE analysis to ensure the immunoprecipitation had worked. The beads were washed 5 times in low stringency buffer and eluted in 30µl of 2 X Laemmli buffer (section 2.1).

The protein complex was separated from the beads, by adding 5% β-ME to each sample and heating the samples at 95°C for 5 minutes. The beads were pelleted by centrifugation at 14000rpm and the supernatant (containing the protein of interest) was collected and subjected to ID electrophorectic separation.

2.4.5 Preparation of Mass spectrometry samples

Protein immunoprecipitations were performed as previously described (section 2.4.4) and eluted in 30µl of fresh 2 X laemmli buffer. A fresh 10% resolving gel and 4% stacking gel was prepared. To prevent as much contamination as possible, all equipment including falcon tubes, Eppendorf tubes, glass plates and a ruler was soaked in methanol and left to air dry. The reagents used to make the gels including the MilliQ dH_20, 30% acrylamide, tris buffer and SDS were drawn into a 20mL sterile plastic syringe (Becton Dickinson LOT: 7500C13LF) and filtered into a sterile falcon tube through a sterile Milllex GP filter unit 0.22µM (Merck Millipore #SLGP033RB). The polymerising agents (10% APS and TEMED) were subsequently added, and the gel mixture was poured into the chamber between the glass plates. A volume of 5% BME was added to each IP sample and the samples were heated at 95°C for 5 minutes.

A volume of 30µl of each IP sample was added to a 10 well gel as shown in the gel template below (Figure 2.5). Each IP sample was surrounded by empty wells (containing only 2 x Laemmli buffer) to prevent protein contamination from the ladder when cutting.

The gel was left unstained to prevent any staining interference with the mass spectrometry. Therefore, after the running of the IP samples, the gel was flipped over and kept on the bottom 1.5mm spacer plate. The wells from the stacking gel were used as a guide to identify each lane. As shown in Figure 2.5. The IP lanes were cut vertically and then a sterile ruler was used to measure and cut out 8 individual pieces horizontally using a clean sterile surgical steel blade scalpel (Swann-Morton Sheffield England, REF 0503, Lot: 6901412) for each individual cut. The gel pieces were added to corresponding labelled tubes. Since the gel was flipped over, the IP samples were located in the opposite direction from the direction the samples were originally loaded. Each gel piece was covered in 1mL of MilliQ H2O and frozen at -80°C.

Samples were sent to Manchester University on dry ice and analysed by research staff using SWATH MS (sequential window acquisition of all theoretical fragment ion spectra mass spectrometry). Analysis of the SWATH MS data is explained in more detail in Chapter 5.

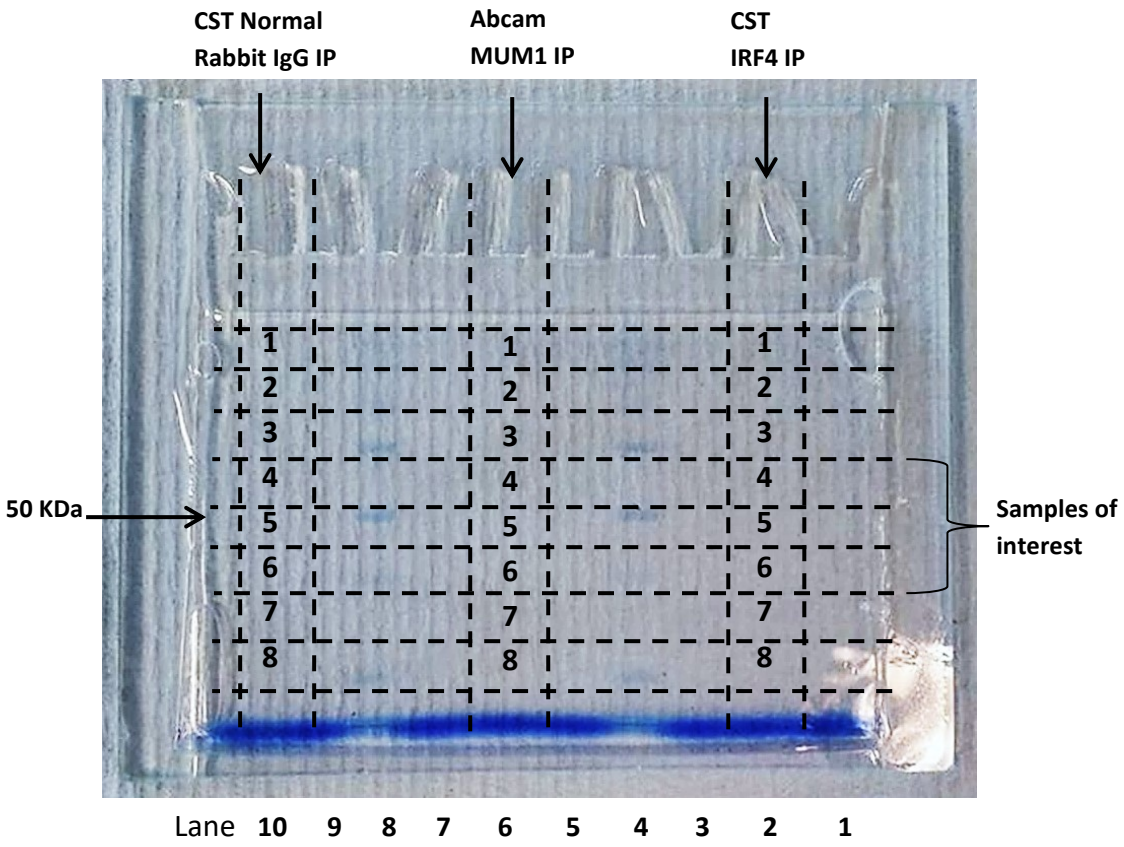

Figure 2.5: Image of gel after separation of IRF4 IP samples. The image shows the approximate position of the cuts and the numbered gel pieces that were sent off for mass spectrometry analysis (samples were cut in the opposite direction from the way they were loaded). Samples 4 and 5 (possibly 6) contain the IRF4 IP at around 50KDa.

2.4.6 Western blotting

Proteins were transferred from the gel onto polyvinylidene difluoride (PVDF) membranes (Biorad #1620177). The PVDF membrane was prepared by immersing in 100% Methanol for 20 seconds. The membranes were then rinsed in dH2O and left to soak in pre-chilled 1X transfer buffer for at least 20 minutes along with the fiber pads and filter paper. The membrane and gel were sandwiched between two pieces of filter paper and two fiber pads, all held together inside a mini gel holder cassette. The cassette was placed inside a Mini Trans-blot central core unit fixed inside the blotting

tank. An ice cold blue cooling unit was placed inside the tank in front of the central core unit and the tank was filled with 1X Transfer buffer. Proteins were transferred at 100V using a Bio-Rad power pack for 1.5 hours.

2.4.6.1 Immunohybridisation

The membranes were rinsed briefly in 1X TBS and then incubated in blocking buffer (section 2.1) for 1 hour at room temperature. The membranes were then incubated with primary antibodies diluted in blocking buffer overnight at 4°C. The membrane was washed for 10 minutes, 3 times in 1X TBST, to remove some of the background from the primary antibody and then incubated with a secondary antibody conjugated to-HRP for one hour at room temperature. Again, the membranes were washed for 10 minutes, 3 times in 1X TBST, to remove some of the secondary antibody background.

2.4.6.2 Detection and analysis

Membranes were enhanced for chemiluminescent visualization following incubation with ECL or ECL Prime western blotting substrate (GE Healthcare) for 1 or 5 minutes (respectively). The membranes were placed in a hyper cassette and exposed to XR film (Fisher Scientific) in a dark room and developed with a Compact X4 Xograph Imaging system (Xograph Healthcare Ltd).

The protein bands detected on the western blot films were quantified using an Image J processing tool. The data was exported to Microsoft Excel where the recorded pixel densities for all data (bands, controls and their backgrounds) were inverted using the following formula; 255 – X, where X is the value recorded by ImageJ. The inverted background value was deducted from the corresponding inverted band value to obtain a net value. The final relative quantification values were determined by the ratio of net

band to net loading control. The ratios were represented as bar graphs and protein expression levels were statistically analysed using Graph pad Prism 5 software.

2.5 Molecular assays

2.5.1 Messenger RNA expression

RNA was extracted from MCL cell lines using the RNeasy Mini Kit (QIAGEN, Hilden, Germany) following manufacturer's instructions. Briefly, 5 x 10^6 cells were added to 1.5mL Eppendorf tubes and centrifuged at 13500 rpm for 5 minutes at 4°C. The cell pellet was lysed in 350µl of denaturing buffer (Buffer RLT), centrifuged for 3 minutes at 13500 rpm and the supernatant was carefully transferred to a clean 1.5mL Eppendorf tube. A volume of 350µl of 70% ethanol was added to the lysate to facilitate the selective binding of the RNA to the silica membrane of the RNeasy spin column. A volume of 700µl of the sample containing ethanol was loaded into a spin column placed inside a 2mL collection tube and centrifuged for 15 seconds at 10000 rpm. The flow through in the collection tube was discarded.

A volume of 700µl of stringent salt buffer (Buffer RW1) was added to the spin column to remove any biomolecules that were non-specifically bound to the silica membrane. The spin column was centrifuged at 10000 rpm and the flow through was discarded. To remove the salt, a volume of 500µl of a mild wash buffer (Buffer RPE) was added to the spin column and centrifuged at 10000 rpm for 15 seconds and the flow through was discarded. This was repeated a second time with a 2 minute centrifugation. The spin columns were placed inside a clean collection tube and centrifuged at 13000 rpm for an extra 1 minute to dry the membrane. The spin columns were then placed inside a clean 1.5mL collection tube.

To elute the RNA, 30µl of RNase free water was added to the spin column and centrifuged for 1 minute at 10000rpm. The spin column was discarded leaving the purified RNA in the 1.5mL collection tube.

The RNA was quantified using a NanoDrop 2000 spectrophotometer (Thermo Scientific). The purity of each RNA sample was determined from the ratio of absorbance at 260nm and 280nm. RNA was considered pure at ratio of ~2. Samples were stored at -80°C.

2.5.2 Reverse transcription (RNA- cDNA)

RNA was converted to complementary DNA (cDNA) using the Tetro cDNA synthesis kit (Bioline #BIO-65042) following manufacturer's instructions. A priming premix was prepared on ice in RNAse free tubes (Fisher Scientific) containing 1µl of oligo dT, 1µl of dNTP mix (10mM), 4µl of reverse transcription buffer, 1µl of Ribosafe RNAse inhibitor and 1µl of Tetro reverse transcriptase enzyme per sample. The quantity of RNA to add to the reaction (no more than 12µl or 2µg) was standardised to obtain equal concentrations for each sample. Diethyl pyrocarbonate (DEPC) treated water was added to the samples to bring the total reaction volume up to 20µl. Samples containing no reverse transcriptase (NRT) were also prepared to control for each test sample reaction. The samples were heated at 45°C for 30 minutes in a GSTORM thermal cycler (Applied Biosystems). The reaction was terminated by denaturing the enzyme at 85°C for 5 minutes. The samples were then chilled on ice and stored at -20°C.

2.5.3 Polymerase chain reaction (PCR)

Regions on *IRF4* and *PU.1* were amplified from cDNA by PCR and analysed against the housekeeping gene *HPRT*. The primers for IRF4 and HPRT were designed previously by the haematology group, the PU.1 primers were taken from Mankai *et al* [189]. All primers were designed to span exon junctions thereby preventing amplification of genomic DNA. Each primer pair was evaluated for target specificity using NCBI primer blast https://www.ncbi.nlm.nih.gov/tools/primer-blast/index.cgi. The oligonucleotide sequences are shown in Table 2.2. All primers were purchased from Sigma Aldrich. Stock solutions of 10µM were prepared in nuclease free water (Fisher Scientific, BP2484-100) and stored at -20°C.

Conventional PCR was used to optimise the primer annealing temperatures (Ta) prior to experimentation by running a temperature gradient (56-62°C). Primers were diluted to a final concentration of 200nM (each) in a PCR mix containing 10X Dream Taq buffer and 2X Dream Taq DNA polymerase (Thermo Fisher Scientific #EP0701), dNTP mix (Thermo Fisher Scientific #R0191), and nuclease free water (Fisher Scientific, BP2484-100), and 2µl of each cDNA sample was added for a total reaction volume of 23µl. IRF4 was amplified using a GSTORM thermal cycler (Applied Biosystems), following the cycle sequence outlined in Table 2.3. The PCR products were analysed by agarose gel electrophoresis (section 2.5.5).

Gene	Primer sequence 5' - 3')	Size (bp)	Amplicon size (bp)
IRF4 Forward	ACCCGCAGATGTCCATGAG	19	90
IRF4 Reverse	GTGGCATCATGTAGTTGTGAACCT	24	
PU.1 Forward	GTGCCCTATGACACGGATCT	20	279
PU.1 Reverse	GTAGAGGACCTGGTGGCC	18	
HPRT Forward	CCTGGCGTCGTGATTAGTGAT	21	131
HPRT Reverse	AGACGTTCAGTCCTGTCCATAA	22	

Table 2.2: Oligonucleotide sequences used for amplifying IRF4, PU.1 and HPRT from cDNA. The IRF4 and HPRT primers were designed previously by the haematology group and the PU.1 (Spi-1) primers were taken from Mankai *et al*[189].

Step	Temperature	Time	No of cycles
Heated lid	112°C		
Automatic hot start	95°C	10 minutes	1
Start cycle amplification			
Denaturation	95°C	30 seconds	40
Annealing	Ta gradient 56, 58, 60, 62°C	30 seconds	
Extension	72°C	60 seconds	
End cycle amplification			
Hold	4°C	Infinite	

Table 2.3: PCR cycle sequence for optimisation of primer annealing.

2.5.4 Real time quantitative PCR (qPCR)

Expression levels of *IRF4* and *PU.1* mRNA were compared against *HPRT* during the exponential growth phase of PCR. Primers were diluted to a final concentration of 200nM in a PCR mix containing 2X SYBR Green Master I and PCR grade water (ROCHE). The PCR mix was added to each test well in a clear optical 96 well plate (ROCHE), and 1-5µl (25-100ng) of each cDNA sample was added in triplicate in a total reaction volume of 15-20µl. The cDNA was amplified using the LightCycler 480 instrument (ROCHE) following the cycle sequence outlined in Table 2.4. A melting curve was included to determine the specificity of the primers for the PCR product and to ensure absence of non-specific amplification. The Cp values (also known as cycle threshold or Ct values) were obtained from the LightCycler 480 instrument and transported to Microsoft Excel. Relative quantification of *IRF4* and *PU.1* expression levels was normalised against *HPRT* and determined using the delta delta Ct method.

Step	Temperature	Time	No of cycles
Pre incubation	95°C	10 minutes	1
Denaturation	95°C	10 seconds	45
Annealing	60°C	20 seconds	
Extension	72°C	10 seconds	
Melting curve	95°C	5 seconds	1
	65°C	60 seconds	
Cooling	40°C	10 seconds	1

Table 2.4: Cycle sequence for qPCR amplification of cDNA regions.

2.5.5 Agarose gel electrophoresis

A 1 or 2% agarose gel was prepared in a glass flask by adding 1 or 2 grams of agarose powder (Fisher Scientific, UK) to 100mL of 1X TBE buffer (section 2.1). After gentle swirling, the mixture was heated for approximately 2 minutes until the agarose was completely dissolved in solution. In order to visualise the DNA, 5µl of GelRed TM (10,000X in water) nucleic acid gel stain (Cambridge Bioscience #BT41003) was added to the mixture. The gel mixture was then poured into a gel tray. A 15 or 20 well comb was added and the gel was left to set for at least 30 minutes before loading the samples.

In order to track the PCR products during electrophoresis the samples were mixed with a 1 in 6 dilution of 6XDNA loading dye buffer (section 2.1) and then loaded into the wells of the agarose gel, alongside a Gene ruler 1Kb plus DNA ladder (Thermo Fisher, UK #10600301) or a 100bp DNA ladder (Norgen, Germany). The samples were electrophoresed through the gel using a Biorad power pack at a constant voltage of 130V for 45 minutes or until the samples had almost migrated the length of the gel. Following electrophoresis, DNA in each sample was visualised using a UVP GelDoc-It® Imager (UVP, Cambridge, UK) aided by the Launch Vision Works LS programme.

2.5.6 Chromatin immunoprecipitation (ChIP)

Chromatin immunoprecipitations were prepared from several cell lines using the SimpleChIP® Enzymatic Chromatin IP Kit (Magnetic Beads) (Cell signalling technology #9003), following manufacturer's instructions.

Preparation of chromatin for ChIP

A cell count was performed for each cell line using a TC20^{TM} automated cell counter (Bio-rad) and cells from each cell line were cultured at 5 x 10^6 in 20mL of fresh culture media in 15cm sterile culture dishes (Thermo Scientific #130183).

Cross-linking chromatin

To cross-link proteins to DNA, cells were fixed in 540µl of 37% formaldehyde to achieve a final concentration of 1% in each 20mL of cell suspension and left to incubate for 10 minutes at room temperature.

To quench the formaldehyde and prevent non-specific cross linking, a volume of 2mL of 10X glycine solution was added to each cell suspension and left at room temperature for 5 minutes.

Each cell suspension was then transferred to a 50mL falcon tube and centrifuged at 1,500rpm for 5 minutes at 4°C. The supernatant was discarded and the remaining pellets were washed twice in 20mL of ice cold 1 X PBS and centrifuged at 1,500rpm for 5 minutes after each wash.

Nuclei preparation

Each pellet was re-suspended in 1mL of ice cold 1X enzymatic lysis buffer A (section 2.1), and incubated on ice for 10 minutes, and mixed by inversion every 3 minutes. The suspension was centrifuged at 3,000rpm for 5 minutes at 4°C and the supernatant discarded. Each pellet was then re-suspended in 1mL of ice cold 1X enzymatic lysis buffer B (section 2.1), the centrifugation was repeated and supernatant was very carefully discarded. Each pellet was then re-suspended in 100µl of 1X enzymatic lysis buffer B, transferred to a 1.5mL Eppendorf tube and placed on ice.

Chromatin digestion and fragmentation

To digest DNA to an optimal length for successful ChIP experiments (approximately 150-900bp), a volume of 0.5 - 0.8µl of micrococcal nuclease (#10011) was added to each chromatin preparation, incubated for 20 minutes at 37°C, and mixed frequently by inversion. The digest was stopped after 20 minutes by adding 10µl of 0.5M EDTA (#7011) and placing the tube on ice. The nuclei was pelleted at 13500rpm for 1 minute at 4°C, the supernatant was discarded and the pellet was re-suspended in 100µl 1X ChIP buffer (section 2.1).

The chromatin from each sample was sonicated in 100µl 1X ChIP buffer (section 2.1) using a Standard Bioruptor ® (Diagenode, Belgium). Nuclei were observed under a light microscope before and after sonication and were determined to be completely lysed (no whole cells visualised) after 10 sonication rounds of 30 seconds ON and 30 seconds OFF. After sonication, the lysates were clarified by centrifugation at 10,000rpm for 10 minutes at 4°C. Approximately 100µl of the supernatant containing the cross-linked chromatin was then transferred to a clean tube.

Confirmation of chromatin fragment length prior to ChIP

One 50µl aliquot of each sonicated chromatin sample was electrophoresed on agarose gel to check the chromatin digestion and fragmentation. A 1% agarose gel was prepared (as described in section 2.5.5). To prepare the samples, cross-linked protein-DNA interactions were reversed (see reversal of cross links) to free up the DNA fragments for electrophoresis. The DNA was purified using spin columns (as described later). Following DNA purification, a 10µl sample was removed, mixed with 6X DNA loading dye buffer and run on agarose gel alongside a 100bp DNA ladder (Norgen, Germany) as previously described.

Determination of DNA concentration in chromatin preparation

DNA concentration and quality was determined using a NanoDrop 2000 spectrophotometer (Thermo Scientific). The optical density was assessed at 260 nm to 280 nm and the DNA quality threshold for the A260/A280 ratio was 1.8- 2.0.

Preparation of the digested chromatin samples for ChIP, and preparation of the input sample.

For each IP sample, the digested cross-linked chromatin was diluted to 1-10µg in 100-500µl of 1X ChIP buffer. Ten microliters of each diluted solution was removed to a separate Eppendorf tube for the 2% input sample and frozen at -20°C.

Indirect binding of chromatin with ChIP antibody

A ChIP validated antibody specific for the protein of interest was added directly to the digested cross-linked chromatin preparation at the concentration specified on the data sheet. A histone (H3) antibody (used as a positive control) and a species matched normal IgG antibody (used as a negative control) were added to separate chromatin preparations at the concentrations specified in the protocol for establishment of the ChIP procedure. Samples were incubated over night at 4°C with rotation on a daisy wheel.

Binding of Protein G magnetic beads to the antibody/chromatin complex

A volume of 30µl of ChIP-grade protein G magnetic beads #9006 was added to each IP sample and incubated for 2 hours at 4°C with rotation on a daisy wheel. Each tube was then placed in a magnetic separation rack (cell signalling technology #7017) for 30 seconds to attract the protein G beads bound to the antibody-antigen complex, to the side of the tube. The supernatant (which should not contain the relative chromatin fragments of interest) was discarded. Each bead pellet was washed 3 times in 1mL of

low salt wash (section 2.1), then washed once in 1mL of high salt wash (section 2.1) at 4°C for 5 minutes with rotation. After each wash the tubes were placed in the magnetic separation rack and the supernatant was discarded.

Elution of chromatin from antibody- protein G magnetic beads

A volume of 150µl of 1X ChIP elution buffer (section 2.1) was added to each IP sample and to the 2% input samples. All samples were heated at 65°C for 30 minutes and gently agitated at 1200rpm in a thermomixer (ThermoFisher) to release the chromatin fragments bound to the antibody from the beads. The tubes were placed in the magnetic separation rack to attract the unbound beads and the supernatant containing the immunoprecipitated chromatin was transferred to fresh tubes.

Reversal of cross links

Cross-links within the antibody chromatin complexes were reversed by adding 6µl of 5M NaCl and 2µl of proteinase K (#10012) to all tubes including the 2% input samples and incubating for 2 hours at 65°C. Proteinase K destroys the antibody-protein complexes, allowing them to be removed from solution, leaving only the DNA fragments.

DNA Purification using spin columns

A volume of 750ul of DNA binding buffer (#10007) was added to each DNA sample and vortexed briefly. Each sample was transferred (450µl at a time) to a spin column placed in a collection tube and centrifuged at 14,000rpm for 30 seconds. The flow through was discarded and the spin column was placed back in the collection tube. A volume of 750µl of DNA wash buffer (#10008) was added to the spin column and centrifuged at 14,000rpm for 30 seconds. The flow through was discarded and the spin column was placed back in the collection tube. The spin columns were centrifuged a second time at

14,000rpm for 30 seconds. The collection tube containing the flow through was discarded and the spin columns were placed into fresh 1.5mL Eppendorf tubes. A volume of 50µl of DNA elution buffer (#10009) was added to each spin column and centrifuged at 14,000rpm for 30 seconds to elute the DNA. The spin columns were discarded and the eluate containing the purified DNA was stored at -20°C.

Confirmation of ChIP procedure by conventional PCR

To determine the success of the ChIP, the purified DNA obtained from each sample (the IP and the input DNA samples) was amplified by conventional PCR for detection of the ribosomal protein L30 (*RPL30*) gene locus.

A PCR reaction-mix was prepared (Table 2.5), the volume of each reagent was multiplied for the required number of samples (to include the positive control (Histone H3), negative control (normal rabbit IgG) and a NTC)). The mix was vortexed and 18µl was added to individual PCR tubes. A volume of 2µl of each DNA sample was added to the individual PCR mixes. The DNA was amplified on a Verity thermal cycler (Applied Biosystems) following the PCR cycle sequence in Table 2.6. For analysis of the *RPL30* amplicons, 10µl of PCR product from each sample was run on a 2% agarose gel (section 2.5.5).

Reagent	Volume for 1 PCR Reaction (18 µl)
Nuclease-free H2O	13.1 µl
10X PCR Buffer	2.0 µl
4mM dNTP Mix	0.4 µl
5µM RPL30 Primers	2.0 µl
Taq DNA Polymerase	0.5 µl

Table 2.5: The PCR reaction mixture for amplification of the *RPL30* locus from ChIP samples

Step	Temperature	Time	Cycles
Initial denaturation	95	5 minutes	1
Denaturation	95	30 seconds	40
Annealing	62	30 seconds	
Extension	72	30 seconds	
	72	5 minutes	1

Table 2.6: The PCR cycle sequence for amplification of the *RPL30* locus from ChIP samples.

Confirmation of DNA concentration and fragment length using Bio-analyser

Following PCR confirmation of the ChIP samples, pre-sequencing assessments were carried out by Dr Michele Kiernan (Plymouth University) using high sensitivity DNA kits. First, the DNA samples were quantified using the Qubit® dsDNA High Sensitivity assay kit (Life Technologies) and a Qubit fluorometer.

Next, the size of the DNA fragments from each sample was assessed on the Agilent 2100 Bio-analyser system (Agilent Technologies, Cheshire, UK) using the High Sensitivity DNA Analysis Kit (Agilent Technologies #50674626,).

In brief, a gel-dye mix was prepared and loaded into a well-marked 'G' (in a black circle) on a High Sensitivity DNA chip fixed to a chip priming station. A plunger was lowered and held in position for 1 minute before slowly pulling the plunger back to the 1mL position. More gel mix was loaded into the remaining 'G' wells to complete loading of the gel-dye mix.

Next, the marker, ladder and samples were loaded into allocated wells. The chip was vortexed for 1 minute at 2400rpm and loaded onto the bio-analyser instrument within 5 minutes. Results were acquired using 2100 Expert Software (version B.02.08, Agilent Technologies).

Prior to the assessment of individual samples, the gel and electropherogram of the DNA Ladder was evaluated to ensure that the required peaks were visible, all peaks were adequately defined, the baseline was flat and there was correct identification of both markers.

2.5.7 Next generation sequencing (NGS)

All sequencing procedures (including library preparation, sequencing and initial analysis) were performed by Dr Michele Kiernan (Plymouth University).

Purified DNA from the ChIP sample was sequenced using an Ion personal genome machine (Ion PGM) (Ion Torrent). The ChIP sequencing data was imported on to a bioinformatics system and analysed using CLC Workbench software (version 11.1). Peaks were aligned to the human genome using the reference HG38.

Chapter 3- Characterising MCL cell line models of BTKi sensitivity and resistance

3.1 Introduction

Inhibitors of BTKi have shown a significant clinical effect in the treatment of MCL, however one third of MCL patients have primary resistance to BTKi and a proportion of responding patients develop secondary resistance and aggressive relapse. Current therapies are less effective in relapsed cases, indicating the need to investigate the mechanisms underlying the cellular sensitivity of MCL to BTKi, and to discover biomarkers of BTKi resistance so that alternative treatments targeting specific resistance mechanisms can be used.

Due to the complications associated with the culturing of primary MCL cells, the characterisation of MCL cell line models which have defined sensitivity or resistance to BTKi was of particular importance.

This chapter describes the characterisation of MCL cell line models of BTKi sensitivity and resistance and subsequent development of a cell line model with acquired BTKi resistance. Our aim was to define these cell line models to allow identification of specific functional and signal responses to BTKi which may ultimately identify biomarkers which predict response to treatment with BTKi in MCL.

Sensitivity to BTKi was assessed through functional assays of apoptosis and proliferation, linking these to responses of key BCR signalling proteins – pBTK and pERK1/2 and assessing the role of IRF4 as a potential biomarker of BTKi sensitivity.

3.2 Methods employed

The methods employed in this chapter involve the general culture of four validated MCL cell lines (REC-1, G519, JEKO-1 and JVM2) (Methods section 2.2.4). These cell lines

were assessed by flow cytometry for apoptosis (annexin V-FITC) and proliferation (Ki-67-FITC) in response to varying concentrations of Ibr or Acal (Methods section 2.2.9).

The cell line displaying BTKi sensitivity (REC-1) was additionally continuously treated with BTKi (Ibr / Acal) to generate an *in vitro* model of acquired BTKi resistance (Methods section 2.2.10).

Assessment of responses by key signalling proteins of the BCR pathway following BTKi treatment were determined through biochemical assays (Methods section 2.4) of 1D-SDS PAGE (section 2.4.3) , western blotting (section 2.4.6) and immunohybridisation (section 2.4.6.1) using cell lysates or by flow cytometry following IgM stimulation (Methods section 2.2.8 and 2.3.2) .

A table of antibodies/probes used in this chapter is shown below (Table 3.1).

All data (flow cytometry and western blotting) were analysed using Microsoft Excel™ and GraphPad Prism™ Version 5 software. The statistical tests employed are described in the figure legend of each experiment.

Antibody/probe	Species	Application	Ref	Source	Conc
Annexin-V-FITC		FC	556419	BD	5ul/test
Ki67 (IgG1k) -FITC	**Mouse anti human**	FC	556026	BD	10ul/test
BTK pY223 (IgG1k) -PE	**Mouse anti human**	FC	562753	BD	5ul/test
BTK pY551 (IgG1k)-PE	**Mouse anti human**	FC	558129	BD	10ul/test
BTK (IgG2a)-PE	**Mouse anti human**	FC	558527	BD	20ul/test
IgG1k isotype-FITC	**Mouse anti human**	FC	556026	BD	10ul/test
IgG1k isotype-PE	**Mouse anti human**	FC	559320	BD	10ul/test
IgG1k isotype-APC	**Mouse anti human**	FC	555751	BD	10ul/test
IgG2ak isotype-PE	**Mouse anti human**	FC	555574	BD	20ul/test
IRF4 primary antibody	**Rabbit anti human**	WB	#4964	CST	1/1000
pERK1/2 primary antibody	**Rabbit anti human**	WB	#9101	CST	1/2000
ERK1/2 primary antibody	**Rabbit anti human**	WB	#9102	CST	1/2000
GAPDH primary antibody	**Rabbit anti human**	WB	#2118	CST	1/5000
Secondary antibody-HRP	**Goat anti rabbit**	WB	#P0448	Dako	1/2000

Table 3.1: Antibodies/probes used in chapter 3. FC = flow cytometry, WB= western blotting, BD = BD Biosciences, CST= Cell signalling technology.

3.3 REC-1 cells demonstrate increased apoptosis in response to Ibr but not Acal.

Of the four mantle cell lymphoma cell lines assessed, REC-1 cells showed sensitivity to Ibr with increased apoptosis in a dose and time dependent manner. This effect on apoptosis was found to be less apparent following treatment with the more selective BTKi Acal.

3.3.1 Assessment of apoptosis in MCL cell lines in response to Ibr

Cell lines were tested for their apoptotic response to increasing concentrations of Ibr or Acal at regular time points over 72 hours. In REC-1 cells, apoptosis was induced by Ibr in a dose and time dependent manner indicating sensitivity to BTKi (Figure 3.1). This was confirmed by linear regression analysis (Figure 3.2) which showed a positive correlation between Ibr concentration and the percentage of apoptosis which was most significant after 72 hours (R^2=0.71). However, more than 60% of the REC-1 cells remained viable after 72 hours even at the highest dose used (10µM).

Unlike REC-1, the G519 cells showed no induction of apoptosis above baseline level at any concentration of Ibr, suggesting resistance to BTKi (Figure 3.1). In the JEKO-1 cells, apoptosis was increased by 7% after 24 hours, although only at a very high concentration (10µM) and there was no further increase over the 72 hours. In the JVM2 cells, there was a slight increase in apoptosis after 24 hours at 1µM, although this was not much higher than the baseline cell death over the 72 hours. Significant apoptosis was observed in this cell line at the highest dose (10µM), however this was not seen at lower doses suggesting this might be an off-target drug effect.

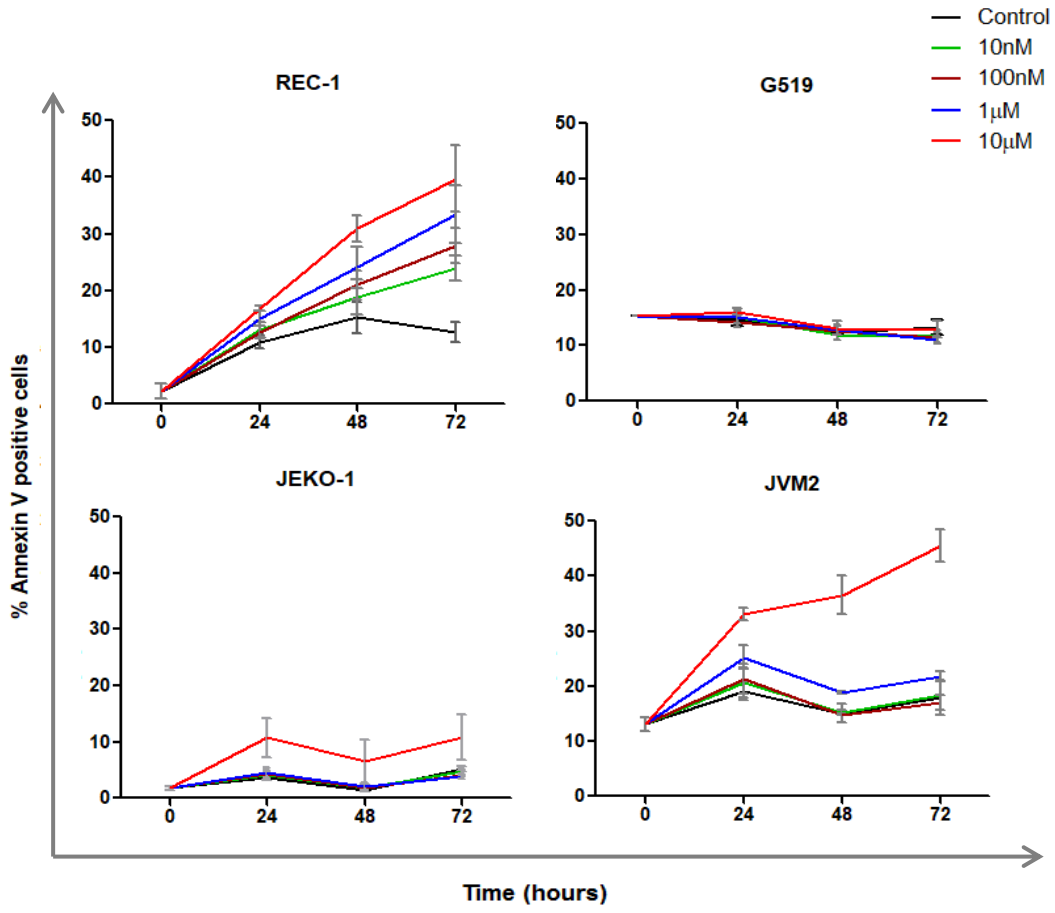

Figure 3.1: Cell death response to Ibr in MCL cell lines. Cells were seeded at 5 x 10^5/mL, treated with DMSO (vehicle) or increasing concentrations of Ibr (FC: 10nM, 100nM, 1μM and 10μM). Cell death was determined by flow cytometry with annexin V-FITC staining at each concentration after 24, 48 and 72 hours incubation (N=3).

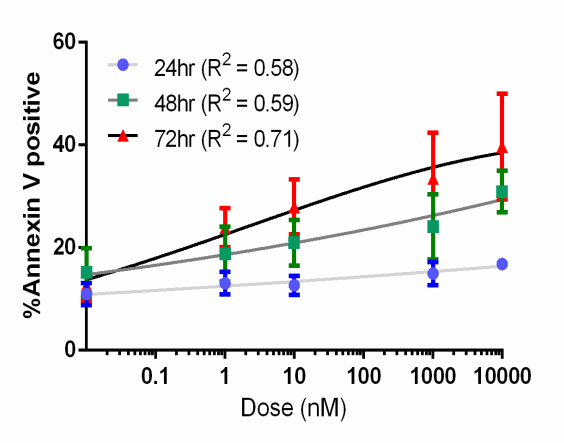

Figure 3.2: Regression analysis of Ibr concentration and apoptosis in REC-1 cells. The graph shows log (Gaussian) non-linear correlation curves showing a positive correlation between concentration of Ibr and apoptosis of REC-1 cells at each time point with the greatest correlation at 72 hours (R^2 =0.71) N=3.

3.3.2 Assessment of apoptosis in MCL cell lines in response to Acal

In response to the more selective BTKi (Acal), apoptosis was only minimally increased in REC-1 cells compared to the control cells and only at doses >100nM. Apoptosis was only increased by Acal by 6% after 72 hours at high dosage (10µM) (Figure 3.3A), indicating that Acal induces less apoptosis when compared to Ibr at the equivalent doses. In G519 cells there was no induction of apoptosis above baseline level at any concentration of Acal (Figure 3.3B), which is equivalent to the lack of apoptosis seen with Ibr. In response to a higher dose range of Acal (1-100µM), apoptosis of REC-1 cells did not significantly increase until the dose reached 100µM (Figure 3.3C), and with approximately 55% of the cells still viable after 48 hours, even this extreme dose was insufficient to cause complete cytotoxicity. Apoptosis of the resistant G519 cells was also increased at this dose, suggesting off target effects due to the very high concentration of Acal (or DMSO).

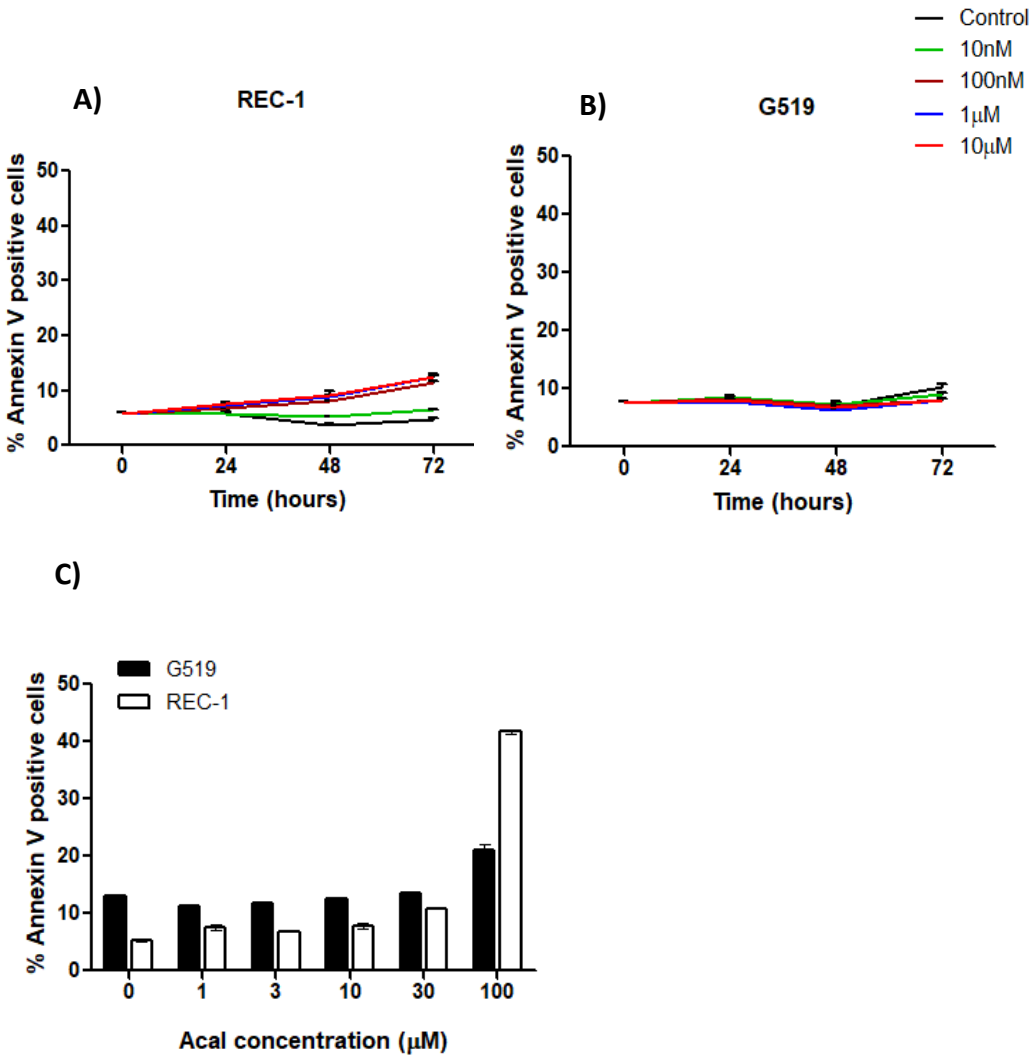

Figure 3.3: Cell death response to Acal in MCL cell lines. Cells were seeded at 5 x 10^5/mL, treated with DMSO (vehicle) or increasing concentrations of Acal. Cell death was determined by flow cytometry with annexin V-FITC staining at each concentration after 24, 48 and 72 hours incubation. A) REC-1, and B) G519 over a 72 hour time course with Acal (FC: 10nM, 100nM, 1µM, 10µM). C) G519 and REC-1 cells after 48 hours Acal treatment using a higher dose range (FC: 1µM, 3µM 10µM, 30µM, 100µM).

3.4 REC-1 cells demonstrate reduced proliferation in response to both Ibr and Acal

The proliferation of REC-1 cells is markedly sensitive to both Ibr and Acal with reduction in proliferation seen early (24 hours) and at very low concentrations (nM). This contrasts to the other MCL cell lines, particularly G519 cells and represents a laboratory assessment to determine BTKi sensitivity.

3.4.1 Assessment of proliferation in MCL cell lines in response to Ibr

The cell lines were tested for changes to proliferation in response to increasing concentrations of Ibr. In REC-1 cells, proliferation was reduced by Ibr equally at all doses tested (10nM, 100nM, 1μM, 10μM) as early as 24 hours after treatment (Figure 3.4A). This reduction was time dependant; with proliferation reduced to approximately 30% of control levels after 72 hours of treatment, but not dose dependant suggesting the proliferation of REC-1 cells may be reduced at lower doses of Ibr.

In response to a lower dose range of Ibr, the reduction of REC-1 cell proliferation was shown to occur at doses as low as 1nM after only 24 hours treatment (Figure 3.4D). In contrast, the G519 cells did not show any reduction of proliferation over baseline levels over the 72 hours treatment with Ibr at the highest dose (10μM) (Figure 3.4B) which correlates with the survival of G519 cells in response to Ibr.

The JEKO-1 and JVM2 cells were also analysed for the percentage of Ki67 positive cells after 48 hours treatment. Like G519, the JEKO-1 cells did not indicate any reduction in proliferation above baseline at any dose but the JVM2 cells showed a considerable reduction in proliferation at the highest dose (10μM) (Figure 3.4C), which correlates

with the increased death of these cells only at 10μM and indicating likely off target drug effects.

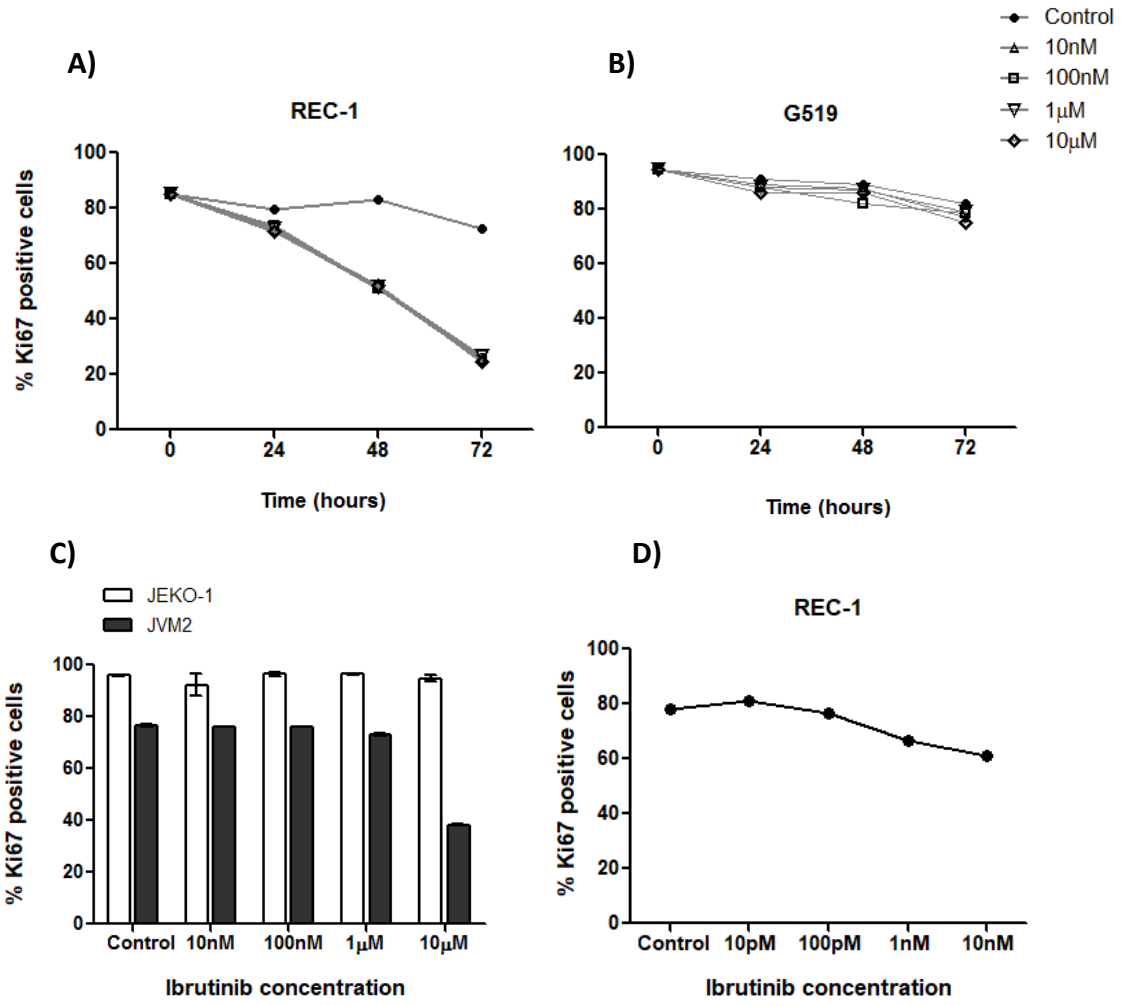

Figure 3.4: Proliferation response to Ibr in MCL cell lines. Cells were seeded at 5 x 10^5/mL, treated with DMSO (vehicle) or increasing concentrations of Ibr as indicated. 1 x 10^6 cells at each concentration were taken at various time points, and stained with a Ki67-FITC antibody for analysis by flow cytometry. Cell proliferation was determined by analysing the percentage of KI67-FITC positive cells against an isotype control using an IgG1-FITC antibody (N=2). A) Proliferation of REC-1 and B) G519 in response to Ibr over a 72 hour time course. C) Proliferation of JEKO-1 and JVM2 cells after 48 hours Ibr treatment. D) Proliferation of REC-1 cells in response to a low dose range of Ibr (10pM, 100pM, 1nM, 10nM).

3.4.2 Assessment of proliferation in MCL cell lines in response to Acal

In response to Acal, the G519 cells showed no reduction of proliferation (<10µM after 72 hours) (Figure 3.5), therefore providing more evidence that these cells are resistant to BTKi. The REC-1 cells showed a 32% reduction in proliferation after 72 hours of Acal treatment at a dose of 100nM (Figure 3.5), 100 fold higher than that seen with Ibr, demonstrating sensitivity to Acal, despite the lack of correlative apoptosis of the cells in response to Acal.

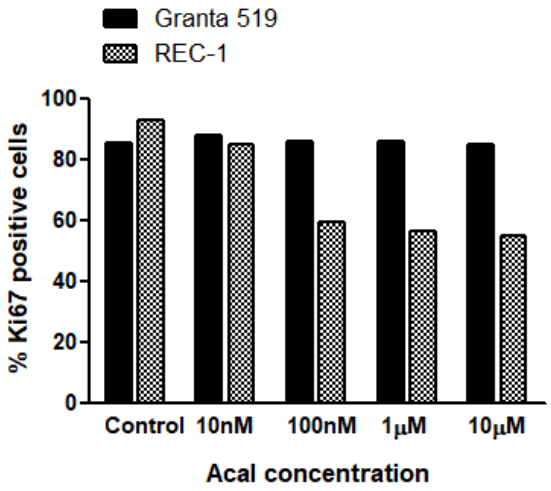

Figure 3.5: Proliferation response to Acal in MCL cell lines. Cells were seeded at 5 x 10^5/mL, treated with DMSO (vehicle) or increasing concentrations of Acal as indicated. 1 x 10^6 cells at each concentration were taken at various time points, and stained with a Ki67-FITC antibody for analysis by flow cytometry. Cell proliferation was determined by analysing the percentage of Ki67-FITC positive cells against an isotype control using an IgG1-FITC antibody. Proliferation of G519 and REC-1 cells after 72 hours Acal treatment.

3.4.3 Comparison of proliferation in REC-1 cells in response to Ibr or Acal

In a separate experiment, the proliferation of REC-1 cells was compared following treatment with either Ibr or Acal at a single effective dose (100nM). Proliferation was reduced equally in response to Ibr and Acal (100nM) from 24 to 72 hours (Figure 3.6). *In vitro* assays assessing proliferation were found to be a more sensitive indicator of BTKi effect than assays of apoptosis. Proliferation was therefore used as a measure of BTKi sensitivity for subsequent experiments.

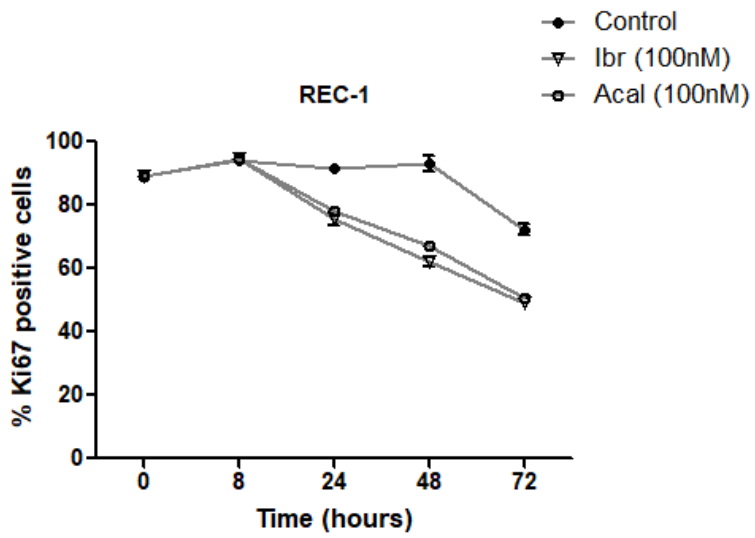

Figure 3.6: Proliferation response to Ibr versus Acal in REC-1 cells. Proliferation of REC-1 cells in response to Ibr or Acal treatment (100nM).

3.5 All MCL cell lines show increased levels of phosphorylated BTK (Y223) following BCR activation and down-regulation with Ibr

The activity of BTK can be assessed through flow cytometric assessment of the intracellular phosphorylation of BTK at tyrosine 233 (Y223). All 4 MCL cell lines irrespective of their sensitivity to treatment with BTKi showed a functional BCR with an increase in phosphorylated BTK (Y233) following anti-IgM stimulation and inhibition of this response by Ibr.

Having established that REC-1 cells were sensitive to BTKi treatment it was important to assess BTK activity between the different cell lines. Previous experiments from the group showed that assessment of BTK phosphorylation was difficult with western blotting and antibody hybridisation. We therefore assessed BTK phosphorylation by flow cytometry (Methods section 2.3.2) using an antibody to BTK, and the Y223 and Y551 phosphorylation sites of BTK (Table 3.1).

3.5.1 Baseline assessment of BTK activity in REC-1 cells following Ibr treatment

The sensitive cell line REC-1 was first analysed for total levels of BTK and BTK phosphorylation at Y551 and Y223 at baseline, and after 1 hour treatment with Ibr (10µM). REC-1 cells showed low levels of total BTK and phosphorylated BTK at Y551, however phosphorylation at Y223 was readily detected in unstimulated REC-1 cells and phosphorylation was reduced by Ibr (10µM) after 1 hour (Figure 3.7). Upon B cell receptor (BCR) stimulation, Y223 is auto-phosphorylated which subsequently activates the enzymatic activity of BTK. With these results, we therefore used phosphorylation of BTK at Y223 as a surrogate marker of BTK activity.

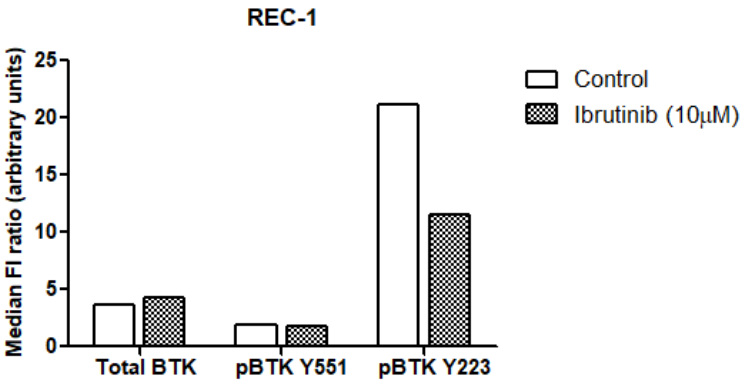

Figure 3.7: Comparison of BTK phosphorylation and total BTK levels in unstimulated REC-1 cells before and after 1 hour of Ibr treatment. REC-1 cells were treated with 10μM Ibr for 1 hour and analysed for phosphorylated BTK and total BTK levels by flow cytometry. Bars represent the median fluorescence intensity ratios (PE marker/PE isotype control), units are arbitrary.

3.5.2 Assessment of Ibr treatment on basal levels of Y223 BTK phosphorylation in all MCL cell lines

All MCL cell lines (REC-1, G519, JEKO-1, JVM2) were subsequently analysed for levels of BTK phosphorylation at Y223 at baseline and after 1 hour treatment with Ibr (100nM, 10μM). Ibr inhibited the activity of BTK in a dose dependent manner in all cell lines (Table 3.2, Figure 3.8) emphasising that sensitivity to BTKi treatment was through modulation of pathways downstream of the BCR and BTK molecule.

Ibr	REC-1	G519	JEKO-1	JVM2
Control	16.03268	5.309242	7.676796	16.12012
100nM	9.558824	3.386256	4.588398	10.48649
10µM	5.348039	2.446682	3.44337	3.45045

Table 3.2: Median fluorescence intensity ratios (MFIR) for BTK phosphorylation at Y223 in unstimulated MCL cell lines in response to Ibr. Each MCL cell line was treated with Ibr (100nM and 10µM) for 1 hour. The table data represents the raw MFIR values for pBTK Y223 obtained for each unstimulated cell line before and after 1 hour incubation with Ibr (100nM and 10µM). Ratios calculated by marker / isotype control. MFIR expressed in arbitrary units.

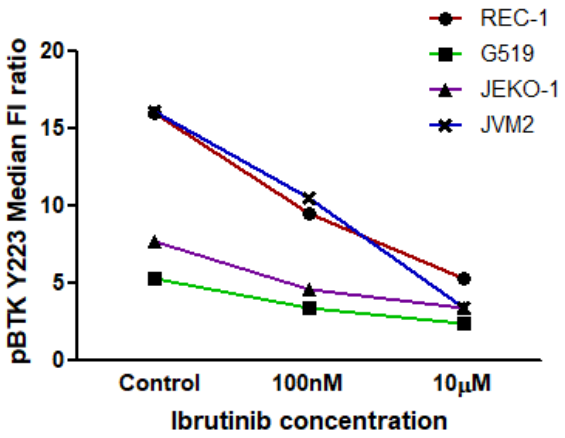

Figure 3.8: Reduction of pBTK Y223 following 1 hour Ibr treatment in unstimulated MCL cell lines. Lines represent the median fluorescence intensity ratios (expressed in arbitrary units) for pBTK Y223 (Table 3.2) illustrating the effect of IgM stimulation on BTK phosphorylation in each cell line at each time point, and the reduction of pBTK Y223 after 1 hour Ibr treatment.

3.5.3 Assessment of Ibr treatment on Y223 BTK phosphorylation following BCR activation

Most BCR in MCL are IgM and can be stimulated via cross-linking with an anti-IgM antibody. MCL cell lines were stimulated with anti-IgM for a varying length of time to determine the optimal response to BTK phosphorylation. In all MCL cell lines, pBTK-Y223 rapidly developed following BCR activation and returned to near basal levels after 60 minutes (Figure 3.9). REC-1 cells showed the greatest increase after 1 minute IgM stimulation.

A)

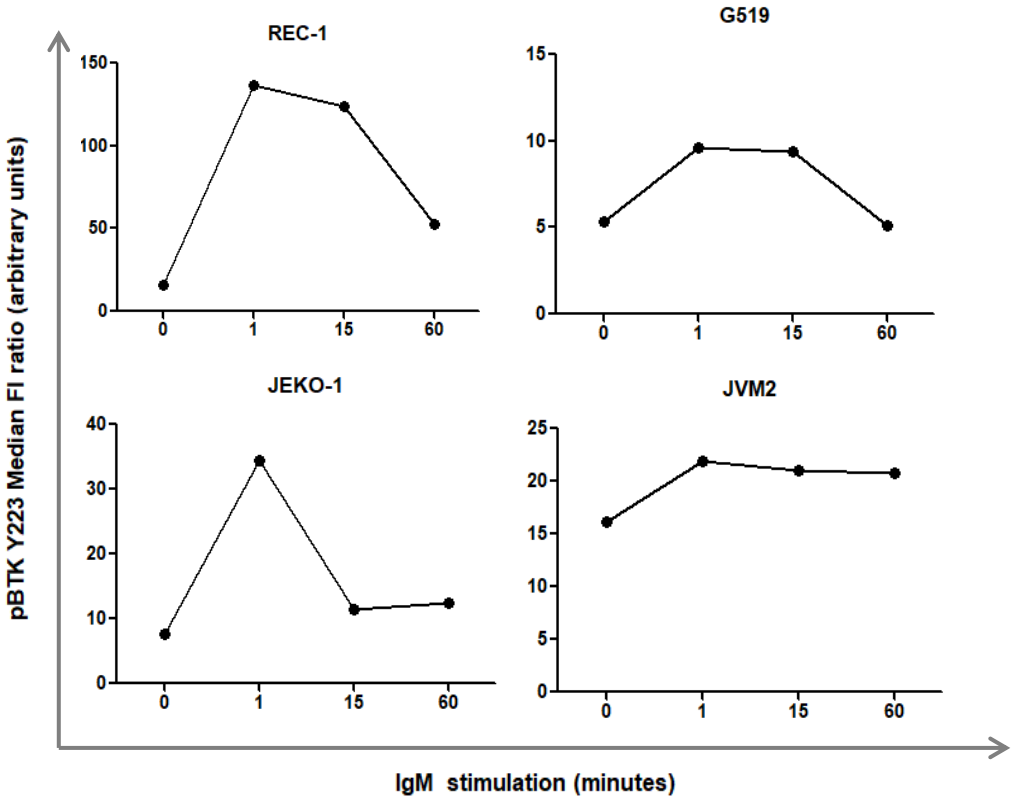

B)

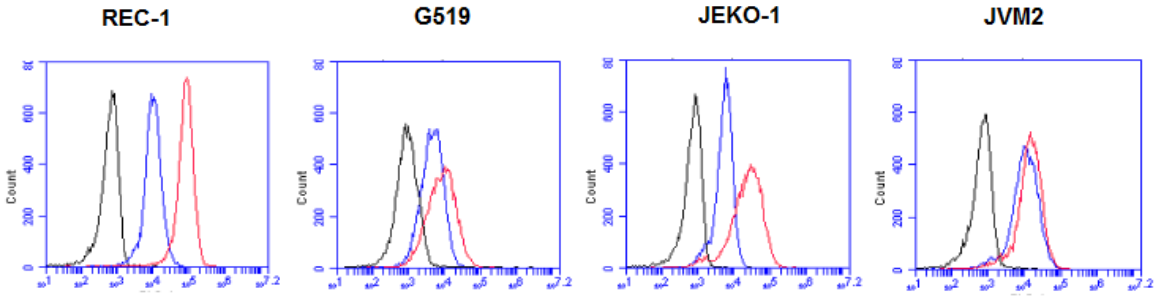

Figure 3.9: Levels of pBTK Y223 in MCL cell lines following IgM stimulation. A) Graphical representations of pBTK Y223 median fluorescence intensity ratios (MFIR) in all MCL cell lines stimulated with IgM at various time intervals over 1 hour. B) Flow cytometry peak plots showing baseline levels of pBTK Y223 (blue) against an IgG1 isotype control (black) and the increase in pBTK Y223 following IgM stimulation for 1 minute (red). All cell lines responded to IgM stimulation at varying degrees but REC-1 showed the greatest increase after 1 minute.

Phosphorylation levels at Y223 of BTK were then determined before and after Ibr treatment in response to BCR stimulation for 1, 15 and 60 minutes. The addition of Ibr reduced phosphorylation of BTK-Y223 in all IgM stimulated cells in a dose dependent manner, as indicated by the reductions in MFI ratio with increasing dosage (Table 3.3, Figure 3.10), emphasising as in Figure 3.8 that all cells behave similarly whether they are sensitive or resistant to BTKi, suggesting that other signalling events further downstream from BTK may define sensitivity or resistance to BTKi in MCL.

	REC-1	**G519**	**JEKO-1**	**JVM2**
Unstimulated				
Control	16.03268	5.309242	7.676796	16.12012
100nM Ibr	9.558824	3.386256	4.588398	10.48649
10µM Ibr	5.348039	2.446682	3.44337	3.45045
IgM: 1 minute				
Control	136.3905	9.640995	34.36602	21.86411
100nM Ibr	130.1757	8.055687	24.65953	14.69745
10µM Ibr	39.52451	2.470379	3.296961	4.310811
IgM: 15 minutes				
Control	123.634	9.356635	11.3826	20.96547
100nM Ibr	105.9273	4.753555	19.96478	14.82432
10µM Ibr	62.98448	2.058057	7.259669	4.283784
IgM: 60 Minutes				
Control	52.58824	5.103081	12.33564	20.7455
100nM Ibr	41.91503	4.712085	8.13674	14.80931
10µM Ibr	29.85621	1.906398	4.05663	5.261261

Table 3.3: Median fluorescence intensity (MFI) ratios for pBTK Y223 following Ibr treatment in IgM stimulated MCL cell lines. The table data represents the raw MFI Ratio values for pBTK Y223 obtained for each IgM stimulated cell line before and after 1 hour incubation with Ibr (100nM and 10µM). MFI ratios were calculated by PE marker / PE isotype control. MFI ratios are expressed in arbitrary units.

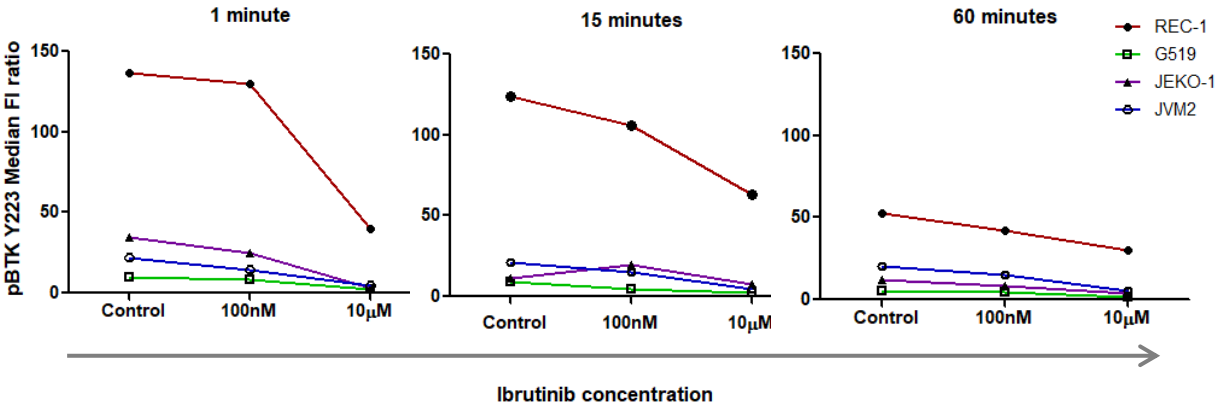

Figure 3.10: Reduction of pBTK Y223 following 1 hour Ibr treatment in four MCL cell lines stimulated with IgM over time. Lines represent the median fluorescence intensity ratios (expressed in arbitrary units) for pBTK Y223 (Table 3.3) illustrating the effect of IgM stimulation on BTK phosphorylation in each cell line at each time point, and the reduction of pBTK Y223 after 1 hour Ibr treatment.

3.6 All MCL cell lines showed downregulation of phosphorylated ERK (pERK) in response to Ibr, however pERK induced by BCR activation was only partially downregulated.

The extracellular signal regulated kinase (ERK), is located directly downstream from BTK. All 4 MCL cell lines whether showing sensitivity to treatment with BTKi showed inhibition of baseline levels of phosphorylated ERK (pERK) with Ibr. Following BCR activation with anti-IgM, levels of pERK were increased but only partly reduced by Ibr in both REC-1 and G519 cells.

3.6.1 Assessment of ERK activity in REC-1 cells following treatment with Ibr

The sensitive REC-1 cells were first treated with three concentrations of Ibr (10nM, 1µM, 10µM) for 4 hours, and levels of ERK1/2 phosphorylation were assessed in protein lysates through immunohybridisation (Methods section 2.4.6.1). Total levels of ERK 1/2 were abundant at each concentration. However, ERK1/2 phosphorylation (pERK) was downregulated by Ibr at all concentrations compared to the control cells (Figure 3.11), suggesting phosphorylation of ERK1/2 results from BTK activity in unstimulated REC-1 cells and that the BTK/ERK signalling pathway is involved in BTKi treatment response in sensitive MCL cells.

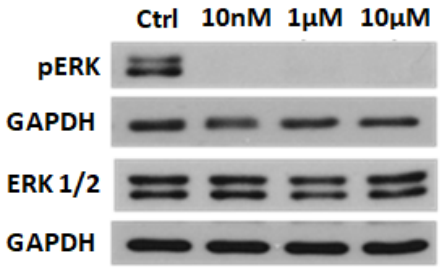

Figure 3.11: Immunoblot analysis of phosphorylated ERK (pERK) levels in REC-1 cells pre and post Ibr treatment for 4 hours. REC-1 cells were seeded at 5 x 10^6/mL and treated with a DMSO vehicle or Ibr at a range of doses (10nM, 1μM and 10μM). The cells were lysed after 4 hours incubation with Ibr. 10% SDS gel. 25μg protein. pERK (Cell Signalling technology #9101) 1 in 2000 dilution, ERK1/2 (Cell signalling technology #9102) 1 in 2000 dilution, GAPDH (Cell Signalling technology #2118) 1 in 5000 dilution in 5% BSA/TBST, o/n at 4°C. Goat anti-rabbit-HRP (Dako, P0448) 1 in 2000 dilution (pERK, ERK1/2) 1 in 5000 dilution (GAPDH) in 5% BSA/TBST, 1 hr, RT. ECL (Pierce, Life Technologies).

3.6.2 Assessment of Ibr action on levels of phosphorylated ERK in all MCL cell lines

To determine whether the downregulation of ERK phosphorylation was observed in all cell lines in response to BTKi and whether it was a transient or a continuous effect sustained over time, all four cell lines including REC-1 were treated with a single concentration of Ibr (10μM), and ERK1/2 phosphorylation was assessed at regular time points (as indicated) over 48 hours (Figure 3.12). Levels of total ERK1/2 in all 4 MCL cell lines remained fairly constant in all unstimulated cells over 48 hours. However inhibition of ERK1/2 activity (measured as pERK) by Ibr, was observed in all MCL cell lines, both sensitive and resistant, therefore levels of pERK do not define sensitivity to BTKi, however it does suggest that BTKi have an effect on the MAP kinase pathway in these cell lines.

For the REC-1 and G519 cells, pERK levels were normalised to ERK1/2. A paired t-test was used to compare pERK levels in control cells versus Ibr treated cells at

corresponding time points (Figure 3.13). In REC-1 cells, pERK was reduced at as early as 1 hour following treatment and this reduction was statistically significant for up to 8 hours compared to the untreated REC-1 cells at corresponding time points ($p=0.0444$). However pERK levels started to increase again after 24 to 48 hours suggesting reactivation of the ERK pathway through alternative, redundant pathways. Levels of pERK were also reduced after 1 hour in G519 cells following Ibr treatment and this reduction was statistically significant for the entire 48 hours ($p=<0.0001$).

For JEKO-1 and JVM2 cells, pERK levels were normalised against GAPDH. The levels of pERK were significantly reduced after 1 hour of Ibr treatment and the reduction was sustained for 48 hours in both JEKO-1 cells ($p=0.0003$) and JVM2 cells ($p=0.0138$).

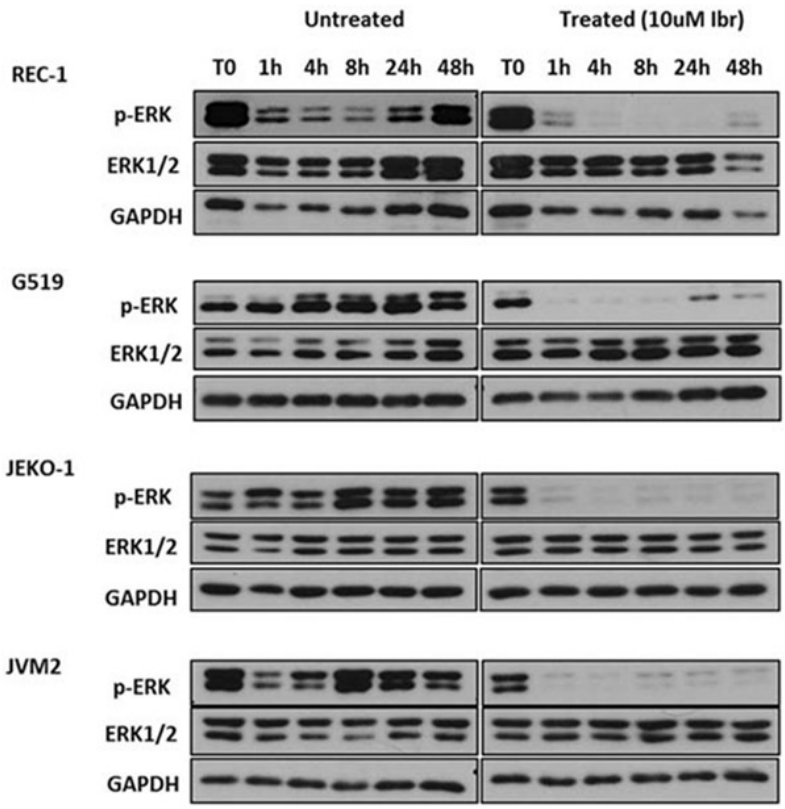

Figure 3.12: Immunoblot analysis of p-ERK and ERK1/2 in MCL cell lines pre and post Ibr treatment. REC-1, G519, JEKO-1 and JVM2 cells were seeded at 5 x 10^6/mL, treated with a DMSO vehicle or Ibr (FC: 10µM). Lysates were taken at time zero (T0), and after 1, 4, 8, 24 and 48 hours. 10% SDS gel. 15µg protein. p-ERK (Cell Signalling technology #9101) 1 in 2000 dilution, ERK1/2 (Cell signalling technology #9102) 1 in 2000 dilution, GAPDH (Cell Signalling technology #2118) 1 in 5000 dilution in 5% BSA/TBST, o/n at 4°C. Goat anti-rabbit-HRP (Dako, P0448) 1 in 2000 dilution (pERK, ERK 1/2) 1 in 5000 dilution (GAPDH) in 5% BSA/TBST, 1 hr, RT. ECL (Pierce, Life Technologies). One of two blots is shown for each cell line representing results of 2 independent experiments.

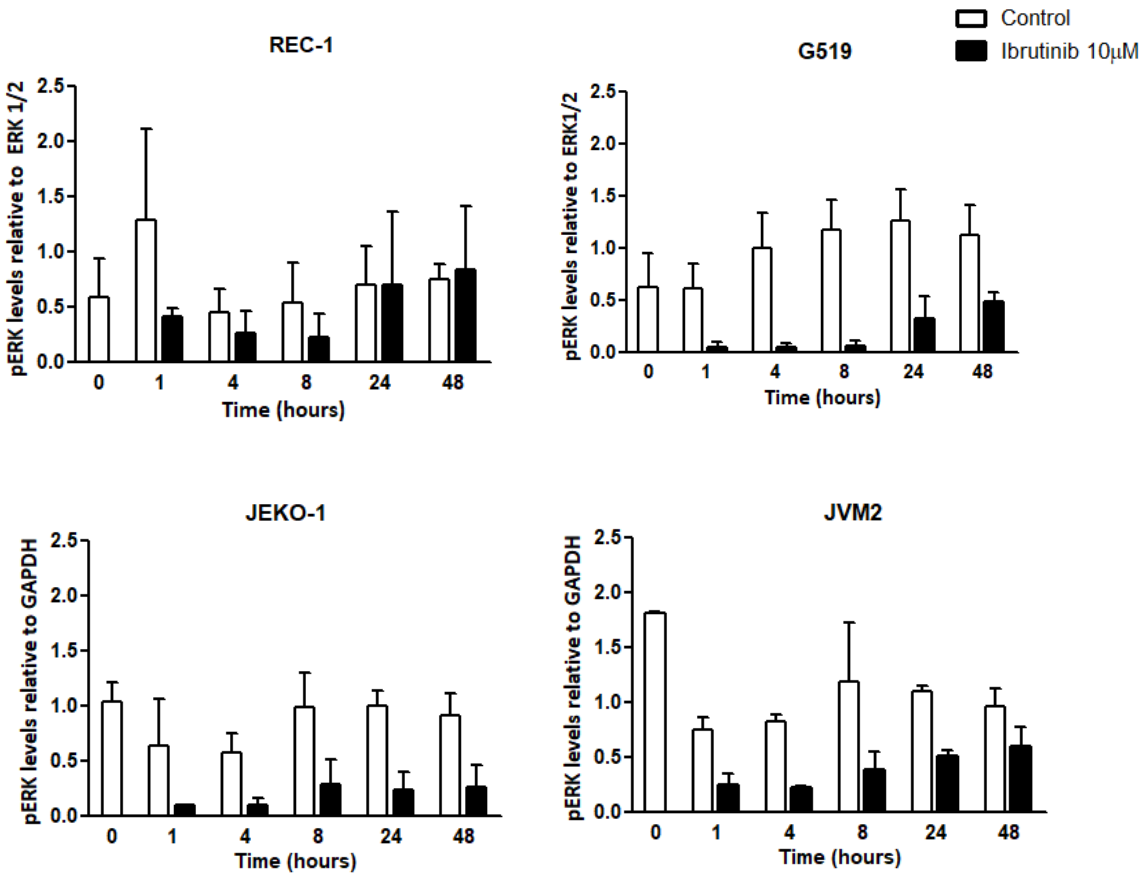

Figure 3.13: Densitometry analysis of the levels of pERK in MCL cell lines before and after treatment with Ibr (10μM). Levels of pERK were assessed by densitometry using Image J. P values were obtained by comparing the levels of pERK in untreated cells vs treated cells at each time point using paired t-test. Levels of pERK in REC-1 and G519 cells were normalised to ERK1/2. pERK was downregulated by Ibr in REC-1 cells for up to 8 hours (p= 0.0444) and for up to 48 hours in G519 cells (p=<0.0001). Levels of pERK in JEKO-1 and JVM2 were normalised to GAPDH. pERK was downregulated by Ibr for up to 48 hours in JEKO-1 cells (p=0.0003) and JVM2 (P= 0.0138).

3.6.3 Assessment of Ibr treatment on levels of phosphorylated ERK following BCR activation

To determine whether pERK expression changed following activation of the BCR, cells of one sensitive cell line (REC-1) and one resistant (G519) were treated with Ibr (10µM) and stimulated with anti-IgM for 15 minutes or 4 hours. Protein lysates were prepared from the cells after 8 hours and 24 hours incubation with Ibr.

Following cross-linkage of the BCR with anti-IgM after 15 minutes or sustained over 4 hours, ERK1/2 activation, as indicated by pERK, was induced in both sensitive REC-1 and resistant G519 cells, as already shown for BTK (pY223). Ibr had no effect on phosphorylated ERK levels following 8 hours of Ibr treatment. In REC-1 cells, levels of pERK appeared to be reduced by Ibr after 24 hours compared to the levels in G519 cells which were sustained (Figure 3.14), therefore upon BCR activation, pERK is only partially reduced by Ibr in both cell lines suggesting that ERK is additionally activated through alternative pathways to BTK and is not defining for sensitivity to BTKi. These results therefore suggest that pERK is not the best candidate for use as a biomarker to determine BTKi sensitivity.

REC-1 cells

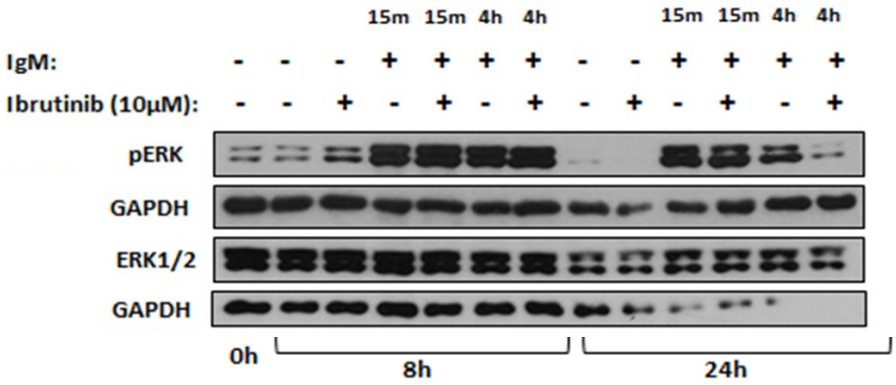

G519 cells

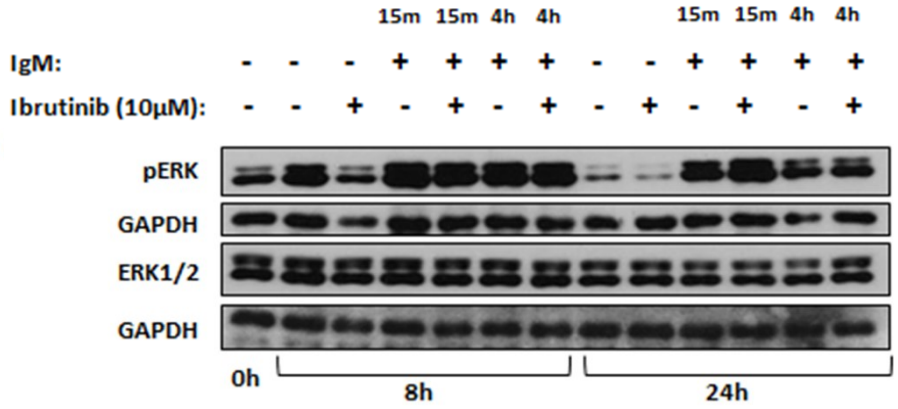

Figure 3.14: Immunoblot analysis of pERK and ERK1/2 in REC-1 and G519 cells (+/- IgM stimulation) pre and post Ibr treatment. REC-1 and G519 cells were seeded at 5 x 10^6/mL, treated with a DMSO vehicle or Ibr (FC: 10µM) and stimulated with anti-IgM (3µg/mL) for 15 minutes or 4 hours. The cells were lysed after 8 hours and 24 hours incubation with Ibr. 10% SDS gel. 15µg protein. p-ERK (Cell Signalling technology #9101) 1 in 2000 dilution, ERK1/2 (Cell signalling technology #9102) 1 in 2000 dilution, GAPDH (Cell Signalling technology #2118) 1 in 5000 dilution in 5% BSA/TBST, o/n at 4°C. Goat anti-rabbit-HRP (Dako, P0448) 1 in 2000 dilution (pERK, ERK1/2) 1 in 5000 dilution (GAPDH) in 5% BSA/TBST, 1 hr, RT. ECL (Pierce, Life Technologies).

3.7 IRF4 protein expression is downregulated following treatment with BTKi in REC-1 cells

IRF4 is downregulated following BTKi treatment (Ibr or Acal) only in sensitive REC-1 cells and not in resistant cell lines. IRF4 was downregulated early (8 hours) and at low concentration (nM). The expression level of IRF4 was not increased following BCR activation with anti-IgM and shows a differential response between sensitive and resistant cells with REC-1 cells showing a persistent down-regulation of IRF4 after 24 hours of Ibr treatment even following BCR activation with anti-IgM.

Preliminary results from this group identified IRF4 as a protein of interest following BTKi treatment in patients with CLL. This is maybe not surprising as IRF4 overexpression is seen in various subtypes of NHL including DLBCL and MM and downregulation of IRF4 in response to a combination of treatment with Ibr and lenolidamide has been shown in the ABC subtype of DLBCL.[173] However the role of IRF4 in response to BTKi treatment in MCL is currently unknown and was therefore investigated.

3.7.1 Assessment of levels of IRF4 in MCL cell lines following treatment with BTKi

All MCL cell lines were tested for baseline expression of IRF4 (by western blotting and immunohybridisation) and subsequent changes in expression following Ibr treatment (10µM). In all non-stimulated cells, IRF4 was consistently expressed in all four cell lines over a 48 hour time course (Figure 3.15). Treatment with Ibr had no effect on IRF4 expression in the resistant cell lines (G519, JEKO-1 and JVM2), however IRF4 was significantly downregulated by Ibr in sensitive REC-1 cells ($p= 0.0078$), commencing at around 4 hours and almost abolished by 48 hours, as determined by a paired t test of

the densitometry data (Figure 3.16). This precedes the Ibr-induced reduction in proliferation observed at 24 hours and the increased apoptosis observed at 24 to 48 hours.

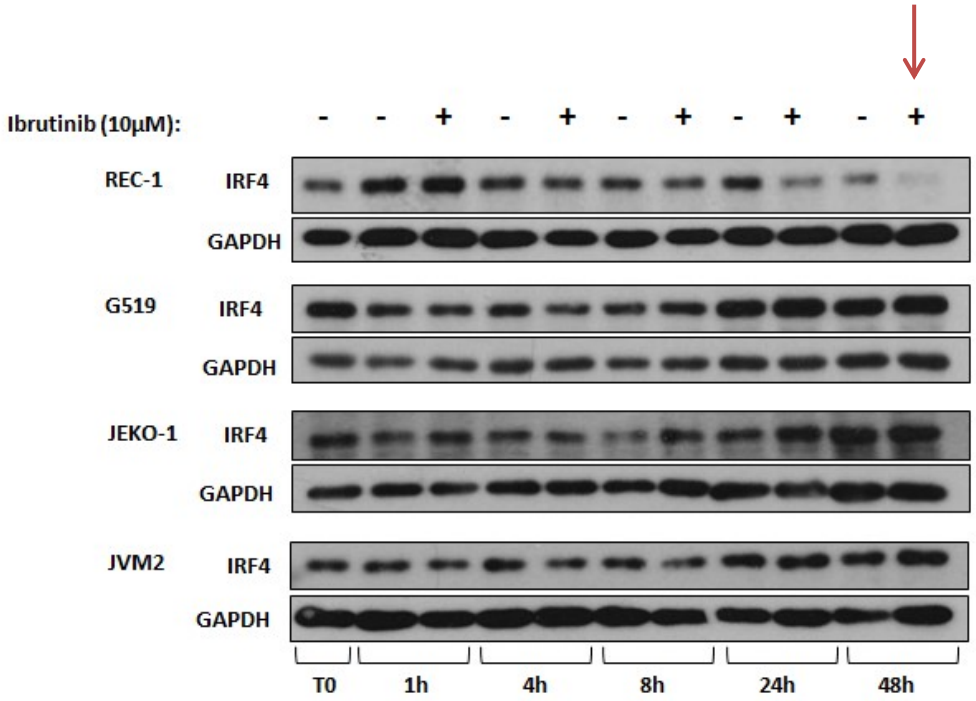

Figure 3.15: Immunoblot analysis of IRF4 in MCL cell lines pre and post Ibr treatment. The red arrow indicates downregulation of IRF4 expression after 48 hours Ibr treatment only in REC-1 cells. 10% SDS gel. 25.0μg protein. IRF4 (Cell Signalling technology #4964) 1 in 1000 dilution, GAPDH (Cell Signalling technology #2118) 1 in 5000 dilution in 5% BSA/TBST, o/n at 4°C. Goat anti-rabbit-HRP (Dako, P0448) 1 in 2000 dilution (IRF4) 1 in 5000 dilution (GAPDH) in 5% BSA/TBST, 1 hr, RT. ECL (Pierce, Life Technologies) (GAPDH) ECL prime (IRF4).

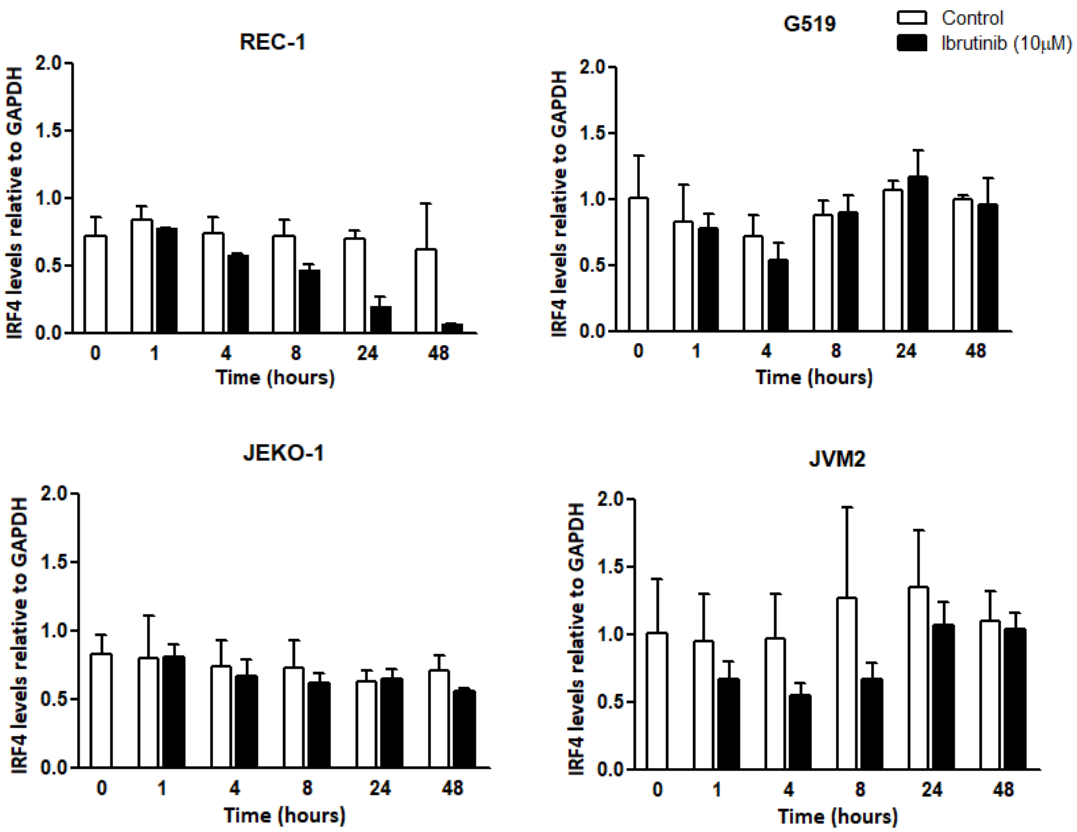

Figure 3.16: Levels of IRF4 in MCL cell lines before and after treatment with Ibr. Levels of IRF4 were assessed by densitometry using Image J and normalised to GAPDH. A paired t test was used to determine the significance of IRF4 downregulation in cells treated with Ibr (10μM) compared to the untreated cells. Error bars represent standard error of the mean of 2 independent experiments for each cell line.

To identify the particular dose of BTKi required to downregulate IRF4, and determine whether this dose would be therapeutically achievable *in vivo*, REC-1 cells were cultured as described above and treated with Ibr or Acal at a range of concentrations (10nM, 100nM, 1µM 10µM). Protein lysates were prepared from cells after 48 hours in culture.

IRF4 was shown to be downregulated by Ibr at a dose of 10nM while the dose required for Acal was 10 fold higher at 100nM (Figure 3.17). However, both doses were below the reported maximum achievable *in vivo* dosage for each drug (400nM for Ibr,[116,145] and 2µM for Acal (personal communication from Acerta Pharma).

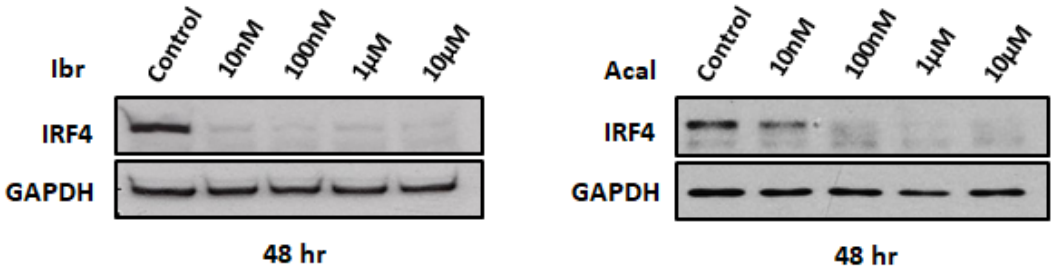

Figure 3.17: Immunoblot analysis of IRF4 in REC-1 cells pre, and 48 hours post BTKi treatment with Ibr and Acal. 10% SDS gel. 30.0µg protein. IRF4 (Cell Signalling technology #4964) 1 in 2000 dilution, GAPDH (Cell Signalling technology #2118) 1 in 5000 dilution in 5% BSA/TBST, o/n at 4°C. Goat anti-rabbit-HRP (Dako, P0448) 1 in 2000 dilution (IRF4) 1 in 5000 (GAPDH) in 5% BSA/TBST, 1 hr, RT. ECL (Pierce, Life Technologies).

3.7.2 Assessment of IRF4 expression in response to BCR activation and treatment with Ibr

To determine the expression of IRF4 following BCR activation with anti-IgM and BTKi treatment, both REC-1 cells and G519 cells were stimulated with anti-IgM for 15 minutes or 4 hours. Proteins were extracted after 8 hours and 24 hours incubation with Ibr (10µM).

Short-term or sustained BCR stimulation did not alter baseline levels of IRF4 in either REC-1 or G519 cells. However, IRF4 was clearly down-regulated in REC-1 cells following 24 hours of Ibr treatment, even in the presence of BCR activation (Figure 3.18).This change possibly occurred as early as 8 hours after Ibr treatment. Importantly in resistant G519 cells there was no downregulation of IRF4 seen in response to Ibr.

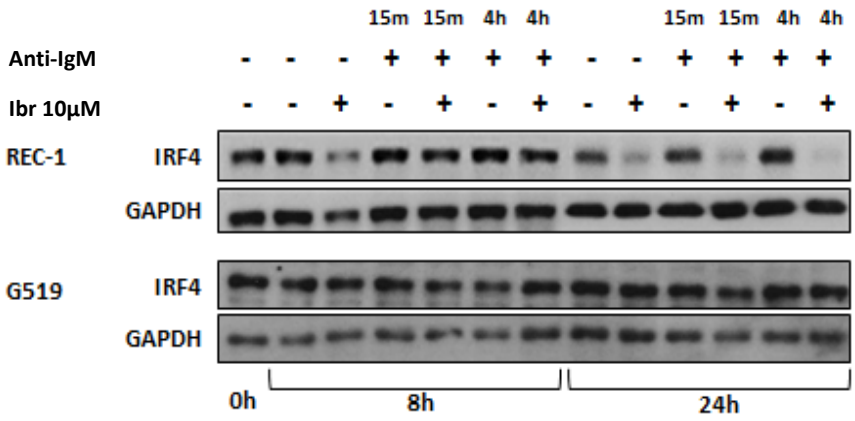

Figure 3.18: Immunoblot analysis of IRF4 in REC-1 and G519 cells treated with Ibr following acute and chronic BCR activation. 10% SDS gel. 20.0µg protein. IRF4 (Cell Signalling technology #4964) 1 in 2000 dilution, GAPDH (Cell Signalling technology #2118) 1 in 5000 dilution in 5% BSA/TBST, o/n at 4°C. Goat anti-rabbit-HRP (Dako, P0448) 1 in 2000 dilution (IRF4), 1 in 5000 dilution (GAPDH) in 5% BSA/TBST, 1 hr, RT. ECL (GAPDH), ECL prime (IRF4) (Pierce, Life Technologies).

3.8 IRF4 downregulation is not seen in cells which have acquired resistance to BTKi. These cells show stable levels of phosphorylated BTK following treatment with BTKi.

An *in vitro* model of acquired Ibr or Acal resistance was created using the REC-1 cell line. In contrast to the parent REC-1 cells, the resistant REC-1 cells demonstrated resistance to the actions of BTKi on survival and proliferation, with a possible increased baseline proliferation. Phosphorylated BTK (Y223) was not downregulated following BTKi treatment and levels of IRF4 were maintained.

3.8.1 Determination of BTKi resistance in REC-1 cells.

REC-1 cells were passaged in the presence of Ibr until stable resistance to Ibr was established, and then continuously treated at concentrations exceeding that of the maximum *in vivo* dose (>400nM). At a later stage in the study, REC-1 cells were also sensitised to Acal in the same way to generate a cell line model of Acal resistance (For full details on developing the resistant cell lines see Methods section 2.2.10).

The resistance status of the cells was determined by assessing the proliferation response to Ibr compared to the sensitive REC-1 cells. The REC-1 cells sensitised to 1μM of Ibr (REC-1/R (Ibr 1μM)) and to 3μM of Ibr (REC-1/R (Ibr 3μM)) were re- treated with 1μM and 3μM Ibr (respectively) along with the parent REC-1 control cells (REC-1/P) at the same dosage. A total volume of 1 x 10^6 cells was harvested from each sample at regular time points over 72 hours for analysis of proliferation by flow cytometry (Methods section 2.3.2).

Compared to the treated parental REC-1 cells, Ibr did not reduce proliferation of the Ibr sensitised REC-1 cells (at either dose). In fact, the sensitised cells were more proliferative than the parent untreated REC-1 control cells. A paired student t test

revealed that proliferation was significantly reduced in the 'parent' REC-1 cells treated with 1µM and 3µM doses of Ibr compared to the sensitised REC-1 cells treated with the corresponding doses at all time points (p= 0.0094) (Figure 3.19).

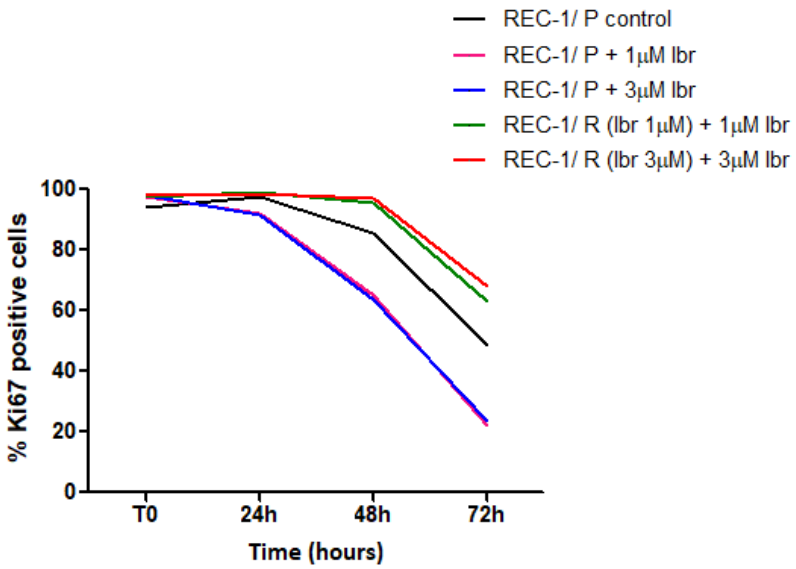

Figure 3.19: Proliferation response to Ibr in parent vs Ibr resistant REC-1 cell lines. Resistant REC-1 cells (one sensitised to 1µM and the other to 3µM Ibr) were washed in media to remove the drug after 72 hours of previous culture with Ibr. A volume of 12mL containing 3 x 10^5/mL cells at each concentration were added to clean culture flasks. An equal volume and density of parent REC-1 cells was added to 3 separate flasks. One flask of parent REC-1 cells was treated with DMSO (vehicle control) and cells in each other flask were treated with either 1µM or 3µM of Ibr. Approximately 1 x 10^6 cells from each flask were taken at the indicated time points over 72 hours, then fixed in PFA and permeablised in triton X-100, and stained with a Ki67-FITC antibody for analysis by flow cytometry. Cell proliferation was determined by analysing the percentage of Ki67-FITC positive cells against an isotype control using an IgG1-FITC antibody**.**

3.8.2 Assessment of IRF4 expression in BTKi resistant REC-1 cells

After resistance to both Ibr and Acal had been established in REC-1 cells (by showing no BTKi induced reduction of proliferation), an experiment was devised to identify changes in IRF4 expression compared to sensitive parent REC-1 cells in response to both BTK inhibitors to determine whether differences in IRF4 expression could be seen in cells of acquired BTKi resistance.

The REC-1 cells sensitised to 1µM of Ibr (REC-1/R (Ibr 1µM), 3µM of Ibr (REC-1/R (Ibr 3µM) and 1µM of Acal (REC-1/R (Acal 1µM) were re- treated with corresponding doses of Ibr or Acal along with the parent REC-1 control cells (REC-1/P) at the same dosage. Cells were removed from each sample after 72 hours incubation for analysis of apoptosis, proliferation and BTK Y223 phosphorylation by flow cytometry, and protein lysates were prepared for analysis of IRF4 expression by western blotting and immunohybridisation.

The parent REC-1 cells treated with Ibr (1µM and 3µM) showed downregulated IRF4 compared to the parent REC-1 control cells (as shown previously), while the acquired resistant REC-1 cells continuously treated with 1µM Ibr showed no downregulation of IRF4 in response to Ibr (Figure 3.20). These results match the findings for IRF4 expression in innate resistant cells (G519, JVM2 and JEKO-1 cells) in response to Ibr, providing more evidence that IRF4 could be a potential biomarker of BTKi sensitivity in MCL.

In the Ibr resistant REC-1 cells continuously treated with 3µM Ibr, IRF4 protein was not as expressed as the parent REC-1 control cells but was clearly more expressed than the parent REC-1 cells treated at this dose, indicating that a dose of 3µM was still having some effect on IRF4 downregulation. A likely explanation for this however looking at

the apoptosis/ proliferation responses is that the cells are yet to become totally resistant to 3μM at the time of this experiment. In the Acal resistant REC-1 cells continuously treated with 1μM Acal, again IRF4 protein was not as expressed as in the parent REC-1 control cells but was clearly more expressed compared to the parent REC-1 cells treated at the same dose of Acal. Again however at the time of the experiment the Acal resistant cell line was still in the process of being sensitised to 1μM suggesting that resistance at this dosage may not have been fully established.

The table below (Table 3.4) compares the survival and proliferation between parental cells treated with BTKi and corresponding acquired resistant cells. Overall survival and proliferation is maintained in acquired resistant cells compared to parental treated cells and is statistically significant (Figure 3.21) compared to parental treated cells. As highlighted above, survival and proliferation in the acquired Ibr resistance cells at 3μM was slightly reduced, suggesting these cells were not entirely resistant to Ibr at this dose.

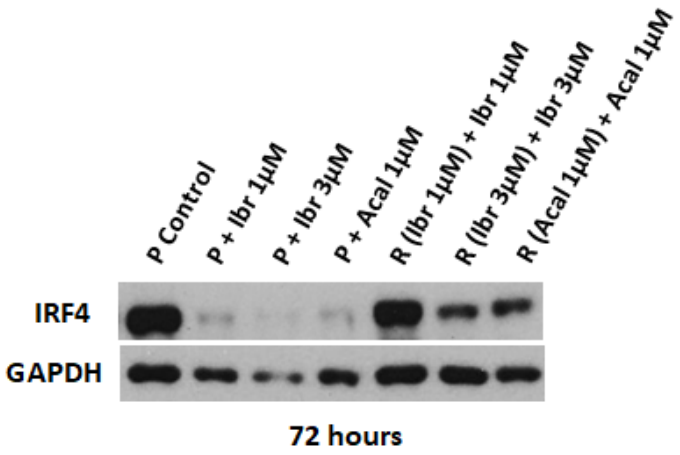

Figure 3.20: Immunoblot analysis of IRF4 expression in parent vs resistant REC-1 cells treated with BTKi. Parent (P) and resistant (R) REC-1 cells were treated with corresponding doses of Ibr or Acal (as indicated). Cells were lysed after 72 hours incubation and analysed for IRF4 expression by western blotting. 10% SDS gel. 20.0μg protein. IRF4 (Cell Signalling technology #4964) 1 in 2000 dilution, GAPDH (Cell Signalling technology #2118) 1 in 5000 dilution in 5% BSA/TBST, o/n at 4°C. Goat anti-rabbit-HRP (Dako, P0448) 1 in 2000 dilution (IRF4), 1 in 5000 dilution (GAPDH) in 5% BSA/TBST, 1 hr, RT. ECL (GAPDH), ECL prime (IRF4) (Pierce, Life Technologies).

	Apoptosis (%)	Proliferation (%)
P control	12.34	89.28
P + Ibr 1µM	19.22	37.84
P + Ibr 3µM	28.44	44.58
P+ Acal 1µM	16.68	47.56
R (Ibr 1µM) + Ibr 1µM	6.78	83.53
R (Ibr 3µM) + Ibr 3µM	16.21	79.82
R (Acal 1µM) + Acal 1µM	8.84	85.15

Table 3.4: Percentage of apoptosis and proliferation in parent vs resistant REC-1 cells treated with BTKi, corresponding to IRF4 expression (Figure 3.20). Parent (P) and resistant (R) REC-1 cells were treated with corresponding doses of Ibr or Acal (as indicated). Cells were removed after 72 hours incubation and analysed for apoptosis (Annexin V-FITC) and proliferation (Ki67-FITC) by flow cytometry.

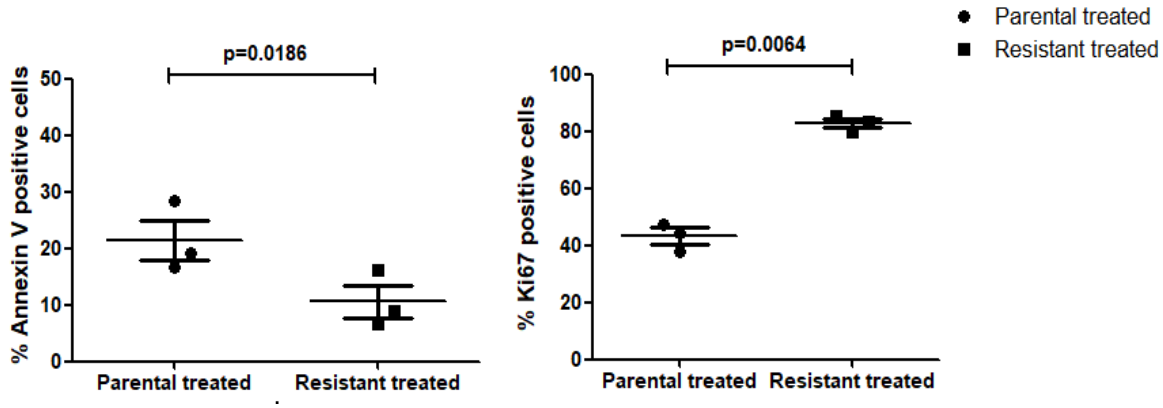

Figure 3.21: Paired t test comparing the percentage of apoptosis and the percentage of proliferation in parent vs resistant REC-1 cells treated with BTKi.

3.8.3 Assessment of BTK activity in REC-1 cells with acquired BTKi resistance

As previously shown, Ibr reduces basal levels of BTK phosphorylation (pBTK-Y223) in all MCL cell lines including REC-1 (Table 3.2). However, in the acquired resistant Ibr and Acal REC-1 cells, no reduction in pBTK Y223 is seen, as demonstrated by the increased median fluorescence intensity ratios for pBTK Y223 compared with the parent REC-1 control cells (Figure 3.22). It is possible that the resistant cell lines have developed a BTK mutation causing ineffective binding of BTKi to the BTK catalytic site and therefore BTK phosphorylation is no longer reduced in response to BTKi.

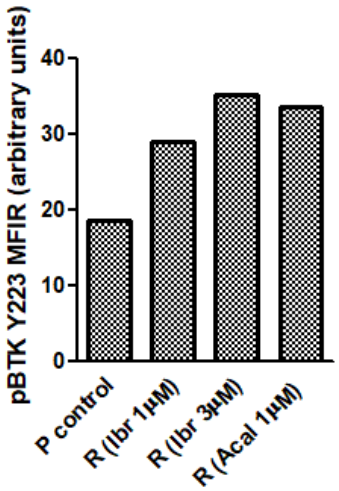

Figure 3.22: Median fluorescence intensity ratios (MFIR) for pBTK Y223 following BTKi treatment in parent REC-1 control cells vs resistant REC-1 cells. Parent (P) REC-1 control cells treated with DMSO and Resistant (R) REC-1 cells treated with corresponding doses of Ibr (1μM/3μM) or Acal (1μM) were removed after 72 hours incubation, and stimulated for 1 minute with anti-IgM. Cells were fixed and permeablised, stained with anti-human pBTK Y223-PE and analysed by flow cytometry. MFIR= pBTK Y223-PE/ IgG1-PE isotype control. Units are arbitrary.

3.9 Discussion

Of the four MCL cell lines tested, the REC-1 cell line proved to be an excellent model to assess responses to the microenvironment, BCR stimulation and BTKi sensitivity. This was shown by the induction of apoptosis in response to Ibr and reduced proliferation in response to Ibr and Acal. The effects on proliferation and apoptosis in REC-1 cells were also achieved at Ibr doses between 1nM and 10nM, which is below the reported maximal achievable dose *in vivo* (400nM).[116,145] The large proportion of REC-1 cells which remained viable after 72 hours Ibr treatment indicated that cell death is not the main mechanism of action in these cells.

In addition to this cell line model of Ibr sensitivity, this study has also identified models of Ibr resistance. The G519 cell line was the most consistently resistant cell type showing no changes in proliferation or apoptosis from baseline over 72 hours even at the highest dose of drug. The JVM2 cells showed a considerable reduction of proliferation at 10µM together with increased cell death. The JEKO-1 cells showed no reduction in proliferation, but like JVM2, had a cell death response at the highest dose (10µM). It can be suggested that since these high concentrations greatly exceed the activity range of Ibr for BTK, the effect on cell death in particular, may represent off-target activity in these cells, through non-specific binding to other kinases, particularly within the TEC family. Additionally, in REC-1 cells, despite Acal being more selective for BTK, the drug did not induce the same level of apoptosis compared with Ibr, and there was an absence of off-target effects in response to high doses of Acal providing further evidence that the apoptotic effect of Ibr is more likely a result of multiple kinase inhibition rather than a direct mechanism of BTKi action. The lack of apoptosis in response to Acal suggests that BTK inhibition may not directly induce cell death and

thus represents a secondary effect of BTKi. The identical reduction of REC-1 cell proliferation in response to both Ibr and Acal suggests that BTKi directly targets proliferation and therefore the Ki67 assay is a better measure to determine sensitivity.

Excluding the results at the highest dose (10µM), the JVM2 and the JEKO-1 cells were characterised as Ibr resistant. This is contrary to other studies which have characterised JVM2 cells as sensitive to Ibr,[190] although that study used a 5µM concentration which again, may cause off-target effects and is not therapeutically achievable *in vivo.* Like JVM2, the JEKO-1 cell line has been shown to be sensitive to Ibr[114,145] and this was achieved at therapeutic doses. Since the JEKO-1 cells used for this study were frozen down at low passage (Passage 4), development of mutations through continued culturing is unlikely. We have noted that the JEKO-1 cells shown by others to be sensitive to Ibr,[114,145] were purchased from the American type culture collection whereas in this study the JEKO-1 cells were purchased from the German collection (DSMZ), indicating possible variation between the two JEKO-1 lines.

In all cell lines there was evidence of basal BTK activation, represented by Y223 phosphorylation that was universally inhibited by Ibr. This BTK activity was shown to induce ERK1/2 activation (pERK) which was reduced following Ibr treatment in all MCL cell lines, suggesting that ERK1/2 activation is dependent on BTK signalling. Activation of the BCR increased Y223-BTK and ERK1/2 phosphorylation in both sensitive and resistant cells, but although levels of pY223-BTK were reduced upon Ibr treatment, the levels of pERK were only partially reduced. This is consistent with other studies [190] and suggests that this subsequent activation of ERK1/2 depends only partly on BTK signals and suggests an additional route for ERK1/2 activation following BCR stimulation, possibly through activation of MAPK and PI3K pathways.

Expression of IRF4 (present in all cell lines), was completely inhibited following Ibr treatment in the REC-1 cells, but not in the resistant cell lines. This change in IRF4 expression was shown to be an early and specific indicator of biological (proliferation and apoptosis) responses to Ibr. This IRF4 down-regulation occurred even in the presence of BCR stimulation in Ibr-sensitive cells (REC-1). Results from these experiments suggest that IRF4 has potential use as a biomarker in monitoring BTKi treatment in MCL by identifying patients who may or may not respond to BTKi and also those who are acquiring resistance to these agents.

To understand the resistance to BTKi agents observed clinically, an *in vitro* model of acquired Ibr resistance was created in the REC-1 cell line. Long-term Ibr treatment (1μM) led to the establishment of a REC-1 cell line with acquired resistance (REC-1/R (Ibr 1μM)), while the passage-matched parent REC-1 cells used as the vehicle control line (REC-1/P) remained sensitive to Ibr as assessed by cell proliferation.

In the presence of both Ibr and Acal, BTK activation was maintained in the REC-1 resistant cell lines, which correlates with the continued proliferation of the cells. Although sequencing for BTK mutations was not carried out in this study, it is possible that the resistant cell lines had developed a BTK mutation causing ineffective binding of each inhibitor to the BTK C481 residue and therefore BTK phosphorylation is no longer reduced in response to Ibr. This would explain the expression of IRF4 in the REC-1/R (Ibr 1μM) cells which was not downregulated with Ibr and matches IRF4 expression seen in the untreated parent REC-1 cells.

This is different from the innate resistant cells (G519, JEKO-1 and JVM2), here, IRF4 is not downregulated by BTKi, although the BTK pY223 response was reduced. This suggests the drug was still able to bind to BTK preventing phosphorylation at Y223,

suggesting other downstream mechanisms are involved in primary resistance (tissue microenvironment).

These results demonstrate that IRF4 is downregulated in sensitive MCL cell lines but not downregulated in the same cells with acquired BTKi resistance or in innate resistant cell lines. These findings suggest that IRF4 is a potential biomarker of treatment response to BTKi. To validate these findings, IRF4 protein levels were assessed in *ex vivo* primary MCL cells taken from MCL patients currently on clinical treatment with BTK inhibitors (discussed in CHAPTER 4) and in models representing the tissue microenvironment.

Chapter 4- Assessing the response of MCL cells to BTK inhibitors within the microenvironment

4.1 Introduction

Within the bone marrow and lymph nodes, mature B-lymphocytes receive essential signals for growth and survival by interacting with specific accessory cells. There is evidence that these signals are essential for the survival of MCL cells *in vitro*.[53,65,117,191] BTKi are thought to have a role in disrupting the interactions which retain the cells in their protective tissue niches; however, processes such as the engagement of CD40L or BCR within the tissues may induce the activation of cellular processes including NFkB, MAPK and PI3K pathways which may be involved in forming resistance pathways, and may allow the malignant cells to bypass the effects of BTK inhibition. It was hypothesised that development of an *in vitro* system which reproduces the *in vivo* tissue microenvironment could be used to explore BTKi resistance pathways in MCL.

This chapter describes the assessment of cell lines and primary MCL cells when co-cultured on a stromal monolayer of murine fibroblasts, focussing on changes to BTKi induced apoptosis, proliferation, and protein expression of pERK1/2 and IRF4 in response to Ibr and Acal. The aim was to determine whether factors from the tissue microenvironment protect MCL cells from the effects of BTK inhibition *in vitro*. Subsequently, paired clinical samples taken before commencement and during BTKi therapy were assessed to confirm the relevance of the cell line findings concerning expression levels of IRF4, and to determine whether IRF4 could be used to predict response to BTKi treatment.

4.2 Methods employed

The methods employed in this section involve the culture of sensitive and resistant REC-1 cells (Methods section 2.2.4 and 2.2.10), the isolation of *ex vivo* primary MCL cells (Methods section 2.2.2), and their co-culture onto two separate monolayers of murine fibroblast cell lines, one expressing CD40L (T-CD40L), and the other not expressing CD40L (NT-CD40L) (Methods section 2.2.6).

The fibroblast cells were characterised for expression of CD40L (CD154) by immunofluorescence and flow cytometry (Methods section 2.2.5). Cells were assessed by flow cytometry for apoptosis (annexin V-FITC), and / or proliferation (Ki67-FITC) with and without fibroblast support and in response to varying concentrations of Ibr or Acal (Methods section 2.2.9 and 2.3). Primary MCL cells were distinguished by their forward and side-scatter characteristics and by their co-expression of CD5 and CD19.

Assessment of signalling proteins following BTKi treatment (*in vitro* and clinical) were determined through biochemical assays (Methods section 2.4) of 1D-SDS PAGE (Methods section 2.4.3), western blotting (Methods section 2.4.6) and immunohybridisation (Methods section 2.4.6.1) on cell lysates or by flow cytometry following IgM stimulation (Methods section 2.3.2 and 2.2.8).

A table of antibodies/probes used in this chapter is shown below (Table 4.1).

All data (flow cytometry and western blotting) were analysed using Microsoft Excel™ and GraphPad Prism™ Version 5 software. The statistical tests employed are described in the figure legend of each experiment.

Antibody/probe	Species	Application	Ref	Source	Conc
Annexin-V-FITC		FC	556419	BD	5µl/test
Ki67 (IgG1k) -FITC	**Mouse anti human**	FC	556026	BD	10µl/test
BTK pY223 (IgG1k) -PE	**Mouse anti human**	FC	562753	BD	5µl/test
CD19 (IgG1k) -FITC	**Mouse anti human**	FC	555412	BD	10µl/test
CD19 (IgG1k) -APC	**Mouse anti human**	FC	555415	BD	10µl/test
CD5 (IgG1k) -PE	**Mouse anti human**	FC	555353	BD	10µl/test
CD5 (IgG1k) -APC	**Mouse anti human**	FC	555355	BD	10µl/test
CD154 (IgG1k) -PE	**Mouse anti human**	FC	555697	BD	20µl/test
IgG1k isotype-FITC	**Mouse anti human**	FC	556026	BD	10µl/test
IgG1k isotype-PE	**Mouse anti human**	FC	559320	BD	10µl/test
IgG1k isotype-APC	**Mouse anti human**	FC	555751	BD	10µl/test
IRF4 primary antibody	**Rabbit anti human**	WB	#4964	CST	1/1000
pERK1/2 primary antibody	**Rabbit anti human**	WB	#9101	CST	1/2000
ERK1/2 primary antibody	**Rabbit anti human**	WB	#9102	CST	1/2000
GAPDH primary antibody	**Rabbit anti human**	WB	#2118	CST	1/5000
Secondary antibody-HRP	**Goat anti rabbit**	WB	#P0448	Dako	1/2000

Table 4.1: Antibodies and stains used in Chapter 4. For flow cytometry the list includes antibodies with corresponding isotype controls used for assessment of apoptosis, proliferation and BTK phosphorylation and for labelling primary MCL cells. For western blotting the list includes antibodies used for immunohybridisation in cell lines and primary MCL cells. FITC - fluorescein isothiocyanate; PE - phycoerythrin; APC –allophycocyanin. FC- Flow cytometry, WB- western blotting, BD- BD Biosciences, CST- Cell signalling technology.

4.3 REC-1 cells show a dependence on CD40L following treatment with BTKi. This dependence is lost when cells acquire resistance to BTKi.

REC-1 cells cultured *in vitro* demonstrated protected survival and proliferation from CD40L-stromal support following treatment with BTKi. In addition, stimulation with CD40L altered signalling, preventing down-regulation of pERK and IRF4 in response to BTKi treatment. These responses were also seen in the resistant REC-1 cells but were independent of stromal support.

4.3.1 Assessment of apoptosis and proliferation within a CD40L co-culture system in response to BTKi.

REC-1 cells were seeded into wells in culture media alone or in co-culture with fibroblast cells, either NT-CD40L or T-CD40L. Cells were treated with Ibr at a range of doses (as indicated) and assessed for rates of apoptosis and proliferation after 48 hours as previously described.

REC-1 cells co-cultured with the NT-CD40L cells demonstrated the same Ibr-induced proliferation effect and cell death response as the REC-1 cells cultured alone suggesting that stromal cell support in the absence of CD40L does not affect the response to BTK inhibition. In contrast (and rather surprisingly a for a cell line), stromal cell support with the T-CD40L cells prevented the reduction in proliferation and attenuated cell death (Figure 4.1), indicating that REC-1 cells were protected from the effects of BTK inhibition by stroma induced CD40-CD40L interactions. This was also shown in response to a dose range of Ibr treatment (10nM-10μM) (Figure 4.2).

Non-linear regression analysis (Figure 4.2) indicated that the rate of death for REC-1 cells following Ibr treatment was approximately 3-fold greater across the dose range when cells were cultured in media alone compared with those cultured with CD40L.

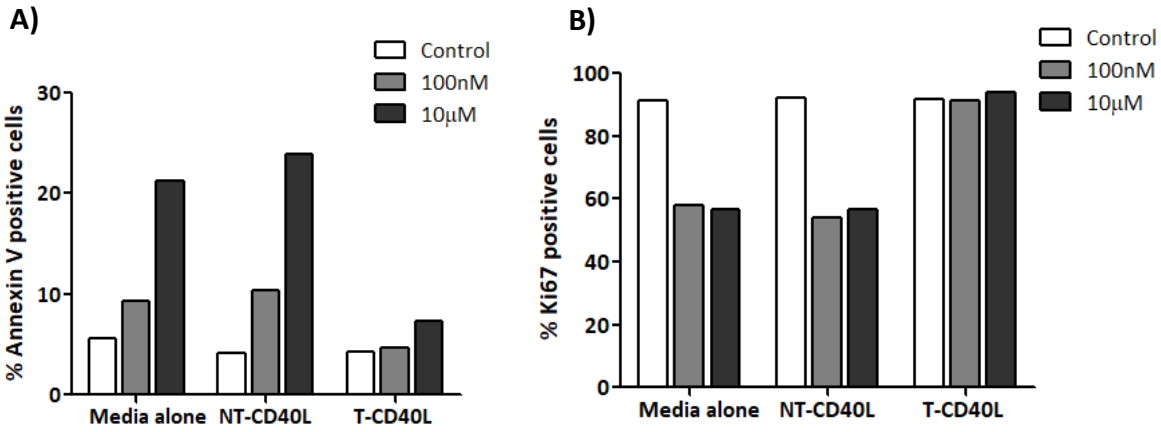

Figure 4.1: Survival and proliferation of REC-1 cells treated with Ibr in response to stromal cell stimulation (+/- CD40L). Murine fibroblast cells (NT-CD40L and T-CD40L) were seeded at 5 x 10^5/mL, irradiated and incubated o/n. REC-1 cells were seeded at 5 x 10^6/mL on to the fibroblast monolayers, and treated with Ibr (FC: 100nM and 10μM). Approximately 1 x 10^6 cells were removed at 48 hours and analysed using flow cytometry. For the apoptosis assay, cells were stained with annexin V-FITC. For the proliferation assay, cells were fixed, permeablised and stained with Ki67-FITC and IgG1-FITC. A) Assessment of apoptosis (%) before and after Ibr treatment, B) Assessment of proliferation (%) before and after Ibr treatment.

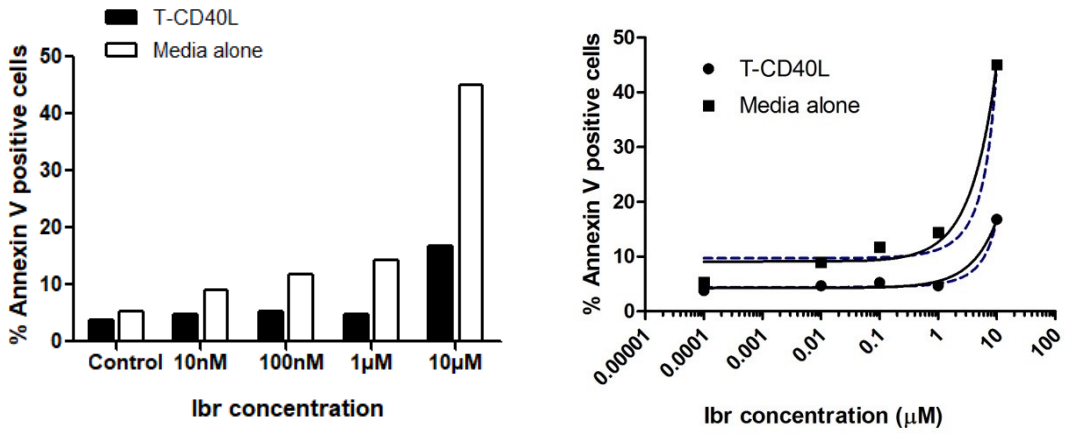

Figure 4.2: Survival of REC-1 cells treated with Ibr in the presence of stromal cell stimulation (T-CD40L). Murine fibroblast cells (T-CD40L) were seeded at 5 x 10^5/mL, and incubated o/n. REC-1 cells were seeded at 5 x 10^6/mL on to the fibroblast monolayer, then treated with Ibr (FC: 10nM, 100nM, 1μM and 10μM). Cells were taken after 48 hours, stained with annexin V-FITC and analysed by flow cytometry (*N*=1). Left: Ibr induced apoptosis (%) at each concentration; Right: Graph of the correlation between apoptosis and Ibr concentration analysed by non-linear regression. The curves of best fit: T-CD40L R^2=0.9845, media alone R^2= 0.9780. The equation of the curves of best fit: T-CD40L y= 1.24x, Media alone y= 3.2x representing an approximate increase in death of 3-fold in the absence of CD40L.

4.3.2 Assessment of ERK1/2 phosphorylation and IRF4 expression in response to BTKi within a co-culture system.

To determine the effects of BTKi treatment on ERK1/2 phosphorylation in the presence or absence of CD40L stimulation, REC-1 cells were seeded onto a fibroblast monolayer expressing CD40L (T-CD40L) and compared with REC-1 cells cultured in media alone. REC-1 cells under both conditions were treated with Ibr at a range of doses (10nM, 100nM, 1µM, 10µM) and incubated for up to 48 hours. Protein was extracted after 24 hours and 48 hours treatment (Methods section 2.4.1).

The presence of CD40L did not significantly effect baseline expression of pERK. However, CD40L did oppose the down-regulation of pERK induced by Ibr treatment in cells cultured in media alone (Figure 4.3).

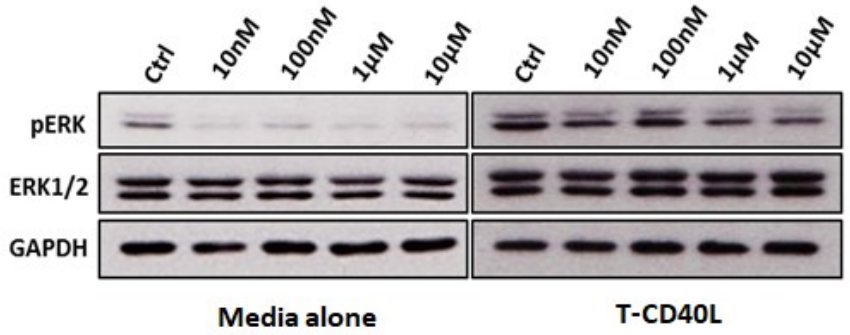

Figure 4.3: Immunoblot analysis of pERK and ERK1/2 in REC-1 cells (cultured in media alone and with T-CD40L fibroblasts) pre, and 24 hours post Ibr treatment. Fibroblast cells (T-CD40L) were seeded at 5 x 10^5/mL and incubated o/n. REC-1 cells were seeded at 2 x 10^6 /mL, on to the fibroblast monolayer and treated with a DMSO vehicle, followed by increasing concentrations of Ibr (10nM, 100nM, 1µM, 10µM). Protein was extracted after 24 hours incubation. 10% SDS gel. 20.0µg protein. pERK (Cell Signalling technology #9101) 1 in 2000 dilution, ERK1/2 (Cell signalling technology #9102) 1 in 2000 dilution, GAPDH (Cell Signalling technology #2118) 1 in 5000 dilution in 5% BSA/TBST, o/n at 4°C. Goat anti-rabbit-HRP (Dako, P0448) 1 in 2000 dilution (pERK, ERK1/2), 1 in 5000 dilution (GAPDH), in 5% BSA/TBST, 1 hr, RT. ECL (Pierce).

The assessment of IRF4 expression of REC-1 cells showed that in the presence of stromal cells that expressed CD40L the baseline expression of IRF4 was increased; and (compared to cells cultured in media alone) these conditions opposed the IRF4 downregulation seen with Ibr over a range of doses at 24 hours and 48 hours (Figure 4.4). These data suggest that signalling following BTKi treatment is modulated in cells cultured on a CD40L-stromal layer preventing down regulation of IRF4 expression.

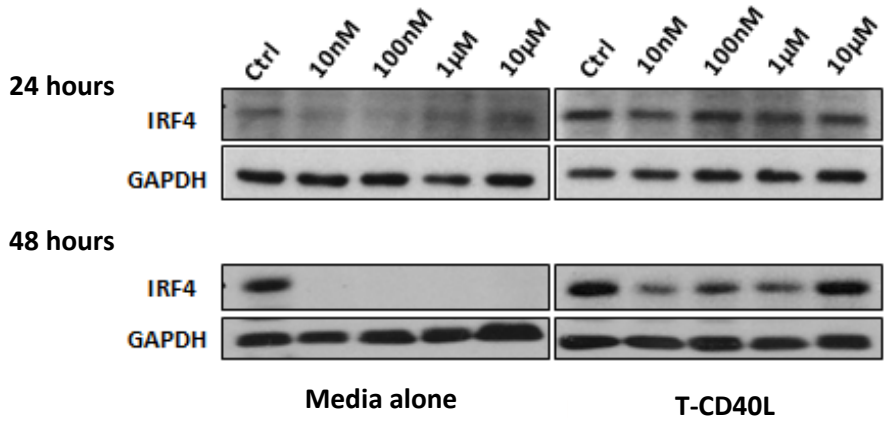

Figure 4.4: Immunoblot analysis of IRF4 in REC-1 cells (cultured in media alone and with T-CD40L fibroblasts) pre, and 24-48 hours post Ibr treatment. Murine fibroblast cells (T-CD40L) were seeded at 5 x 10^5/mL and incubated o/n. REC-1 cells were seeded at 2 x 10^6 /mL, on to the fibroblast monolayer and treated with a DMSO vehicle, followed by increasing concentrations of Ibr (10nM, 100nM, 1μM, 10μM). Protein was extracted after 24 and 48 hours incubation. Upper panel IRF4 expression after 24 hours; Lower panel IRF4 expression after 48 hours. 10% SDS gel. 20.0μg protein. IRF4 (Cell Signalling technology #4964) 1 in 2000 dilution, GAPDH (Cell Signalling technology #2118) 1 in 5000 dilution in 5% BSA/TBST, o/n at 4°C. Goat anti-rabbit-HRP (Dako, P0448) 1 in 2000 dilution (IRF4), 1 in 5000 dilution (GAPDH) in 5% BSA/TBST, 1 hr, RT. ECL (GAPDH), ECL prime (IRF4) (Pierce, Life Technologies).

To confirm CD40L was responsible for these IRF4 results as opposed to stromal cell interactions alone, REC-1 cells were seeded onto both fibroblast monolayers, T-CD40L and NT-CD40L. In addition, the response to both Ibr and the more specific BTKi Acal was assessed. Protein was extracted after 48 hours as described previously and assessed for IRF4 expression.

As shown in Figure 4.5, IRF4 was downregulated by both Ibr and Acal when cultured with the NT-CD40L stromal cells correlating with the reduced survival and proliferation data of REC-1 cells cultured in the absence of CD40L (Figure 4.1). However in REC-1 cells cultured with T-CD40L stromal cells, as demonstrated above, IRF4 expression was upregulated in the control cells with no/ or limited downregulation of IRF4 seen with Ibr and Acal treatment respectively and correlates with the previously shown data of enhanced survival and proliferation in the presence of CD40L (Figure 4.1).

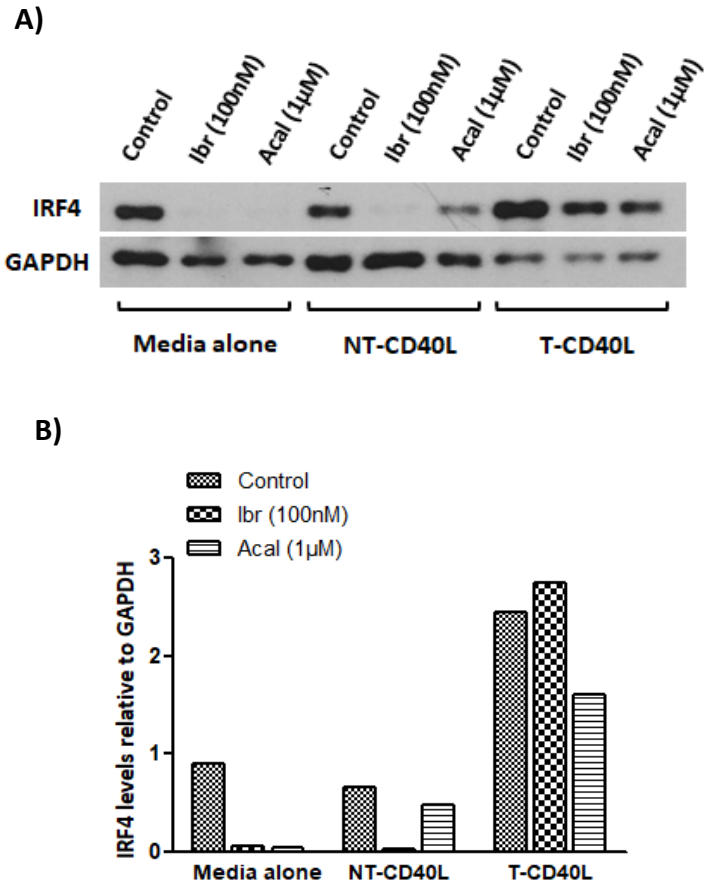

Figure 4.5: IRF4 expression in REC-1 cells co-cultured with stromal cells NT-CD40L and T-CD40L following 48 hours treatment with BTKi. REC-1 cells were seeded at 5 x 10^6/mL in culture media alone and onto two fibroblast monolayers NT-CD40L and T-CD40L. Cells were treated with a DMSO vehicle control, Ibr (100nM) and Acal (1μM). Protein was extracted after 48 hours incubation. A) Immunoblot analysis of IRF4 expression B) Densitometry analysis of IRF4 levels relative to GAPDH (units are arbitrary). 10% SDS gel. 25.0μg protein, IRF4 (Cell Signalling technology #4964) 1 in 2000 dilution, GAPDH (Cell Signalling technology #2118) 1 in 5000 dilution in 5% BSA/TBST, o/n at 4°C. Goat anti-rabbit-HRP (Dako, P0448) 1 in 2000 dilution (IRF4), 1 in 5000 dilution (GAPDH) in 5% BSA/TBST, 1 hr, RT. ECL (GAPDH), ECL prime (IRF4) (Pierce, Life Technologies).

4.3.3 Functional and biochemical response of acquired BTKi resistant REC-1 cells when cultured on a CD40L co-culture system.

As determined in chapter 3, acquired BTKi resistant REC-1 cells show no reduction in survival, proliferation or levels of IRF4 expression in the presence of BTK inhibitors. To determine whether stromal interaction would modulate this response, the acquired BTKi resistant REC-1 cells were co-cultured on NT-CD40L and T-CD40L fibroblast monolayers and treated with Ibr at a range of doses (as indicated) and assessed for changes in apoptosis, proliferation and IRF4 expression.

The below results show that survival and proliferation were not affected when the acquired BTKi resistant REC-1 cells were cultured on either of the NT-CD40L or T-CD40L fibroblast monolayers (Figure 4.6) and IRF4 expression was not downregulated (Figure 4.7).

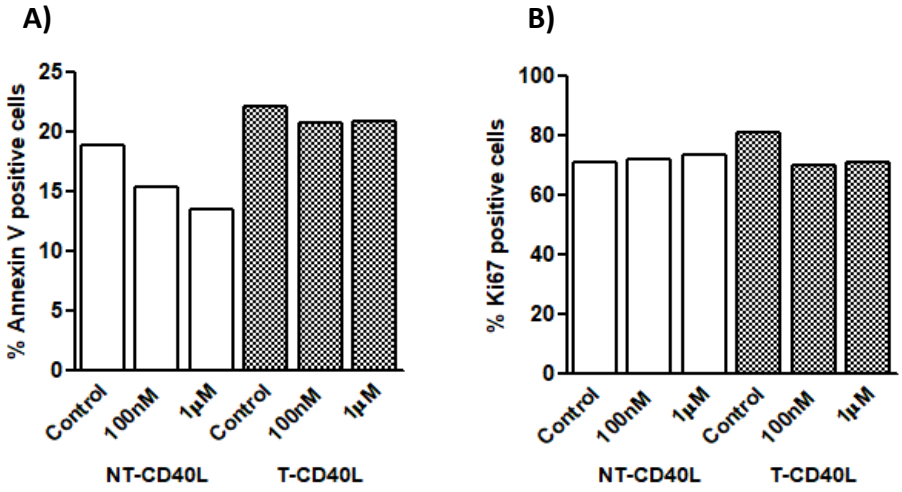

Figure 4.6: Survival and proliferation of acquired Ibr resistant REC-1 cells co-cultured with NT-CD40L and T-CD40L stromal cells following treatment with Ibr. Resistant REC-1 cells were seeded at 5 x 10^6/mL onto two fibroblast monolayers; NT-CD40L and T-CD40L and treated with Ibr (FC: 100nM and 1µM). Cells were harvested from the monolayers after 48 hours incubation for analysis of survival and proliferation by flow cytometry. A) Assessment of apoptosis (%), B) Assessment of proliferation (%).

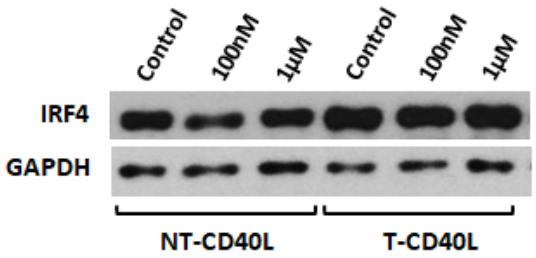

Figure 4.7: Immunoblot analysis of IRF4 expression in acquired resistant REC-1 cells co-cultured with NT-CD40L and T-CD40L stromal cells following treatment with Ibr. Resistant REC-1 cells were seeded at 5 x 10^6/mL onto two fibroblast monolayers; NT-CD40L and T-CD40L and treated with a DMSO vehicle control or Ibr (100nM or 1μM). Protein was extracted after 48 hours incubation for analysis of IRF4 expression. 10% SDS gel. 25.0μg protein, IRF4 (Cell Signalling technology #4964) 1 in 2000 dilution, GAPDH (Cell Signalling technology #2118) 1 in 5000 dilution in 5% BSA/TBST, o/n at 4°C. Goat anti-rabbit-HRP (Dako, P0448) 1 in 2000 dilution (IRF4), 1 in 5000 dilution (GAPDH) in 5% BSA/TBST, 1 hr, RT. ECL (GAPDH), ECL prime (IRF4) (Pierce, Life Technologies).

4.4 Primary MCL cells cultured *ex vivo* demonstrate a functioning BCR and when co-cultured with CD40L, and behave similarly to REC-1 cells following BTKi treatment.

Primary MCL cells cultured *ex vivo* demonstrate a functional BCR with inhibition of phosphorylated BTK (Y223) following BTKi treatment. Primary MCL cells are heterogeneous, but generally behave similarly to REC-1 cells when co-cultured with stromal support and in response to BTKi. Co culture with CD40L induced survival, prevented BTKi-induced IRF4 downregulation and protected the primary cells from BTKi-induced death.

4.4.1 Assessment of BCR signalling in response to BTKi treatment

In all MCL cell lines (REC-1, G519, JEKO-1 and JVM2), Y223 BTK phosphorylation was reduced 1 hour following Ibr treatment. To determine whether the data was comparable in primary MCL cells, pre-treatment primary cells taken from four individual MCL patients were treated *in vitro* with Ibr or Acal (100nM), and incubated for 1 hour (MCL01, MCL02, MCL04) or 90 minutes (MCL03). Levels of BTK phosphorylation were assessed in both unstimulated and in anti-IgM stimulated cells (Methods section 2.3.2 and 2.2.8).

As was seen in the MCL cell lines, phosphorylation of BTK-Y223 in primary cells was much greater following anti-IgM stimulation for 1 minute than at baseline (Figure 4.8). In BCR activated primary cells, phosphorylation of BTK-Y223 was significantly reduced by 100nM concentrations of Ibr ($p=0.0047$) after 1 hour, but not significantly by Acal ($p=0.06$) at this time point (Figure 4.9). Further reductions may have been seen after a longer incubation with BTKi but this could not be achieved in primary MCL cells unsupported in culture due to the rapid rates of apoptosis.

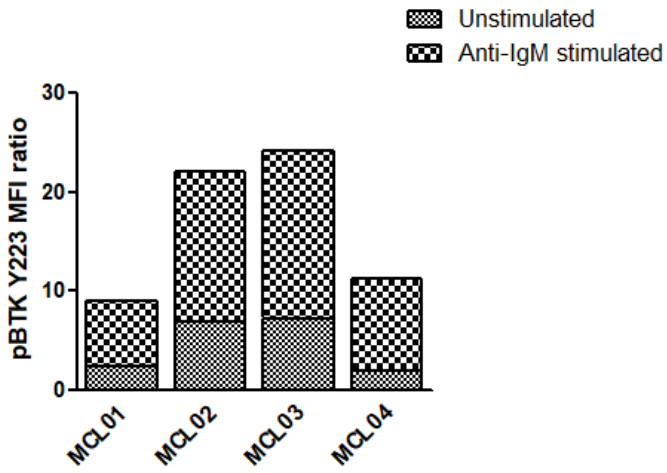

Figure 4.8: Increase in BTK-Y223 phosphorylation in patient samples after anti-IgM stimulation for 1 minute. Median Fluorescence Intensity ratios of BTK-Y223 phosphorylation in unstimulated cells vs anti-IgM stimulated primary cells (Units are arbitrary).

Case	Untreated	Ibr (100nM)
MCL01	6.585928	5.15917
MCL02	15.18704	12.54907
MCL03	11.47	8.86
MCL04	9.3681592	6.6355721

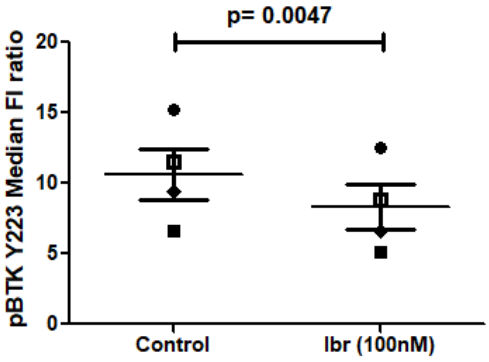

Case	Untreated	Acal (100nM)
MCL01	6.585928	5.716263
MCL02	15.18704	12.71481
MCL03	11.47	11.07
MCL04	9.3681592	7.9415423

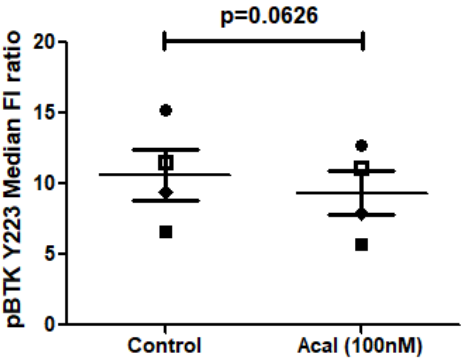

Figure 4.9: Reduction of pBTK-Y223 in patient samples after *in vitro* Ibr and Acal treatment (100nM) for 1 hour. The tables show the Median Fluorescence Intensity ratios of BTK-Y223 phosphorylation in 4 primary MCL cell cases. Cells were stimulated with anti-IgM and treated *in vitro* with Ibr (upper panel) and Acal (lower panel) (100nM). * MCL03 cells were treated for 1.5 hours. Data were analysed using a student's paired t-test.

4.4.2 Assessment of CD40L co-cultures on the survival of BTKi-treated MCL cells

Due to the poor proliferative response of primary MCL cultured *ex vivo,* even with CD40L stimulation (data from studies performed by Dr D Tucker as part of a completed MD from this group), the effects of BTKi treatment on the proliferation of primary MCL cells was not assessed. However, those studies did demonstrate that CD40L protected primary MCL cells from apoptosis. Therefore we assessed whether CD40L also protected cells from BTKi- induced apoptosis. Initially we assessed the effects of stromal cell support on primary MCL cell survival before BTK inhibition. E*x vivo* primary cells from five MCL cases were seeded into wells in culture media alone or with murine fibroblast cells, either NT-CD40L or T-CD40L. The primary cells were removed for assessment of apoptosis after 24 and / or 48 hours.

Although the response was variable (Table 4.2), most MCL cases showed enhanced survival in the presence of CD40L. This is very clearly demonstrated in the cases analysed at 24 hours ($p=0.0201$ paired t-test) although less clear in those cases analysed at 48 hours (Figure 4.10) largely as a result of the low apoptotic rates of cases MCL03 and MCL09 which are clinically indolent cases (the disease characteristics for these samples are shown in Table 4.3).

		% Apoptosis NT-CD40L	% Apoptosis T-CD40L
MCL03	24 hours	10.3	7.5
	48 hours	0.7	1.0
MCL05	24 hours	10.7	3.8
	48 hours	14	2
MCL06	24 hours	20.37	12.53
MCL07	24 hours	14.4	10.4
	48 hours	10.0	2.5
MCL08	48 hours	8.5	4.5
MCL09	48 hours	1.5	2.6

Table 4.2: Survival of primary MCL cells after 24 and 48 hours co-culture on a stromal layer. Primary MCL cells were seeded at 4 x 10^6/mL onto two fibroblast monolayers; NT-CD40L and T-CD40L. Cells were harvested from the fibroblast layer after 24 and 48 hours incubation, labelled with MCL surface markers and annexin V-FITC for 20 minutes at RT and assessed for apoptosis by flow cytometry. The table shows the percentage of apoptotic cells from 4 cases of primary MCL after 24 hours and from 5 cases of primary MCL after 48 hours of co-culture.

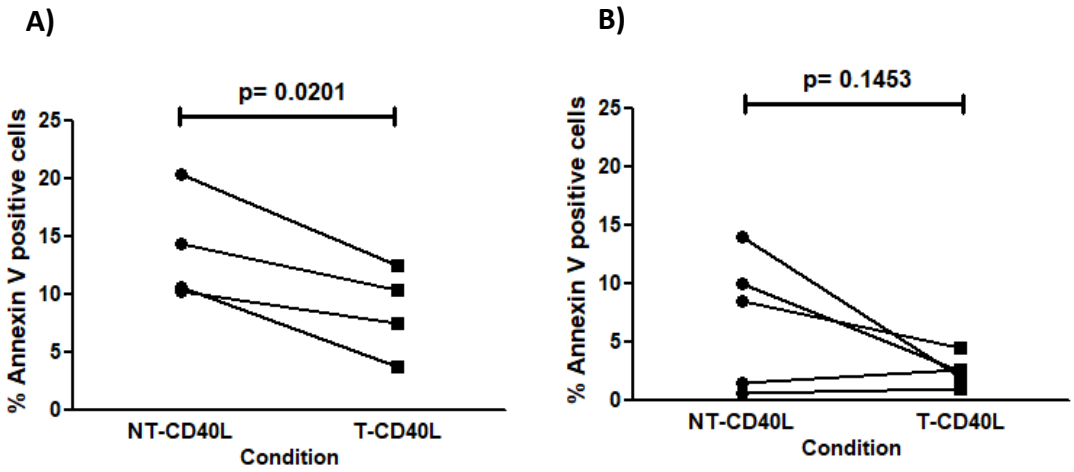

Figure 4.10: Survival of primary MCL cells after 24 and 48 hours co-culture on a stromal layer with and without CD40L. Paired t test comparing rates of apoptosis for 4-5 cases of primary MCL cells cultured with NT-CD40L and T-CD40L murine fibroblasts. A) Cases assessed at 24 hours B) Cases assessed at 48 hours. Some cases analysed at 48 hours were different to the cases analysed at 24 hours.

Case	Indolent/ aggressive subtype of MCL disease
MCL01	Aggressive
MCL03	Indolent
MCL06	Aggressive
MCL07	Aggressive
MCL08	Aggressive
MCL09	Indolent

Table 4.3: Disease characteristics of MCL cases whose cells were analysed for survival in section 4.4.2.

To determine whether the survival of primary MCL cells was reduced in response to BTKi, the cells co-cultured on NT-CD40L and T-CD40L fibroblasts were treated *in vitro* with Ibr or Acal at the doses indicated and analysed for apoptosis by flow cytometry.

Again results are heterogeneous with overall low levels of apoptosis seen in all cases. However for cells co-cultured for 24 hours with CD40L, apoptosis was significantly reduced in response to BTKi ($p=0.0004$) (Table 4.4, Figure 4.11), suggesting that CD40L protects primary cells from apoptosis even in the presence BTK inhibition. This finding is similar to the results previously shown for REC-1 cells. As before, results are less clear at 48 hours mainly as a result of the outlaying MCL08 case in response to Acal (Table 4.5, Figure 4.11).

		Apoptosis (%)	
Case		**NT-CD40L**	**T-CD40L**
MCL03	**Control**	10.27	7.46
	Ibr (100nM)	10.28	5.65
	Acal (1µM)	13.72	6.46
MCL05	**Control**	20.37	12.53
	Ibr (100nM)	22.27	13.48
	Acal (1µM)	20.09	15.69
MCL 06	**Control**	10.70	3.82
	Ibr (100nM)	15.28	4.22
	Acal (1µM)	14.30	4.07
MCL 07	**Control**	14.39	10.35
	Ibr (100nM)	15.58	12.80
	Acal (1µM)	16.56	11.68

Table 4.4: Survival of primary MCL cells in response to BTKi after 24 hours co-culture on NT-CD40L and T-CD40L fibroblasts. Primary MCL cells were co-cultured on a monolayer of NT-CD40L and T-CD40L fibroblasts and treated with Ibr (100nM) or Acal (1µM). Approximately 1 x 10^6 cells were removed after 24 hours and stained with annexin-V-FITC for analysis of apoptosis by flow cytometry.

		Apoptosis (%)	
Case		**NT-CD40L**	**T-CD40L**
MCL03	**Control**	0.72	0.97
	Ibr (100nM)	0.86	1.00
	Acal (1µM)	0.79	0.97
MCL06	**Control**	10.70	3.82
	Ibr (100nM)	15.28	4.22
	Acal (1µM)	14.30	4.07
MCL07	**Control**	10.00	2.50
	Ibr (100nM)	8.90	2.20
	Acal (1µM)	6.30	1.40
MCL08	**Control**	8.51	4.51
	Ibr (100nM)	5.10	5.77
	Acal (1µM)	7.44	13.43
MCL09	**Control**	1.46	2.60
	Ibr (100nM)	1.65	5.24
	Acal (1µM)	1.45	4.21

Table 4.5: Survival of primary MCL cells in response to BTKi after 48 hours co-culture on NT-CD40L and T-CD40L fibroblasts. Primary MCL cells were co-cultured on a monolayer of NT-CD40L and T-CD40L fibroblasts and treated with Ibr (100nM) or Acal (1µM). Approximately 1 x 10^6 cells were removed after 48 hours and stained with annexin-V-FITC for analysis of apoptosis by flow cytometry.

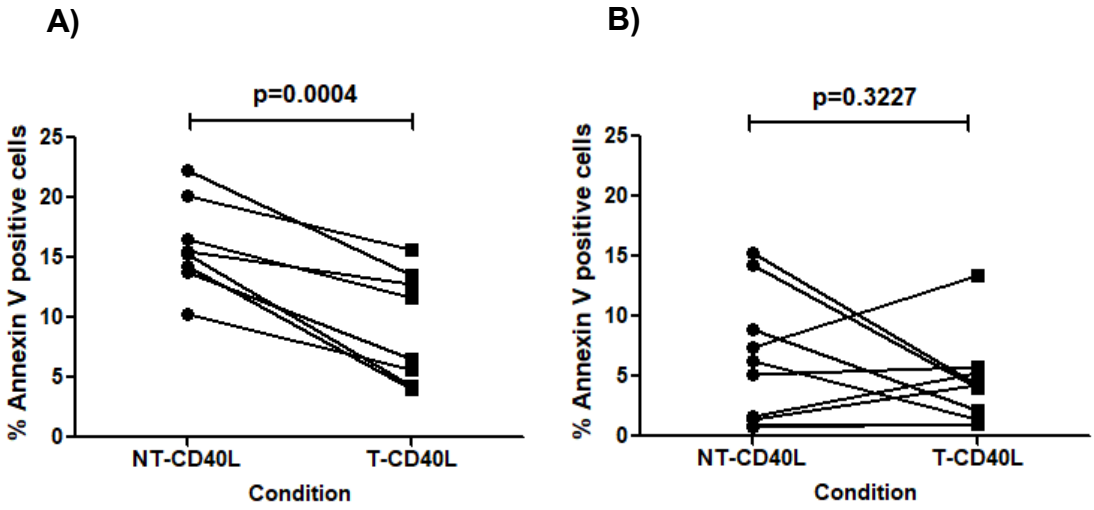

Figure 4.11: Survival of primary MCL cells co-cultured with stromal cells with and without CD40L in response to *in vitro* BTKi treatment. Paired t-test comparing the rates of apoptosis in response to Ibr (100nM) and Acal (1µM) (treatment groups combined), in primary MCL cells co-cultured with NT-CD40L and T-CD40L murine fibroblasts. A) 24 hours, B) 48 hours. Some cases analysed at 48 hours were different to the cases analysed at 24 hours.

4.4.3 Analysis of IRF4 expression in BTKi-treated primary MCL cells in response to CD40L co-culture

In the BTKi sensitive REC-1 cell line, IRF4 expression was upregulated by CD40L and IRF4 levels were sustained in response to BTKi (both Ibr and Acal). To determine whether these findings were also features in primary MCL cells, *ex vivo* primary MCL cells from 8 untreated patients were co-cultured with murine fibroblasts; NT-CD40L and T-CD40L, and treated *in vitro* with BTKi (Ibr or Acal). The cells were removed from the fibroblasts after 48 hours incubation with BTKi and lysed to obtain protein for analysis of IRF4 expression.

Results from those experiments are shown in Figure 4.12. A representative immunoblot is shown in Figure 4.12A. In the absence of treatment, IRF4 expression was significantly upregulated by CD40L in all eight MCL patient samples (paired t-test p= 0.0012) (Figure 4.12B). IRF4 expression was significantly down regulated by Ibr (p=0.0393) and almost significantly by Acal (p=0.0590) in all primary MCL cases co-cultured without CD40L (Figure 4.12C). However, stromal co-culture with CD40L prevented BTKi-induced downregulation of IRF4 in all 8 primary MCL cases (Ibr p=0.3398, Acal p=0.3802) (Figure 4.12D).

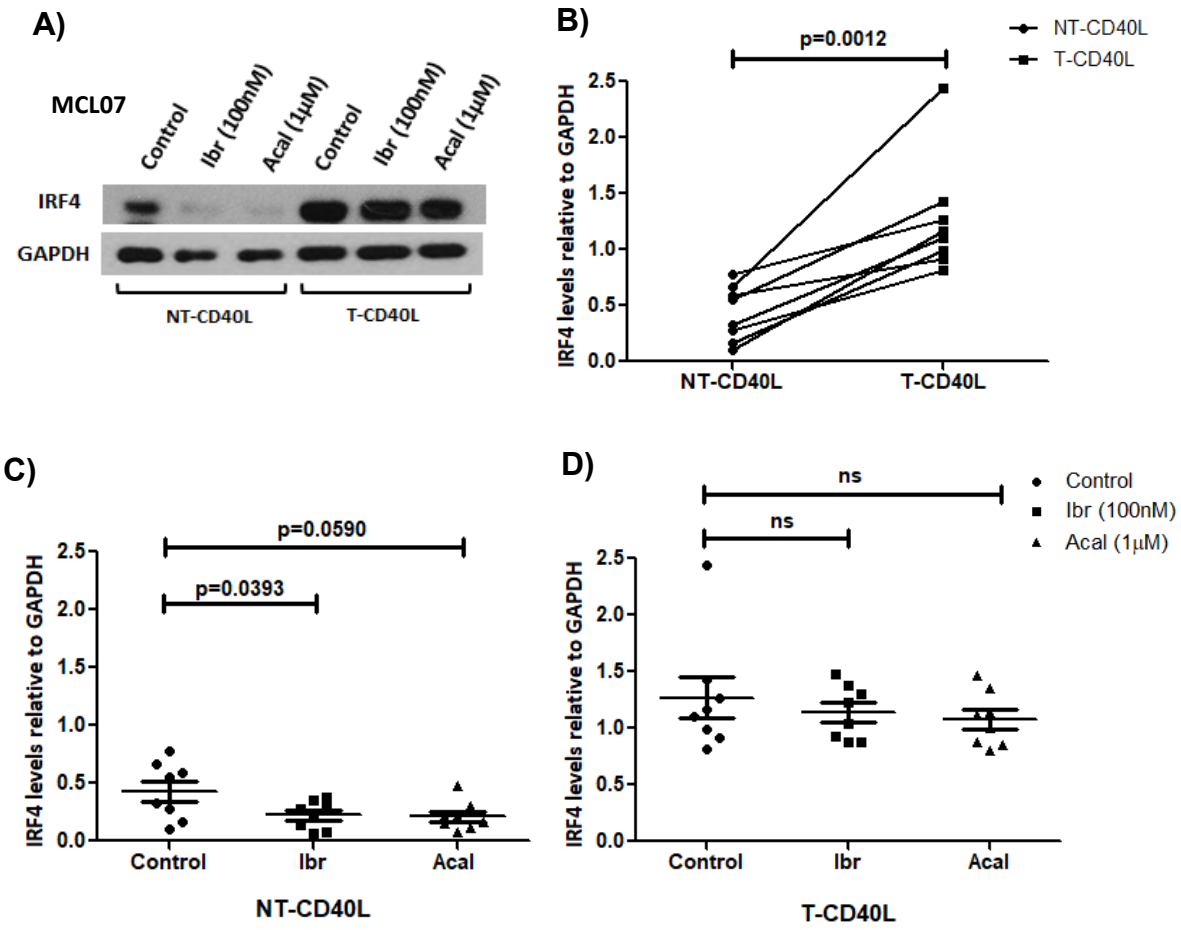

Figure 4.12: Assessment of IRF4 expression in BTKi-treated primary MCL cells in response to CD40L co-culture. A) Representative immunoblot analysis of IRF4 expression (Case MCL07) co-cultured with/without CD40L and treated *in vitro* with BTKi for 48h. **B)** CD40L upregulates IRF4 expression in 8/8 patient samples (Paired t-test p= 0.0012). **C)** IRF4 is significantly down regulated by Ibr and almost significantly downregulated by Acal in 8 patient samples co-cultured without CD40L (paired t-test). **D)** CD40L stimulation prevents downregulation of IRF4 by BTK inhibitors (Paired t-test; Ibr p=0.3398, Acal p=0.3802). Blot details: 10% SDS gel. 30.0µg protein. Rabbit anti-human IRF4 (CST #4964) 1 in 1000 dilution, rabbit anti-human GAPDH (CST #2118) 1 in 5000 dilution, in 5% BSA/TBST, o/n at 4°C. Goat anti-rabbit-HRP (Dako, P0448) 1 in 2000 dilution in 5% BSA/TBST, 1 hr, RT. ECL (GAPDH), ECL prime (IRF4) (Pierce, Life Technologies).

4.5 IRF4 expression can predict response to BTKi treatment.

In primary MCL patient samples, downregulation of IRF4 was associated with clinical response to BTKi therapy. In these patients, downregulation of IRF4 expression was an early response to BTKi therapy and sustained over time. Results suggest that sustained or loss of IRF4 downregulation in response to BTKi treatment can signify primary or acquired resistance.

Results from cell line and *ex vivo* BTKi-treated primary MCL cells have shown that IRF4 expression is downregulated in cells sensitive to BTKi treatment, but that IRF4 expression can be affected by either primary resistance seen in BTK resistant MCL cell lines, or by factors within the microenvironment such as stimulation by CD40L. However data from *in vivo* BTKi-treated patient samples would provide further rationale of the use of IRF4 as a predictor of response to BTKi treatment.

4.5.1 Assessment of IRF4 expression in MCL patient samples following BTKi treatment

Blood samples from 8 patients on monotherapy with BTK inhibitor agents Ibr and Acal were collected over the course of the PhD and were compared with pre-treatment samples. Samples were taken from patients responding to BTKi therapy, and from one patient who was treatment refractory and not responding to BTKi therapy. The specific BTK inhibitor monotherapy given to patients and their response to therapy is shown in Table 4.6. Following isolation of the PBMCs (Methods section 2.2.2), the primary MCL cells were lysed in a RIPA buffer (Methods section 2.4.1) to obtain protein for analysis of IRF4 expression.

Case	BTKi Treatment	Status
MCL01	Acalabrutinib	Responding
MCL02	Acalabrutinib	Responding
MCL04	Acalabrutinib	Refractory
MCL10	Ibrutinib	Responding
MCL11	Acalabrutinib	Responding
MCL12	Acalabrutinib	Responding
MCL13	Ibrutinib	Responding
MCL14	Ibrutinib	Responding

Table 4.6: The specific BTK inhibitor monotherapy used in the clinical treatment of 8 primary MCL cases examined for IRF4 expression levels and their response to treatment.

The results are shown in Figure 4.13. IRF4 expression was downregulated in 7 out of 8 MCL patient samples tested. These samples were taken from patients clinically responding to BTKi treatment. Statistical analysis of those 7 samples (three patients on Ibr treatment and four patients on Acal treatment) show significant IRF4 down-regulation (paired t-test; p=0.0009). Sample MCL04 shows sustained levels of IRF4 expression and was clinically refractory to BTKi treatment.

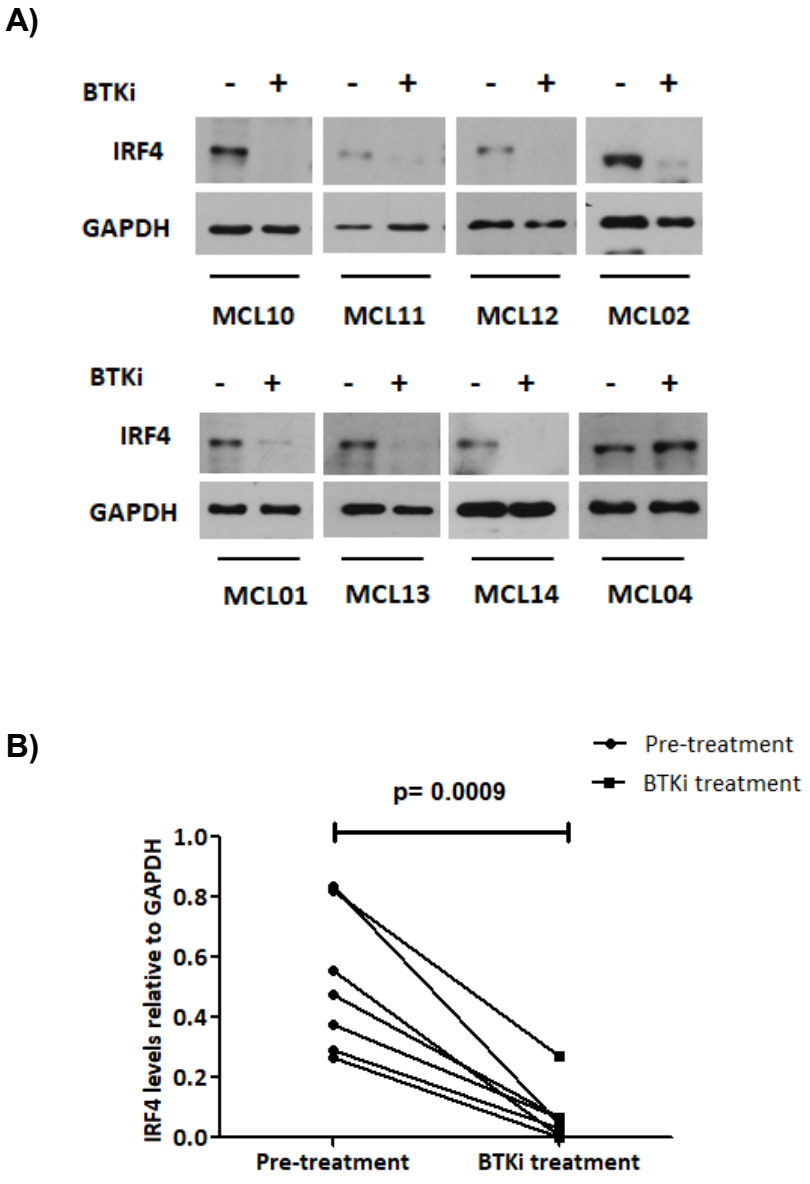

Figure 4.13: IRF4 expression levels in patient samples on clinical therapy with BTKi. A) IRF4 expression in 8 patient samples on BTKi treatment compared to their matched pre-treatment sample, in all but one case there is a clear downregulation of IRF4. **B)** In the 7 cases which are responding to clinical BTKi treatment, IRF4 is significantly downregulated. Data was statistically analysed using paired t-test (p=0.0009). Blot details: 10% SDS gel. 30.0µg protein. Rabbit anti-human IRF4 (CST #4964) 1 in 1000 dilution, rabbit anti-human GAPDH (CST #2118) 1 in 5000 dilution, in 5% BSA/TBST, o/n at 4°C. Goat anti-rabbit-HRP (Dako, P0448) 1 in 2000 dilution in 5% BSA/TBST, 1 hr, RT. ECL (GAPDH), ECL prime (IRF4) (Pierce, Life Technologies).

We next assessed the expression of IRF4 during time on BTKi-treatment to determine how quickly downregulation of IRF4 expression occurred. IRF4 expression was assessed in two clinically responding cases over several treatment cycles with Acal. The cycle- associated white cell count (WCC)/ lymphocyte count is shown in Table 4.7. Immunoblot analysis shows that downregulation of IRF4 expression occurs within the first treatment cycle and was sustained over time, (Figure 4.14 and 4.15), not surprisingly response was variable between and within patient samples but expression levels were independent of the reported WCC.

A)

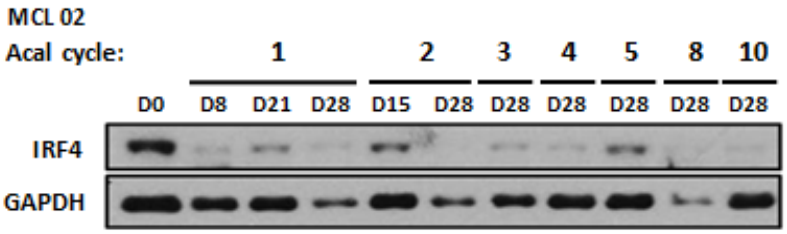

B)

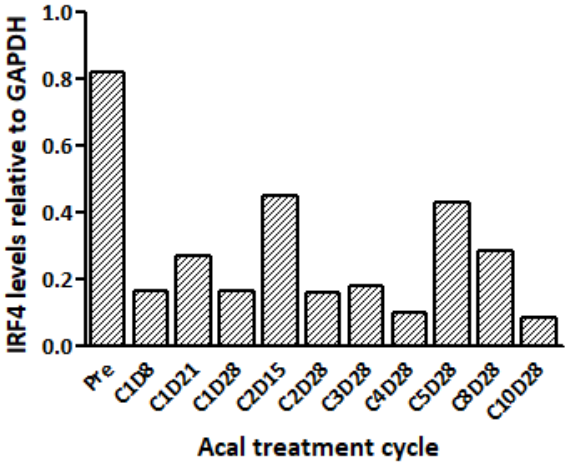

Figure 4.14: IRF4 expression over several Acal treatment cycles in a patient responding to therapy. A) Immunoblot analysis of IRF4 expression **B)** Densitometry analysis of IRF4 expression relative to GAPDH expressed in arbitrary units. C= cycle, D = day. Blot details: 10% SDS gel. 30.0µg protein. Rabbit anti-human IRF4 (CST #4964) 1 in 1000 dilution, rabbit anti-human GAPDH (CST #2118) 1 in 5000 dilution, in 5% BSA/TBST, o/n at 4°C. Goat anti-rabbit-HRP (Dako, P0448) 1 in 2000 dilution in 5% BSA/TBST, 1 hr, RT. ECL (GAPDH), ECL prime (IRF4) (Pierce, Life Technologies).

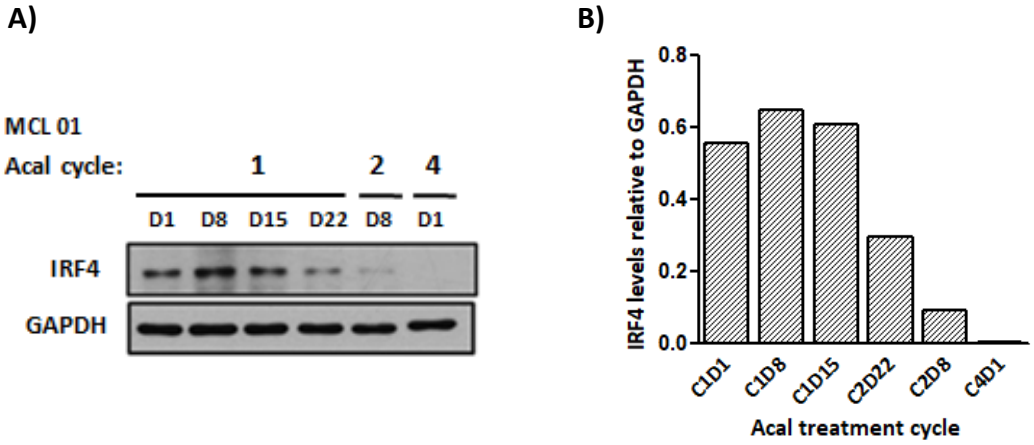

Figure 4.15: IRF4 expression over several Acal treatment cycles in a patient responding to therapy. A) Immunoblot analysis of IRF4 expression B) Densitometry analysis of IRF4 expression relative to GAPDH expressed in arbitrary units. C= cycle, D = day. Blot details: 10% SDS gel. 30.0µg protein. Rabbit anti-human IRF4 (CST #4964) 1 in 1000 dilution, rabbit anti-human GAPDH (CST #2118) 1 in 5000 dilution, in 5% BSA/TBST, o/n at 4°C. Goat anti-rabbit-HRP (Dako, P0448) 1 in 2000 dilution in 5% BSA/TBST, 1 hr, RT. ECL (GAPDH), ECL prime (IRF4) (Pierce, Life Technologies).

Case	Acal treatment cycle	WCC (x10^9/L)	
MCL02	Pre	36	
	C1D8	345	
	C1D21	339	
	C1D28	258	
	C2D15	155	
	C2D28	118	
	C3D28	73.9	
	C4D28	43.8	
	C5D28	34	
	C8D28	15	
	C10D28	12.9	lymphocytes: 9.4

Case	Acal Treatment cycle	WCC (x10^9/L)	
MCL01	C1D1	89	
	C1D8	335	
	C1D15	196	
	C1D22	122	
	C2D8	32	
	C4D1	9.2	lymphocytes: 5.5

Table 4.7: White blood cell counts obtained from two patients corresponding to individual Acal treatment cycles. Lymphocyte counts were obtained for the two samples demonstrating low WCC.

4.6 IRF4 expression can be used to monitor for BTKi-treatment resistance in primary MCL cases.

All primary MCL cases whether sensitive or resistant to BTKi demonstrated a normal functional BCR with inhibition of phosphorylated BTK Y223 in treated samples, but showed differential expression of IRF4. Loss of clinical response to BTKi treatment corresponded to increasing IRF4 expression and lack of downregulation with sustained IRF4 levels corresponded to primary BTKi resistance.

4.6.1 Assessment of BTK phosphorylation and IRF4 expression in MCL patient cells with primary and acquired resistance to BTKi treatment

To validate whether IRF4 expression can be used as a biomarker to detect patients with primary or acquired BTKi resistance, further detailed studies on two individual MCL cases was undertaken. One case (MCL04) was treatment refractory demonstrating primary resistance to BTKi and the other was an acquired resistance case from a previously responding patient (MCL02) who subsequently relapsed after 23 months on BTKi therapy. The primary MCL cells isolated from these cases were assessed for BTK phosphorylation following IgM stimulation (Methods section 2.2.8 and 2.3.2) by flow cytometry. In the acquired resistance case, BTK phosphorylation was assessed in a pre-treatment sample and compared to a BTKi-treatment sample with relapsed disease. In the primary resistance case, BTK phosphorylation was assessed in a pre-treatment sample following *in vitro* treatment with Ibr and Acal at the doses indicated.

In both cases of BTKi resistance, phosphorylation of BTK-Y223 was reduced by BTKi as shown by the reductions in the median fluorescence intensity ratios for pBTK-Y223-PE against a corresponding isotype control (Figure 4.16).

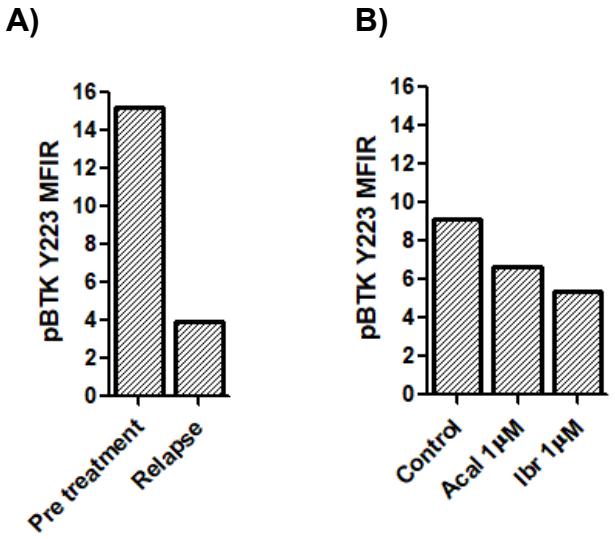

Figure 4.16: Flow cytometry analysis of phosphorylated BTK-Y223 in MCL patient cells with primary and acquired resistance to BTKi. A) MFIR of pBTK-Y223 in a pre-treatment sample vs. a BTKi-treatment sample from a patient with acquired BTKi resistance (case MCL02). B) MFIR of pBTK-Y223 in a pre-treatment sample from a patient with primary BTKi resistance following *in vitro* treatment with Ibr and Acal (1µM) (case MCL04). MFIR denotes the median fluorescence intensity ratio of pBTK-Y223-PE / IgG-PE isotype control. Units are arbitrary.

IRF4 expression was assessed in both the acquired and primary resistant BTKi cases (MCL02 and MCL04, respectively).

In the acquired BTKi resistance case, protein was extracted from PBMCs during BTKi treatment until relapse. IRF4 was initially downregulated over several treatment cycles with Acal as shown previously (Figure 4.14) and shown again in Figure 4.17A. However, comparison of the patient's pre-treatment sample with their relapse sample showed that IRF4 was not downregulated at relapse (Figure 4.17B) and appeared as a band slightly lower than that seen pre-treatment.

In the primary resistance case, protein was extracted from PBMCs pre-treatment and during the first 3 cycles on treatment. IRF4 was consistently expressed over several treatment cycles with Acal therapy and was not downregulated even after three months on therapy (Figure 4.18).

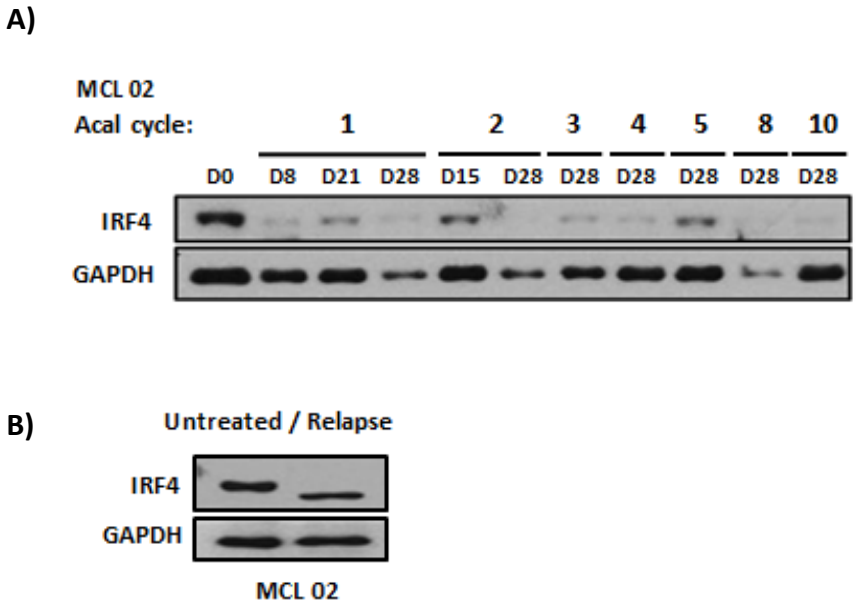

Figure 4.17: Immunoblot of IRF4 expression in primary MCL cells in a patient with acquired BTKi resistance. A) Shows downregulation of IRF4 expression during treatment response, **B)** shows loss of IRF4 downregulation at disease relapse. Blot details: 10% SDS gel. 30.0µg protein. Rabbit anti-human IRF4 (CST #4964) 1 in 1000 dilution, rabbit anti-human GAPDH (CST #2118) 1 in 5000 dilution, in 5% BSA/TBST, o/n at 4°C. Goat anti-rabbit-HRP (Dako, P0448) 1 in 2000 dilution in 5% BSA/TBST, 1 hr, RT. ECL (GAPDH), ECL prime (IRF4) (Pierce, Life Technologies).

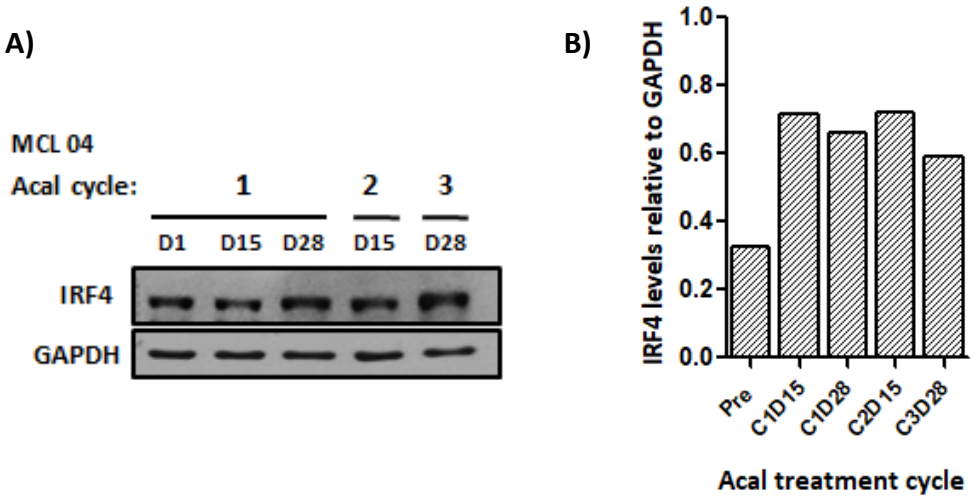

Figure 4.18: Expression of IRF4 in primary MCL cells in a patient with primary BTKi resistance. IRF4 expression is not downregulated over several Acal treatment cycles in a patient clinically not responding to treatment. **A)** Immunoblot analysis of IRF4 expression **B)** Densitometry analysis of IRF4 expression relative to GAPDH expressed in arbitrary units. C= cycle, D = day. Blot details: 10% SDS gel. 30.0µg protein. Rabbit anti-human IRF4 (CST #4964) 1 in 1000 dilution, rabbit anti-human GAPDH (CST #2118) 1 in 5000 dilution, in 5% BSA/TBST, o/n at 4°C. Goat anti-rabbit-HRP (Dako, P0448) 1 in 2000 dilution in 5% BSA/TBST, 1 hr, RT. ECL (GAPDH), ECL prime (IRF4) (Pierce, Life Technologies).

4.7 Discussion

The tissue microenvironment is recognised to contribute to the development of chemo-resistance, and has been proposed as a mechanism of Ibr resistance in MCL and other B cell malignancies.[191-194] Like their normal B cell counterparts, MCL cells are attracted into the tissues by chemotactic factors secreted by accessory cells such as stromal cells in the microenvironment, where important interactions take place with other cell types including T cells. CD40L is expressed on T cells, and in normal cells has an important role in providing co-stimulatory signals following stimulation of the BCR which increase the survival and growth of specific B cell clones.

In this study, REC-1 cells treated with either Ibr or Acal demonstrated enhanced survival and proliferation in the presence of CD40L-stromal support. We found it surprising that a cell-line model would show such dependency, mimicking the behaviour of MCL cells *in vivo,* but this behaviour provides further support for the use of REC-1 cells as a model to investigate mechanisms of BTKi resistance in MCL.

Stromal cell support in the absence of CD40L did not affect functional or signalling responses of REC-1 cells to BTK inhibition. However, the presence of CD40L stroma prevented downregulation of ERK1/2 phosphorylation following BTKi treatment of the REC-1 cells, suggesting that there is a BTK-independent pathway for ERK1/2 activation that is induced by CD40L possibly by MAPK and PI3K pathways. In addition, IRF4 expression in REC-1 cells following CD40L stimulation was sustained and not down-regulated in response to treatment with either Ibr or Acal. These data suggest that CD40L stimulation provides a pathway for REC-1 cells to resist effects of BTKi treatment. Increased levels of IRF4 expression are seen following CD40L stimulation, as we see with BCR stimulation. However, unlike effects of BCR stimulation, IRF4

expression is sustained following BTKi treatment in the presence of CD40L, reflecting a possible mechanism of resistance and/or a biomarker of resistance. Studies suggest that both the canonical and non-canonical NF-κB pathways can be activated by MCL stromal cell interaction, either alone or through secretion of B-cell activating factor (BAFF),[53] and may be a possible pathway mediating the effect of IRF4. There was no evidence of increased IRF4 expression in REC-1 cells co-cultured with stromal cells in the absence of CD40L.

Unsurprisingly, REC-1 cells with acquired BTKi resistance were independent of CD40L; they required no additional stimulation from CD40L to overcome BTKi effect suggesting that the increased survival, proliferation and the sustained levels of IRF4 in these cells was independent of the effects of CD40L. This suggests that acquired resistance to BTKi may occur through an intrinsic mechanism, such as mutations in the BTK molecule.

Like the MCL cell lines described in Chapter 3, primary MCL cells whether sensitive or resistant to BTKi all showed a normal functional BCR with increased pBTK-Y223 following IgM stimulation which was reduced following BTKi treatment. Phosphorylated BTK-Y223 was significantly reduced by Ibr but not Acal, however given the near significance (p=0.06) this was possibly due to the low dosage of Acal treatment (100nM) used to treat the cells *in vitro*. It is likely that this result would be significant at higher dosage. These results are suggestive that in cells with innate resistance, resistance mechanisms may occur further downstream from BTK or via alternative pathway activation possibly by effects of the tissue microenvironment.

Primary MCL cells behaved similarly to REC-1 cells when co-cultured with fibroblast support and in response to BTKi treatment. Survival was significantly increased after 24 hours co-culture with CD40L although not at 48 hours, which could be due to patient variability given that some patient samples analysed at 48 hours were different to samples analysed at 24 hours, two of which were indolent cases which generally have lower rates of apoptosis. In addition, the data is only representative of 5 individual MCL cases at 48 hours, it is likely therefore that significance would increase with a larger sample size.

Similar results were shown in response to BTKi; CD40L significantly prevented apoptosis of primary MCL cells in response to BTKi after 24 hours co-culture but not after 48 hours which again may be influenced by the small sample size and indolent cases with low apoptosis rates.

CD40L significantly upregulated IRF4 levels in all 8 MCL patient samples analysed ($p= 0.0012$) (Figure 4.12B). In the absence of CD40L, IRF4 was downregulated by BTKi (both Ibr and Acal), but in the presence of CD40L, no downregulation of IRF4 expression was seen in response to BTKi (both Ibr and Acal).

These findings suggest that signals from the tissue microenvironment may modulate drug response in MCL and that CD40L-CD40 signalling may have a role in primary resistance to BTK inhibitors by modulating expression of IRF4. To validate whether IRF4 could be a biomarker of BTKi treatment response in MCL, *ex vivo* samples from clinically treated patients (n=8) were analysed before and during BTKi treatment. The results showed that IRF4 was downregulated in 7 samples from patients shown to be clinically responding to BTKi and was not downregulated in 1 refractory case. In responding patients, IRF4 downregulation was shown to be an early response to

therapy occurring within the first treatment cycle and was sustained over several treatment cycles until relapse when its downregulation was prevented and IRF4 expression was sustained. Here however, we noticed that the IRF4 band was detected lower than that predicted which may reflect a post translational modification/alteration in phosphorylation sites which could be explored further using 2 dimensional SDS-gel electrophoresis. Commercially available phospho- IRF4 antibodies are not widely available. The group of Wang & Ning [195] have developed a polyclonal antibody specific to phospho-IRF4 (Y121/124) offering the opportunity for collaborative studies.

Similarly, IRF4 was not downregulated over several treatment cycles in a primary resistance case. These findings provide further evidence that IRF4 expression is associated with response to BTKi treatment in MCL and could have potential use as a biomarker in a clinical setting. The mechanisms of IRF4 regulation by BTKi in MCL are discussed in Chapter 5.

Chapter 5 - Investigating IRF4 regulation, interactions and effects of BTKi.

5.1 Introduction

The findings from this study have indicated that IRF4 is linked to the treatment response to BTKi, both in MCL cell lines and in primary cells. However, to understand the role that IRF4 has in cells treated with BTKi, it is important to understand its regulation and function in MCL. Therefore, further studies were undertaken to test the control of IRF4 within MCL, and to investigate the complex relationship between protein translation and degradation through assessment of mRNA levels. Subsequent studies then went on to explore the interactions between IRF4 and other cell proteins: initially exploring known interactions (specifically the interaction with the ETS family member PU.1 - as discussed in the Introduction section 1.4.1). Then subsequently, and perhaps more importantly, interactions with previously unreported proteins were studied using co-immunoprecipitation studies and SWATH mass spectrometry. Finally, since IRF4 is a known transcription factor, studies were performed to identify IRF4 target genes through sequencing of IRF4-DNA chromatin precipitates from either BTKi sensitive or resistant cells, aiming to determine DNA binding sites of IRF4 which can be mapped to the human genome to further identify its interactions.

5.2 Methods employed

The methods employed in this chapter involve the isolation of RNA (Methods section 2.5.1) from REC-1 and G519 cells following BTKi treatment, conversion of the RNA to cDNA (Methods section 2.5.2) and analysis of IRF4 and PU.1 mRNA expression by quantitative real time PCR (qPCR) (Methods section 2.5.4).

Co-expression of IRF4 and PU.1 was investigated using biochemical assays of co-immunoprecipitation (Co-IP) (Methods section 2.4.4), western blotting (Methods section 2.4.6) and immunohybridisation (Methods section 2.4.6.1) of IRF4 protein precipitates from REC-1 cells. Further assessment of IRF4-protein interactions was determined using SWATH mass spectrometry of co-precipitated proteins (Methods section 2.4.5). Functional relationships of the proteins identified using SWATH were determined using STRING (Search Tool for the Retrieval of Interacting Genes/Proteins) database, using highest confidence analysis (predicted significance >0.9).

Chromatin immunoprecipitation (ChIP) of IRF4 (Methods section 2.5.6) was optimised in REC-1 and G519 cells. The ChIP procedure was confirmed by amplification of the *RPL30* locus using conventional methods of PCR (Methods section 2.5.3) and agarose gel electrophoresis (Methods section 2.5.5). The DNA sequences bound to IRF4 were detected by next generation sequencing (Methods section 2.5.7) on purified IRF4 DNA from G519 cells.

The list of antibodies used in this chapter is shown below (Table 5.1), accompanied with the antibody dilutions relating to the applications in which they were used.

The mRNA expression data (qPCR) was analysed using the delta delta Ct (2^-ddCt) method in Microsoft Excel™. Sequencing reads obtained from the IRF4 ChIP sample

were aligned to the human genome reference HG38 using CLC Workbench version 11 software.

Antibody/probe	Species	Application	Ref	Source	Conc
IRF4 primary antibody	**Rabbit anti human**	WB IP/ChIP	#4964	CST	1/1000 1/25
MUM-1 primary antibody	**Rabbit anti human**	WB IP/ ChIP	ab133298	Abcam	1/5000 1/25
PU.1/Spi-1 primary antibody	**Mouse anti human**	WB	MAB5870	R & D systems	1/250
GAPDH primary antibody	**Rabbit anti human**	WB	#2118	CST	1/5000
Histone H3 (D2B12) XP primary antibody	**Rabbit anti human**	ChIP	#4620	CST	1/50
Normal Rabbit IgG primary antibody	**Rabbit anti human**	IP/ChIP	#2729	CST	1/250
Secondary antibody-HRP	**Goat anti rabbit**	WB	#P0448	Dako	1/2000
Secondary antibody-HRP	**Goat anti mouse**	WB	#P0447	Dako	1/2000
IgG light chain secondary antibody-HRP	**Mouse anti rabbit**	WB	ab99697	Abcam	1/2000

Table 5.1: Antibodies used in Chapter 5. HRP= Horseradish peroxidase, WB= western blotting, IP = immunoprecipitation ChIP=chromatin immunoprecipitation, CST= Cell signalling technology. All antibodies used for ChIP were validated except for the MUM-1 antibody from Abcam.

5.3 Downregulation of IRF4 mRNA is an early and specific response to BTKi treatment in sensitive REC-1 cells, but not in resistant cells (innate or acquired).

Downregulated expression of IRF4 mRNA was shown to be an early response to BTKi treatment in the BTKi sensitive REC-1 cells. However, downregulation was not demonstrated in the acquired resistant REC-1 cells or the G519 cells; these findings corresponded to the retained expression of IRF4 protein in these latter cells.

5.3.1 Assessment of IRF4 mRNA expression in REC-1 cells following BTKi treatment

Expression of IRF4 mRNA was first assessed in REC-1 cells following treatment with Ibr (10µM). RNA was extracted from the cells at regular time points over 48 hours and converted to cDNA. The cDNA was amplified by qPCR using primers specific for regions on *IRF4* and the control gene *HPRT*.

Expression of IRF4 mRNA was found to be downregulated (relative to HPRT) in REC-1 cells as an early response to Ibr, and was maximally reduced after 4 hours of treatment (Figure 5.1). This timescale related well to the results already reported in chapter 3 (Figure 5.2) where the downregulation of IRF4 protein expression occurred at 4-8 hours following BTKi treatment. This suggested that the changed IRF4 protein expression might be due to altered mRNA transcription and biosynthesis rather than degradation, and the down regulation of IRF4 was therefore a specific transcriptionally-regulated response to treatment. However, IRF4 mRNA was not persistently downregulated at this level and appeared to increase with time (although relative to baseline expression was still lower). The IRF4 protein expression did not follow the same trend (Figure 5.2), suggesting alternative/additional mechanisms must

underlie the persistent downregulation of IRF4 protein expression seen in REC-1 treated cells.

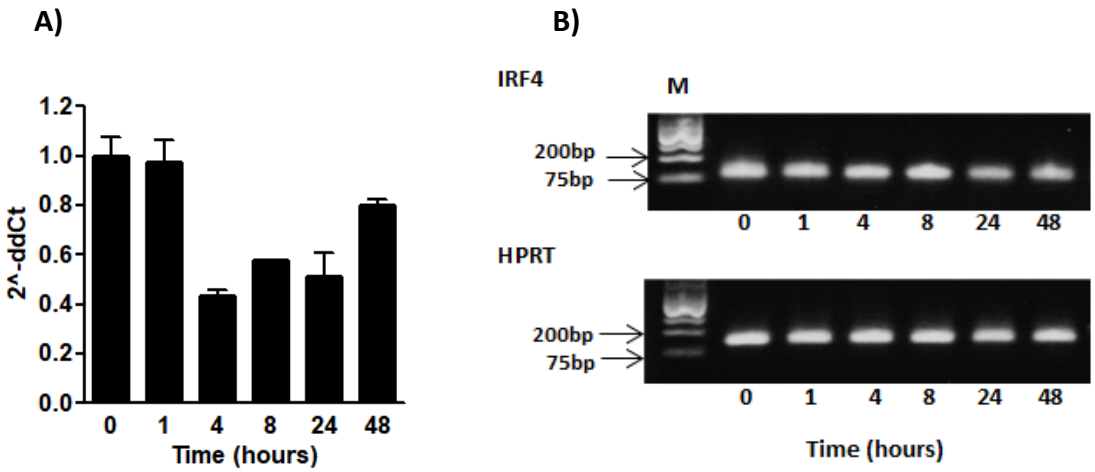

Figure 5.1: Expression of IRF4 mRNA in REC-1 cells in response to Ibr. REC-1 cells were treated with Ibr (10µM). RNA was extracted from the cells at regular time points over 48 hours. *IRF4* and *HPRT* regions were amplified from cDNA using qPCR. A) 2^-ddCt of IRF4 mRNA levels normalised to HPRT (N=2). B) Agarose gel electrophoresis analysis of the qPCR amplicons for IRF4 (91bp) and HPRT (131bp) (representative image from one experiment).

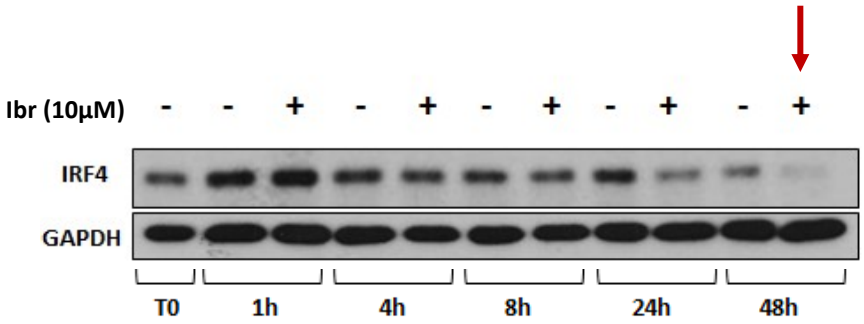

Figure 5.2: Expression of IRF4 protein in REC-1 cells in response to Ibr. REC-1 cells were treated with Ibr (10µM). Protein was extracted from the cells at regular time points over 48 hours and separated by SDS-PAGE. 10% SDS gel. 25µg protein, Rabbit anti-IRF4 Ab (CST #4964) 1 in 1000, GAPDH (CST #2118) 1 in 5000 in 5% BSA/TBST, o/n at 4°C. Goat anti-rabbit-HRP (Dako, P0448) 1 in 2000 dilution (IRF4), 1 in 5000 dilution (GAPDH) in 5% BSA/TBST, 1 hr, RT. ECL (Pierce, Life Technologies) (GAPDH) ECL prime (IRF4). Expression of IRF4 protein after 48 hours Ibr treatment is indicated by the red arrow.

To determine whether the response to Ibr was similar with a more specific BTKi, expression of IRF4 mRNA was compared in REC-1 cells treated with either Ibr or Acal at 1μM concentrations. IRF4 mRNA was again found to be downregulated by Ibr by 4 hours (as previously); and slightly later (after 4 hours) following treatment with Acal (Figure 5.3). Despite the differences in the first 4 hours following treatment, there was a similar trend in IRF4 mRNA expression in response to either Ibr or Acal.

Note that in this experiment, the time 0 control was excluded from analysis, since the PCR amplicons assessed by agarose gel electrophoresis showed reduced expression of the IRF4 cDNA in the time 0 control sample compared to the treated samples (Figure 5.4), which was not seen in the previous experiment (Figure 5.1B). This was possibly due to poor quality RNA as shown in Table 5.2. Since there was no difference seen between IRF4 mRNA expression at 0 or 1 hour (as shown in Figure 5.1) and is in accordance with what is generally considered to be the case with mRNA transcription, analysis of IRF4 mRNA was compared relative to the 1 hour treated samples for both Ibr and Acal.

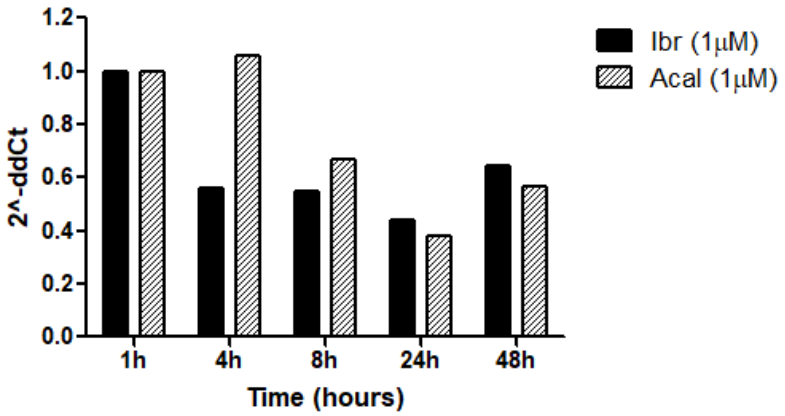

Figure 5.3: Expression of IRF4 mRNA in REC-1 cells in response to Ibr and Acal. REC-1 cells were treated with Ibr or Acal (1μM). RNA was extracted from the cells at regular time points over 48 hours. *IRF4* and *HPRT* regions were amplified from cDNA using qPCR. IRF4 mRNA levels were normalised to HPRT (2^-ddCt).

Sample	Concentration ng/µl	A260/280 (2.0)	A260/230 (2.0-2.2)
Ctrl 0h	167.8	2.8	1.5
Ibr 1h	202.3	2.1	1.9
Ibr 4h	251.4	2.1	2.0
Ibr 8h	308.9	2.1	1.9
Ibr 24h	298.9	2.1	2.0
Ibr 48h	357.9	2.1	1.7
Acal 1h	190.1	2.1	1.7
Acal 4h	275.1	2.1	1.8
Acal 8h	335.7	2.1	1.7
Acal 24h	247.4	2.1	1.9
Acal 48h	328.7	2.1	1.7

Table 5.2: Nanodrop assessment of RNA concentration and purity. The time 0 sample (highlighted in red), shows poor RNA purity compared to treated samples.

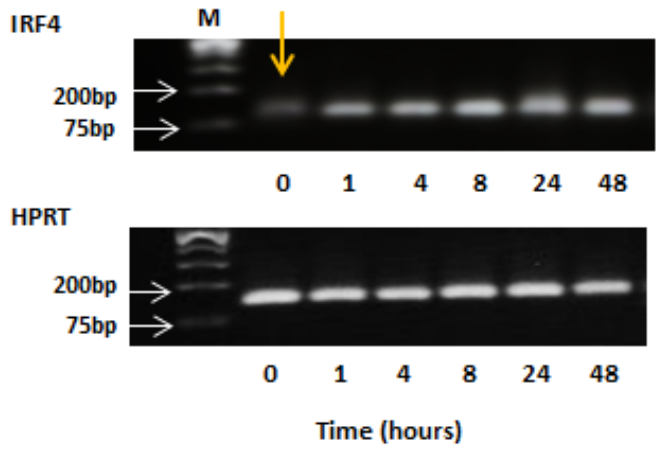

Figure 5.4: Agarose gel analysis of the PCR products showing poor expression of IRF4 cDNA in the time 0 sample. IRF4 and HPRT cDNA amplicons from the time 0 sample (indicated by orange arrow) compared to the samples treated with Ibr (1µM) after 1, 4, 8, 24 and 48 hours.

5.3.2 Assessment of IRF4 mRNA in BTKi- treated MCL cells with innate or acquired resistance

IRF4 mRNA expression was next assessed in cells with either innate or acquired BTKi resistance to provide evidence of whether the differences seen in protein expression between BTKi sensitive and resistant cells were consistent with changes to IRF4 transcription.

The innate resistant G519 cells were assessed following treatment with Ibr or Acal (1µM). RNA was extracted from the cells at regular time points over 48 hours. IRF4 mRNA expression was found to differ between treatment with Ibr and Acal (although again, the trends are similar but delayed with Acal); however both showed increased mRNA expression at 24 and 48 hours relative to the control time 0 sample (Figure 5.5). The pattern of IRF4 mRNA following Ibr treatment corresponds well to the IRF4 protein expression in G519 treated cells - although direct correlation cannot be made due to different doses used, it is clear that there is increased protein expression seen at 24 and 48 hours (Figure 5.6). Further analysis shows that IRF4 mRNA expression was significantly different in G519 cells compared to REC-1 cells in response to BTKi treatment (unpaired t test p=0.0006) (Figure 5.7) suggesting differences in IRF4 gene transcription between BTKi sensitive and innately resistant cells.

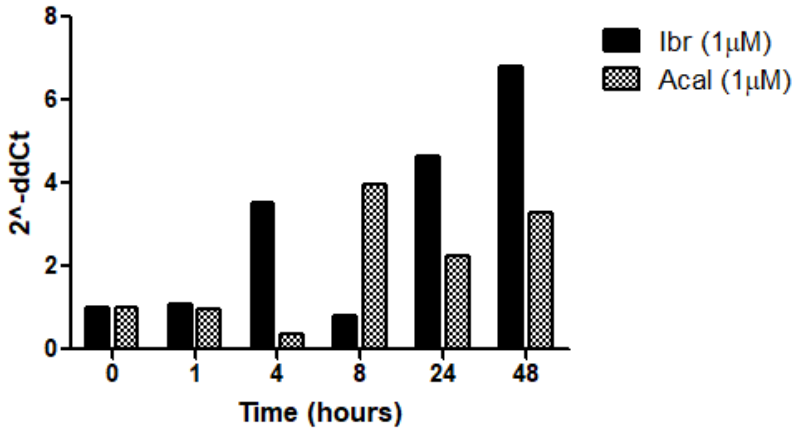

Figure 5.5: Expression of IRF4 mRNA in G519 cells in response to Ibr and Acal. G519 cells were treated with Ibr or Acal (1μM). RNA was extracted from the cells at regular time points over 48 hours. IRF4 and HPRT regions were amplified from cDNA using qPCR. IRF4 mRNA levels normalised to HPRT (2^-ddCt).

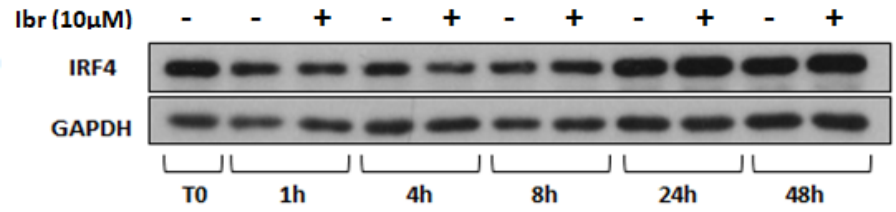

Figure 5.6: Protein expression of IRF4 in G519 cells following Ibr treatment. G519 cells were treated with Ibr (10μM). Protein was extracted from the cells at regular time points over 48 hours and separated by SDS-PAGE. 10% SDS gel. 25μg protein, Rabbit anti-IRF4 Ab (CST #4964) 1 in 1000, GAPDH (CST #2118) 1 in 5000 in 5% BSA/TBST, o/n at 4°C. Goat anti-rabbit-HRP (Dako, P0448) 1 in 2000 dilution (IRF4), 1 in 5000 dilution (GAPDH) in 5% BSA/TBST, 1 hr, RT. ECL (Pierce, Life Technologies) (GAPDH) ECL prime (IRF4).

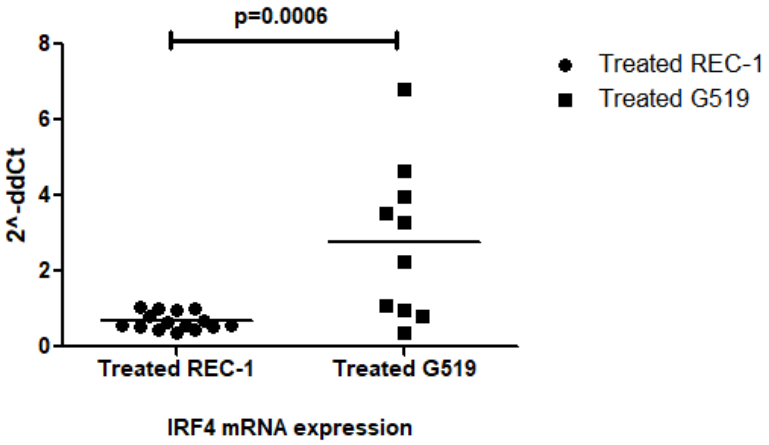

Figure 5.7: Comparison of IRF4 mRNA expression in REC-1 and G519 cells in response to BTKi. The average relative expression values (2^-ddCt) of IRF4 mRNA from 3 x data sets for REC-1 and 2 x data sets for G519. Data was analysed using an unpaired t test on treated samples only.

To confirm whether differences in IRF4 gene transcription were additionally seen in acquired resistant MCL cells, the acquired resistant REC-1 cells (R (Ibr 1μM)) and parent REC-1 cells (P) were treated with a corresponding dose of Ibr (1μM) and incubated for 4 hours. RNA was extracted from each cell line along with untreated parent REC-1 cells (P control) at the same time point for assessment of IRF4 mRNA expression. In the acquired resistant REC-1 cells, IRF4 mRNA was upregulated relative to the untreated control cells at 4 hours which differed to that observed with parental treated cells (Figure 5.8). These findings are suggestive that differences in protein expression that we see in cells resistant to BTKi are additionally reflected at the level of IRF4 gene transcription.

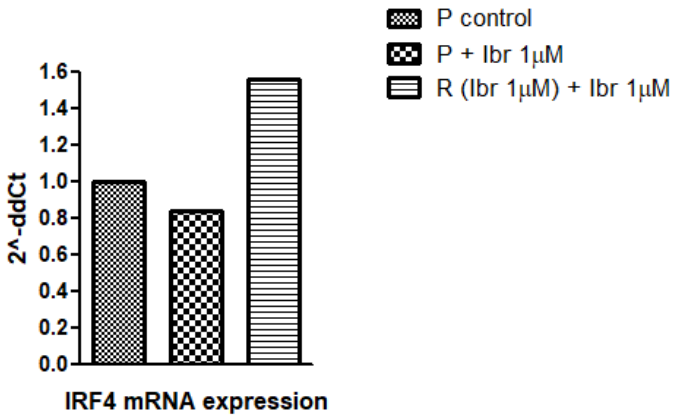

Figure 5.8: Expression of IRF4 mRNA in parent vs acquired resistant REC-1 cells in response to Ibr. REC-1 cells and acquired resistant REC-1 cells (R (Ibr 1μM)) were treated with Ibr (1μM). RNA was extracted after 4 hours treatment. IRF4 and HPRT regions were amplified from cDNA using qPCR. IRF4 mRNA levels were normalised to HPRT (2^-ddCt).

5.4 PU.1 does not interact with IRF4 in REC-1 cells and is not linked to the downregulation of IRF4 in response to BTKi.

PU.1 was not detected in IRF4 protein precipitates from REC-1 cells following co-immunoprecipitation. Assessment of protein expression showed that, in contrast to IRF4 expression, PU.1 was not downregulated in primary MCL cells treated *in vitro* with BTKi. In addition, expression of PU.1 mRNA in REC-1 cells was increased in response to BTKi which did not correlate with downregulation of IRF4 mRNA expression. These studies suggest that PU.1 does not interact with IRF4 in REC-1 cells and is not linked to the downregulation of IRF4 in response to BTKi.

Having determined that IRF4 protein expression and transcription are specific changes seen in MCL cells in response to BTKi treatment, we wanted to understand more about the role IRF4 in MCL cells and how differences in IRF4 protein expression could influence the response of MCL cells to BTKi. Little is known about the interactions of IRF4 in MCL either at the protein or chromatin level. As described in the introduction we know that IRF4 activates transcription of its target genes by forming homo or hetero-dimers either with other IRF family members or with other proteins including AP.1 and ETS family members. The most recognised binding partners for IRF4 are ETS family members PU.1 and SPI-B.[150] We therefore assessed the interaction of PU.1 with IRF4 in MCL cells through co-immunoprecipation assays, and through comparison of expression of IRF4 to PU.1 proteins and transcription in response to BTKi treatment.

5.4.1 Assessment of IRF4- PU.1 interaction in REC-1 cells

To investigate whether PU.1 interacts with IRF4 in MCL, co-immunoprecipitation was performed. Briefly, REC-1 cells were lysed in a low stringency (LS) lysis buffer (100µl / 1 X 10^7 cells). Protein was extracted for immunoprecipitation (IP) of IRF4 using a 1 in 25 dilution of rabbit anti-human IRF4 antibody (CST #4964) and an IgG control IP using a normal rabbit IgG antibody (CST #2729) (Methods section 2.4.4).

Samples of the IRF4 precipitated protein, the post IP sample, the normal IgG control and the REC-1 whole cell lysate were run on a 10% SDS gel and transferred onto a PVDF membrane. The membrane was cut into two pieces. One half was incubated with rabbit anti-human IRF4 primary Ab (1:1000) and the other, with mouse anti-human PU.1/Spi-1 primary Ab (1:250) in 5% BSA/TBST over night at 4°C. Both membranes were incubated for 1 hour with a light chain specific secondary antibody-HRP (abcam #ab99697) diluted 1:2000 in 5% BSA/TBST.

As shown in Figure 5.9, both IRF4 and PU.1 were present in the whole cell lysate confirming their expression by REC-1 cells. IRF4 was also shown to be present in the IRF4 precipitated sample and was enriched compared to the whole cell lysate; IRF4 was not expressed in the IgG precipitated control sample confirming the absence of non-specific binding. Expression of PU.1 was not detected in the IRF4 test IP sample, although IRF4 and PU.1 were weakly expressed in the IRF4 post-IP sample suggesting that not all of the IRF4 protein was successfully precipitated from the lysate. As IRF4 showed enrichment in the test IP sample and with the effectiveness of the PU.1 antibody at detecting PU.1, there should have been sufficient IRF4 protein present to identify any co-precipitated PU.1. These results therefore suggest that PU.1 and IRF4 were not physically associated in REC-1 cells.

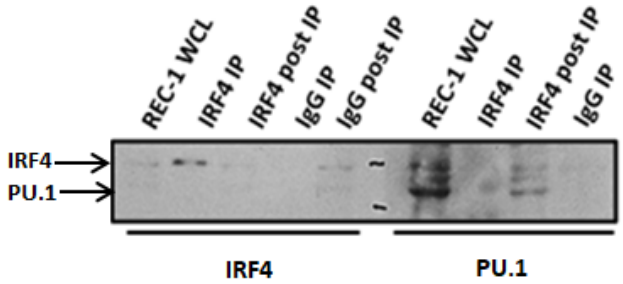

Figure 5.9: Co-immunoprecipitation of IRF4 and PU.1 in REC-1 cells. REC-1 cells were lysed in LS buffer (100µl per 1 x 10^7 cells). For each IP, 600µg protein was diluted in 200µl of immunoprecipitation buffer and incubated with Rabbit anti human IRF4 antibody (CST #4964) (1/25 dilution), or Normal rabbit IgG antibody (CST #2729) (1:250) o/n at 4°C. Membranes were incubated with Rabbit anti-human IRF4 primary Ab (1:1000) or mouse anti-human PU.1/Spi-1 primary Ab (1:500) in 5% BSA/TBST o/n at 4°C. Membranes were incubated with a light chain specific secondary antibody-HRP (Abcam) (1:2000) in 5% BSA/TBST for 1 hour. IRF4 (MW: 50kD) PU.1 (MW: 42kD).

5.4.2 Assessment of PU.1 protein expression in primary MCL cells treated *in vitro* with BTKi

Primary MCL cells co-cultured on a stromal layer (both NT-CD40L and T-CD40L), were treated *in vitro* with Ibr and Acal. Protein was extracted after 48 hours and analysed for expression of IRF4 and PU.1. As shown previously (Chapter 4), in primary cells cultured on the NT-CD40L stromal layer, IRF4 was downregulated by BTKi (both Ibr and Acal) and both upregulated and sustained when cultured on a CD40L stromal layer. This differs to the expression of PU.1 which shows stable expression in response to BTKi treatment and appears downregulated in response to CD40L co-culture (Figure 5.10).

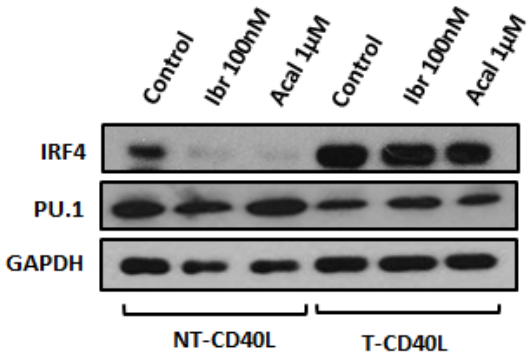

Figure 5.10: Expression of IRF4 and PU.1 in primary MCL cells. Immunoblot analysis of IRF4 and PU.1 in primary MCL cells (Case MCL07) co-cultured on a stromal layer (both NT-CD40L and T-CD40L) and treated *in vitro* with BTKi for 48 hours. 10% SDS gel. 30μg protein. Membranes were incubated with Rabbit anti human IRF4 primary Ab (CST #4964) 1 in 1000 dilution and GAPDH (CST #2118) 1 in 5000 dilution, o/n at 4°C and detected using Goat anti Rabbit-HRP secondary 1 in 2000 dilution following 1 hour incubation at room temperature. The membrane was washed and re-incubated with Mouse anti human PU.1/Spi-1 primary Ab (1:500) o/n at 4°C and detected using Goat anti mouse –HRP secondary antibody.

5.4.3 Assessment of PU.1 mRNA levels following BTKi treatment in REC-1 cells

REC-1 cells were treated with Ibr (1µM) and incubated for 48 hours. RNA was extracted from the cells at regular time points (as indicated) and converted to cDNA. The cDNA was amplified by qPCR using primers specific for regions on *IRF4, PU.1* and the control gene *HPRT* for assessment of both IRF4 and PU.1 mRNA expression.

As shown earlier (section 5.3.1) IRF4 mRNA expression relative to the control *HPRT* gene was downregulated by Ibr in REC-1 cells. However an almost inverse pattern was seen with PU.1 mRNA expression. PU.1 mRNA expression appeared to increase with almost a log greater difference in PU.1 mRNA expression compared to IRF4 mRNA seen at 48 hours (Figure 5.11). These results are again suggestive that PU.1 and IRF4 are not binding partners.

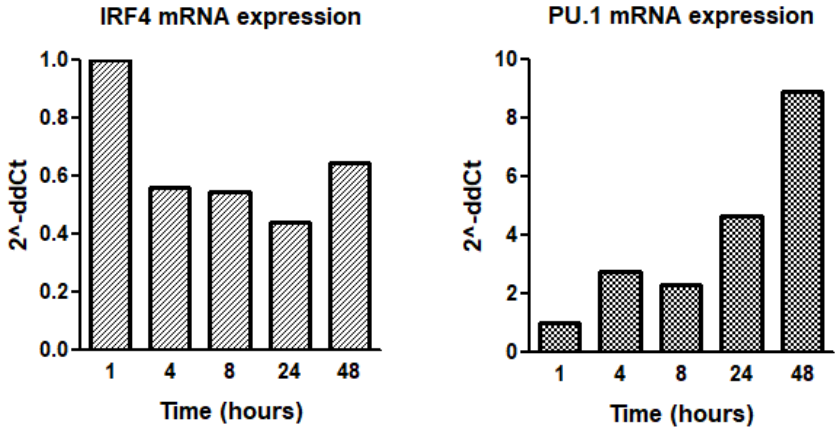

Figure 5.11: Expression of IRF4 and PU.1 mRNA in REC-1 cells in response to Ibr. REC-1 cells were treated with Ibr 1µM. RNA was extracted from the cells at regular time points over 48 hours for assessment of both IRF4 and PU.1 mRNA. IRF4, PU.1 and HPRT regions were amplified from cDNA using qPCR. IRF4 and PU.1 mRNA levels were normalised to HPRT (2^-ddCt).

5.5 IRF4 interactions identified by mass spectrometry reveals a role for IRF4 in mitochondrial ribogenesis

Proteomic study of IRF4 immunoprecipitation of REC-1 cells reveals a particular association with mitochondrial ribosomal proteins and related functional processes.

Previous studies revealed that it was unlikely that one of IRF4's known binding partners, PU.1, was associated with IRF4 in MCL cells. We therefore went on to explore other potential protein interactions of IRF4 in REC-1 cells through studies of co-immunoprecipitation using SWATH mass spectrometry. This study employed the same IRF4 antibody used in earlier precipitation (CST #4964), but also a second IRF4 antibody (rabbit anti-human MUM-1 (abcam #ab133298)) for immunoprecipitation to allow better comparison of precipitated proteins (Figure 5.12).

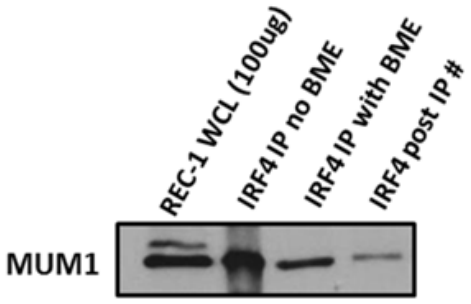

Figure 5.12: Testing the efficiency of the abcam MUM-1 antibody for the immunoprecipitation of IRF4 from REC-1 cells. REC-1 cell lysate (600µg) was incubated with rabbit anti-human MUM-1 antibody (abcam #ab133298) 1:25 in 5% BSA/TBST, o/n at 4°C. A volume of 50µl of protein G beads was added for 1 hour at 4°C. Membrane was incubated with abcam rabbit anti-human MUM-1 antibody (1:1000) o/n at 4°C. Membrane was then incubated with mouse anti-rabbit light chain specific secondary antibody- HRP (1:5000) for 1 hour. WCL = whole cell lysate, BME = β-mercaptoethanol.

Briefly, IRF4 protein precipitations were prepared from REC-1 cell lysate using both CST IRF4 and abcam MUM-1 antibodies and an IgG control antibody. The denatured precipitates were run on a 10% resolving gel prepared under sterile conditions, and each IP lane was cut into 8 individual gel slices (Methods section 2.4.5, Figure 2.5). The gel was left unstained to prevent any staining interference with the mass spectrometry.

The proteomic analysis was performed in Manchester by Drs Cieran and Bobby Graham, and data analysis was then performed with the help of Dr Karen Rees-Unwin and Dr John Burthem in Manchester.

In brief, sequential window acquisition of all theoretical fragment ion spectra (SWATH) was used to identify proteins in the IP samples and to allow quantitative comparison of the protein abundance. Essentially, the technique simply acquires all ions from proteins in the samples using an isolation window that covers the whole mass/charge range. The fragmentation spectra then enable retrospective identification of the peptides allowing the parent proteins to be identified. Quantitation is derived from the quantity of ions related to each protein in relation to the total amount of protein in the sample. SWATH therefore generates a list of proteins within a sample and a supports a relative comparison of protein abundance between samples. Proteins present can then be further analysed by data analysis tools to determine likely significance, and can be further analysed using bioinformatics approaches (in this case analysis using STRING) to determine likely functional relationships.

The results below describe in more detail the analysis of these studies and the significance of the results. The initial analysis focussed on proteins that were precipitated by both IRF4 and MUM-1 antibodies and were not seen in the IgG control IP. The specificity was confirmed since the IRF4 protein itself was found only in precipitates where the specific antibodies were used and not seen in the control precipitates. In addition, both these antibodies co-precipitated a range of proteins that were not found in the control. Analysis showed that the probability that the proteins had been co-precipitated by chance by the specific antibodies but not the control was < 0.00001 (Chi Squared test). This confirmed that many of the precipitated proteins were likely to be associated with IRF4 in some form, although some would be non-specific.

To further analyse the data and identify the major associated proteins with IRF4, the functional relationships of these proteins were assessed by exporting to STRING analysis database. This database combines a range of data mining and experimental sources to establish linked functional characteristics of proteins. All high confidence interactions were initially considered in the analysis, but due to the extensive level of interaction (Figure 5.13) only the highest confidence interactions (STRING algorithm confidence >0.9) were examined in more detail (Figure 5.14). Single proteins without linkage which more likely represented non-specific interactions or unknown associations were excluded to simplify the analysis. The identities of proteins present in each string cluster were determined and used to ascribe the functional group to that cluster (Figures 5.15). These functional proteins clustered to Ribosomal proteins and translation and ribosomal assembly (Figure 5.16), Mitochondrial ribosome proteins and mitochondria and mitochondrial RNA (Figure 5.17), DNA processing and

transcription (Figure 5.18), RAS and signalling functions (Figure 5.19) and Metabolism (general) (Figure 5.20).

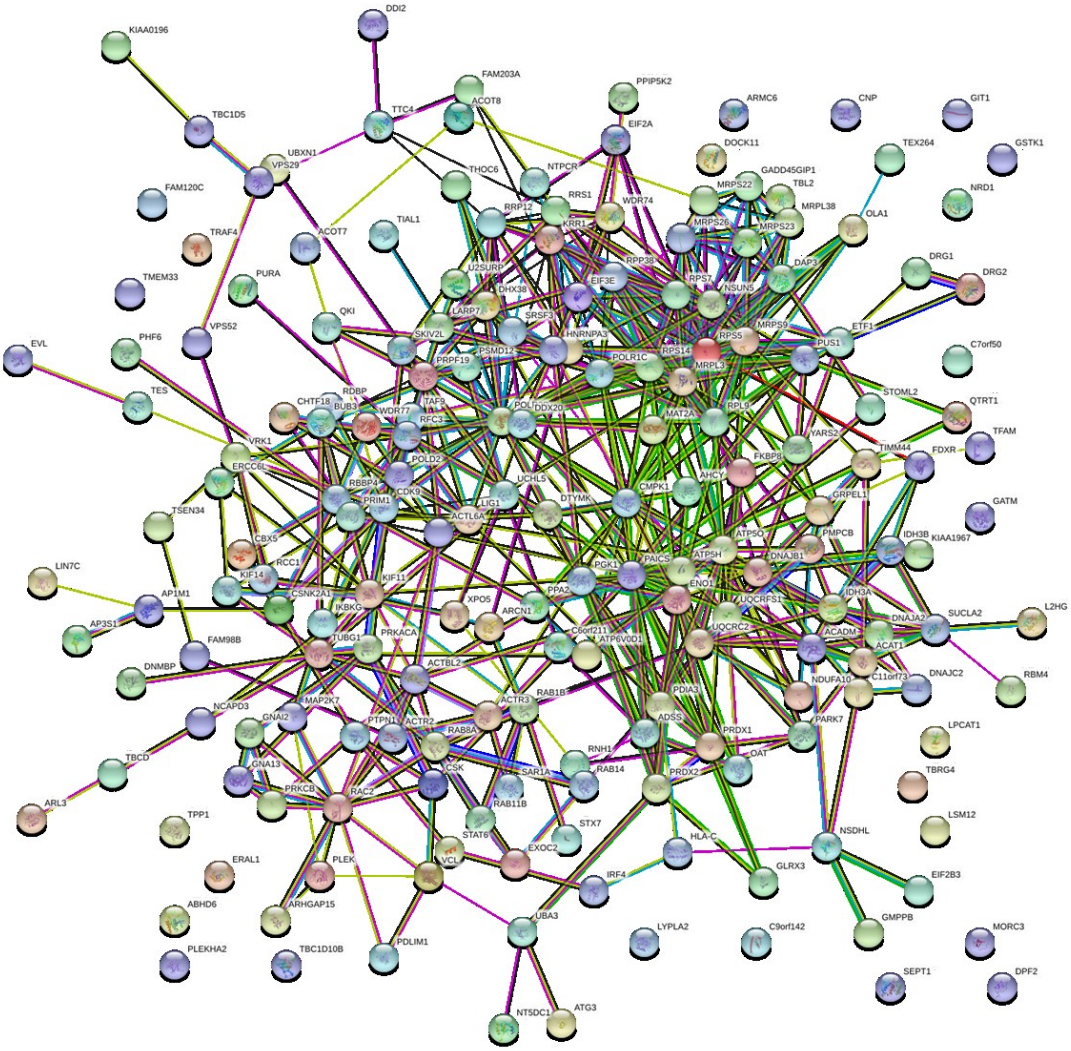

Figure 5.13: STRING analysis of high confidence relationships. Results suggested high level of interaction for the majority of precipitated proteins, but was too complex for detailed functional analysis.

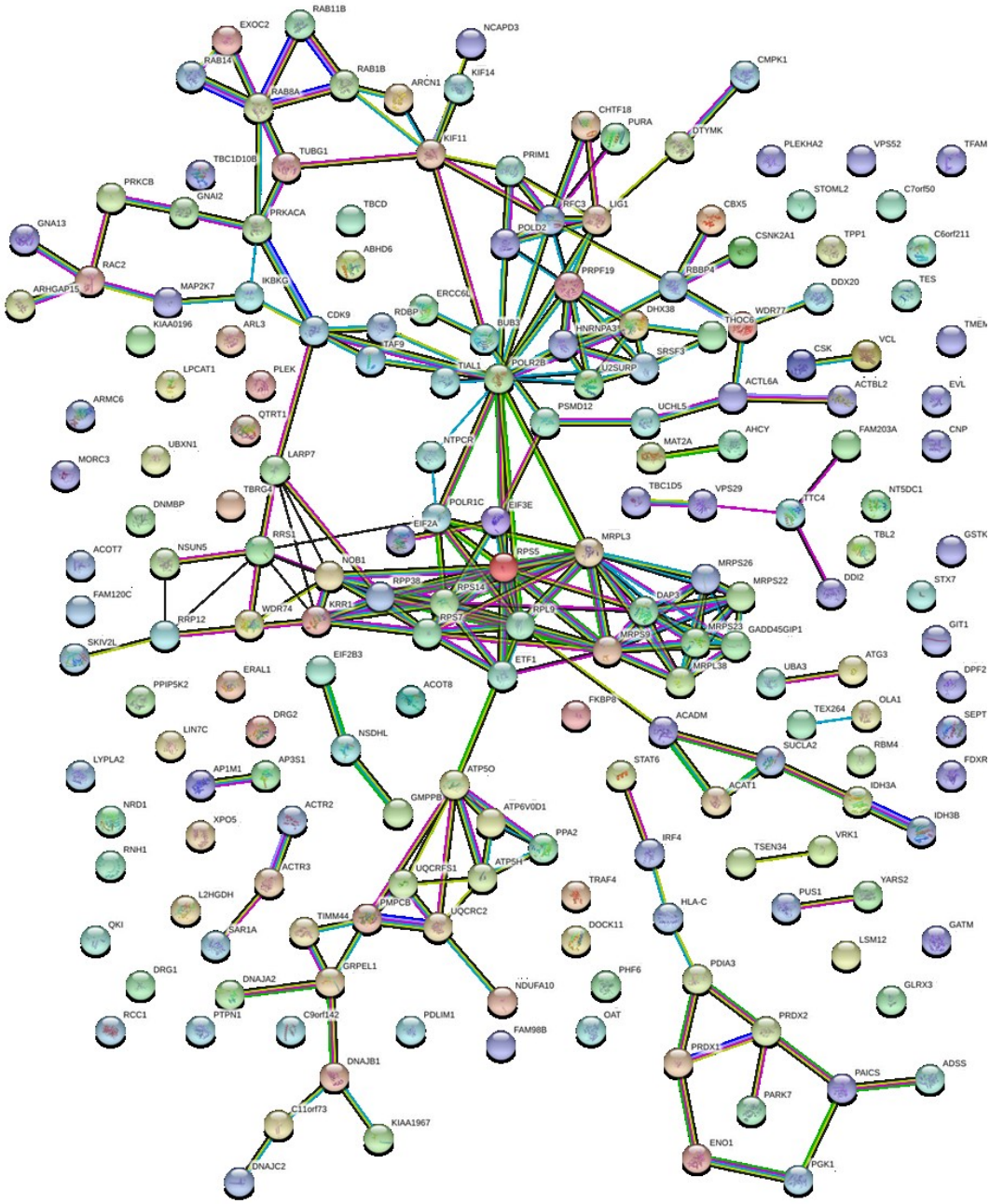

Figure 5.14: Profile of relationships analysed with highest confidence (STRING algorithm confidence >0.9). Single proteins are shown without linkage and may be non-specific or unreported interactions.

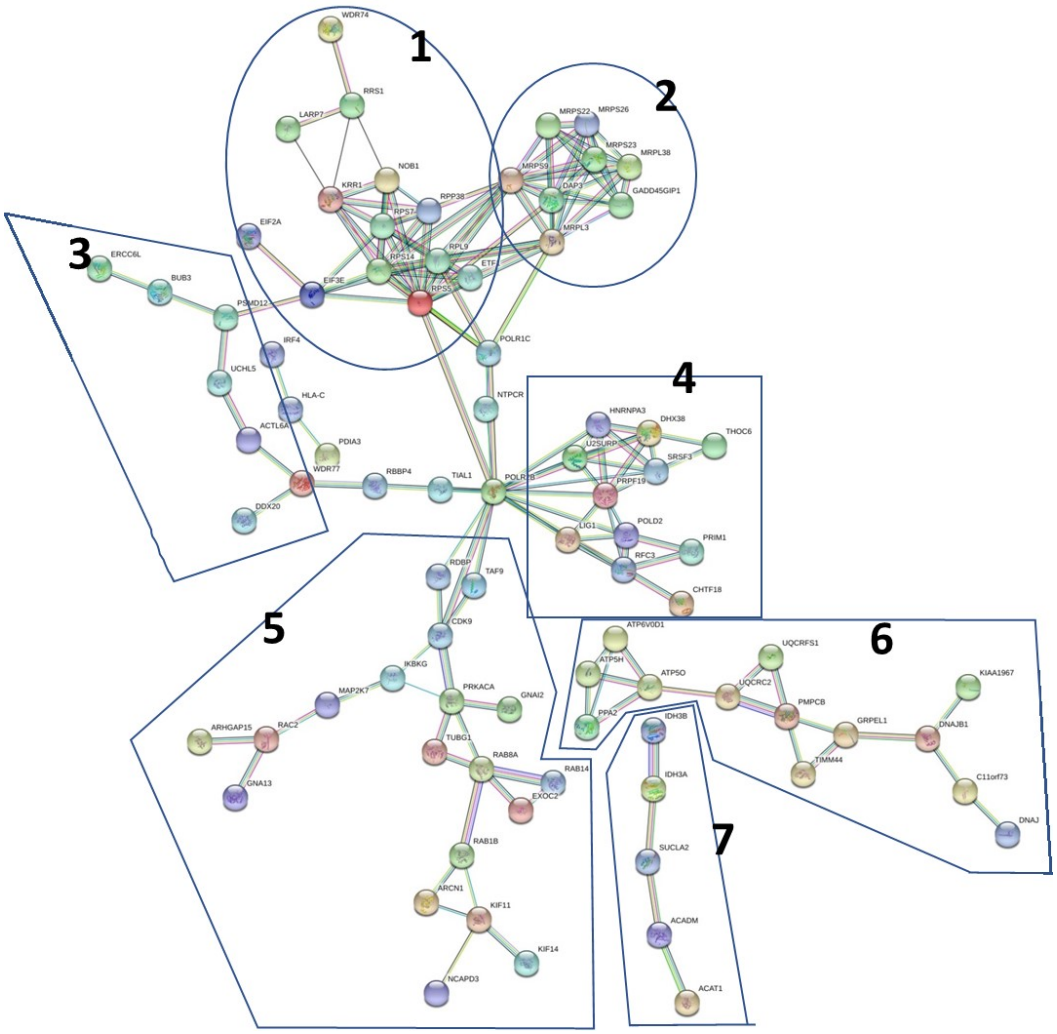

Figure 5.15: Profile of relationships analysed with highest confidence with functional annotation. Data analysed with highest confidence with all single proteins or doublets excluded from the analysis. The groups are assigned function according to protein function of the majority of precipitated elements. Group (1) Ribosomal proteins and translation, (2) Mitochondrial ribosome proteins, (3) Ribosome assembly, (4) DNA processing and transcription (5) RAS and signalling functions, (6) Mitochondria and mitochondrial RNA, (7) Metabolism (general).

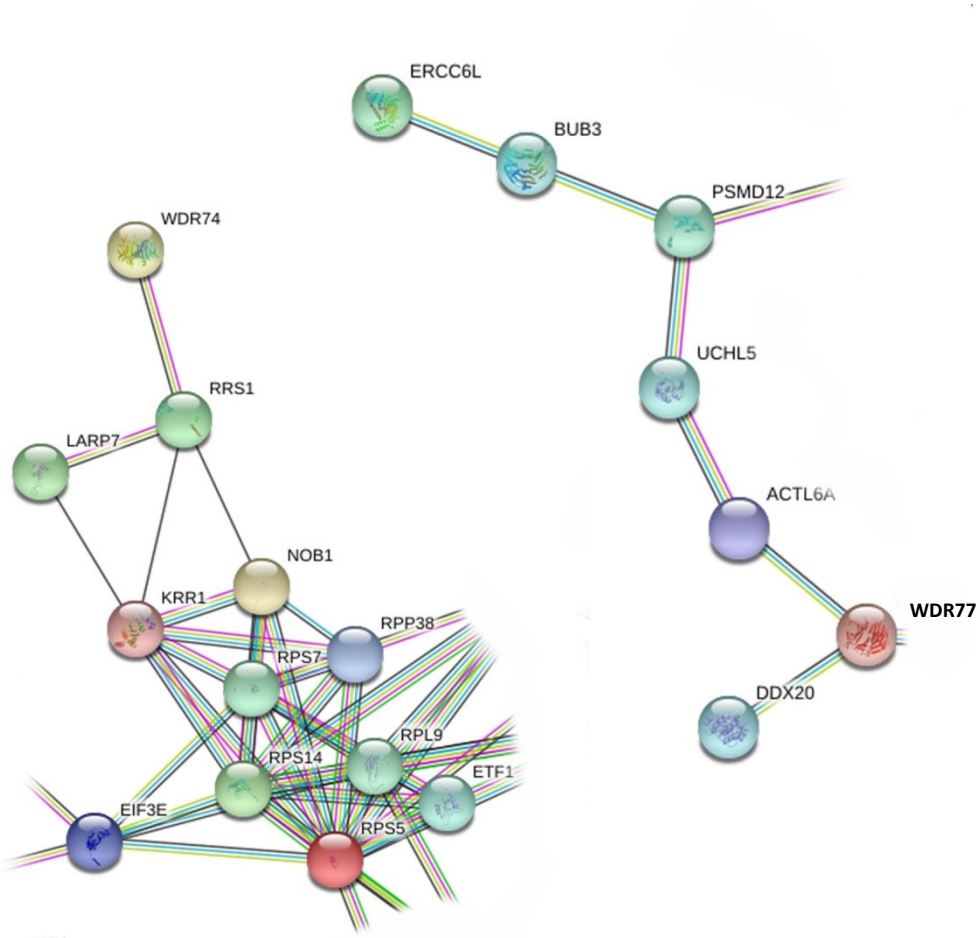

Figure 5.16: Ribosome proteins and proteins of translation and ribosomal assembly. Proteins identified in functional groups 1 and 3.

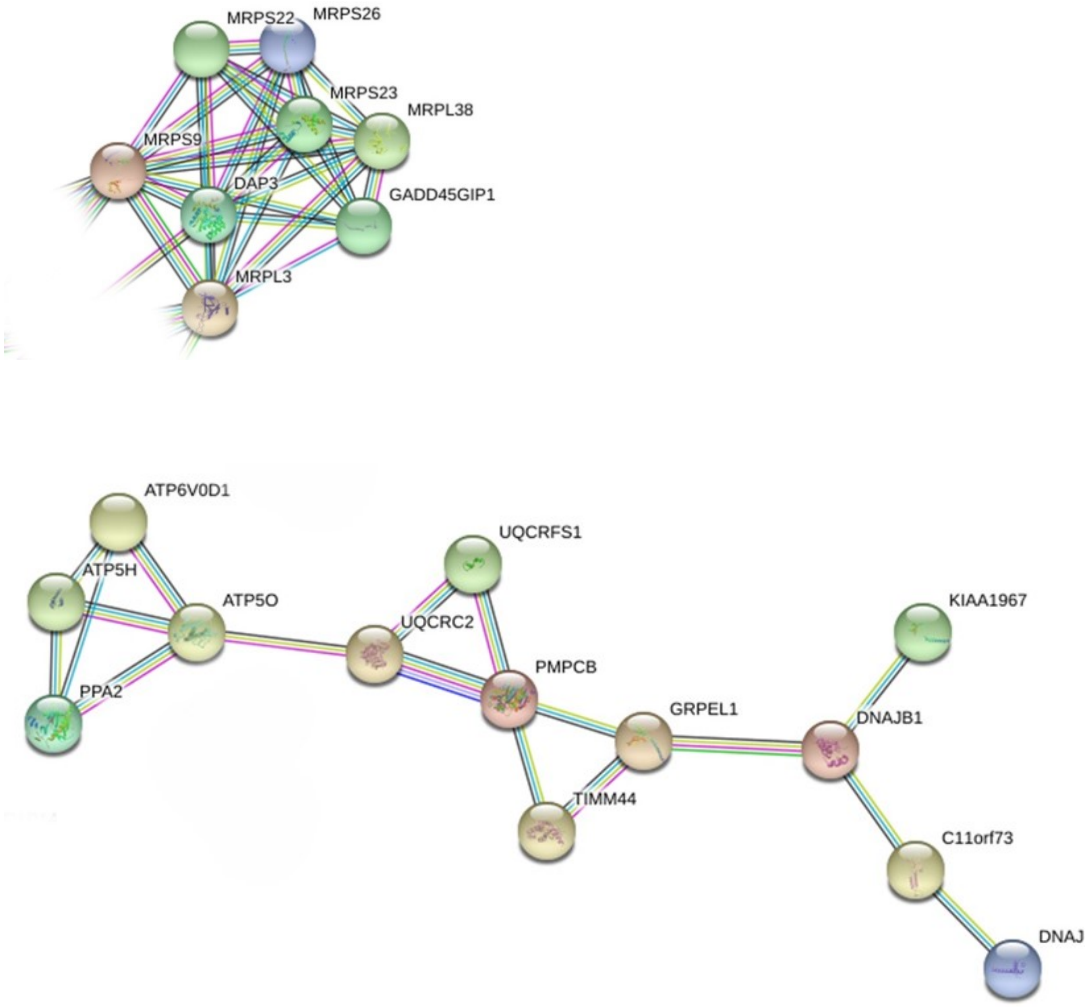

Figure 5.17: Mitochondrial ribosome proteins and mitochondria and mitochondrial RNA proteins. Proteins identified in functional groups 2 and 6.

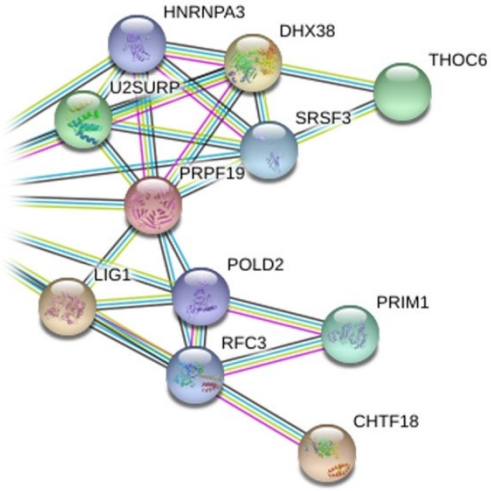

Figure 5.18: Proteins of DNA processing and transcription. Proteins identified in functional group 4.

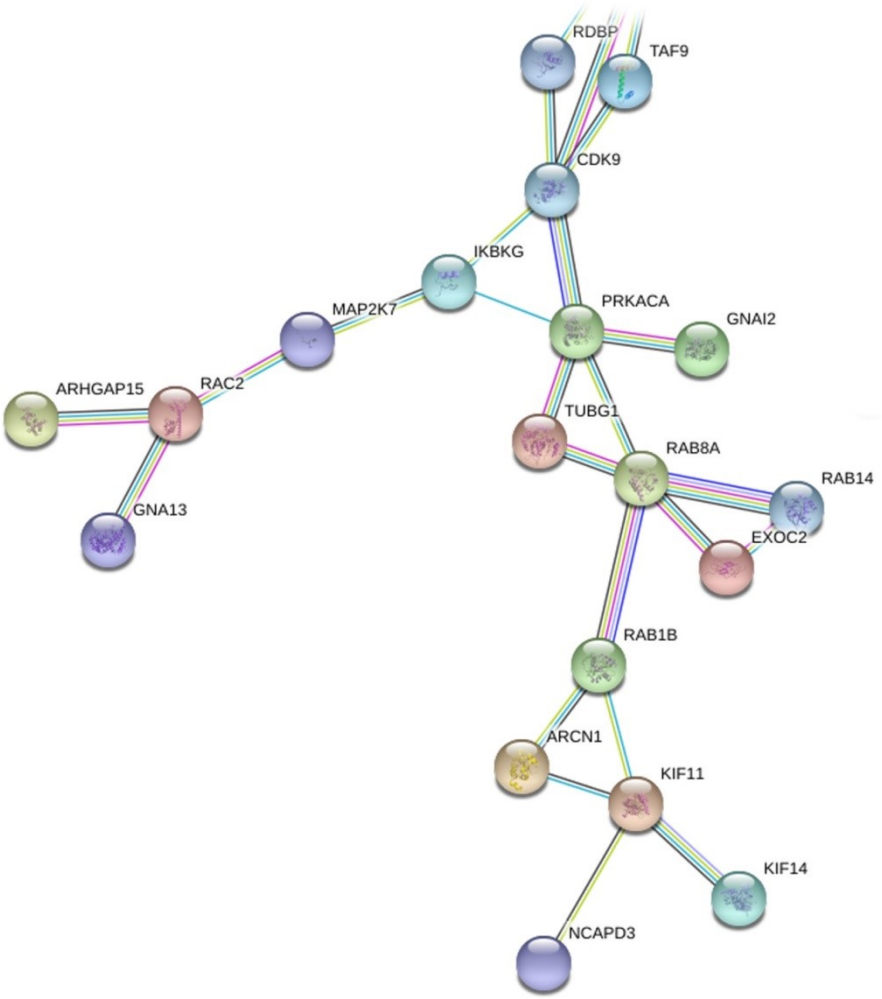

Figure 5.19: RAS and signalling function proteins. Proteins identified in functional group 5.

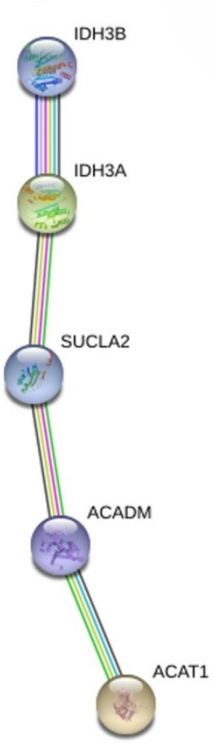

Figure 5.20: Proteins of Metabolism (general). Proteins identified in functional group 7.

Further validation steps were undertaken to determine whether these IRF4 associations were specific, since a possible criticism would be is that there are a large number of co-precipitated proteins detected in both test and control samples. The aim of this validation step was to see if the types of protein that were non-specifically precipitated (i.e. seen with control antibody alone or control antibody and IRF4 antibodies) differed from the specific proteins (precipitated by the IRF4 antibody only). This analysis used a slightly extended dataset including both those that were solely present in control or IRF4 precipitates, but also proteins that were significantly enriched (>2-fold) in either sample. Comparison of the functional protein groups precipitated by control vs. test antibodies (as revealed by the STRING analysis database) is shown in Figure 5.21 and 5.22.

This analysis showed that ribosomal elements including RNA translational factors were a frequent finding in both the control and the IRF4 fractions suggesting that some of these protein types might be non-specific elements. However, one of the major aspects from the initial findings was confirmed – only the IRF4 antibodies precipitated mitochondrial RNA, shown as the distinct cluster in Figure 5.22 and enhanced in Figure 5.23. The presence of mitochondrial ribosomal components only in IRF4 samples was highly significant ($p<0.01$ Chi square test). In comparison to a STRING analysis of known IRF4 interactions (Figure 5.24), the findings identified in this study are currently unknown and warrant further investigation. In addition, analysis of known IRF4, BTK and BCR interactions revealed a direct link for BTK and BCR but only an indirect link with IRF4 (Figure 5.25).

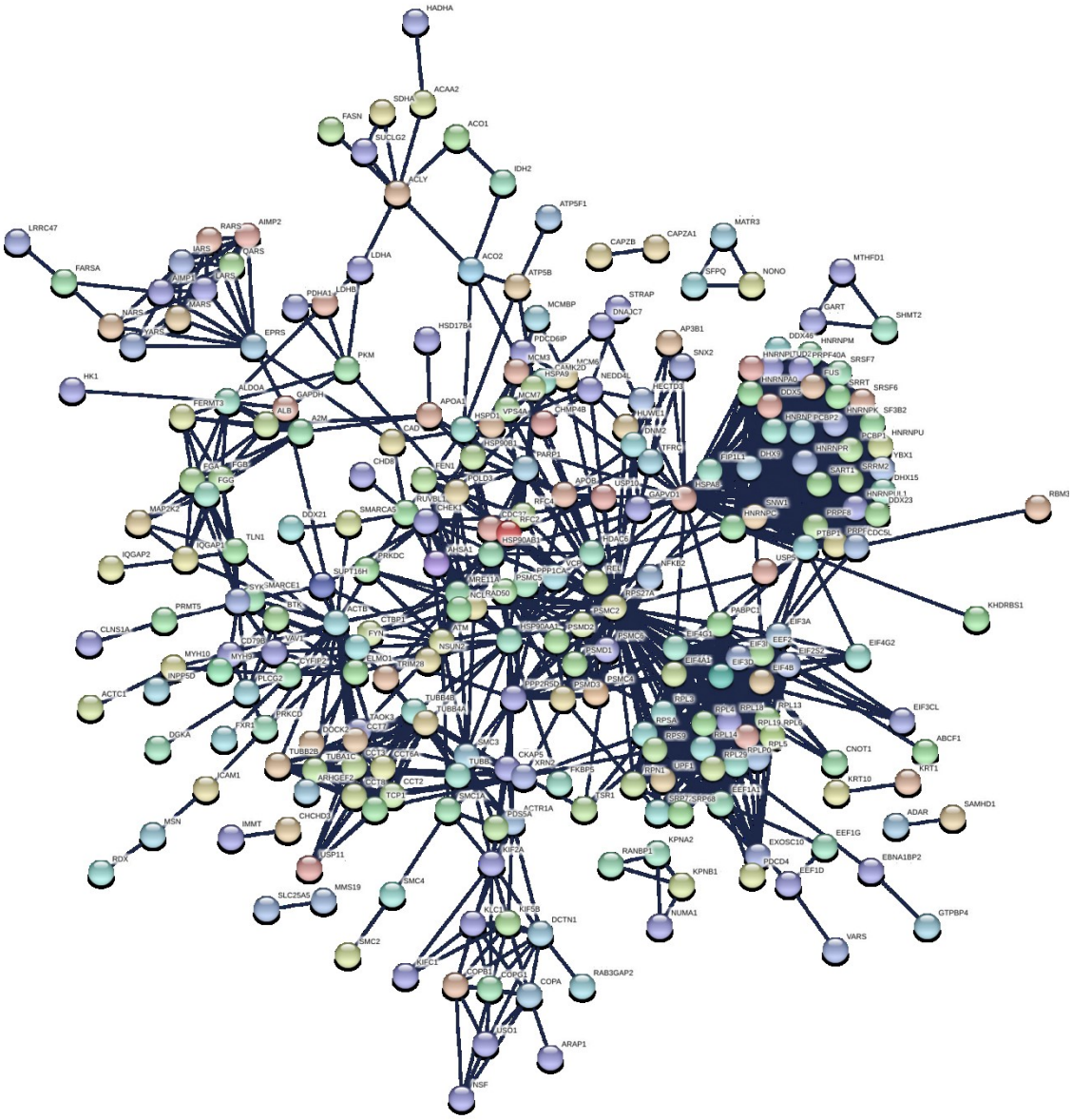

Figure 5.21: Profile of the relationships of the non-specific proteins precipitated by the control sample. Of note there are 2 significant functional clusters which both relate to cellular ribosomal RNA or RNA translation.

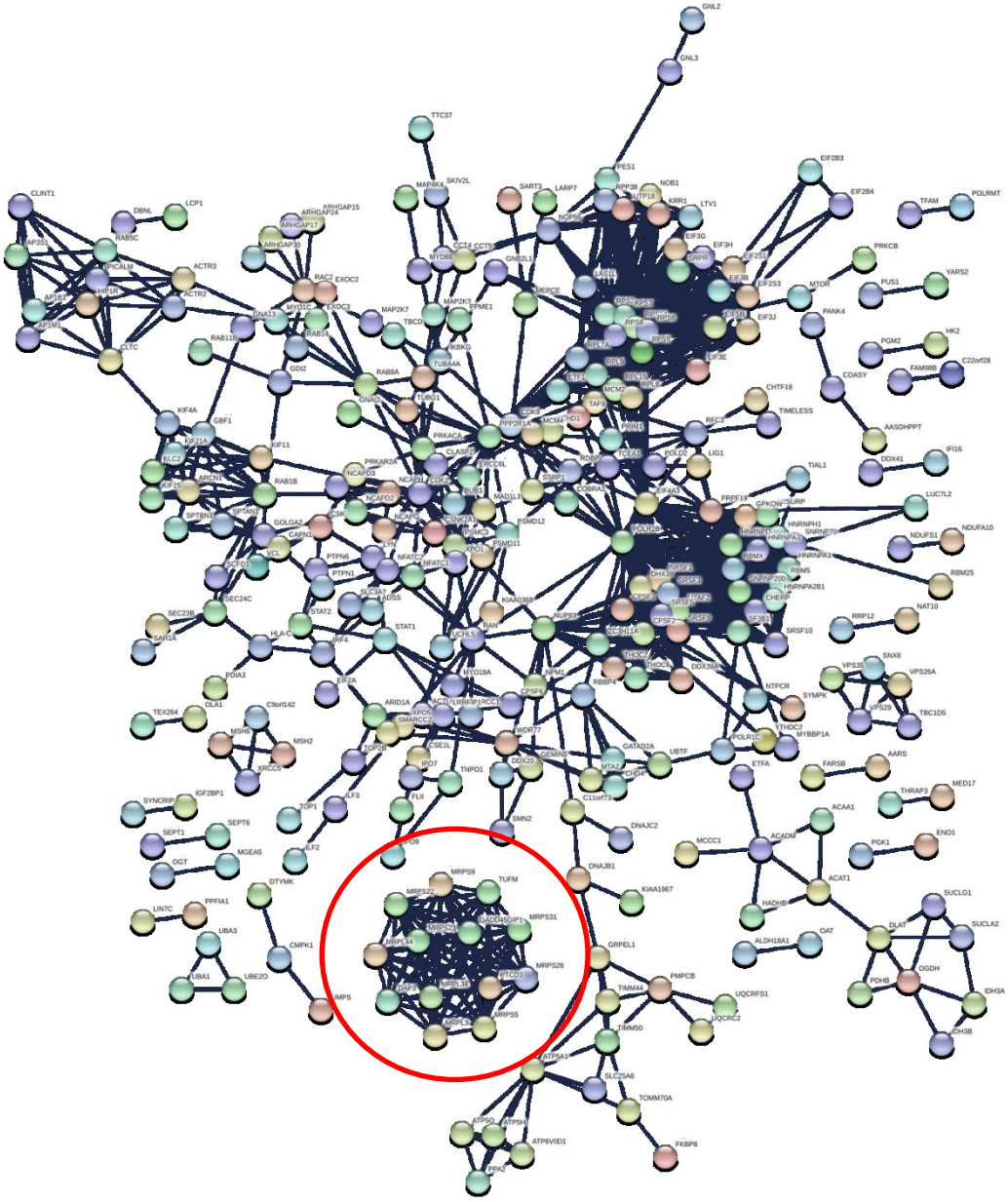

Figure 5.22: Profile of the relationships of the specific proteins precipitated by the IRF4 test antibodies. The two big clusters contain different proteins to the control, but they are functionally similar – relating to cellular RNA and RNA processing. However the highly distinct group (red circle) are mitochondrial ribosome elements which were not present in the control IP.

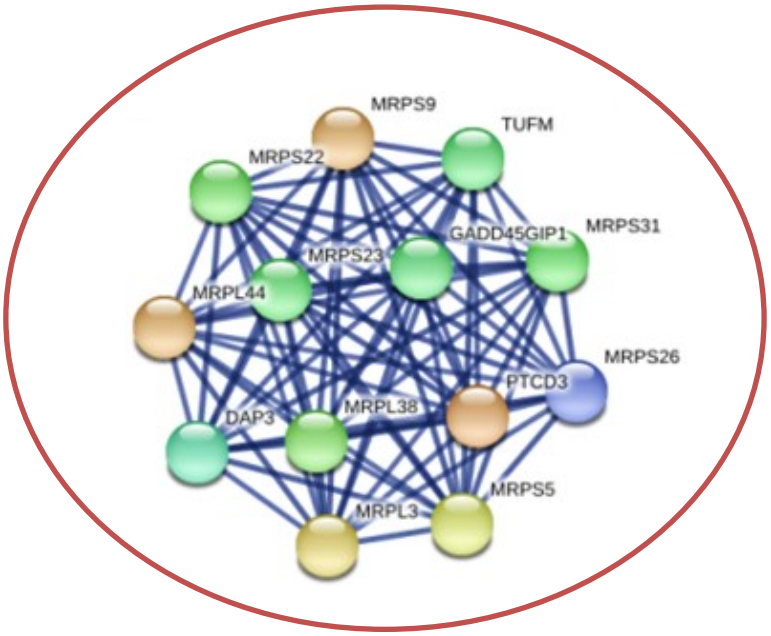

Figure 5.23: Enhanced detail of the distinct cluster of mitochondrial ribosome elements bound to IRF4. IRF4 precipitated proteins included MRPS5, MRPS9, MRPS22, MRPS26, MRPS23, MRPS31, MRPL3, MRPL38 and MRPL44 (mitochondrial ribosomal proteins), PTCD3 (mitochondrial RNA-binding protein), TUFM (mitochondrial elongation factor Tu), DAP3 (mitochondrial 28S ribosomal protein S29), and GADD45GIP1 (Growth arrest and DNA damage-inducible proteins-interacting protein 1).

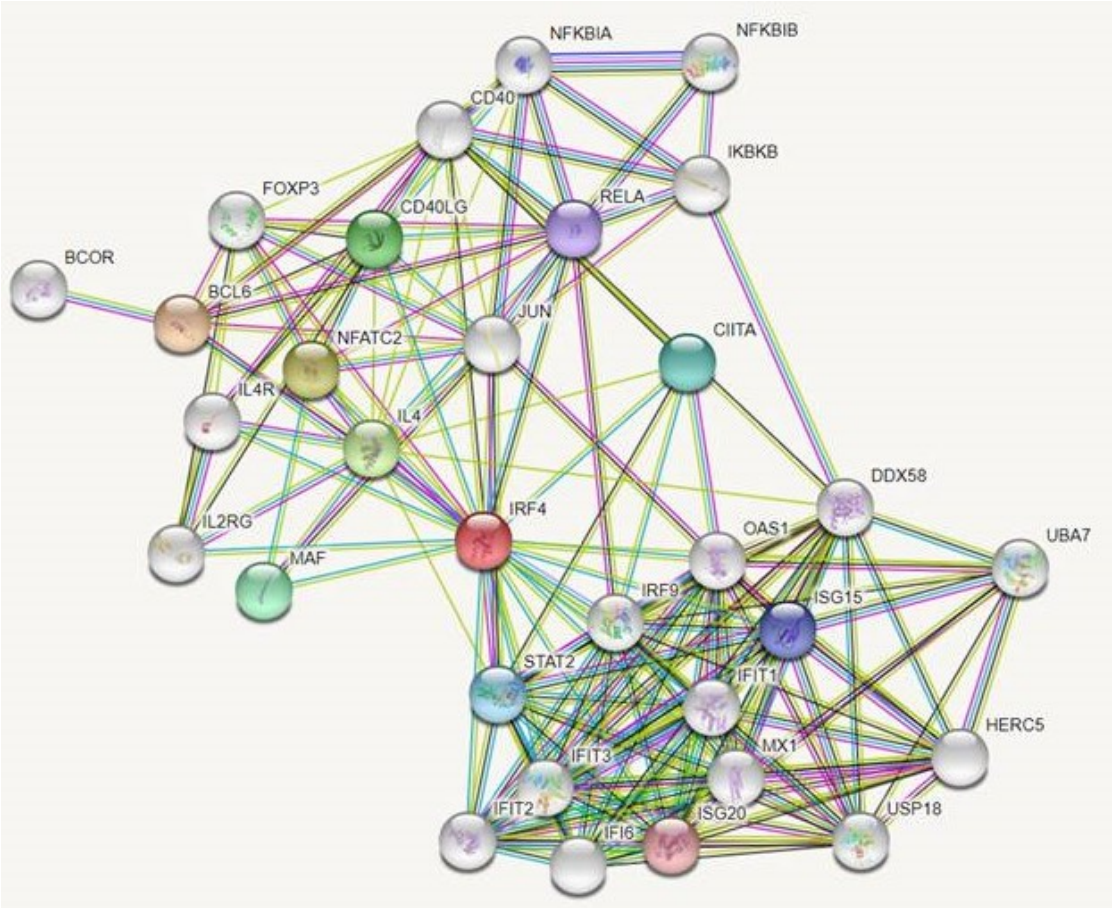

Figure 5.24: STRING analysis of known IRF4 interactions. The figure shows networks that are already known for IRF4 (Uniprot ID: Q15306). The findings from this study were not identified.

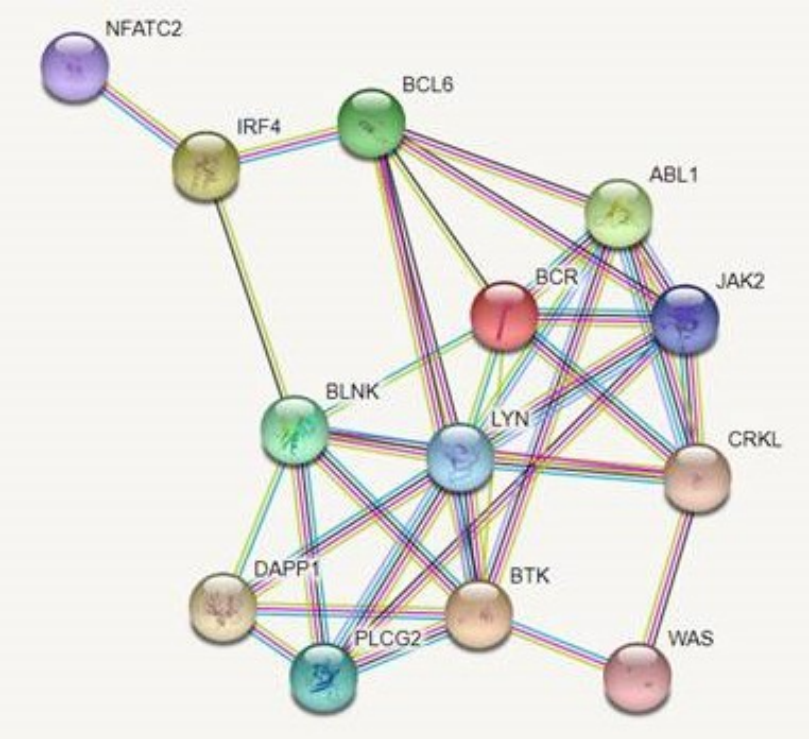

Figure 5.25: STRING analysis of known interactions for IRF4, BTK and BCR. Results showed a direct link for BTK (Uniprot ID: Q06187) and BCR (Uniprot ID: P11274), but no direct link with IRF4 (Uniprot ID: Q15306) (only indirect links).

5.6 Chromatin immunoprecipitation of IRF4 and detection of IRF4 transcriptional targets can be achieved in MCL cell lines.

Assessment of DNA interactions associated with IRF4 may indicate novel targets with the potential to overcome resistance to BTKi. Chromatin immunoprecipitation (ChIP) followed by high throughput DNA sequencing (ChIP-seq) is a useful method to identify binding sites for transcription factors on a genome-wide scale.

The initial purpose of this section was to sequence DNA purified from chromatin precipitates of IRF4 and identify DNA sequences bound to IRF4 in MCL cell lines demonstrating sensitivity and resistance to BTKi. However, work was complex due to the extensive quality control steps required by the ChIP assay limiting the experimental results that could be analysed. Therefore the following section describes the work flow of the intended experiment, highlighting the problems encountered along the way and finishes with a summary of the optimised conditions required for ChIP-seq of IRF4 which will be useful in future studies.

Chromatin immunoprecipitation of IRF4 from MCL cell lines was performed using the Simple Chip Enzymatic Chromatin IP kit (CST #9003). This kit was chosen since the company had previously validated the rabbit anti-IRF4 antibody (CST #4964) (used throughout this study) for ChIP, in experiments with Hela cells. For details on the materials and reagents refer to methods section 2.1.5 and 2.5.6.

5.6.1 Introduction and general principle

ChIP-Seq uses antibodies to detect proteins that are bound to DNA directly or that interact within DNA-bound protein complexes. Protein- DNA interactions are first preserved using a formaldehyde solution for cross-linking. A series of lysis steps then disrupt cell and nuclear membranes, isolating only the nuclear contents for the ChIP. The chromatin is then digested using an enzyme and / or sheared into smaller fragments using sonication. An antibody specific to the protein of interest is then incubated with the cross-linked protein-DNA complexes and then bound to magnetic beads, which pulls the relative chromatin fragments out of solution. The cross-links are then reversed, and the resulting purified DNA can be used in subsequent DNA fragment library construction for DNA sequencing. Following sequencing, the sequence reads are analysed using peak-calling tools that align reads to a reference sequence and identify known DNA regions associated to proteins.

5.6.2 Optimisation of chromatin digestion and fragmentation

The first step in a ChIP assay is to optimise the chromatin digestion and fragmentation. This will depend on the size of the fragments required for the downstream application. Appropriate length fragments required for ChIP can be anywhere in the range of 150-900bp. However DNA sequencing requires shorter fragments normally between 200-400bp.

Chromatin was first prepared from REC-1 cells at a concentration of 5 X 10^6 in 20mL culture media dispersed within a 15cm culture dish. Proteins were cross-linked to DNA by fixing cells in paraformaldehyde to a final concentration of 1%. Glycine was added to quench the formaldehyde and the cells were lysed in enzymatic 1 X lysis buffer A. The nuclei was pelleted and re-suspended in 1 X buffer B.

The protocol provided evidence that chromatin from Hela cells was digested to the appropriate length fragments (1-5 nucleosomes in length (900-150bp)) using 0.5µl of micrococcal enzyme and 3 sets of 20 second pulses with a sonication probe.

To test these conditions in REC-1 cells, the chromatin was digested with 0.5µl of micrococcal enzyme for 20 minutes, washed and re-suspended in 1 X ChIP buffer and sonicated 3 times for 20 seconds using a Vibra-cell ultrasonic probe (SONICS).

The crosslinks were reversed and the DNA from the chromatin was purified and analysed on 2% agarose gel. Most of the chromatin was digested to 3 nucleosomes in length (between 75bp and 500bp) (Figure 5.26) indicating that the length of time incubated with the enzyme or the volume could be reduced slightly in subsequent experiments to prevent over digestion. However these conditions were considered as optimal for this study since the downstream application was to sequence the ChIP samples.

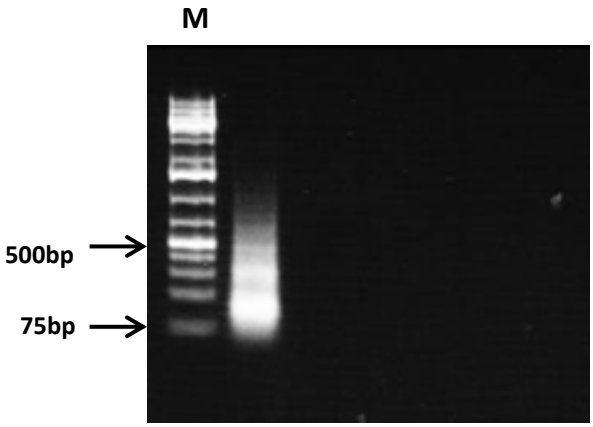

Figure 5.26: Optimisation of chromatin digestion and fragmentation in REC-1 cells. Chromatin was digested with 0.5µl of micrococcal enzyme for 20 minutes and sonicated 3 times for 20 seconds using a Vibra-cell ultrasonic probe. Chromatin was digested to 3 nucleosomes in length (between 75bp and 500bp). M= DNA ladder/marker.

5.6.3 Preparation of chromatin samples for ChIP

Using the same culture conditions and digestion and sonication conditions outlined above, chromatin samples were prepared from the following cell lines; REC-1, G519, and the acquired BTKi resistant cell lines REC-1/R (Ibr 1µM) and REC-1/R (Acal 1µM). A 50µl aliquot was taken from each sample, the cross links were reversed (as before) and DNA was purified and quantified using a NanoDrop 2000 spectrophotometer. The DNA quantification values are shown in Table 5.3 and were used to standardise concentration of each sample in preparation for IP.

Next, the original chromatin preparations from each cell line were diluted to 2µg in 500µl of 1X ChIP buffer. This was recommended by the ChIP protocol to provide sufficient chromatin for immunoprecipitation and an optimal concentration for antibody binding using their CST ChIP validated antibodies. Ten microliters of each 2µg

suspension was removed to a separate Eppendorf tube for the 2% input samples which were frozen at -20°C until a later stage of the protocol. The input DNA is used as a control for PCR effectiveness and is important in ChIP-sequencing data analysis.

5.6.4 Immunoprecipitation of IRF4 from chromatin samples

ChIP was performed using histone (H3), IRF4, and species-matched (normal rabbit) IgG antibodies (Table 5.1) on REC-1, G519 and acquired BTKi resistant REC-1 chromatin. The histone (H3) antibody was used as a positive control and the normal rabbit IgG was used as a negative control for establishment of the ChIP protocol.

The indirect method of immunoprecipitation was performed by adding the appropriate volume of ChIP validated antibody to the 500µl of digested cross-linked chromatin. The amount of histone (H3) and normal IgG antibodies to add to the chromatin was specified by the kit protocol. The amount of ChIP validated IRF4 antibody added to the chromatin was a 1 in 25 dilution (specified on the product datasheet).

The antigen/antibody complexes were separated from the solution on a magnet following incubation with ChIP grade protein G magnetic dynabeads. The beads containing the complex were then washed, the cross links were reversed and the DNA was purified. The efficiency of the ChIP was assessed by successful amplification of the ribosomal protein L30 (*RPL30*) locus using conventional PCR.

Sample	A260/280 (1.8-2.0)	DNA Conc (ng/µl)
REC-1 control 1	1.91	91.3
REC-1 control 2	1.89	140.2
REC-1 control 3	1.88	151.1
REC-1/R (Ibr 1µM)	1.87	106.1
REC-1/R (Acal 1µM)	1.86	91.2
G519	1.86	146.0

Table 5.3: Nanodrop assessment of DNA concentration and purity following DNA purification of various chromatin preparations pre immunoprecipitation.

5.6.5 Assessment of the efficiency of immunoprecipitation from chromatin samples

Histone H3 is an essential component of chromatin in the cell and is bound to most DNA sequences throughout the genome, including the *RPL30* locus. Thus, IP of chromatin with the histone H3 antibody will enrich for the *RPL30* gene and can be used as a positive control IP for almost any locus, including IRF4, while IP with the normal rabbit IgG will not result in *RPL30* enrichment and is used as a negative control.

A volume of 5µl of each sample including the 2% input samples for REC-1 and G519 was added to a PCR mix containing RPL30 primers and amplified with 40 rounds of PCR. A volume of 10µl of each sample was run on 2% agarose gel.

Clear bands were present for the REC-1 2% input sample (taken from 2µg DNA) and the Histone H3 (positive control) sample but not the normal IgG sample (negative control) thereby confirming the efficiency of the ChIP procedure (Figure 5.27). The

RPL30 locus was amplified in all the IRF4 samples but to varying degrees. A very clear band was seen in the REC-1/R (Ibr 1µM) sample suggesting that the 2µg concentration of chromatin incubated with the IRF4 antibody was sufficient for effective IP of IRF4. Since all the chromatin samples were diluted to 2µg, it was suggested that some of the chromatin may have been lost during the wash steps in some of the samples.

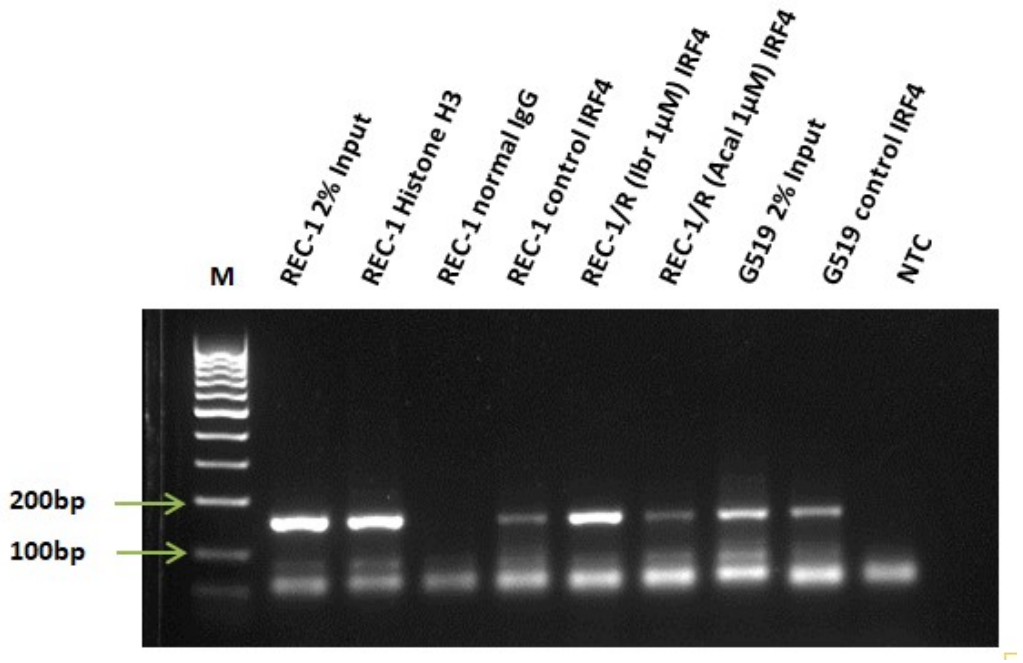

Figure 5.27: PCR validation of the ChIP samples. Chromatin immunoprecipitations were performed using digested chromatin from REC-1, G519 and REC-1/R cells and either Histone H3, IRF4 or Normal Rabbit IgG. Purified DNA was analysed by standard PCR methods using Human RPL30 Exon 3 Primers. PCR products were observed for RPL30 in the input samples for REC-1 (lane 1) and for G519 (lane 7) and for the IRF4 ChIP samples with and without BTKi, but not in the Normal Rabbit IgG ChIP sample (lane 3) or NTC (lane 9). RPL30 (161bp). M= DNA ladder/marker.

The ChIP samples underwent a number of pre-sequencing tests to confirm concentration and fragment length using high sensitivity DNA kits. A DNA concentration of 50ng is required for sequencing on the Ion Torrent, Ion personal genome machine (Ion PGM). Due to slight non-selective variation in results associated with UV spectrophotometry on the Nanodrop, final DNA concentrations before sequencing were determined using the Qubit® dsDNA High Sensitivity assay kit (Life Technologies).

Despite the presence of DNA from all samples after 40 rounds of PCR, analysis of DNA concentration obtained using a qubit fluorimeter showed that the concentration of DNA in the original sample was too low for sequencing in 4 of the samples (Table 5.4).

Furthermore, analysis of the 4 samples containing DNA using a bio-analyser showed a big peak of DNA in all samples at around 2kb. These fragments were too large to sequence on the Ion PGM. Smaller fragments were also present but were very faint suggesting the chromatin was not fully digested to the required length. Figure 5.28 shows a gel like image of the DNA fragment size for each sample and Figure 5.29 shows the Electropherograms, both obtained following analysis on the bio-analyser.

Sample	DNA Conc (ng/µl)	Amount of DNA (µl) for sequencing (50ng)	dH2O to 39.5µl
REC-1 2% Input	4.6	10.9	28.6
REC-1 H3	10.2	4.9	34.6
REC-1 IgG	-	39.5	-
REC-1 IRF4	-	39.5	-
REC-1/R (Ibr 1µM) IRF4	2.7	18.5	21
REC-1/R (Acal 1µM) IRF4	-	39.5	-
G519 2% input	5.34	9.4	30.1
G519 IRF4	-	39.5	

Table 5.4: High sensitivity analysis of DNA concentration for each ChIP sample and 2% inputs. Samples were re quantified using a Qubit high sensitivity DNA detection kit. Results show an adequate quantity of DNA in the input samples for REC-1 and G519 and in one of the IRF4 IP samples, but insufficient DNA quantity in four other IP samples precipitated from 2µg of chromatin.

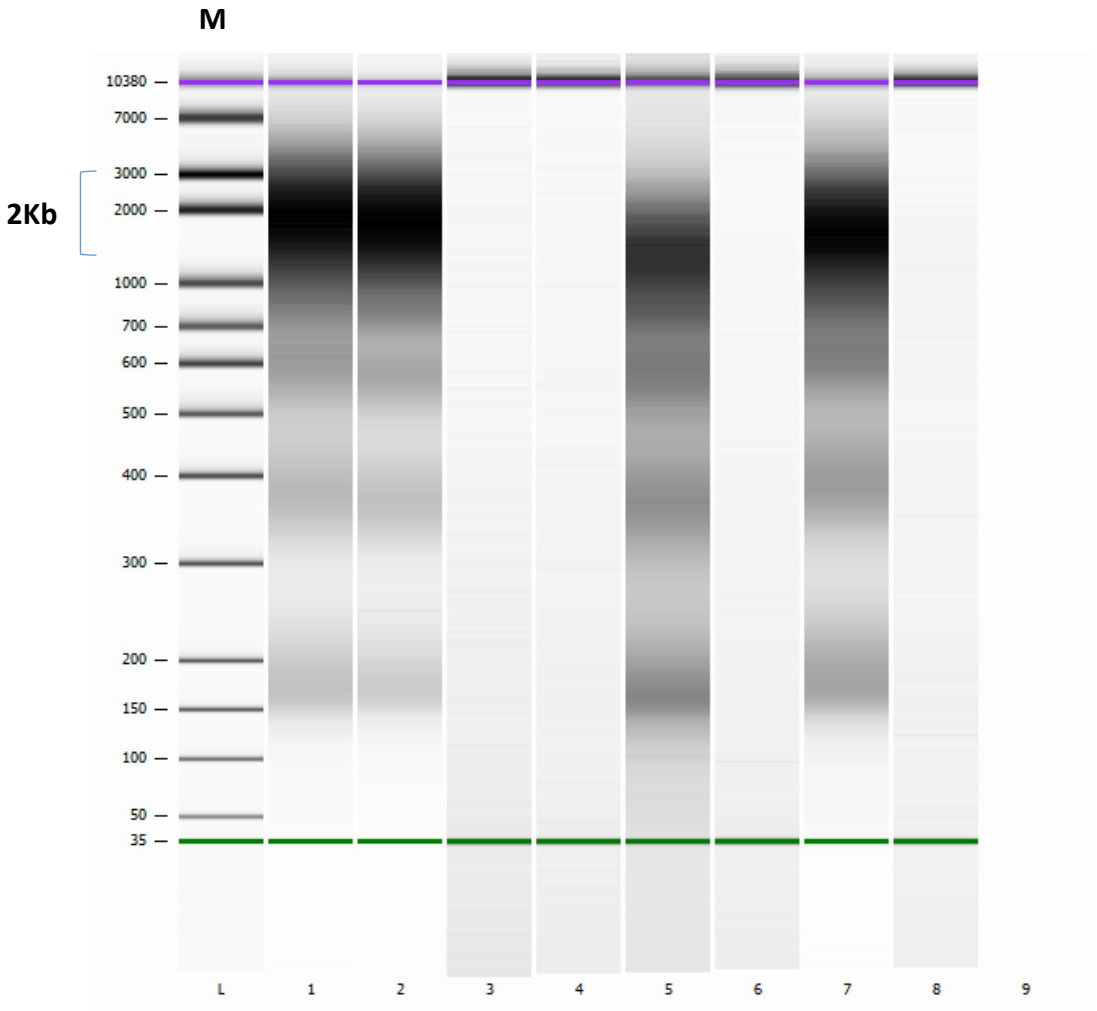

Figure 5.28: Electrophoresis gel-like image of each ChIP sample and the input samples. The four samples in Lane 3 (REC-1 IgG IP), Lane 4 (REC-1 IRF4 IP), Lane 6 (REC-1/R (Acal 1µM) IRF4 IP)) and Lane 8 (G519 IRF4 IP) demonstrated complete absence of DNA. The four samples in Lane 1 (REC-1 2% input), Lane 2 (REC-1 Histone H3 IP), Lane 5 (REC-1/R (Ibr 1µM) IRF4 IP)) and lane 7 (G519 2% input) show presence of DNA however strong bands were present at around 2000bp (2kb) as indicated. M= DNA ladder/marker.

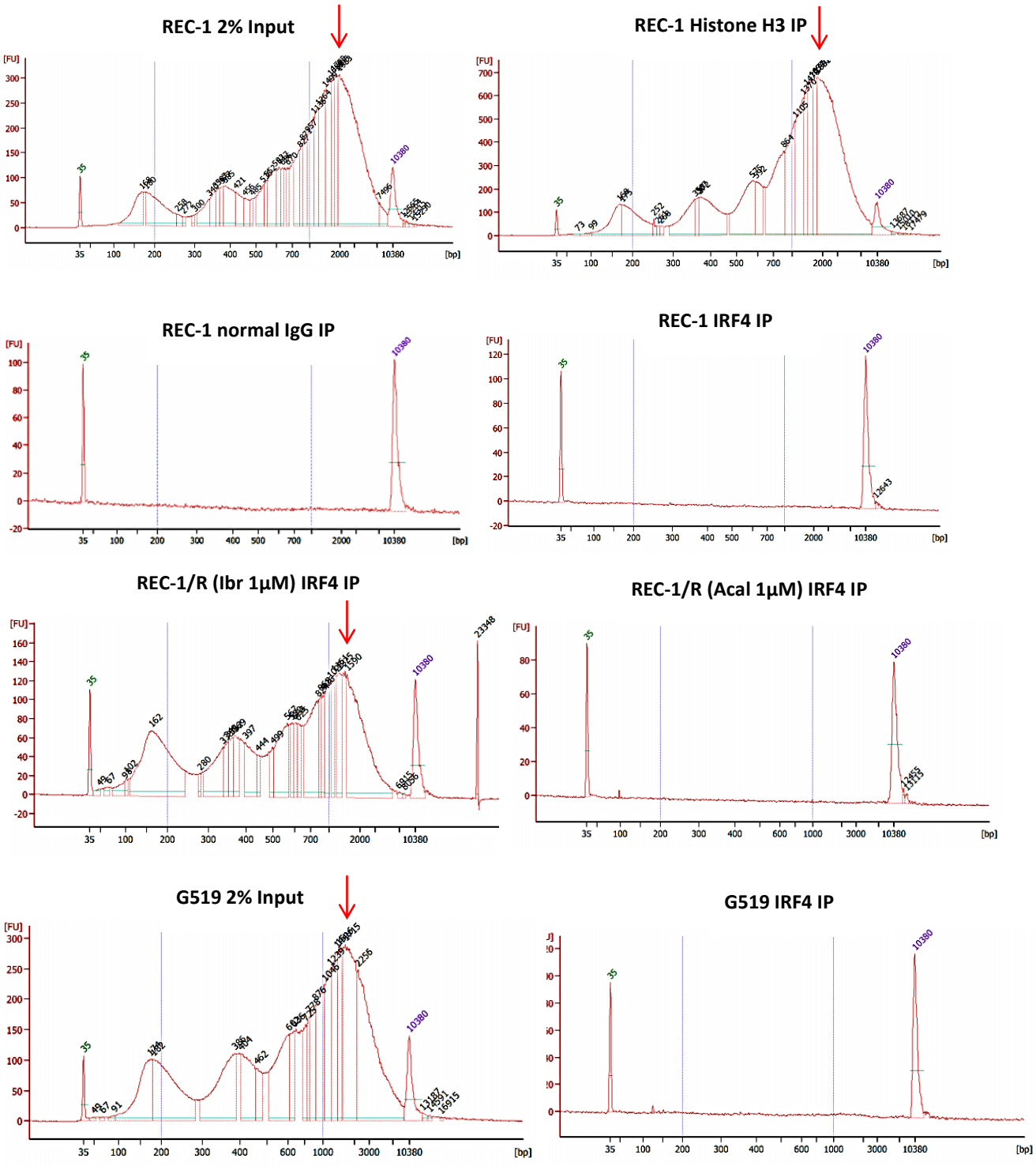

Figure 5.29: Electropherograms obtained from the Bio-analyser showing DNA fragment size of each ChIP sample including the 2% inputs. The size of the DNA fragments is indicated by the numbers on the peaks. Red arrows point toward peaks of around 2Kb.

Given that there was no DNA in four of the samples, the experiment was repeated with the following optimisation steps.

The seeding concentration of cells from each cell line remained the same at 5 X 10^6 in 20ml culture media. However this time, the chromatin was digested using 0.8µl of micrococcal enzyme for 20 minutes with additional sonication in a water based bioruptor (Diagnode). For assessment of chromatin digestion and fragmentation, a 'no sonication' REC-1 control sample was added for comparison. Ten cycles of 30 seconds ON, and 30 seconds OFF produced appropriate length fragments (Figure 5.30). The purified DNA concentrations are shown in Table 5.5.

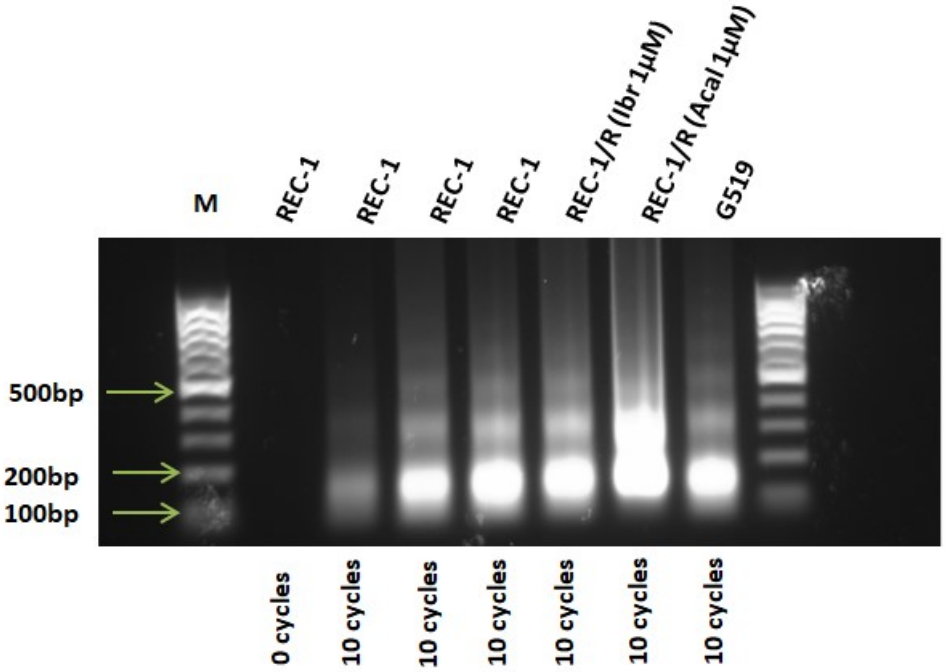

Figure 5.30: Analysis of chromatin digestion and fragmentation pre immunoprecipitation-Experiment 2. Chromatin from 5 X 10^6 cells per sample was digested with 0.8µl of micrococcal nuclease and 10 rounds of sonication. The DNA was purified and 10µl was separated by electrophoresis on a 1% agarose gel. Lane 1 shows absence of DNA in the un digested/no sonication control, while lanes 2 – 7 show that the majority of chromatin from each sample was digested to 1 to 4 nucleosomes in length (150 to 500bp). M= DNA ladder/marker.

Sample	A260/280	DNA Conc (ng/µl)
REC-1	1.92	62.6
REC-1	1.91	56.9
REC-1	1.92	78.7
REC-1/R (Ibr 1µM)	1.90	92.1
REC-1/R (Acal 1µM)	1.89	195.8
G519	1.90	118.8

Table 5.5: Nanodrop assessment of DNA concentration and purity following DNA purification of various chromatin preparations pre immunoprecipitation- Experiment 2.

Each chromatin sample was diluted to 2µg in 1X ChIP buffer. The same concentrations of antibodies were incubated with the chromatin. PCR validation of the ChIP procedure showed a clear band was present for the REC-1 and G519 input samples and the REC-1 Histone H3 (positive control) but not the IgG sample, again confirming the efficiency of the ChIP procedure (Figure 5.31). However bands were very faint in all of the IRF4 samples using the CST antibody at a concentration of 1 in 25. The DNA concentrations following IRF4 IP from 2µg of DNA were very low. The integrity of the DNA was also poor (Table 5.6). This suggested that concentration of chromatin to the specific IRF4 antibody required further optimisation.

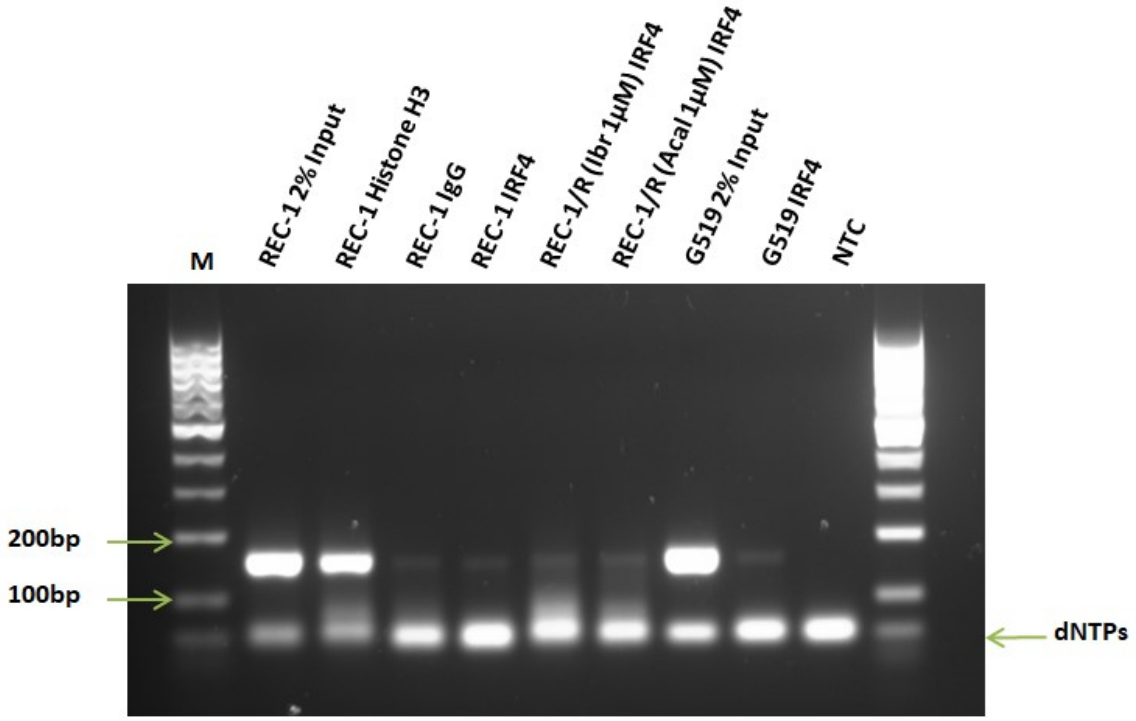

Figure 5.31: PCR validation of ChIP procedure- Experiment 2. Chromatin immunoprecipitations were performed using digested chromatin from REC-1 and G519 cells and either Histone H3, IRF4 or Normal Rabbit IgG. Purified DNA was analysed by standard PCR methods using Human *RPL30* Exon 3 Primers. PCR products were observed for RPL30 in the input samples for REC-1 (lane 1) and for G519 (lane 7), and the Histone H3 positive control (lane 2), but not in the Normal Rabbit IgG ChIP sample (lane 3), NTC (lane 9), or any of the IRF4 ChIP samples (lanes 4, 5, 6 and 8). M= DNA ladder/marker.

Sample	A260/280	DNA Conc (ng/µl)
REC-1 (2% input)	1.97	10.2
REC-1 (H3)	2.05	9.4
REC-1 (IgG)	2.00	7.9
REC-1 (IRF4)	2.20	3.0
REC-1/R (Ibr 1µM) (IRF4)	3.62	1.6
REC-1/R (Acal 1µM) (IRF4)	1.92	3.0
G519 (2% input)	2.20	5.4
G519 (IRF4)	2.23	3.6

Table 5.6: Nanodrop assessment of DNA concentration and purity following DNA purification of ChIP samples and 2 % inputs post immunoprecipitation- Experiment 2.

A third experiment was performed using chromatin prepared from REC-1 and G519 cells. This time, the chromatin was not diluted and the antibodies were added directly to the chromatin preparations at their original concentrations (also suggested by the protocol), therefore the chromatin concentration was increased but the antibody concentration was kept the same. In addition to using the CST IRF4 antibody, the alternative abcam MUM-1 antibody was tested.

Immunoprecipitation of IRF4 was more defined using the anti-MUM-1 antibody and a chromatin concentration of 12µg (Figure 5.32, blue arrow), however whether this was due to the antibody or the higher concentration of chromatin was unclear.

To determine whether the CST IRF4 antibody would be more effective at higher chromatin concentration, a 1 in 25 dilution of the antibody was incubated with 10µg of G519 chromatin and compared with results at 2µg.

At 2µg, IRF4 was not successfully pulled out, however at 10µg, IP of IRF4 was much more defined (Figure 5.32, orange arrow).

The DNA concentrations following IP from 10µg and 12µg chromatin were much higher than at 2µg, the quality of the DNA was also better (Table 5.7).

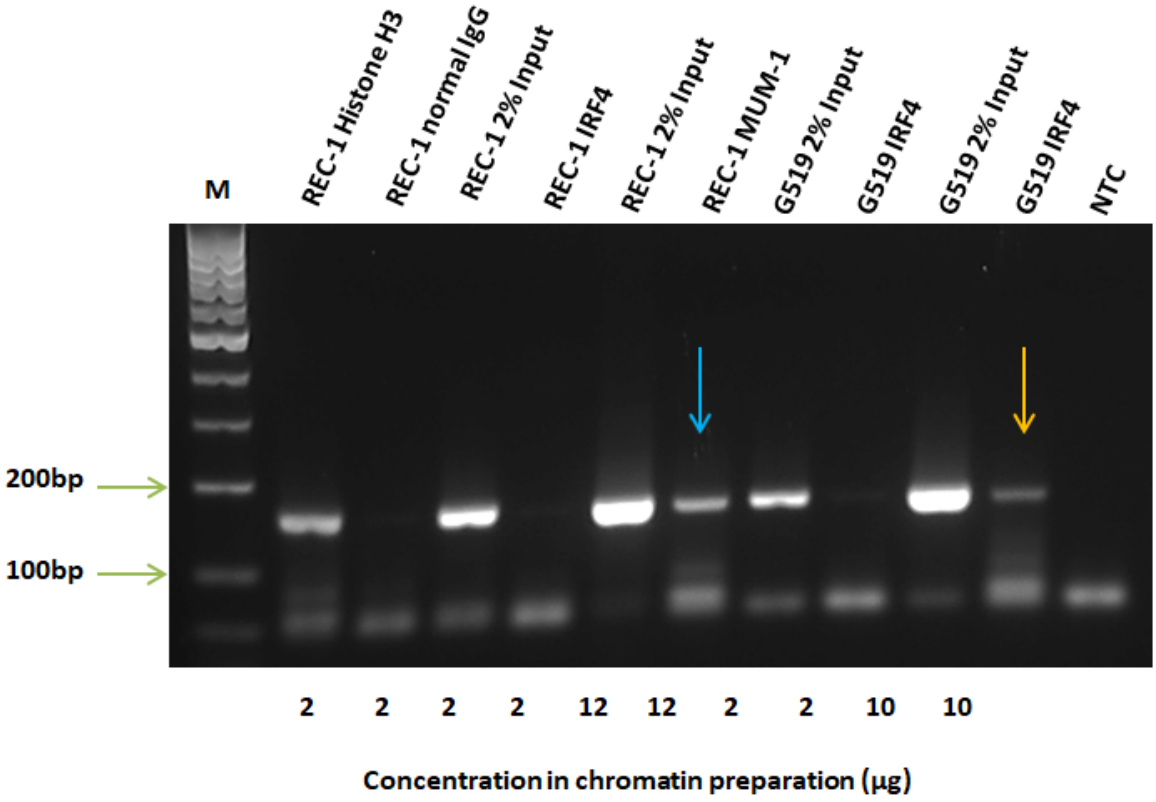

Figure 5.32: Immunoprecipitation of IRF4 at higher chromatin concentration. Chromatin immunoprecipitations were performed from different concentrations of digested chromatin from REC-1 and G519 cells and either Histone H3, Normal Rabbit IgG or IRF4 from cell signalling technology or MUM-1 from abcam. PCR products were observed for *RPL30* in all 2% input samples including REC-1 (2µg), REC-1 (12µg), G519 (2µg) and G519 (10µg). PCR products were not present for IRF4 IP from REC-1 (2µg), or G519 (2µg). Products were clear for IRF4 IP from REC-1 chromatin (12µg) using the abcam anti MUM-1 antibody (blue arrow), and from G519 chromatin (10µg) using the CST anti-IRF4 antibody (orange arrow). No amplification of *RPL30* was present in the Normal Rabbit IgG IP sample or NTC. M= DNA ladder/marker.

Sample	A260/280	DNA Conc (ng/µl)
REC-1 2% input	1.94	61.9
REC-1 (abcam MUM-1 IP)	1.91	40.5
G519 2% input	1.95	34.4
G519 (CST IRF4 IP)	1.86	21.1

Table 5.7: Nanodrop assessment of DNA concentration and purity following ChIP at higher chromatin concentration. IRF4 was precipitated from higher concentrations of chromatin; 10µg from G519, and 12µg from REC-1 chromatin.

The DNA fragments from the G519 samples were analysed and re-quantified on the Bio-analyser using the high sensitivity DNA detection kit. DNA was detected in the G519 2% input sample and most of the DNA fragments indicated on a gel-like image were between 150 and 200bp (Figure 5.33) and were sufficient for sequencing. Larger fragments were also present as shown on the electropherogram (Figure 5.34) but can be cleaned up using beads for size selection. The quantity of DNA detected in the G519 2% input sample from the Bio-analyser using the high sensitivity kit was 10.9ng/µl, different to the nanodrop quantification 34.4ng/µl (Table 5.7). However, as shown in the gel-like image and electropherogram (Figure 5.33 and 5.34, respectively) no DNA was detected in the G519 IRF4 IP prepared from 10µg chromatin, despite the better DNA quantification and quality results obtained from the nanodrop. Again, it appeared that there was not sufficient DNA for sequencing. However, given the presence of DNA for the *RPL30* locus following 40 rounds of PCR as shown on the agarose gel image (Figure 5.32, orange arrow), the G519 IRF4 sample was sequenced with the idea that the DNA would also be amplified in the process.

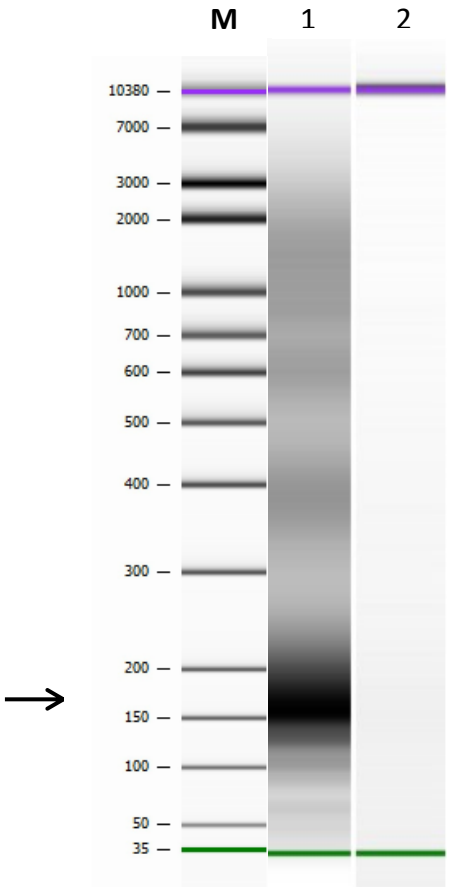

Figure 5.33: Electrophoresis gel-like image of the G519 2% input sample and the G519 IRF4 sample following ChIP at higher chromatin concentration. ChIP of IRF4 was performed from 10µg of G519 chromatin. DNA was detected by the Bio-analyser in the G519 2% input sample and most of the DNA fragments were between 150 and 200bp (lane 1). No DNA was detected in the G519 IRF4 IP prepared from 10µg chromatin (lane 2). M= DNA ladder/marker.

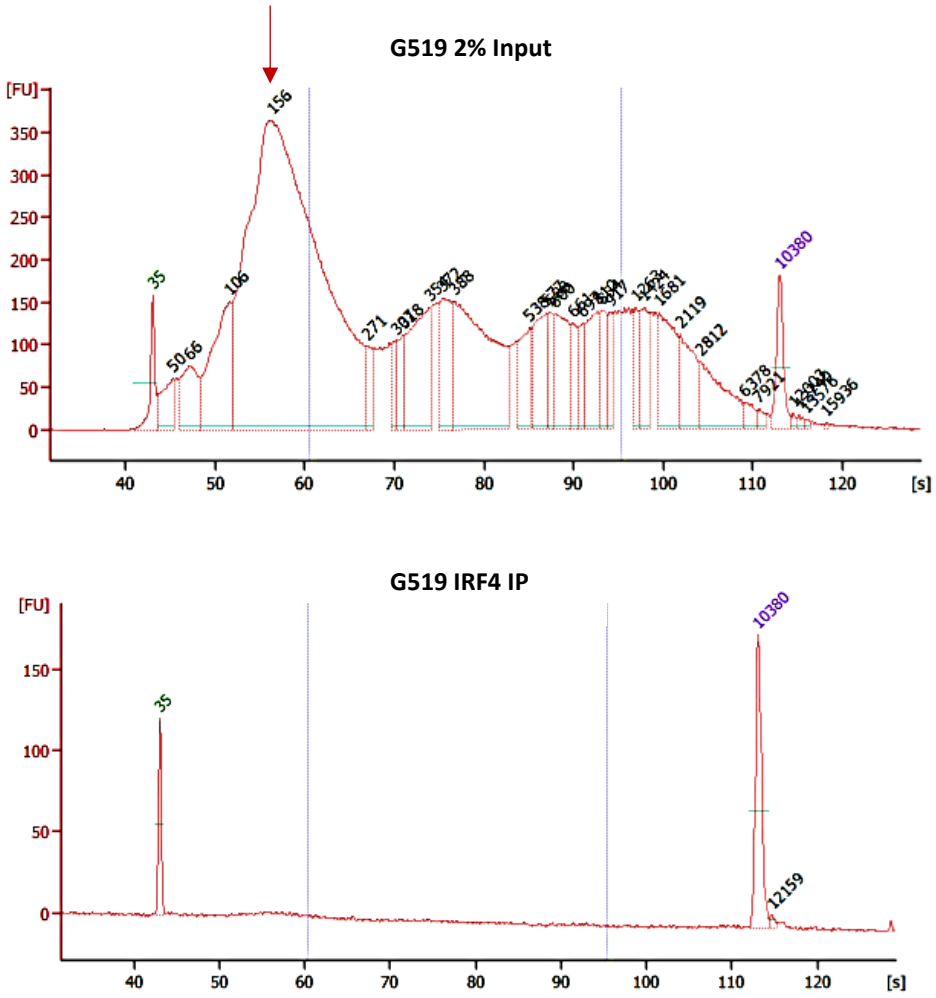

Figure 5.34: Electropherograms obtained from the Bio-analyser showing DNA fragment size for the G519 2% input sample and the IRF4 IP sample. The size of the DNA fragments is indicated by the numbers on the peaks. Small fragments were indicated by peaks of around 100-250bp (red arrow) for the G519 2% input sample. No fragments were detected for the G519 IRF4 IP sample. Bio-analyser assessment of DNA concentration for the G519 2% input sample and the G519 IRF4 IP sample was 10.9ng/µl and 0.1ng/µl (respectively).

The G519 IRF4 sample (10µg) was sequenced on the Ion PGM by Dr Michele Kiernan (University of Plymouth). Despite the absence of DNA obtained from the Bio-analyser, a successful library was generated from the sample and 79,000 reads were obtained.

At this stage, the G519 IRF4 ChIP sample was only sequenced to see if sequencing reads could be obtained from the low amount of DNA.

Therefore, the G519 IRF4 sample reads were aligned to the human genome with peak annotation (Figure 5.35). This generated a list of all peaks of > 0.0001 significance to either the 3' or 5' of genes and the distance the peak was from these genes (Table 5.8). However, in order to properly identify DNA sequences specifically bound to IRF4 in G519 cells, the normal IgG sample and the 2% G519 input sample should have been included to eliminate non-specific bias. Therefore detailed analysis was not undertaken, although given the interesting results from the protein co-immunoprecipitation studies, a comparison of mitochondrial associated proteins (proteins from function group 2 and 6) was undertaken with potential IRF4 associated genes (Table 5.9). This showed that IRF4 in G519 cells can be associated with DNA fragments from some of those proteins identified.

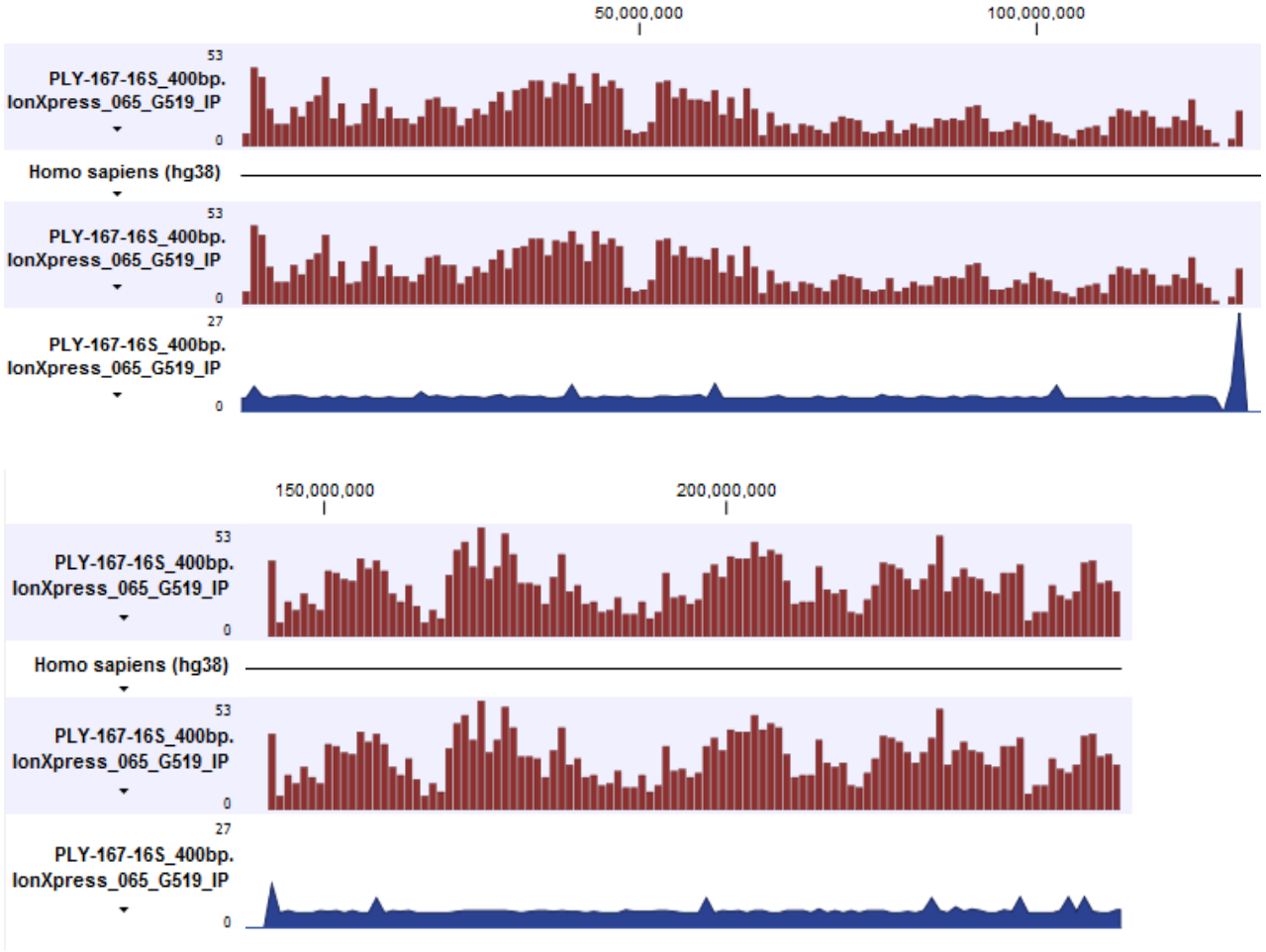

Figure 5.35: Peak annotations generated from the G519 ChIP sequencing reads.

Chr	Region	Center of peak	Length	Peak shape score	P-value	5' gene	5' distance	3' gene	3' distance
1	125180106..125180314	1.25E+08	209	26.53298	2E-155	RP11-344P13.1	3599581	CH17-333M13.2	18162865
5	49661458..49661574	49661504	117	23.14485	8.2E-119	CTD-2013M15.1	3765487	EMB	734617
4	49153148..49153288	49153198	141	17.90544	5.35E-72	TPI1P4	135993	RP11-1281K21.2	49882
16	46388681..46388807	46388743	127	17.09306	8.36E-66	PPP1R1AP2	10476164	ANKRD26P1	80533
18	108404..108557	108470	154	15.32276	2.69E-53	RP11-683L23.6	14073	ROCK1P1	507
3	93470653..93470775	93470728	123	13.63451	1.25E-42	ABBA01000934.1	1956877	RNU6-488P	372988
3	93470416..93470545	93470449	130	13.57463	2.83E-42	ABBA01000934.1	1956640	RNU6-488P	373218
16	34583066..34583185	34583141	120	13.50516	7.29E-42	BCLAF1P2	314416	CTD-2144E22.9	358791
Y	11747623..11747716	11747669	94	12.75345	1.49E-37	RP11-295P22.2	273385	RCC2P1	33335
5	49659765..49659900	49659820	136	12.0967	5.5E-34	CTD-2013M15.1	3763794	EMB	736291

Table 5.8: Sample of G519 sequencing read data. The list shows the results for the first 10 IRF4 DNA targets.

Mitochondrial and ribosome proteins		IRF4-DNA binding sites	Comments
MRPS22	Mitochondrial Ribosomal Protein S22	0	
MRPS26	Mitochondrial Ribosomal Protein S26	0	
MRPS23	Mitochondrial Ribosomal Protein S23	0	
MRPS9	Mitochondrial Ribosomal Protein S9	0	
MRPL38	Mitochondrial Ribosomal Protein L38	0	Sites were found for MRPL 32,33,35,37 and 39
MRPL3	Mitochondrial Ribosomal Protein L3	1	
DAP3	Death-associated protein 3	1	
GADD45GIP1	Growth arrest and DNA-damage-inducible proteins-interacting protein 1	0	
Mitochondria and mitochondrial RNA			
ATP6V0D1	ATPase H+ transporting V0 subunit D1	2	
ATP5H	ATP synthase, H+ transporting, mitochondrial Fo complex, subunit D	0	Sites were found for ATP5HP2, P3, P4
PPA2	Pyrophosphatase (Inorganic) 2	4	
ATP5O	ATP Synthase Subunit O	0	
UQCRFS1	Ubiquinol-Cytochrome C Reductase, Rieske Iron-Sulfur Polypeptide 1	3	
UQCRC2	Ubiquinol-Cytochrome C Reductase Core Protein 2)	0	Sites were found for UQCRC2P1
PMPCB	Peptidase, Mitochondrial Processing Beta Subunit	5	
TIMM44	Translocase Of Inner Mitochondrial Membrane 44	2	
GRPEL1	GrpE Like 1, Mitochondrial	1	
KIAA1967	Deleted in Breast Cancer 1	0	
DNAJB1	DnaJ Heat Shock Protein Family (Hsp40) Member B1	0	Sites were found for DNAJB8, 11, 12, 13, 14
C11orl73	Chromosome 11, open reading frame 73	0	Sites were found for 33 other Cllorf's
DNAJ	HSP40 (heat shock protein 40)	0	

Table 5.9: Comparison of mitochondrial associated proteins with potential IRF4 associated genes.

5.7 Discussion

The results shown in this chapter attempt to characterise the role IRF4 has in neoplastic MCL cells. Results shown in chapter 3 and 4 demonstrate that the protein expression of IRF4 in MCL cells is downregulated in the neoplastic cells of both BTKi-sensitive cell lines and primary cells, and that BTKi- resistance either innate or acquired either from pronged exposure to BTKi or through the influence of microenvironmental interactions do not show IRF4 downregulation. The initial question we asked was whether this downregulation was as a result of reduced gene transcription rather than because of increased protein degradation. In REC-1 cells, IRF4 mRNA levels were found to be downregulated following Ibr treatment after 1 hour and maximally by 4 hours correlating with the downregulation of IRF4 protein expression at 4-8 hours shown in previous chapters, suggesting that initial IRF4 expression-changes result from change to mRNA transcription as a specific response to treatment. However, IRF4 mRNA levels were not maintained at this lower level with an increase seen over time although remaining lower relative to control. This differs to the protein expression of IRF4 in response to BTKi treatment which appears more downregulated with time suggesting additional/alternative mechanisms such as protein degradation are also involved in the control of IRF4. This response in mRNA levels was mirrored with Acal treatment although the response appeared delayed and may reflect the increased specificity of Acal and the higher reported IC50 dose.

Further experiments indicated considerable differences in IRF4 mRNA expression in response to BTKi between sensitive and resistant cells. In the G519 cells IRF4 mRNA levels were shown to increase over time relative to the control cells with both Ibr and Acal BTKi, with an almost 10 fold increase seen at 48 hours in response to Ibr. This is

consistent with the observed changes to IRF4 protein expression in G519 cells particularly after 24 and 48 hours treatment. This analysis clearly showed that the pattern of mRNA expression by G519 cells differed from that seen in BTKi treated REC-1 cells. Similarly, in cells with acquired Ibr resistance (Ibr resistant REC-1 cells) IRF4 mRNA was upregulated relative to the untreated control cells at 4 hours which differed to that observed with parental treated cells.

These results suggest that the changes observed in IRF4 protein expression , at least at early stages, are at the level of transcription and differences exist in the transcription of IRF4 mRNA between cells with BTKi sensitivity and resistance which reflect IRF4 protein expression. However, although these results are suggestive of a transcriptional control mechanism for IRF4, particularly given that IRF4 mRNA expression generally matched protein expression in each case, the fold change difference seen in REC-1 cells following BTKi treatment was small and the sample size was small. Therefore more replicates with the addition of measurement of mRNA in control cells at the same time points (mRNA levels can vary under normal conditions) would be required in order to confirm the significance of the data.

To further determine the role IRF4 may have in response to BTKi treatment we looked for the protein associations of the molecule using co-immunoprecipitation. Initially this focussed on investigating the known interactions with the ETS family member PU.1 which on binding with IRF4, results in release of the auto-inhibitory effect on the DNA binding region allowing IRF4 to bind its target sequence with much greater affinity (introduction section 1.4.1). These interactions play an important role in B-cells maturation and development. However PU.1 was not detected in IRF4 protein precipitates from REC-1 cells following co-immunoprecipitation studies or in the mass

spectrometry analysis. In addition, we appreciate that failing to detect PU.1 in IRF4 precipitates doesn't prove lack of interaction. We therefore performed some further assessments of PU.1 expression in response to BTKi treatment. In assessing the response of PU.1 to BTKi treatment we found that in primary MCL cells co-cultured on stromal cells, unlike IRF4 expression, protein PU.1 expression was not downregulated in response to BTKi when CD40L was absent and that PU.1 expression following MCL cell stimulation with CD40L remained stable (again the converse to what was seen with IRF4 protein expression). We would have expected if IRF4 and PU.1 were associated that they would show similar levels of expression. Assessment of levels of PU.1 mRNA in REC-1 cells further supports this contention. Expression of PU.1 mRNA in REC-1 cells in comparison to IRF4 mRNA levels was increased in response to BTKi with almost a log greater difference in PU.1 mRNA expression compared to IRF4 mRNA seen at 48 hours. Taken together these studies are suggestive that PU.1 is not a principal binding partner of IRF4 in our MCL cell lines, and that IRF4 regulates expression of its target genes through binding to other protein partners.

Having explored the proteins of known associations with IRF4 we undertook further experiments to explore protein associations that had not previously been reported which might give insight into the role IRF4 plays in MCL biology.

This element of the study employed immunoprecipitation as before, but in this case used mass spectrometry to determine protein association. The analysis identified a large number of co-precipitated proteins, the IRF4 protein itself was found only in precipitates where the specific antibodies were used and not seen in the control precipitates, confirming that the IP had worked. Further analysis of the co-precipitated proteins was therefore undertaken.

Initial analysis focussed on the subset of proteins (190 proteins) that were precipitated by both IRF4 test antibodies, but were not present in the control IP. This was done to focus on the proteins that were most likely to be significant. The proteins precipitated by both specific antibodies showed high similarity and data confidence analysis suggested that the probability of these proteins being co-precipitated by IRF4 but not control was $p<0.00001$ (chi squared test). Furthermore, analysis of functional relationships using STRING demonstrated that the proteins that were precipitated were linked at a functional level being mainly proteins with positive biosynthetic function: anabolic elements and were functionally consistent with a known function of IRF4 – to enhance anabolic processes[196,197] and therefore the findings were biologically plausible. In particular, the link with mitochondrial proteins is interesting, this finding was not expected, however mitochondria have a recognised link to IRF4 [196,197] and one that can be linked to chemo-resistance.[198,199]

Further analysis to evaluate the specificity of IRF4 protein participates was undertaken. This analysis compared proteins which were present in control and IRF4 samples (presumed non-specific) with those present in both IRF4 precipitates (presumed specific), including proteins that were present or absent but also those that were significantly enriched (>2-fold) in either sample. This wider protein group was again analysed by STRING. This analysis showed that ribosomal elements including RNA translational factors were a frequent finding in both the control and the IRF4 fractions, suggesting that some these protein types might be non-specific elements. However, one of the major aspects from the initial findings was confirmed – only the IRF4 test antibodies precipitated mitochondrial ribosomal elements. The presence of

mitochondrial ribosomal components only in IRF4 samples was highly significant ($p<0.01$ Chi square test).

Therefore, the Proteomic study of IRF4 immunoprecipitation of REC-1 cells strongly suggests a particular association of IRF4 in REC-1 cells with mitochondrial ribosomal and functional processes. These results require confirmation by additional analysis, but are interesting. Mitochondrial proteins (while forming part of mitochondria) are encoded and synthesised by the main cellular DNA, not mitochondrial DNA, and are then exported to the cytoplasm where they are imported into the mitochondria and assembled. In short, it is plausible that IRF4 may associate with these proteins in nucleus, nucleolus or cytoplasm, the IRF4 does not have to enter the mitochondria to encounter them. We cannot say at what point the IRF4 binds to mitochondrial ribosomal proteins but given the functional link as referenced above it is certainly plausible that it might do so and that activation of mitochondrial function may contribute to the chemo-resistance associated with IRF4 expression.

Experiments aiming to identify IRF4 target genes in BTKi sensitive and resistant MCL cell lines using ChIP analysis were limited due time constraints of this PhD and the extensive optimisation steps required for successful precipitation of IRF4 using the CST Simple ChIP enzymatic chromatin IP protocol.

It was determined that a 20 minute incubation using 0.8ul of micrococcal nuclease with an additional 10 rounds of sonication was required in order to generate appropriate length fragments for ChIP-seq. This was confirmed by agarose gel electrophoresis and following assessment of the input DNA sample on the bio-analyser. A concentration of 2µg of REC-1 chromatin was enough for successful ChIP of the histone H3 positive control as confirmed by amplification of the *RPL30* locus, but

not for IRF4. At least 10µg of chromatin was required for immunoprecipitation of IRF4 which showed a clear band for the *RPL30* locus, however DNA from the G519 ChIP sample could not be detected using high sensitivity DNA quantification kits.

Despite the absence of DNA, a successful library was generated from the G519 IRF4 ChIP sample which may be due to the additional rounds of PCR required during DNA library preparation. In addition, a total of 79,000 reads were produced from the sample following sequencing of the DNA on the Ion Torrent PGM.

Although the purified DNA from the G519 IRF4 ChIP sample was successfully sequenced, the resulting peaks are only relevant with an input DNA control. This would normally be sequenced in parallel with the ChIP sample.

Furthermore, even though the reads generated were aligned to the human genome, the DNA sequences bound to IRF4 could not be accurately determined due to the absence of an appropriate IgG control. However it was noted that Spi-1 (the gene which gives rise to PU.1), was not detected in the G519 IRF4 DNA, providing further evidence for the lack of association with IRF4 in MCL. In addition, within the limitations outlined above and that this analysis was performed in G519 cells , it is interesting to note that genes which denote mitochondrial /ribosomal function were detected in the G519 IRF4 DNA again suggesting a link of IRF4 to mitochondrial function.

Chapter 6 – Discussion and future work

MCL is a rare B-cell lymphoproliferative disorder that generally has poor outcome following conventional therapy. Inhibitors of BTK have significantly improved treatment outcomes for MCL patients. However it remains that a significant fraction of patients have primary resistance to BTKi and responding patients inevitably develop acquired resistance with aggressive relapse of the disease. Resistance to BTKi is therefore a major challenge in the management of MCL.

This thesis builds on from existing knowledge of the mechanisms underlying the sensitivity of MCL cells to the first in class BTKi Ibr, and contributes further knowledge using the more selective BTKi Acal.

In addition, this thesis contributes a significant body of evidence implicating IRF4 in BTKi response in both MCL cell lines and in primary cells possibly arising from activation of alternative survival pathways which modulate ERK1/2 phosphorylation. The findings with respect to IRF4 suggest it may have a role as a mediator of BTKi treatment-resistance in MCL and as a biomarker to predict response to BTKi therapy in the clinical setting.

The downregulation of IRF4 in response to BTKi was significantly opposed following CD40L stimulation, therefore implicating CD40 signalling as a possible mechanism of resistance to BTKi within the cellular microenvironment of MCL. Further assessment of IRF4 protein interactions using the MCL cell line REC-1 identified a novel group of proteins associated with mitochondria which may be involved in mediating the IRF4-mediated resistance to treatment with BTKi. Further investigation of these interactions may indicate novel targets for the design of therapeutic combinations which can overcome BTKi resistance in MCL.

6.1.1 Cellular responses to BTKi in MCL

Given the spontaneous apoptosis of primary MCL cells *in vitro,* this study set out to characterise MCL cell line models of BTKi sensitivity and resistance. Previous studies have reported that the REC-1 cell line is valuable for the analysis of BTKi in MCL [26,106,200] and this was confirmed and extended in this study: The REC-1 cells demonstrated sensitivity to BTKi showing dose dependant apoptosis in response to Ibr and a reduction of proliferation in response to both Ibr and Acal. In contrast, BTKi had no effect on G519 cells, again supporting other studies which have characterised these cells as BTKi resistant.[145,201]

The JEKO-1 and JVM2 cells were also characterised as BTKi resistant as they only responded to Ibr at high dosage (10µM) which is likely to cause off-target activity in the cells due to the broad specificity of the Ibr kinome and indicates that effects observed at high dosage may not be a direct effect of BTK inhibition. This was supported by results using the more selective BTKi Acal, which compared with Ibr, did not induce substantial apoptosis in REC-1 cells or show any evidence of off-target effects even at exceptionally high dose.

The findings with REC-1 are in accordance with another study reporting that minimal apoptosis was observed in REC-1 cells in response to the second generation BTKi, Spebrutinib (CC-292).[106] Rather, inhibition of BTK in this study and others identify predominant effects on proliferation.[145] In our studies, the effects on proliferation were not only induced by Ibr but also by Acal and both inhibitors reduced proliferation of REC-1 cells equally at low dosage (100nM).

The observed low levels of apoptosis seen with treatment of MCL cells with BTKi is supported by both others in the field and by clinical observations - in patients treated

with BTKi, rapid apoptosis of circulating neoplastic cells is not seen. However one of the known mechanisms of action of BTKi is to disrupt integrin mediated adhesion to the tissues rather than to directly inhibit survival. Again this is supported by clinical observations of the lymphocytosis seen in MCL and CLL patients directly following BTKi therapy which is accompanied by lymph node shrinkage. This lack of cell attachment to the extracellular matrix (ECM)[132,202] has been suggested to result in anoikis (a form of programmed cell death) of the leukaemia cells. Certainly the mechanisms resulting in MCL cell death following BTKi treatment are not fully understood and could be a consideration for future work.

6.1.2 Effect of the MCL microenvironment on the cellular response to BTKi

MCL cells are recognised to be supported by accessory cells within a microenvironment providing signals for growth and survival, and known to be a major factor in causing resistance to chemotherapy. To investigate whether this MCL microenvironment influences responses to BTKi, this study developed a 2D *in vitro* model using two murine fibroblasts cell lines, one expressing CD40L and the other not expressing CD40L.

It was rather surprising to find that REC-1 cells demonstrated dependency on CD40L; co-culture with fibroblast cells in the absence of CD40L did not alter the cellular response to BTKi, but co-culture in the presence of CD40L prevented the reduction in proliferation and attenuated cell death in response to BTKi. The murine fibroblasts expressing CD40L were also shown to support the survival of *ex vivo* primary MCL cells. The aggressive MCL subtypes demonstrated increased dependence on CD40L over the indolent subtypes, which has been shown in previous unpublished results by our group (Dr David Tucker, MD awarded 2017). In response to BTKi, the primary MCL cells

behaved similarly to REC-1 cells showing increased apoptosis in response to Ibr while apoptosis was prevented in the presence of CD40L.

In summary, these results demonstrated that REC-1 cells have a dependency on the tissue microenvironment in response to CD40L which mimics the behaviour of the cells *in vivo* and therefore represents a useful model to explore BTKi resistance pathways in MCL, and also suggests that CD40 signalling may play an important role in resistance to BTKi by increasing survival.

6.1.3 Signalling responses to BTKi in MCL

All MCL cell lines whether sensitive or resistant to Ibr, showed increased phosphorylation of BTK (pBTK-Y223) following IgM stimulation which was reduced following BTKi treatment. Similar results were seen in primary MCL cells although the degree of pBTK-Y223 following IgM stimulation was variable between cases.

Again, in all cell lines, activation of the downstream effector molecule ERK1/2, appeared to be dependent on BTK signals as it was inhibited following Ibr treatment. These findings do not correlate with the cellular responses of each cell line following BTKi treatment and indicate that resistance mechanisms occur further downstream from ERK1/2. However, in the presence of BCR activation and CD40 stimulation, ERK1/2 phosphorylation was only partially reduced, suggesting that there is an additional route for ERK1/2 activation induced by BCR or CD40 signalling, possibly through activation of MAPK and PI3K pathways. A previous study by Ma *et al* [145] showed that reduced phosphorylation of ERK and AKT levels after Ibr treatment correlated with cytotoxic sensitivity of MCL cells. It has been suggested by others that activation of PI3K-AKT causes primary resistance to Ibr in MCL.[138,145] Therefore it would

seem mechanistically plausible for clinical studies to use BTKi in combination with PI3K inhibitors.

6.1.4 IRF4 expression in response to BTKi in MCL

The role of IRF4 in the pathogenesis of other NHLs such as DLBCL and MM is well understood. Both DLBCL and MM respond well to treatment which downregulates IRF4 expression. IRF4 also has defined roles in CLL, HL and ALL and is believed to contribute to disease pathogenesis. Evidence supporting a role for IRF4 in MCL biology is lacking, so given the preliminary results by the group indicating downregulation of IRF4 in CLL patients treated with BTKi, it was of particular interest to investigate its expression in response to BTKi treatment in MCL.

This study showed that IRF4 was downregulated by BTKi (both Ibr and Acal) in sensitive REC-1 cells, but not in REC-1 cells with acquired Ibr resistance or any of the innate resistant cell lines. Expression of IRF4 mRNA showed that downregulation of IRF4 was an early response to BTKi treatment in REC-1 cells and was prevented / increased in REC-1 cells with acquired Ibr resistance. These findings were validated in primary MCL cell samples from treated patients (n=8) analysed before and during BTKi treatment showing that IRF4 was downregulated in 7 samples from patients shown to be clinically responding to BTKi and was not downregulated in 1 refractory case.

Consistent with the protein and mRNA expression of IRF4 in sensitive REC-1 cells in response to Ibr, IRF4 downregulation was also shown to be an early response to therapy occurring within the first treatment cycle and was sustained over several treatment cycles until relapse when its downregulation was prevented. Furthermore, IRF4 was not downregulated over several treatment cycles in a patient demonstrating primary resistance to BTKi (determined clinically).

These findings indicated that IRF4 may be involved in the development of both primary and acquired resistance to BTKi in MCL. In addition the observation that IRF4 was involved in treatment response to BTKi indicated it may have potential use as a biomarker in a clinical setting.

Although only representative of 8 cases, these results represent the largest study of IRF4 expression in matched pre and post BTKi treatment patient samples thus far and show encouraging results. A larger panel of MCL patient samples would however strengthen the data.

Modulation of IRF4 by CD40 signalling, a potential mechanism of BTKi resistance

Unlike pERK, the downregulation of IRF4 was not altered in response to BCR activation in sensitive REC-1 cells; IRF4 was however modulated by CD40L stimulation which prevented its down-regulation in response to Ibr and Acal. This correlates with the enhanced survival and proliferation of the REC-1 cells and suggests an alternative route for IRF4 activation, possibly via CD40L induced activation of NFκB which is a direct target of IRF4.[147] *In vitro* experiments with primary MCL cells were consistent with results from REC-1 cells, IRF4 was downregulated by BTKi (both Ibr and Acal) in the absence of CD40L, but this effect was prevented in the presence of CD40L.

Recently, it has been demonstrated that CD40L activation of the alternative NFκB pathway has a major impact on the drug response in MCL. Rauert-Wunderlich *et al* [203] showed that CD40L activation of the alternative NFκB pathway in MCL led to independency of classical NFκB signalling which resulted in resistance to BCR inhibitors.

Taken together these findings suggest that signals from the tissue microenvironment may modulate drug response in MCL and that CD40L signalling may have a role in resistance to BTK inhibitors by modulating expression of IRF4 through NFκB. On the other hand, dependency on CD40L was lost in REC-1 cells with acquired BTKi resistance (both Ibr and Acal) suggesting that 'acquired resistance' to BTKi more likely occurs through an intrinsic mechanism. Furthermore, BTK activation was restored in these cells in the presence of both Ibr and Acal and correlated with the sustained proliferation of the cells.

It is possible that the REC-1 cells with acquired BTKi resistance had developed a BTK mutation, as has been described in patients on BTKi in CLL and MCL and discussed in further detail in the introduction (section 1.3.7), causing ineffective binding of each inhibitor to the BTK C481 residue, and therefore BTK phosphorylation was no longer reduced in response to BTKi. Indeed in these cells we saw an increased level of pBTK-Y223 suggesting a more aggressive proliferative phenotype. This would also explain the sustained levels of IRF4 in REC-1 cells with acquired Ibr resistance which were not downregulated by Ibr and matched IRF4 expression seen in the untreated parent REC-1 cells.

However, this is different from the innate resistant cells (G519, JEKO-1 and JVM2) in which pBTK Y223 was reduced and IRF4 was not downregulated by BTKi suggesting the drug was still able to bind, only it was ineffective suggesting modulation via other mechanisms, such as alternative pathway activation via stimulation from the microenvironment, are involved in primary resistance. Detection of the BTK C418S mutation was not carried out in this study but would be a consideration in future studies in order to confirm the predictions made above. This could be carried out on

parent REC-1 cells and compared with the acquired BTKi resistant REC-1 cells and an MCL cell line with innate BTKi resistance such as G519.

Assessment of IRF4-protein interactions in REC-1 cells

It is well known that the most common binding partner for IRF4 in B-cells is ETS family member PU.1.[150,151,159] This study showed no evidence of IRF4 interacting with PU.1 in BTKi sensitive REC-1 cells, and no link between PU.1 and IRF4 response to BTKi in primary MCL cells. Interestingly, detailed assessment of IRF4- protein interactions by SWATH mass spectrometry revealed a strong relationship with mitochondrial proteins. This finding was novel, however mitochondria have a recognised link to IRF4 [197] and one that can be linked to chemo-resistance. In studies of CLL, resistance to chemotherapy has been associated with increased mitochondrial mass which reduced sensitivity to fludarabine nucleoside [198] and correlated with the apoptotic response of the CLL cells.

Further work will need to be carried out to prove the significance of these protein interactions and whether BTKi have effects on mitochondrial function.

Use of IRF4 as a biomarker of BTKi response

Findings from this study provide evidence that IRF4 is associated with response to BTKi treatment in MCL and could have potential use as a biomarker to predict response to BTKi therapy in a clinical setting.

This would prevent unnecessary administration of BTKi to patients who do not respond to therapy (identified by absence of IRF4 downregulation within the first treatment cycle) and also those who are acquiring resistance to BTKi (identified by sustained IRF4 expression following a period of downregulation). Early prediction of response to BTKi

would allow patients to be treated with alternative treatment options and thus improve treatment outcomes.

Other studies have suggested early detection of the relapse specific mutation during Ibr treatment by identification of an evolving minute mutant clone.[135] At present, this can only be achieved using deep targeted sequencing of the *BTK* gene either through NGS, which is costly, or Sanger sequencing (less sensitive), this however would not benefit cases of primary BTKi resistance where it has been shown in previous studies that the mutation is not present.[138]

Therefore monitoring IRF4 protein levels by flow cytometry or ELISA (enzyme-linked immunosorbent assay), would be a cheaper alternative to sequencing and would determine both primary BTKi resistance as well as onset of secondary resistance to Ibr and other BTK inhibitors. The use of flow cytometry to assess IRF4 levels along with pBTK-Y223 expression in the neoplastic B-cells would be a rapid and cost effective method to monitor patients on BTKi treatment compared to screening all patient samples for the presence of BTK mutations by NGS.

Using data generated from this study, our group are currently optimising a method for assessment of IRF4 expression by flow cytometry in paired pre-treatment / BTKi-treated samples in patients with CLL where IRF4 expression specifically in the neoplastic B-cells can be determined. CLL cases were chosen for optimisation studies due to the more frequent condition and guaranteed peripheral lymphocytosis which can be validated against detection of IRF4 by western blotting and immunohybridisation studies. It is however anticipated that this will be assessed in MCL patients on BTKi treatment once these initial optimisation and validation steps are confirmed.

6.1.5 Alternative therapy combinations

It was hoped that results from the chromatin IP studies would have generated insights into the role IRF4 may have in BTKi treatment in MCL. This work is on-going but having performed initial optimisation experiments with the generation of gene-annotated reads it can be continued. The proteomic study revealed some interesting insights, again which need validation, but which confirmed, could potentiate the evaluation of drugs which target mitochondrial function. Venetoclax is an oral selective BCL2 inhibitor which is known to target mitochondrial metabolism and indeed combinations of Ibr with Venetoclax are showing promise [204] and are currently being evaluated in on-going clinical trials.

Our studies also show that MCL cells can overcome sensitivity to BTK inhibition through alternative pathway activation. It has been shown by others that one consequence of relapse-specific mutation is the activation of PI3K and CDK4 pathways which promote cell survival and proliferation.[138] MCL is driven by cyclin D1 overexpression, and it has been shown that blocking CDK4 (which normally interacts with cyclin D1 to promote cell cycle progression) makes Ibr-resistant cells carrying the relapse-specific mutation sensitive to drugs that inhibit PI3K and also re-sensitises cells to Ibr. Therefore it has been suggested that targeting CDK4 with palbociclib plus a BTK inhibitor may be able to override acquired resistance in MCL.

Given the knowledge that in both DLBCL and MM IRF4 expression is downregulated upon treatment with lenolidomide it was interesting to note that during the course of this study a clinical trial was initiated testing lenolidamide in combination with Ibr in MCL (Trial ID: NCT02446236) and has shown encouraging results. This again is suggestive of the role IRF4 may have in the BTKi-treatment response in MCL.

6.1.6 Conclusion

This thesis contributes significantly to the understanding on the particular sensitivity of MCL cells to BTK inhibition. Overall, this study has identified that BTKi induces downregulation of IRF4 in sensitive but not resistant MCL cell lines, and that downregulation is opposed by CD40L. CD40L encountered in the cellular microenvironment supports the proliferation and survival of MCL cells, and protects them from the effects of BTK inhibition. This suggests that the expression of IRF4 following treatment with BTKi might be a biomarker for BTKi-sensitivity in MCL, and that mitochondrial proteins modulated by IRF4 may play an important role in MCL treatment response.

Appendix

Analysis of flow cytometry data

Results were acquired using a BD Accuri^{TM} C6 flow cytometer (BD) and data were analysed using BD Accuri^{TM} CFlow Plus software (BD Biosciences).

For analysis of apoptosis, a two dimensional (2D) plot of forward/side scatter identified populations of apoptotic or dead cells (small with low-forward scatter and irregular with increased side scatter) (Figure_Apx 1). This population was confirmed to express Annexin V consistent with the occurrence of apoptosis. Using this plot, the viable and apoptotic/dead cells were separately gated to determine the percentage viability within the sample (Figure_Apx 2).

For the remainder of analyses, a gate was placed only around the viable lymphocyte population and assessed in relation to fluorescence of an isotype control. Proliferation was assessed using the nuclear proliferation antigen Ki67 and expressed according to the percentage of permeabilised viable cells expressing Ki67 –FITC (Figure_Apx 3). The activation of BTK was assessed using an antibody recognising phosphorylation of one of the activation epitopes of BTK (pBTK-Y223-PE) in permeabilised cells. The activation of BTK in these cells was expressed as the median fluorescence intensity of the peak. The median rather than the mean was chosen as the peaks produced from primary cells would often be skewed (Figure_Apx 4).

For experiments using primary MCL cells, a forward / side scatter plot was obtained and a gate was placed on the population of cells containing lymphocytes (similar to the cell line approach above). The CD5 / CD19 dual-staining population of cells (mantle cell population) within this gate were identified according to their fluorescence (compared with isotype control antibody). Apoptosis, proliferation and BTK phosphorylation data was determined as previously described, but only from the

CD5/19 positive population of cells. Example of analysis plots to determine the percentage of apoptosis of primary cells labelled with MCL surface markers is shown (Figure_Apx 5) or median fluorescence intensity of BTK Y223 phosphorylation in primary MCL cells (Figure_Apx 6).

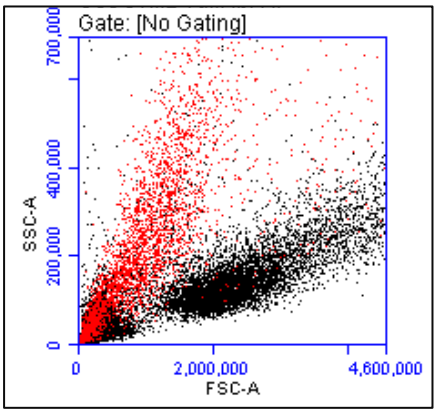

Figure_Apx 1: Populations of viable or apoptotic lymphocytes using a forward (FSC-A) vs side scatter (SSC-A) plot. Viable lymphocytes with high forward scatter are shown in black, apoptotic/dead cells with low forward scatter and high side-scatter are shown in red.

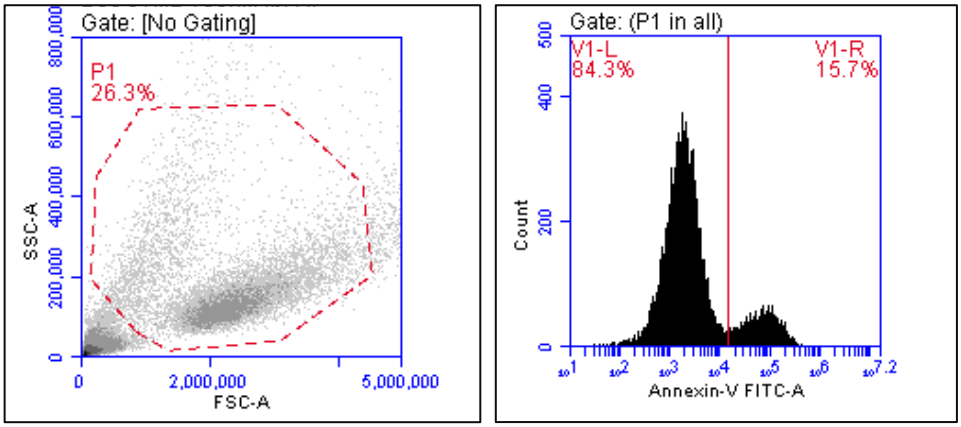

Figure_Apx 2: Example of FACS analysis plots used to determine the percentage of apoptosis of MCL cell lines. Using a forward/side scatter plot, a gate was placed around the population of cells containing both viable and apoptotic lymphocytes (labelled P1) (left). Analysis on these cells using a peak plot of FITC fluorescence determined two defined populations. A threshold line was placed between these defined populations to determine the percentage of annexin V-positive cells, shown in V1-R (right).

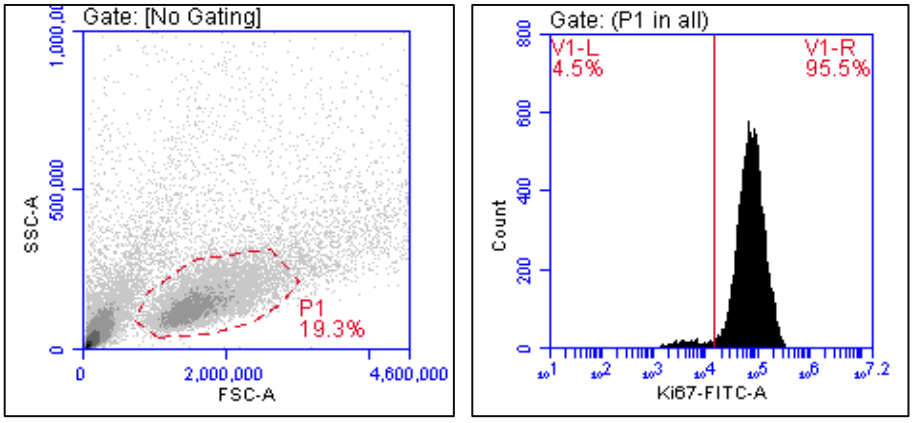

Figure_Apx 3: Example of FACS analysis plots used to determine the percentage of proliferation of MCL cell lines. Using a forward/side scatter plot, a gate was placed around the population of cells containing only the viable lymphocytes (labelled P1) (left). Using a peak plot, fluorescence from FITC labelled Ki67 positive cells was gated on the P1 cell population. A threshold line was placed between the Ki67 negative and positive cells to determine the percentage of the peak containing Ki67 positive cells, shown in V1-R (right).

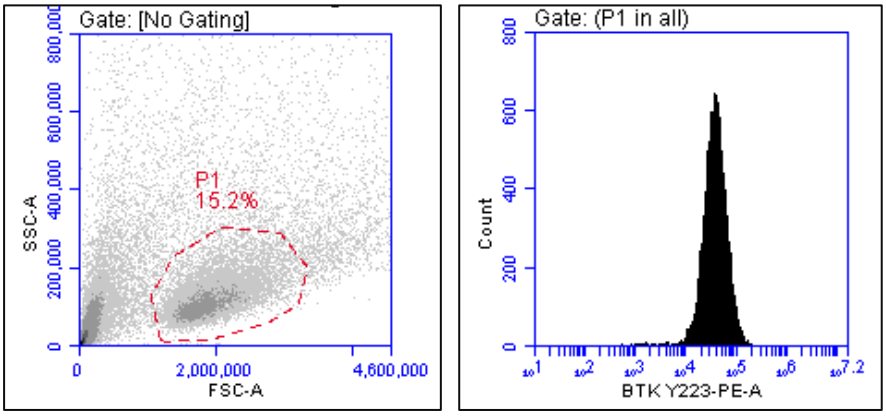

Figure_Apx 4: Example of FACS analysis plots used to calculate the median fluorescence intensity for BTK phosphorylation in MCL cell lines. Using a forward/side scatter plot, a gate was placed around the population of cells containing only the viable lymphocytes (labelled P1) (left). The median fluorescence intensity was calculated for PE labelled BTK Y223 positive cells gated on P1.

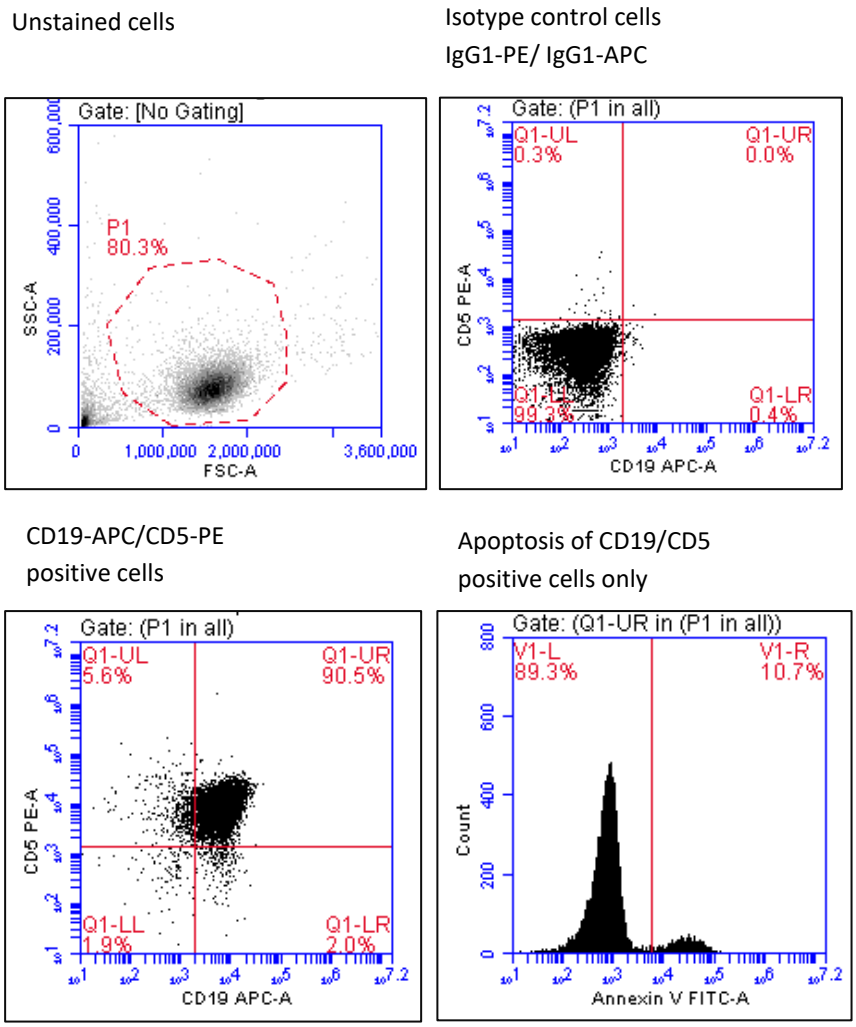

Figure_Apx 5: Example analysis plots of apoptosis in primary MCL cells. Using a forward/side scatter plot, a gate was placed around the population of cells containing lymphocytes (labelled P1) (top left). An isotype control (top right) and CD5/CD19 positive population (bottom left) allowed MCL cells to be identified. The percentage of annexin V-positive cells was applied to the CD5/CD19 positive cells to obtain the level of apoptosis (bottom right).

Unstained viable cells shown in P1

Isotype control cells
IgG1-FITC/ IgG1-PE/ IgG1-APC

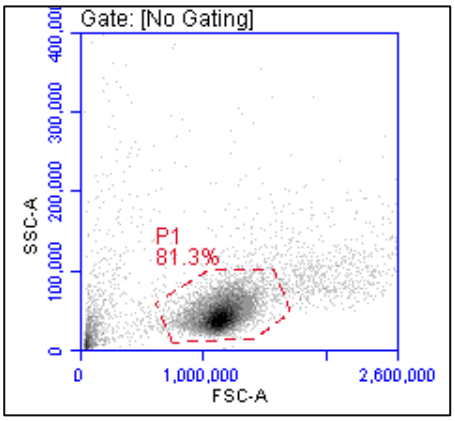

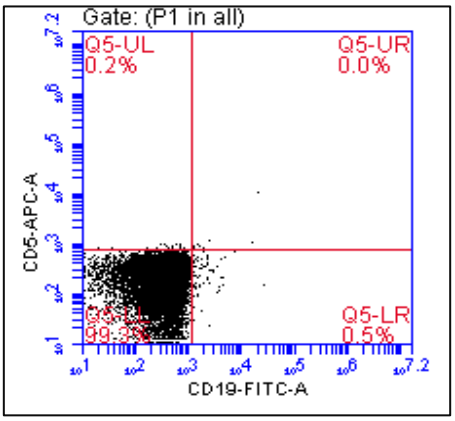

CD19-FITC/CD5-APC positive
cells shown in Q5-UR

Phosphorylation of BTK Y223-PE in
CD19/CD5 positive cells only

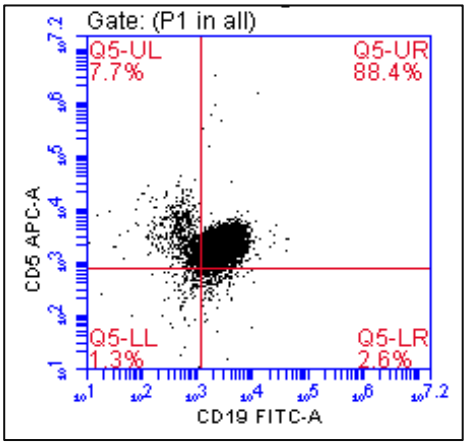

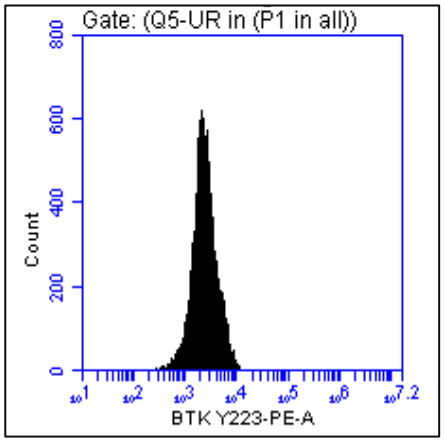

Figure_Apx 6: Analysis to determine median fluorescence intensity of BTK Y223 phosphorylation in primary MCL cells. Using the gating strategy described in Figure_Apx 5, the median fluorescence intensity of the BTK Y223-PE peak was determined for the CD5/CD19 positive cells.

References

1 Jares, P. & Campo, E. Advances in the understanding of mantle cell lymphoma. *British journal of haematology* **142**, 149-165, doi:10.1111/j.1365-2141.2008.07124.x (2008).

2 Swerdlow, S. H. *et al.* The 2016 revision of the World Health Organization classification of lymphoid neoplasms. *Blood* **127**, 2375-2390, doi:10.1182/blood-2016-01-643569 (2016).

3 Fu, S. *et al.* Trends and variations in mantle cell lymphoma incidence from 1995 to 2013: A comparative study between Texas and National SEER areas. *Oncotarget* **8**, 112516-112529, doi:10.18632/oncotarget.22367 (2017).

4 Zhou, Y. *et al.* Incidence trends of mantle cell lymphoma in the United States between 1992 and 2004. *Cancer* **113**, 791-798, doi:10.1002/cncr.23608 (2008).

5 Shah, N., Hutchinson, C. & Rule, S. Ibrutinib for the treatment of mantle cell lymphoma. *Expert Review of Hematology* **7**, 521-531, doi:10.1586/17474086.2014.951323 (2014).

6 Dreyling, M. *et al.* Newly diagnosed and relapsed mantle cell lymphoma: ESMO Clinical Practice Guidelines for diagnosis, treatment and follow-up†. *Annals of Oncology* **28**, iv62-iv71, doi:10.1093/annonc/mdx223 (2017).

7 Martins, C., Teixeira, C., Gamito, É. & Oliveira, A. P. Mantle cell lymphoma presenting as multiple lymphomatous polyposis of the gastrointestinal tract. *Revista Brasileira de Hematologia e Hemoterapia* **39**, 73-76, doi:10.1016/j.bjhh.2016.11.005 (2017).

8 Swerdlow SH, C. E., Harris NL, Jaffe ES, Pileri SA, Stein H, Thiele J. *WHO Classification of Tumours of Haematopoietic and Lymphoid Tissues*. 4th edn, Vol. 2 (International Agency for Research on Cancer (IARC), 2017).

9 Herrmann, A. *et al.* Improvement of overall survival in advanced stage mantle cell lymphoma. *Journal of clinical oncology : official journal of the American Society of Clinical Oncology* **27**, 511-518, doi:10.1200/jco.2008.16.8435 (2009).

10 Sandoval-Sus, J. D., Sotomayor, E. M. & Shah, B. D. Mantle Cell Lymphoma: Contemporary Diagnostic and Treatment Perspectives in the Age of Personalized Medicine. *Hematology/oncology and stem cell therapy* **10**, 99-115, doi:10.1016/j.hemonc.2017.02.003 (2017).

11 Dreyling, M. *et al.* Newly diagnosed and relapsed mantle cell lymphoma: ESMO Clinical Practice Guidelines for diagnosis, treatment and follow-up†. *Annals of Oncology* **25**, iii83-iii92, doi:10.1093/annonc/mdu264 (2014).

12 Fernandez, V. *et al.* Genomic and gene expression profiling defines indolent forms of mantle cell lymphoma. *Cancer research* **70**, 1408-1418, doi:10.1158/0008-5472.can-09-3419 (2010).

13 Furtado, M. & Rule, S. Indolent mantle cell lymphoma. *Haematologica* **96**, 1086-1088, doi:10.3324/haematol.2011.047357 (2011).

14 Martin, P. *et al.* Outcome of deferred initial therapy in mantle-cell lymphoma. *Journal of clinical oncology : official journal of the American Society of Clinical Oncology* **27**, 1209-1213, doi:10.1200/jco.2008.19.6121 (2009).

15 Campo, E., Raffeld, M. & Jaffe, E. S. Mantle-cell lymphoma. *Seminars in hematology* **36**, 115-127 (1999).

16 Jares, P., Colomer, D. & Campo, E. Molecular pathogenesis of mantle cell lymphoma. *The Journal of Clinical Investigation* **122**, 3416-3423, doi:10.1172/JCI61272 (2012).

17 Neganova, I. & Lako, M. G1 to S phase cell cycle transition in somatic and embryonic stem cells. *Journal of Anatomy* **213**, 30-44, doi:10.1111/j.1469-7580.2008.00931.x (2008).

18 Sherr, C. J. & Roberts, J. M. CDK inhibitors: positive and negative regulators of G1-phase progression. *Genes & development* **13**, 1501-1512 (1999).

19 Jiang, W. *et al.* Overexpression of cyclin D1 in rat fibroblasts causes abnormalities in growth control, cell cycle progression and gene expression. *Oncogene* **8**, 3447-3457 (1993).

20 Fu, K. *et al.* Cyclin D1–negative mantle cell lymphoma: a clinicopathologic study based on gene expression profiling. *Blood* **106**, 4315-4321, doi:10.1182/blood-2005-04-1753 (2005).

21 Salaverria, I. *et al.* Specific Secondary Genetic Alterations in Mantle Cell Lymphoma Provide Prognostic Information Independent of the Gene Expression–Based Proliferation Signature. *Journal of clinical oncology : official journal of the American Society of Clinical Oncology* **25**, 1216-1222, doi:10.1200/JCO.2006.08.4251 (2007).

22 Hirt, C. *et al.* Circulating t(14;18)-Positive Cells in Healthy Individuals – Association with Age and Sex but not with Smoking. *Leukemia & lymphoma* **54**, 2678-2684, doi:10.3109/10428194.2013.788177 (2013).

23 Greiner, T. C. *et al.* Mutation and genomic deletion status of ataxia telangiectasia mutated (ATM) and p53 confer specific gene expression profiles in mantle cell lymphoma. *Proceedings of the National Academy of Sciences of the United States of America* **103**, 2352-2357, doi:10.1073/pnas.0510441103 (2006).

24 Zhang, J. *et al.* The genomic landscape of mantle cell lymphoma is related to the epigenetically determined chromatin state of normal B cells. *Blood* **123**, 2988-2996, doi:10.1182/blood-2013-07-517177 (2014).

25 Kridel, R. *et al.* Whole transcriptome sequencing reveals recurrent NOTCH1 mutations in mantle cell lymphoma. *Blood* **119**, 1963-1971, doi:10.1182/blood-2011-11-391474 (2012).

26 Rahal, R. *et al.* Pharmacological and genomic profiling identifies NF-kappaB-targeted treatment strategies for mantle cell lymphoma. *Nature medicine* **20**, 87-92, doi:10.1038/nm.3435 (2014).

27 Saba, N. S. *et al.* Pathogenic role of B-cell receptor signaling and canonical NF-kappaB activation in mantle cell lymphoma. *Blood* **128**, 82-92, doi:10.1182/blood-2015-11-681460 (2016).

28 Bertoni, F. & Ponzoni, M. The cellular origin of mantle cell lymphoma. *The international journal of biochemistry & cell biology* **39**, 1747-1753, doi:10.1016/j.biocel.2007.04.026 (2007).

29 Pileri, S. A. & Falini, B. Mantle cell lymphoma. *Haematologica* **94**, 1488-1492, doi:10.3324/haematol.2009.013359 (2009).

30 Hadzidimitriou, A. *et al.* Is there a role for antigen selection in mantle cell lymphoma? Immunogenetic support from a series of 807 cases. *Blood* **118**, 3088-3095, doi:10.1182/blood-2011-03-343434 (2011).

31 Navarro, A. *et al.* Molecular subsets of mantle cell lymphoma defined by the IGHV mutational status and SOX11 expression have distinct biological and clinical features. *Cancer research* **72**, 5307-5316, doi:10.1158/0008-5472.CAN-12-1615 (2012).

32 Orchard, J. *et al.* A subset of t(11;14) lymphoma with mantle cell features displays mutated IgVH genes and includes patients with good prognosis, nonnodal disease. *Blood* **101**, 4975-4981, doi:10.1182/blood-2002-06-1864 (2003).

33 Hsu, P. *et al.* Mantle cell lymphoma with in situ or mantle zone growth pattern: a study of five cases and review of literature. *International journal of clinical and experimental pathology* **7**, 1042-1050 (2014).

34 Gao, J., Peterson, L., Nelson, B., Goolsby, C. & Chen, Y. H. Immunophenotypic variations in mantle cell lymphoma. *American journal of clinical pathology* **132**, 699-706, doi:10.1309/ajcpv8ln5enmzovy (2009).

35 Dorfman, D. M. & Pinkus, G. S. Distinction between small lymphocytic and mantle cell lymphoma by immunoreactivity for CD23. *Modern pathology : an official journal of the United States and Canadian Academy of Pathology, Inc* **7**, 326-331 (1994).

36 Garcia, D. P., Rooney, M. T., Ahmad, E. & Davis, B. H. Diagnostic usefulness of CD23 and FMC-7 antigen expression patterns in B-cell lymphoma classification. *American journal of clinical pathology* **115**, 258-265, doi:10.1309/vwtk-xyt5-d0dk-06hq (2001).

37 Xu, J. *et al.* CD10-positive mantle cell lymphoma: clinicopathologic and prognostic study of 30 cases. *Oncotarget* **9**, 11441-11450, doi:10.18632/oncotarget.23571 (2018).

38 Majlis, A., Pugh, W. C., Rodriguez, M. A., Benedict, W. F. & Cabanillas, F. Mantle cell lymphoma: correlation of clinical outcome and biologic features with three histologic variants. *Journal of clinical oncology : official journal of the American*

Society of Clinical Oncology **15**, 1664-1671, doi:10.1200/jco.1997.15.4.1664 (1997).

39 Kimura, Y. *et al.* Small cell variant of mantle cell lymphoma is an indolent lymphoma characterized by bone marrow involvement, splenomegaly, and a low Ki-67 index. *Cancer science* **102**, 1734-1741, doi:10.1111/j.1349-7006.2011.01988.x (2011).

40 Ott, G. *et al.* Blastoid variants of mantle cell lymphoma: frequent bcl-1 rearrangements at the major translocation cluster region and tetraploid chromosome clones. *Blood* **89**, 1421-1429 (1997).

41 Zucca, E., Stein, H. & Coiffier, B. European Lymphoma Task Force (ELTF): Report of the workshop on Mantle Cell Lymphoma (MCL). *Annals of oncology : official journal of the European Society for Medical Oncology* **5**, 507-511 (1994).

42 Hoster, E. *et al.* The Addition of Rituximab to First-Line Chemotherapy (R-CHOP) Results in Superior Response Rates, Time to Treatment Failure and Response Duration in Patients with Advanced Stage Mantle Cell Lymphoma: Long Term Results of a Randomized GLSG Trial. *Blood* **112**, 3049-3049 (2008).

43 Tucker, D. L. & Rule, S. A. A critical appraisal of ibrutinib in the treatment of mantle cell lymphoma and chronic lymphocytic leukemia. *Therapeutics and Clinical Risk Management* **11**, 979-990, doi:10.2147/TCRM.S73559 (2015).

44 Schieber, M., Gordon, L. I. & Karmali, R. Current overview and treatment of mantle cell lymphoma. *F1000Research* **7**, F1000 Faculty Rev-1136, doi:10.12688/f1000research.14122.1 (2018).

45 Pérez-Galán, P. *et al.* The proteasome inhibitor bortezomib induces apoptosis in mantle-cell lymphoma through generation of ROS and Noxa activation

independent of p53 status. *Blood* **107**, 257-264, doi:10.1182/blood-2005-05-2091 (2006).

46 Hambley, B., Caimi, P. F. & William, B. M. Bortezomib for the treatment of mantle cell lymphoma: an update. *Therapeutic Advances in Hematology* **7**, 196-208, doi:10.1177/2040620716648566 (2016).

47 Samad, N. & Younes, A. Temsirolimus in the treatment of relapsed or refractory mantle cell lymphoma. *OncoTargets and therapy* **3**, 167-178 (2010).

48 Zinzani, P. L. *et al.* Long-term follow-up of lenalidomide in relapsed/refractory mantle cell lymphoma: subset analysis of the NHL-003 study. *Annals of Oncology* **24**, 2892-2897, doi:10.1093/annonc/mdt366 (2013).

49 Candido, J. & Hagemann, T. Cancer-related inflammation. *Journal of clinical immunology* **33 Suppl 1**, S79-84, doi:10.1007/s10875-012-9847-0 (2013).

50 Coussens, L. M. & Werb, Z. Inflammation and cancer. *Nature* **420**, 860-867, doi:10.1038/nature01322 (2002).

51 Grivennikov, S. I., Greten, F. R. & Karin, M. Immunity, inflammation, and cancer. *Cell* **140**, 883-899, doi:10.1016/j.cell.2010.01.025 (2010).

52 Burger, J. A. & Ford, R. J. The microenvironment in mantle cell lymphoma: cellular and molecular pathways and emerging targeted therapies. *Seminars in cancer biology* **21**, 308-312, doi:10.1016/j.semcancer.2011.09.006 (2011).

53 Medina, D. J. *et al.* Mesenchymal stromal cells protect mantle cell lymphoma cells from spontaneous and drug-induced apoptosis through secretion of B-cell activating factor and activation of the canonical and non-canonical nuclear factor κB pathways. *Haematologica* **97**, 1255-1263, doi:10.3324/haematol.2011.040659 (2012).

54 Papin, A., Le Gouill, S. & Chiron, D. Rationale for targeting tumor cells in their microenvironment for mantle cell lymphoma treatment. *Leuk Lymphoma* **59**, 1064-1072, doi:10.1080/10428194.2017.1357177 (2018).

55 Fowler, N. H. *et al.* Role of the tumor microenvironment in mature B-cell lymphoid malignancies. *Haematologica* **101**, 531-540, doi:10.3324/haematol.2015.139493 (2016).

56 Scott, D. W. & Gascoyne, R. D. The tumour microenvironment in B cell lymphomas. *Nature reviews. Cancer* **14**, 517-534, doi:10.1038/nrc3774 (2014).

57 Meads, M. B., Gatenby, R. A. & Dalton, W. S. Environment-mediated drug resistance: a major contributor to minimal residual disease. *Nature reviews. Cancer* **9**, 665-674, doi:10.1038/nrc2714 (2009).

58 Barroso, M., Tucker, H., Drake, L., Nichol, K. & Drake, J. R. Antigen-B Cell Receptor Complexes Associate with Intracellular major histocompatibility complex (MHC) Class II Molecules. *The Journal of Biological Chemistry* **290**, 27101-27112, doi:10.1074/jbc.M115.649582 (2015).

59 Elgueta, R. *et al.* Molecular mechanism and function of CD40/CD40L engagement in the immune system. *Immunological reviews* **229**, 152-172, doi:10.1111/j.1600-065X.2009.00782.x (2009).

60 Aloui, C. *et al.* The signaling role of CD40 ligand in platelet biology and in platelet component transfusion. *International journal of molecular sciences* **15**, 22342-22364, doi:10.3390/ijms151222342 (2014).

61 Kawabe, T., Matsushima, M., Hashimoto, N., Imaizumi, K. & Hasegawa, Y. CD40/CD40 ligand interactions in immune responses and pulmonary immunity. *Nagoya journal of medical science* **73**, 69-78 (2011).

62 Ma, D. Y. & Clark, E. A. The role of CD40 and CD40L in Dendritic Cells. *Seminars in immunology* **21**, 265-272, doi:10.1016/j.smim.2009.05.010 (2009).

63 Andersen, N. S. *et al.* Soluble CD40 ligand induces selective proliferation of lymphoma cells in primary mantle cell lymphoma cell cultures. *Blood* **96**, 2219-2225 (2000).

64 Chiron, D. *et al.* Microenvironment-dependent proliferation and mitochondrial priming loss in mantle cell lymphoma is overcome by anti-CD20. *Blood*, doi:10.1182/blood-2016-06-720490 (2016).

65 Kurtova, A. V., Tamayo, A. T., Ford, R. J. & Burger, J. A. Mantle cell lymphoma cells express high levels of CXCR4, CXCR5, and VLA-4 (CD49d): importance for interactions with the stromal microenvironment and specific targeting. *Blood* **113**, 4604-4613, doi:10.1182/blood-2008-10-185827 (2009).

66 Lwin, T. *et al.* Lymphoma cell adhesion-induced expression of B cell-activating factor of the TNF family in bone marrow stromal cells protects non-Hodgkin's B lymphoma cells from apoptosis. *Leukemia* **23**, 170, doi:10.1038/leu.2008.266 (2008).

67 Lwin, T. *et al.* Bone marrow stromal cells prevent apoptosis of lymphoma cells by upregulation of anti-apoptotic proteins associated with activation of NF-kappaB (RelB/p52) in non-Hodgkin's lymphoma cells. *Leukemia* **21**, 1521-1531, doi:10.1038/sj.leu.2404723 (2007).

68 Marr, H. *Regulation of CD38 by IRF4 in chronic lymphocytic leukaemia* Doctor of Philosophy thesis, Newcastle University (2016).

69 Chen, Z., Teo, A. E. & McCarty, N. ROS induced CXCR4 signaling regulates mantle cell lymphoma (MCL) cell survival and drug resistance in the bone marrow microenvironment via autophagy. *Clinical cancer research : an official*

journal of the American Association for Cancer Research **22**, 187-199, doi:10.1158/1078-0432.CCR-15-0987 (2016).

70 Kim, Y.-R. & Eom, K.-S. Simultaneous Inhibition of CXCR4 and VLA-4 Exhibits Combinatorial Effect in Overcoming Stroma-Mediated Chemotherapy Resistance in Mantle Cell Lymphoma Cells. *Immune Network* **14**, 296-306, doi:10.4110/in.2014.14.6.296 (2014).

71 Hombach, J., Tsubata, T., Leclercq, L., Stappert, H. & Reth, M. Molecular components of the B-cell antigen receptor complex of the IgM class. *Nature* **343**, 760-762, doi:10.1038/343760a0 (1990).

72 Rolli, V. *et al.* Amplification of B cell antigen receptor signaling by a Syk/ITAM positive feedback loop. *Molecular cell* **10**, 1057-1069 (2002).

73 Yamamoto, T., Yamanashi, Y. & Toyoshima, K. Association of Src-family kinase Lyn with B-cell antigen receptor. *Immunological reviews* **132**, 187-206 (1993).

74 Woyach, J. A., Johnson, A. J. & Byrd, J. C. The B-cell receptor signaling pathway as a therapeutic target in CLL. *Blood* **120**, 1175-1184, doi:10.1182/blood-2012-02-362624 (2012).

75 Kabak, S. *et al.* The Direct Recruitment of BLNK to Immunoglobulin α Couples the B-Cell Antigen Receptor to Distal Signaling Pathways. *Molecular and Cellular Biology* **22**, 2524-2535, doi:10.1128/MCB.22.8.2524-2535.2002 (2002).

76 Dal Porto, J. M. *et al.* B cell antigen receptor signaling 101. *Molecular immunology* **41**, 599-613, doi:10.1016/j.molimm.2004.04.008 (2004).

77 Huang, K. P. The mechanism of protein kinase C activation. *Trends in neurosciences* **12**, 425-432 (1989).

78 Yokoyama, K. *et al.* BANK regulates BCR-induced calcium mobilization by promoting tyrosine phosphorylation of IP(3) receptor. *The EMBO Journal* **21**, 83-92, doi:10.1093/emboj/21.1.83 (2002).

79 Dang, C. V. MYC, metabolism, cell growth, and tumorigenesis. *Cold Spring Harb Perspect Med* **3**, a014217, doi:10.1101/cshperspect.a014217.

80 Merolle, M. I., Ahmed, M., Nomie, K. & Wang, M. L. The B cell receptor signaling pathway in mantle cell lymphoma. *Oncotarget* **9**, 25332-25341, doi:10.18632/oncotarget.25011 (2018).

81 Roskoski, R., Jr. Ibrutinib inhibition of Bruton protein-tyrosine kinase (BTK) in the treatment of B cell neoplasms. *Pharmacological research* **113**, 395-408, doi:10.1016/j.phrs.2016.09.011 (2016).

82 Johnson, G. L. & Lapadat, R. Mitogen-activated protein kinase pathways mediated by ERK, JNK, and p38 protein kinases. *Science (New York, N.Y.)* **298**, 1911-1912, doi:10.1126/science.1072682 (2002).

83 Colomer, D. & Campo, E. Unlocking new therapeutic targets and resistance mechanisms in mantle cell lymphoma. *Cancer cell* **25**, 7-9, doi:10.1016/j.ccr.2013.12.011 (2014).

84 Cang, S., Iragavarapu, C., Savooji, J., Song, Y. & Liu, D. ABT-199 (venetoclax) and BCL-2 inhibitors in clinical development. *Journal of Hematology & Oncology* **8**, 129, doi:10.1186/s13045-015-0224-3 (2015).

85 Braun, T. *et al.* Targeting NF-kappaB in hematologic malignancies. *Cell death and differentiation* **13**, 748-758, doi:10.1038/sj.cdd.4401874 (2006).

86 Davids, M. S. Targeting BCL-2 in B-cell lymphomas. *Blood* **130**, 1081, doi:10.1182/blood-2017-04-737338 (2017).

87 Karvonen, H. *et al.* Crosstalk between ROR1 and BCR pathways defines novel treatment strategies in mantle cell lymphoma. *Blood advances* **1**, 2257-2268, doi:10.1182/bloodadvances.2017010215 (2017).

88 Chiron, D. *et al.* Biological rational for sequential targeting of Bruton tyrosine kinase and Bcl-2 to overcome CD40-induced ABT-199 resistance in mantle cell lymphoma. *Oncotarget* **6**, 8750-8759, doi:10.18632/oncotarget.3275 (2015).

89 Li, Y. *et al.* Synergistic Co-Targeting of BTK and BCL2 in Mantle Cell Lymphoma. *Blood* **126**, 708 (2015).

90 Li, Y. *et al.* FBXO10 deficiency and BTK activation upregulate BCL2 expression in mantle cell lymphoma. *Oncogene* **35**, 6223-6234, doi:10.1038/onc.2016.155 (2016).

91 Thijssen, R. *et al.* Resistance to ABT-199 induced by microenvironmental signals in chronic lymphocytic leukemia can be counteracted by CD20 antibodies or kinase inhibitors. *Haematologica* **100**, e302-306, doi:10.3324/haematol.2015.124560 (2015).

92 Leverson, J. D. & Cojocari, D. Hematologic Tumor Cell Resistance to the BCL-2 Inhibitor Venetoclax: A Product of Its Microenvironment? *Frontiers in Oncology* **8**, doi:10.3389/fonc.2018.00458 (2018).

93 Jain, N. *et al.* Combined Venetoclax and Ibrutinib for Patients with Previously Untreated High-Risk CLL, and Relapsed/Refractory CLL: A Phase II Trial. *Blood* **130**, 429-429 (2017).

94 Tam, C. S. *et al.* Ibrutinib plus Venetoclax for the Treatment of Mantle-Cell Lymphoma. *The New England journal of medicine* **378**, 1211-1223, doi:10.1056/NEJMoa1715519 (2018).

95 Smith, C. I. *et al.* Expression of Bruton's agammaglobulinemia tyrosine kinase gene, BTK, is selectively down-regulated in T lymphocytes and plasma cells. *Journal of immunology (Baltimore, Md. : 1950)* **152**, 557-565 (1994).

96 de Weers, M. *et al.* The Bruton's tyrosine kinase gene is expressed throughout B cell differentiation, from early precursor B cell stages preceding immunoglobulin gene rearrangement up to mature B cell stages. *European journal of immunology* **23**, 3109-3114, doi:10.1002/eji.1830231210 (1993).

97 Smith, C. I. E. From identification of the BTK kinase to effective management of leukemia. *Oncogene* **36**, 2045-2053, doi:10.1038/onc.2016.343 (2017).

98 Hutchinson, C. V. & Dyer, M. J. Breaking good: the inexorable rise of BTK inhibitors in the treatment of chronic lymphocytic leukaemia. *British journal of haematology* **166**, 12-22, doi:10.1111/bjh.12895 (2014).

99 Mao, C., Zhou, M. & Uckun, F. M. Crystal structure of Bruton's tyrosine kinase domain suggests a novel pathway for activation and provides insights into the molecular basis of X-linked agammaglobulinemia. *J Biol Chem* **276**, 41435-41443, doi:10.1074/jbc.M104828200 (2001).

100 Tsukada, S. *et al.* Deficient expression of a B cell cytoplasmic tyrosine kinase in human X-linked agammaglobulinemia. *Cell* **72**, 279-290 (1993).

101 Vetrie, D. *et al.* The gene involved in X-linked agammaglobulinaemia is a member of the src family of protein-tyrosine kinases. *Nature* **361**, 226-233, doi:10.1038/361226a0 (1993).

102 Bruton, O. C. Agammaglobulinemia. *Pediatrics* **9**, 722-728 (1952).

103 Wang, Q. *et al.* Autoinhibition of Bruton's tyrosine kinase (Btk) and activation by soluble inositol hexakisphosphate. *eLife* **4**, doi:10.7554/eLife.06074 (2015).

104 Liu, C. *et al.* A balance of Btk and SHIP activation regulates B-cell receptor cluster formation by controlling actin remodeling. *Journal of immunology (Baltimore, Md. : 1950)* **187**, 230-239, doi:10.4049/jimmunol.1100157 (2011).

105 Lowry, W. E. & Huang, X. Y. G Protein beta gamma subunits act on the catalytic domain to stimulate Bruton's agammaglobulinemia tyrosine kinase. *J Biol Chem* **277**, 1488-1492, doi:10.1074/jbc.M110390200 (2002).

106 Vidal-Crespo, A. *et al.* The Bruton tyrosine kinase inhibitor CC-292 shows activity in mantle cell lymphoma and synergizes with lenalidomide and NIK inhibitors depending on nuclear factor-κB mutational status. *Haematologica* **102**, e447-e451, doi:10.3324/haematol.2017.168930 (2017).

107 Pan, Z. *et al.* Discovery of selective irreversible inhibitors for Bruton's tyrosine kinase. *ChemMedChem* **2**, 58-61, doi:10.1002/cmdc.200600221 (2007).

108 Gayko, U. *et al.* Development of the Bruton's tyrosine kinase inhibitor ibrutinib for B cell malignancies. *Annals of the New York Academy of Sciences* **1358**, 82-94, doi:10.1111/nyas.12878 (2015).

109 Honigberg, L. A. *et al.* The Bruton tyrosine kinase inhibitor PCI-32765 blocks B-cell activation and is efficacious in models of autoimmune disease and B-cell malignancy. *Proceedings of the National Academy of Sciences of the United States of America* **107**, 13075-13080, doi:10.1073/pnas.1004594107 (2010).

110 Barf, T. *et al.* Acalabrutinib (ACP-196): A Covalent Bruton Tyrosine Kinase Inhibitor with a Differentiated Selectivity and In Vivo Potency Profile. *The Journal of pharmacology and experimental therapeutics* **363**, 240-252, doi:10.1124/jpet.117.242909 (2017).

111 Herman, S. E. *et al.* Bruton tyrosine kinase represents a promising therapeutic target for treatment of chronic lymphocytic leukemia and is effectively targeted

by PCI-32765. *Blood* **117**, 6287-6296, doi:10.1182/blood-2011-01-328484 (2011).

112 Ponader, S. *et al.* The Bruton tyrosine kinase inhibitor PCI-32765 thwarts chronic lymphocytic leukemia cell survival and tissue homing in vitro and in vivo. *Blood* **119**, 1182-1189, doi:10.1182/blood-2011-10-386417 (2012).

113 de Rooij, M. F. *et al.* The clinically active BTK inhibitor PCI-32765 targets B-cell receptor- and chemokine-controlled adhesion and migration in chronic lymphocytic leukemia. *Blood* **119**, 2590-2594, doi:10.1182/blood-2011-11-390989 (2012).

114 Cinar, M. *et al.* Bruton tyrosine kinase is commonly overexpressed in mantle cell lymphoma and its attenuation by Ibrutinib induces apoptosis. *Leukemia research* **37**, 1271-1277, doi:10.1016/j.leukres.2013.07.028 (2013).

115 Pham, L. V. *et al.* Targeting BCR Activated STAT3 By Ibrutinib In Mantle Cell Lymphoma. *Blood* **122**, 3079-3079 (2013).

116 Advani, R. H. *et al.* Bruton tyrosine kinase inhibitor ibrutinib (PCI-32765) has significant activity in patients with relapsed/refractory B-cell malignancies. *Journal of clinical oncology : official journal of the American Society of Clinical Oncology* **31**, 88-94, doi:10.1200/jco.2012.42.7906 (2013).

117 Wang, M. L. *et al.* Targeting BTK with ibrutinib in relapsed or refractory mantle-cell lymphoma. *The New England journal of medicine* **369**, 507-516, doi:10.1056/NEJMoa1306220 (2013).

118 Treon, S. P. *et al.* Ibrutinib in previously treated Waldenstrom's macroglobulinemia. *The New England journal of medicine* **372**, 1430-1440, doi:10.1056/NEJMoa1501548 (2015).

119 Noy, A. *et al.* Targeting Bruton tyrosine kinase with ibrutinib in relapsed/refractory marginal zone lymphoma. *Blood* **129**, 2224-2232, doi:10.1182/blood-2016-10-747345 (2017).

120 Wilson, W. H. *et al.* Targeting B cell receptor signaling with ibrutinib in diffuse large B cell lymphoma. *Nature medicine* **21**, 922-926, doi:10.1038/nm.3884 (2015).

121 Byrd, J. C. *et al.* Targeting BTK with ibrutinib in relapsed chronic lymphocytic leukemia. *The New England journal of medicine* **369**, 32-42, doi:10.1056/NEJMoa1215637 (2013).

122 Howard, S. C., Jones, D. P. & Pui, C.-H. The Tumor Lysis Syndrome. *The New England journal of medicine* **364**, 1844-1854, doi:10.1056/NEJMra0904569 (2011).

123 Stephens, D. M. & Spurgeon, S. E. Ibrutinib in mantle cell lymphoma patients: glass half full? Evidence and opinion. *Therapeutic Advances in Hematology* **6**, 242-252, doi:10.1177/2040620715592569 (2015).

124 Walter, H. S. *et al.* A phase 1 clinical trial of the selective BTK inhibitor ONO/GS-4059 in relapsed and refractory mature B-cell malignancies. *Blood* **127**, 411-419, doi:10.1182/blood-2015-08-664086 (2016).

125 Wu, J., Liu, C., Tsui, S. T. & Liu, D. Second-generation inhibitors of Bruton tyrosine kinase. *Journal of Hematology & Oncology* **9**, 80, doi:10.1186/s13045-016-0313-y (2016).

126 Sarkissian, S., O'Brein S. Second-Generation Brutons Tyrosine Kinase Inhibitors. *AJHO* **13**, 29-34 (2017).

127 Harrington, B. K. *et al.* Preclinical Evaluation of the Novel BTK Inhibitor Acalabrutinib in Canine Models of B-Cell Non-Hodgkin Lymphoma. *PLOS ONE* **11**, e0159607, doi:10.1371/journal.pone.0159607 (2016).

128 Wang, M. *et al.* Acalabrutinib in relapsed or refractory mantle cell lymphoma (ACE-LY-004): a single-arm, multicentre, phase 2 trial. *Lancet (London, England)* **391**, 659-667, doi:10.1016/s0140-6736(17)33108-2 (2018).

129 Dreyling, M. *et al.* Ibrutinib versus temsirolimus in patients with relapsed or refractory mantle-cell lymphoma: an international, randomised, open-label, phase 3 study. *Lancet (London, England)* **387**, 770-778, doi:10.1016/s0140-6736(15)00667-4 (2016).

130 Wang, M. L. *et al.* Ibrutinib in combination with rituximab in relapsed or refractory mantle cell lymphoma: a single-centre, open-label, phase 2 trial. *The Lancet. Oncology* **17**, 48-56, doi:10.1016/s1470-2045(15)00438-6 (2016).

131 Tam, C. *et al.* The BTK Inhibitor, Bgb-3111, Is Safe, Tolerable, and Highly Active in Patients with Relapsed/ Refractory B-Cell Malignancies: Initial Report of a Phase 1 First-in-Human Trial. *Blood* **126**, 832-832 (2015).

132 Pal Singh, S., Dammeijer, F. & Hendriks, R. W. Role of Bruton's tyrosine kinase in B cells and malignancies. *Molecular Cancer* **17**, 57, doi:10.1186/s12943-018-0779-z (2018).

133 Herman, S. E. M. *et al.* The Bruton Tyrosine Kinase (BTK) Inhibitor Acalabrutinib Demonstrates Potent On-Target Effects and Efficacy in Two Mouse Models of Chronic Lymphocytic Leukemia. *Clinical cancer research : an official journal of the American Association for Cancer Research* **23**, 2831-2841, doi:10.1158/1078-0432.CCR-16-0463 (2017).

134 Medicine, U. S. N. L. o. *Clinical Trials.gov*.

135 Sharma, S. *et al.* Identification of a structurally novel BTK mutation that drives ibrutinib resistance in CLL. *Oncotarget* **7**, 68833-68841, doi:10.18632/oncotarget.11932 (2016).

136 Valiaho, J., Smith, C. I. & Vihinen, M. BTKbase: the mutation database for X-linked agammaglobulinemia. *Human mutation* **27**, 1209-1217, doi:10.1002/humu.20410 (2006).

137 Cheng, S. *et al.* Functional characterization of BTK(C481S) mutation that confers ibrutinib resistance: exploration of alternative kinase inhibitors. *Leukemia* **29**, 895-900, doi:10.1038/leu.2014.263 (2015).

138 Chiron, D. *et al.* Cell Cycle Reprogramming for PI3K Inhibition Overrides Relapse-Specific C481S BTK Mutation Revealed by Longitudinal Functional Genomics in Mantle Cell Lymphoma. *Cancer discovery* **4**, 1022-1035, doi:10.1158/2159-8290.CD-14-0098 (2014).

139 Furman, R. R. *et al.* Ibrutinib resistance in chronic lymphocytic leukemia. *The New England journal of medicine* **370**, 2352-2354, doi:10.1056/NEJMc1402716 (2014).

140 Maddocks, K. J. *et al.* Etiology of Ibrutinib Therapy Discontinuation and Outcomes in Patients With Chronic Lymphocytic Leukemia. *JAMA oncology* **1**, 80-87, doi:10.1001/jamaoncol.2014.218 (2015).

141 Woyach, J. A. *et al.* Resistance mechanisms for the Bruton's tyrosine kinase inhibitor ibrutinib. *The New England journal of medicine* **370**, 2286-2294, doi:10.1056/NEJMoa1400029 (2014).

142 Burger, J. A. *et al.* Clonal evolution in patients with chronic lymphocytic leukaemia developing resistance to BTK inhibition. *Nature Communications* **7**, 11589, doi:10.1038/ncomms11589

https://www.nature.com/articles/ncomms11589#supplementary-information (2016).

143 Komarova, N. L., Burger, J. A. & Wodarz, D. Evolution of ibrutinib resistance in chronic lymphocytic leukemia (CLL). *Proceedings of the National Academy of Sciences* **111**, 13906-13911, doi:10.1073/pnas.1409362111 (2014).

144 Zhao, X. *et al.* Unification of de novo and acquired ibrutinib resistance in mantle cell lymphoma. *Nature Communications* **8**, 14920, doi:10.1038/ncomms14920

https://www.nature.com/articles/ncomms14920#supplementary-information (2017).

145 Ma, J. *et al.* Characterization of ibrutinib-sensitive and -resistant mantle lymphoma cells. *British journal of haematology* **166**, 849-861, doi:doi:10.1111/bjh.12974 (2014).

146 De Silva, N. S., Simonetti, G., Heise, N. & Klein, U. The diverse roles of IRF4 in late germinal center B-cell differentiation. *Immunological reviews* **247**, 73-92, doi:10.1111/j.1600-065X.2012.01113.x (2012).

147 Shaffer, A. L., Tolga Emre, N. C., Romesser, P. B. & Staudt, L. M. IRF4: Immunity. Malignancy! Therapy? *Clinical cancer research : an official journal of the American Association for Cancer Research* **15**, 2954-2961, doi:10.1158/1078-0432.CCR-08-1845 (2009).

148 Grumont, R. J. & Gerondakis, S. Rel induces interferon regulatory factor 4 (IRF-4) expression in lymphocytes: modulation of interferon-regulated gene expression by rel/nuclear factor kappaB. *The Journal of experimental medicine* **191**, 1281-1292 (2000).

149 Gualco, G., Weiss, L. M. & Bacchi, C. E. MUM1/IRF4: A Review. *Applied immunohistochemistry & molecular morphology : AIMM* **18**, 301-310, doi:10.1097/PAI.0b013e3181cf1126 (2010).

150 Shukla, V. & Lu, R. IRF4 and IRF8: Governing the virtues of B Lymphocytes. *Frontiers in biology* **9**, 269-282, doi:10.1007/s11515-014-1318-y (2014).

151 Brass, A. L., Kehrli, E., Eisenbeis, C. F., Storb, U. & Singh, H. Pip, a lymphoid-restricted IRF, contains a regulatory domain that is important for autoinhibition and ternary complex formation with the Ets factor PU.1. *Genes & development* **10**, 2335-2347 (1996).

152 Mamane, Y. *et al.* Interferon regulatory factors: the next generation. *Gene* **237**, 1-14 (1999).

153 Escalante, C. R. *et al.* Crystal structure of PU.1/IRF-4/DNA ternary complex. *Molecular cell* **10**, 1097-1105 (2002).

154 Glasmacher, E. *et al.* A genomic regulatory element that directs assembly and function of immune-specific AP-1-IRF complexes. *Science (New York, N.Y.)* **338**, 975-980, doi:10.1126/science.1228309 (2012).

155 Li, P. *et al.* BATF-JUN is critical for IRF4-mediated transcription in T cells. *Nature* **490**, 543-546, doi:10.1038/nature11530 (2012).

156 Tussiwand, R. *et al.* Compensatory dendritic cell development mediated by BATF-IRF interactions. *Nature* **490**, 502-507, doi:10.1038/nature11531 (2012).

157 Wang, L., Yao, Z. Q., Moorman, J. P., Xu, Y. & Ning, S. Gene Expression Profiling Identifies IRF4-Associated Molecular Signatures in Hematological Malignancies. *PLoS ONE* **9**, e106788, doi:10.1371/journal.pone.0106788 (2014).

158 Pridans, C. *et al.* Identification of Pax5 target genes in early B cell differentiation. *Journal of immunology (Baltimore, Md. : 1950)* **180**, 1719-1728 (2008).

159 Brass, A. L., Zhu, A. Q. & Singh, H. Assembly requirements of PU.1-Pip (IRF-4) activator complexes: inhibiting function in vivo using fused dimers. *Embo j* **18**, 977-991, doi:10.1093/emboj/18.4.977 (1999).

160 Ma, S., Turetsky, A., Trinh, L. & Lu, R. IFN regulatory factor 4 and 8 promote Ig light chain kappa locus activation in pre-B cell development. *Journal of immunology (Baltimore, Md. : 1950)* **177**, 7898-7904 (2006).

161 Ma, S., Pathak, S., Trinh, L. & Lu, R. Interferon regulatory factors 4 and 8 induce the expression of Ikaros and Aiolos to down-regulate pre–B-cell receptor and promote cell-cycle withdrawal in pre–B-cell development. *Blood* **111**, 1396-1403, doi:10.1182/blood-2007-08-110106 (2008).

162 Ma, S. *et al.* Ikaros and Aiolos Inhibit Pre-B-Cell Proliferation by Directly Suppressing c-Myc Expression. *Molecular and Cellular Biology* **30**, 4149-4158, doi:10.1128/MCB.00224-10 (2010).

163 Johnson, K. *et al.* Regulation of immunoglobulin light-chain recombination by the transcription factor IRF-4 and the attenuation of interleukin-7 signaling. *Immunity* **28**, 335-345, doi:10.1016/j.immuni.2007.12.019 (2008).

164 Tokoyoda, K., Egawa, T., Sugiyama, T., Choi, B. I. & Nagasawa, T. Cellular niches controlling B lymphocyte behavior within bone marrow during development. *Immunity* **20**, 707-718, doi:10.1016/j.immuni.2004.05.001 (2004).

165 Klein, U. *et al.* Transcription factor IRF4 controls plasma cell differentiation and class-switch recombination. *Nature immunology* **7**, 773-782, doi:10.1038/ni1357 (2006).

166 Ochiai, K. *et al.* Transcriptional regulation of germinal center B and plasma cell fates by dynamical control of IRF4. *Immunity* **38**, 918-929, doi:10.1016/j.immuni.2013.04.009 (2013).

167 Saito, M. *et al.* A signaling pathway mediating downregulation of BCL6 in germinal center B cells is blocked by BCL6 gene alterations in B cell lymphoma. *Cancer cell* **12**, 280-292, doi:10.1016/j.ccr.2007.08.011 (2007).

168 Sciammas, R. *et al.* Graded expression of interferon regulatory factor-4 coordinates isotype switching with plasma cell differentiation. *Immunity* **25**, 225-236, doi:10.1016/j.immuni.2006.07.009 (2006).

169 Simonetti, G. *et al.* IRF4 controls the positioning of mature B cells in the lymphoid microenvironments by regulating NOTCH2 expression and activity. *The Journal of experimental medicine* **210**, 2887-2902, doi:10.1084/jem.20131026 (2013).

170 Chang, C.-C. *et al.* Expression of MUM1/IRF4 correlates with clinical outcome in patients with B-cell chronic lymphocytic leukemia. *Blood* **100**, 4671-4675, doi:10.1182/blood-2002-01-0104 (2002).

171 Shaffer, A. L. *et al.* IRF4 Addiction in Multiple Myeloma. *Nature* **454**, 226-231, doi:10.1038/nature07064 (2008).

172 Hans, C. P. *et al.* Confirmation of the molecular classification of diffuse large B-cell lymphoma by immunohistochemistry using a tissue microarray. *Blood* **103**, 275-282, doi:10.1182/blood-2003-05-1545 (2004).

173 Yang, Y. *et al.* Exploiting synthetic lethality for the therapy of ABC diffuse large B cell lymphoma. *Cancer cell* **21**, 723-737, doi:10.1016/j.ccr.2012.05.024 (2012).

174 Di Bernardo, M. C. *et al.* A genome-wide association study identifies six susceptibility loci for chronic lymphocytic leukemia. *Nature genetics* **40**, 1204-1210, doi:10.1038/ng.219 (2008).

175 Allan, J. M. *et al.* Variant IRF4/MUM1 associates with CD38 status and treatment-free survival in chronic lymphocytic leukaemia. *Leukemia* **24**, 877-881, doi:10.1038/leu.2009.298 (2010).

176 Crowther-Swanepoel, D. *et al.* Fine-scale mapping of the 6p25.3 chronic lymphocytic leukaemia susceptibility locus. *Human molecular genetics* **19**, 1840-1845, doi:10.1093/hmg/ddq044 (2010).

177 Naushad, H. *et al.* Mantle cell lymphoma with flow cytometric evidence of clonal plasmacytic differentiation: a case report. *Cytometry. Part B, Clinical cytometry* **76**, 218-224, doi:10.1002/cyto.b.20463 (2009).

178 Young, K. H. *et al.* Mantle cell lymphoma with plasma cell differentiation. *The American journal of surgical pathology* **30**, 954-961 (2006).

179 Pérez-Galán, P. *et al.* Bortezomib resistance in mantle cell lymphoma is associated with plasmacytic differentiation. *Blood* **117**, 542-552, doi:10.1182/blood-2010-02-269514 (2011).

180 Moros, A. *et al.* Synergistic antitumor activity of lenalidomide with the BET bromodomain inhibitor CPI203 in bortezomib-resistant mantle cell lymphoma. *Leukemia* **28**, 2049-2059, doi:10.1038/leu.2014.106 (2014).

181 Forero, A., Moore, P. S. & Sarkar, S. N. Role of IRF4 in IFN-stimulated gene induction and maintenance of Kaposi sarcoma-associated herpesvirus latency in primary effusion lymphoma cells. *Journal of immunology (Baltimore, Md. : 1950)* **191**, 1476-1485, doi:10.4049/jimmunol.1202514 (2013).

182 Wang, M. *et al.* Observational study of lenalidomide in patients with mantle cell lymphoma who relapsed/progressed after or were refractory/intolerant to ibrutinib (MCL-004). *Journal of Hematology & Oncology* **10**, 171, doi:10.1186/s13045-017-0537-5 (2017).

183 Sun, Z., Zhou, D., Wei, M. & Luo, L. Abstract 4563: Mechanism of action of Ibrutinib in mantle cell lymphoma. *Cancer research* **74**, 4563-4563, doi:10.1158/1538-7445.am2014-4563 (2014).

184 Amin, H. M. *et al.* Characterization of 4 mantle cell lymphoma cell lines. *Archives of pathology & laboratory medicine* **127**, 424-431, doi:10.1043/0003-9985(2003)127<0424:comclc>2.0.co;2 (2003).

185 Drexler, H. G. & MacLeod, R. A. F. Malignant hematopoietic cell lines: in vitro models for the study of mantle cell lymphoma. *Leukemia research* **26**, 781-787, doi:10.1016/S0145-2126(02)00026-7 (2002).

186 Young, L., Sung, J., Stacey, G. & Masters, J. R. Detection of Mycoplasma in cell cultures. *Nature protocols* **5**, 929-934, doi:10.1038/nprot.2010.43 (2010).

187 Niemann, C. U. & Wiestner, A. B-cell receptor signaling as a driver of lymphoma development and evolution. *Seminars in cancer biology* **23**, 410-421, doi:10.1016/j.semcancer.2013.09.001 (2013).

188 Young, R. M. & Staudt, L. M. Targeting pathological B cell receptor signalling in lymphoid malignancies. *Nature reviews. Drug discovery* **12**, 229-243, doi:10.1038/nrd3937 (2013).

189 Mankai, A. *et al.* Improvement of rituximab efficiency in chronic lymphocytic leukemia by CpG-mediated upregulation of CD20 expression independently of PU.1. *Annals of the New York Academy of Sciences* **1173**, 721-728, doi:10.1111/j.1749-6632.2009.04614.x (2009).

190 Balasubramanian, S., Chen, J., Crowley, R. & Buggy, J. J. Abstract 856: Biomarkers of sensitivity and resistance to the BTK inhibitor PCI-32765 in mantle cell lymphoma. *Cancer research* **72**, 856-856, doi:10.1158/1538-7445.am2012-856 (2012).

191 Zhang, L. *et al.* Role of the microenvironment in mantle cell lymphoma: IL-6 is an important survival factor for the tumor cells. *Blood* **120**, 3783-3792, doi:10.1182/blood-2012-04-424630 (2012).

192 Burger, J. A., Ghia, P., Rosenwald, A. & Caligaris-Cappio, F. The microenvironment in mature B-cell malignancies: a target for new treatment strategies. *Blood* **114**, 3367-3375, doi:10.1182/blood-2009-06-225326 (2009).

193 Senthebane, D. A. *et al.* The Role of Tumor Microenvironment in Chemoresistance: To Survive, Keep Your Enemies Closer. *International journal of molecular sciences* **18**, 1586, doi:10.3390/ijms18071586 (2017).

194 Son, B. *et al.* The role of tumor microenvironment in therapeutic resistance. *Oncotarget* **8**, 3933-3945, doi:10.18632/oncotarget.13907 (2017).

195 Wang, L. & Ning, S. Interferon Regulatory Factor 4 Is Activated through c-Src-Mediated Tyrosine Phosphorylation in Virus-Transformed Cells. *Journal of Virology* **87**, 9672-9679, doi:10.1128/JVI.01435-13 (2013).

196 Adams, W. C. *et al.* Anabolism-associated Mitochondrial Stasis Driving Lymphocyte Differentiation over Self-renewal. *Cell reports* **17**, 3142-3152, doi:10.1016/j.celrep.2016.11.065 (2016).

197 Kong, X. *et al.* IRF4 is a key thermogenic transcriptional partner of PGC-1alpha. *Cell* **158**, 69-83, doi:10.1016/j.cell.2014.04.049 (2014).

198 Carew, J. S. *et al.* Increased mitochondrial biogenesis in primary leukemia cells: the role of endogenous nitric oxide and impact on sensitivity to fludarabine. *Leukemia* **18**, 1934-1940, doi:10.1038/sj.leu.2403545 (2004).

199 Guerra, F., Arbini, A. A. & Moro, L. Mitochondria and cancer chemoresistance. *Biochimica et biophysica acta. Bioenergetics* **1858**, 686-699, doi:10.1016/j.bbabio.2017.01.012 (2017).

200 Rauert-Wunderlich, H., Rudelius, M., Ott, G. & Rosenwald, A. Targeting protein kinase C in mantle cell lymphoma. *British journal of haematology* **173**, 394-403, doi:10.1111/bjh.13973 (2016).

201 Ponader, S. *et al.* Activity of Bruton's Tyrosine Kinase (Btk) Inhibitor PCI-32765 in Mantle Cell Lymphoma (MCL) Identifies Btk As a Novel Therapeutic Target. *Blood* **118**, 3688-3688 (2011).

202 Mason, J. A., Hagel, K. R., Hawk, M. A. & Schafer, Z. T. Metabolism during ECM Detachment: Achilles Heel of Cancer Cells? *Trends in cancer* **3**, 475-481, doi:10.1016/j.trecan.2017.04.009 (2017).

203 Rauert-Wunderlich, H., Rudelius, M., Berberich, I. & Rosenwald, A. CD40L mediated alternative NFκB-signaling induces resistance to BCR-inhibitors in patients with mantle cell lymphoma. *Cell death & disease* **9**, 86, doi:10.1038/s41419-017-0157-6 (2018).

204 Portell, C. A. *et al.* Initial Report of a Multi-Institution Phase I/Ib Study of Ibrutinib with Venetoclax in Relapsed or Refractory Mantle Cell Lymphoma. *Blood* **128**, 2958-2958 (2016).